UNIVERSITY OF PRETORIA

DEPARTMENT OF CIVIL ENGINEERING

The Influence of Binder Composition and Content on the Early Age Behaviour of Concrete

---

Sophia Visser

DECEMBER 2019

THE INFLUENCE OF BINDER COMPOSITION AND CONTENT ON THE EARLY AGE BEHAVIOUR OF CONCRETE

SOPHIA VISSER

A dissertation submitted in partial fulfilment of the requirements for the degree of

MASTER OF ENGINEERING (STRUCTURAL ENGINEERING)

in the

FACULTY OF ENGINEERING

UNIVERSITY OF PRETORIA

December 2019

PROJECT REPORT SUMMARY

THE INFLUENCE OF BINDER COMPOSITION AND CONTENT ON THE EARLY AGE BEHAVIOUR OF CONCRETE

S. VISSER

Supervisor: Professor E.P. Kearsley

Department: Civil Engineering

University: University of Pretoria

Degree: Master of Engineering (Structural Engineering)

With the increased use of high performance concrete a lower water-to-binder ratio is employed to improve the properties of concrete and mineral and chemical admixtures are introduced. With a low water-to-binder ratio, considerable early-age volume changes can occur and compromises the durability of the concrete. Early age shrinkage is often not tested in practice due to the difficulty in measuring and the lack of standardisation of measuring techniques.

The tensile capacity of concrete is lowest at an early age and therefore the most susceptible to cracking and material faults when stresses are induced by, for instance, drying shrinkage. Drying shrinkage can be prevented by proper placing and curing techniques but even then, cracking has been observed soon after casting. This occurrence can be attributed to factors such as high thermal gradients and autogenous shrinkage. Autogenous shrinkage is defined as a change in volume while no moisture is allowed to leave the material system and is present at low water-to-binder ratios. The influence of supplementary cementitious materials (SCMs) on autogenous shrinkage is not well understood but is well documented.

SCMs are used to improve the properties of concrete but significantly affect the exothermic hydration process of cement. The strength and heat of hydration is altered, and this is dependent on the water-to-binder ratio but also on the type of SCM used and the amount present. Autogenous shrinkage is caused by hydration reactions and the heat of hydration is linked to strength development. There may thus exist a relationship between autogenous shrinkage, the thermal processes and strength development.

The primary objective of this study was to investigate the relationship between autogenous shrinkage, the thermal processes and the strength development of concrete. The influence of binder composition and content on the early age behaviour of concrete was studied. The results indicated a correlation between autogenous shrinkage and cumulative heat released where the autogenous shrinkage observed increased with cumulative heat released. A weak correlation was found between compressive strength and autogenous shrinkage. Generally, the shrinkage increased with concrete strength and the early age strength attributed more to autogenous shrinkage than later age strength. A correlation was observed between the compressive strength and cumulative heat released. SCM replacement led to a lower cumulative heat but SCM addition was detrimental in that more heat was released for an equivalent strength than for SCM replacement samples.

Notably, GGBS replacement led to more shrinkage with a lower cumulative heat released and a lower strength as well. This was mitigated by additional CSF replacement which was also not expected as CSF is known to exacerbate autogenous shrinkage. It was believed that the CSF used in this study conglomerated to behave as a material with a larger particle size.

DECLARATION

I, the undersigned hereby declare that:

- I understand what plagiarism is and I am aware of the University's policy in this regard;
- The work contained in this dissertation is my own original work;
- I did not refer to work of current or previous students, lecture notes, handbooks or any other study material without proper referencing;
- Where another person's work has been used this has been properly acknowledged and referenced;
- I have not allowed anyone to copy any part of my dissertation;
- I have not previously in its entirety or in part submitted this dissertation at any university for a degree.

Disclaimer:

The work presented in this report is that of the student alone. Students were encouraged to take ownership of their projects and to develop and execute their experiments with limited guidance and assistance. The content of the research does not necessarily represent the views of the supervisor or any staff member of the University of Pretoria, Department of Civil Engineering. The supervisor did not read or edit the final report and is not responsible for any technical inaccuracies, statements or errors. The conclusions and recommendations given in the report are also not necessarily that of the supervisor, sponsors or companies involved in the research.

Signature: 

Name of student: Sophia Visser

Student number: 10094289

Date: December 2019

ACKNOWLEDGEMENT

I wish to express my sincere gratitude to my supervisor *Professor E.P. Kearsley* for her continuous support and guidance throughout this research, for believing in me and encouraging me to pursue postgraduate studies. I would like to thank and convey my gratitude to all of those who have contributed and have been a part of this dissertation and I would like to recognise the following persons in particular:

- The *Concrete Institute* for financial assistance during my postgraduate studies.
- *Mr. Derek Mostert*, the concrete technologist at the University of Pretoria, for his technical assistance and guidance.
- *Mr. Johan Scholtz* and *Mr. Jaco Botha* for their technical and practical assistance during testing in this study.
- *Dr. Grizelda du Toit*, *Mr. Mike Mc Donald* and *AfriSam* for the use of their laboratory facilities for the isothermal calorimeter measurements during this study.
- The *concrete laboratory personnel* for assisting me in carrying out my testing. Without them this experimental undertaking would have been insurmountable.

Finally, my deep and sincere gratitude to my family, friends and most of all my husband for the enthusiasm, encouragement, support and continuous optimism without which this dissertation would not have been possible. Thank you for all the sacrifices you have made to enable me to pursue my studies.

CONTENTS

LIST OF TABLES

LIST OF FIGURES

LIST OF ABBREVIATIONS

CSF	Condensed Silica Fume
FA	Fly Ash
GGBS	Ground Granulated Blast-furnace Slag
HPC	High Performance Concrete
HRWR	High-range-water-reducer
PC	Portland Cement
RH	Relative Humidity
SCMs	Supplementary Cementitious Materials
SF	Silica Fume
SP	Superplasticiser
TSTM	Temperature Stress Testing Machine
VTT	Valtion Teknillinen Tutkimuskeskus (State Technical Research Centre of Finland)
WRA	Water Reducing Admixture

CHAPTER 1: INTRODUCTION

1.1 BACKGROUND

The increase in the use of high-performance concrete (HPC) has given rise to the use of supplementary cementitious materials (SCMs) and chemical admixtures. The exothermic hydration process of cement is complex and SCMs can affect the hydration process and subsequently the concrete properties significantly. The chemical reaction of cement to form hydrates generates heat which has a great influence on the early age strength and stress development due to differential volume changes in concrete. A high early age heat of hydration can promote early age strength to the detriment of long-term strength and conversely a low early age heat of hydration may give rise to a lower early age strength, but a high long-term strength may occur. Silica fume (SF) generally increases the early heat of hydration and early age strength, fly ash (FA) generally reduces the early heat of hydration and early age strength and the effect of ground granulated blast-furnace slag (GGBS) used in concrete varies with source and composition.

Emphasis is frequently placed on the later age properties of the concrete, measured after acceptable strength has been achieved. When water from the concrete evaporates into the environment, drying shrinkage takes place. Cracking can occur and adversely affect the durability of the concrete. The tensile capacity of concrete is lowest at an early age and therefore the most susceptible to cracking and material faults when stresses are induced by, for instance, drying shrinkage. Drying shrinkage can be prevented by employing proper placing and curing procedures to prevent moisture loss to the environment and to allow the concrete to gain sufficient strength.

Even with proper placing and curing techniques, cracking has been observed soon after casting. This occurrence can be attributed either to volume change caused by thermal gradients resulting from heat released during cement hydration or to autogenous shrinkage. Autogenous shrinkage mostly takes place within the first couple of days after casting and it is defined as a change in volume while no moisture is allowed to leave the material system. Autogenous shrinkage results from the internal chemical reactions of the concrete constituents. In traditional concrete, autogenous shrinkage is deemed negligible compared to, for example, drying shrinkage while in high performance concrete (HPC) autogenous shrinkage can be significant. Autogenous shrinkage is generally increased by SF and mitigated by FA, while the effect of GGBS on

autogenous shrinkage depends on the source and composition. Early age shrinkage is often not tested in practice due to the difficulty in measuring and the lack of standardisation of measuring techniques.

HPC contains high volumes of cementitious material to enable the development of high strength. This high volume of cementitious material in turn results in a high heat of hydration. There may therefore be a relationship between autogenous shrinkage, the thermal processes and strength development.

1.2 RESEARCH OBJECTIVES

The primary objective of this study was to investigate the relationship between autogenous shrinkage, the thermal processes and the strength development of concrete. The influence of binder composition and content on the early age volume change of concrete was studied.

Secondary objectives included:

- To determine the most suitable technique for measuring autogenous shrinkage.
- Finding a suitable reference point in time to start autogenous shrinkage measurements by comparing different methods for obtaining concrete setting times.
- To determine a method to quantify the reactivity of different cementitious materials in concrete mixes.

1.3 SCOPE OF STUDY

In this study the effect of binder composition and content were evaluated for Portland cement, condensed silica fume, fly ash and ground granulated blast-furnace slag. The materials were obtained from the same suppliers throughout this study. It would thus be possible to obtain different results when different materials are used. Aggregate type is known to have a significant effect on concrete properties and only one type of aggregate, namely dolomite, was used in this study. Only fine aggregate was used so that small samples could be tested. The effect of concrete batch size and sample size were not considered in this study.

Thermal effects were investigated while setting time, early age shrinkage and strength development were recorded. Environmental effects (such as temperature and relative humidity) were not part of the study and were kept constant. The thermal influence from the concrete itself was also not considered.

1.4 METHODOLOGY

The following methodology was implemented to investigate the effect of binder content and composition on early age concrete behaviour. A literature study was conducted to study the relationship between admixtures and mix proportions on autogenous shrinkage. The relationship between heat of hydration, admixture additions and mixture proportions were also investigated.

Mortar samples were prepared and the methodology below was followed:

- The hydration processes were studied in different ways to understand the principle mechanisms for each method.
- Two experimental procedures to determine the concrete setting time were selected, modified and compared.
- Two experimental procedures to study the effect of mix proportions on autogenous shrinkage were selected and modified. Materials were prepared, various mixes were tested, and the results were compared
- The heat of hydration and setting times were investigated in the first part of the study. In the second part the autogenous shrinkage of various mixes was investigated and lastly the mechanical properties were measured as well.

1.5 ORGANIZATION OF REPORT

This document consists of the following chapters and appendices:

- Chapter 1 serves as an introduction to the report.
- Chapter 2 contains a technical introduction based on a literature study.
- Chapter 3 describes the experimental procedure and materials used during the study.
- Chapter 4 describes the analysis of the study observations.
- Chapter 5 contains the conclusions and recommendations of the study.
- The list of references follows at the end of the report.
- The appendices contain data obtained and used in this study.

CHAPTER 2: LITERATURE REVIEW

2.1 INTRODUCTION

High performance concrete (HPC) is increasingly being used in structures due to the high strength, improvement in durability and long-term performance. A lower water to binder ratio is employed to improve the performance of concrete and mineral and chemical admixtures are introduced. With a low water to binder ratio, considerable early-age volume changes can occur compromising the durability of HPC. Internal and external restraints in concrete structures results in tensile stresses where structures cannot move freely. Early age cracking occurs when the tensile stresses exceeds the tensile strength of the concrete. Early age volume changes are primarily due to autogenous shrinkage, thermal deformation as well as drying shrinkage and is caused by self-desiccation of capillary porosity, by temperature and moisture gradients between concrete and exterior surroundings, respectively (Aïtcin, 1998). Autogenous shrinkage accounts for the most significant volume change of HPC at early ages, compared to that of thermal deformation and drying shrinkage (Lura, 2003).

Shrinkage of concrete can be divided into two distinct stages: early age and long term. Early age is typically taken as the first day, when concrete is setting and starting to harden. Long term refers to 24 hours and later. Long term shrinkage is usually measured on samples which are demoulded after 24 hours and tested according to standardised shrinkage measurements. Long term shrinkage is typically the only type of shrinkage that is discussed and addressed in literature and considered in structural design (Holt, 2001).

Concrete is also subjected to chemical shrinkage and carbonation reactions which are noted here but fall outside the scope of this study. Figure 2.1 illustrates the types of shrinkage with the corresponding time frame at which each type of shrinkage tends to occur.

2.2 PROPERTIES OF FRESH CONCRETE

Stresses are generated in concrete as water is lost to evaporation or internal reactions. A volume reduction occurs due to the formation of menisci resulting in high internal tensile stresses (Seddik Meddah and Tagnit-Hamou, 2011). At early ages, the concrete has not yet developed a high strength and the shrinkage is more critical. A small stress can induce large strains in the early age

concrete (Holt, 2001). The risk of cracking as a result of early age shrinkage is increased as a result of the relatively low early age strength.

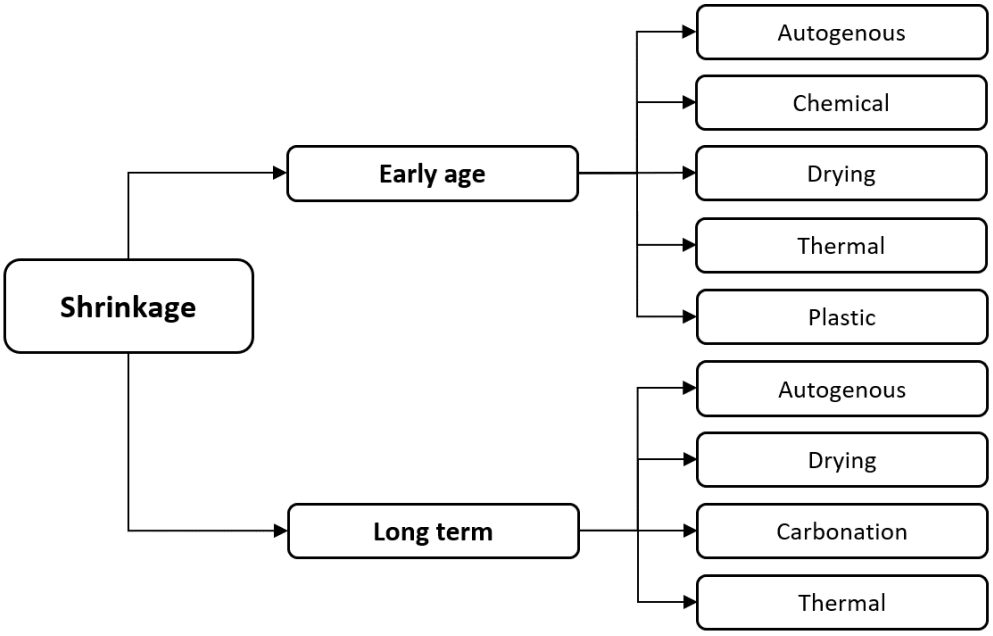

Figure 2.1 Types of shrinkage at early age and long-term stages

2.2.1 Liquid Phase

The concrete is still a liquid immediately after mixing and casting. Any force applied to the mixture will be corrected by a shift in the material. There is no skeletal structure holding the body in place and the concrete has no strength. Bleeding can occur as the heavier particles suspended in the fresh concrete mix move downward with the accompanying movement of water to the surface.

2.2.2 Skeleton formation phase

Strength develops when the cement and additions chemically react to form a complex series of hydrates. The cement particles are fixed into a weak structure surrounded by water-filled space. The spacing between the cement particles increases with water content. The cement particles will continue to hydrate and fill the space between the cement particles with hydrates and pores. The strength of the concrete is highly dependent on the volume of pores. The higher the water-to-cement-ratio, the more pores and the weaker the concrete. Hydration continues to take place for years as long as there is water available for cement hydration (i.e. the concrete is not allowed to

dry out) and there is cement and/or additions available to react (Harrison, 2003). Setting occurs during this phase.

2.2.3 Hardening phase

When the skeleton system is well established the concrete will often have sufficient strength to resist additional stresses during the early ages. The rate of drying shrinkage and autogenous shrinkage will decrease due to the developing stable skeleton. Holt (2001) and Kronlöf et al. (1995) found that the point where concrete can withstand drying shrinkage forces is approximately 2 hours after the initial setting time. When the concrete strength is less than the forces caused by drying then the concrete will crack.

Volume changes will occur for a long time as the concrete is still reacting. A measure of the reactions that has taken place is the degree of hydration. Figure 2.2 illustrates the progression of hydration of a single grain of Portland cement (PC) (Domone and Illston, 2010). Pores, that were not entrapped or entrained at mixing, are created by pockets that were originally filled with mixing water. The capillary pores fill with hydration products over time. The capillary pores become discontinuous after approximately 3 days for a water-to-cement ratio of 0.4 and at a water-to-cement ratio of 0.8 or higher pores will never become discontinuous (ACI, 2014). Figure 2.3 illustrates the pore size distribution and volume of pores for different water-to-cement ratio cement pastes, a lower water-to-cement ratio paste typically yields a lower volume and size of pores than a higher water-to-cement ratio paste.

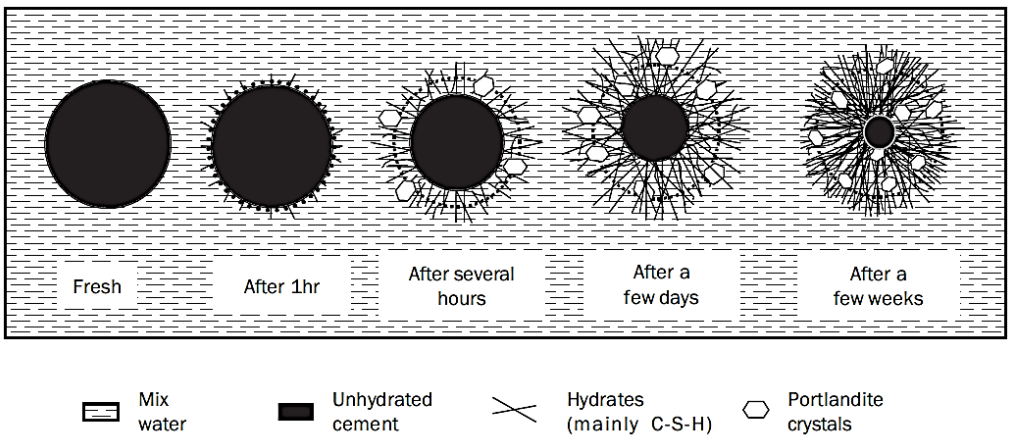

Figure 2.2 Illustration of the hydration of a single grain of Portland cement (Domone and Illston, 2010)

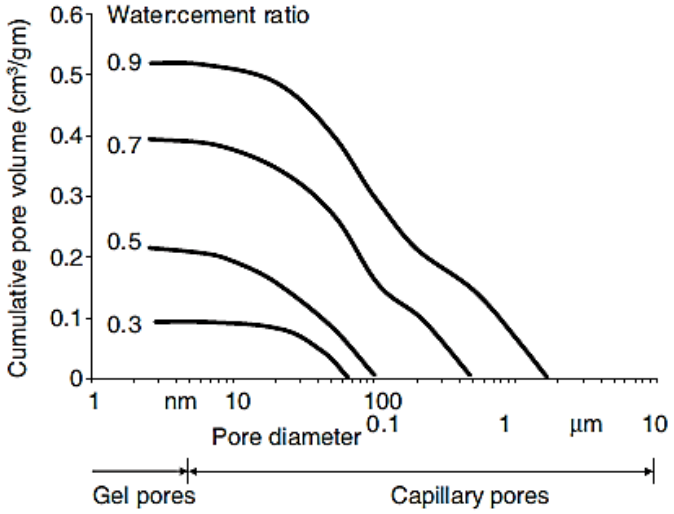

Figure 2.3 Pore size distribution of 28 day old cement paste at different water-to-cement ratios (Domone and Illston, 2010)

When the water-to-cement ratio is equal to 0.4 and all the cement hydrates fully, the hydrates will fill the available space completely. Pastes with a water-to-cement ratio higher than 0.4 will have capillary pores after all the cement has hydrated. Unhydrated cement will be present in pastes with a water-to-cement ratio of less than 0.4 when further hydration is constrained by lack of space (Addis, 1994). Capillary porosity (P_c) and the volume fraction of unhydrateable cement (V_{uc}) with water-to-cement ratio is shown graphically in Figure 2.4. Powers and Brownyard (1947) used their developed model to study the minimum water-to-cement ratio for complete hydration using Cement 15754 and found it to be between 0.42 and 0.44. Later analysis done with CEM I revealed a value of 0.39.

2.2.4 Tensile strain capacity

Early age shrinkage is a concern due to the stresses developing at a critical time when the concrete strain capacity is at a minimum. Many researchers have found that the strain capacity decreases at an early age before increasing again at roughly 10 hours. Nguyen et al. (2017) summarised data from their study and previous major studies in Figure 2.5.

Early age cracks can occur a few hours after casting, the cracks can propagate and seriously decrease the serviceability of the structure due to subsequent shrinkage and loading. Even when early age cracks do not occur, the residual restrained stresses due to early age deformation remain

in the structure which can reduce the tensile capacity of the structure and cause problems with serviceability (Nguyen et al., 2017).

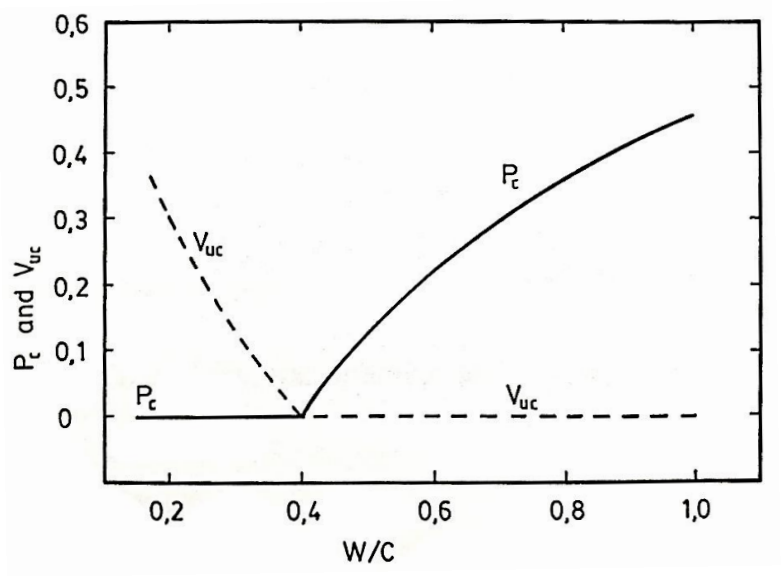

Figure 2.4 Capillary porosity (P_c) and volume of unhydratable cement (V_{uc}) versus water-to-cement ratio (Addis, 1994)

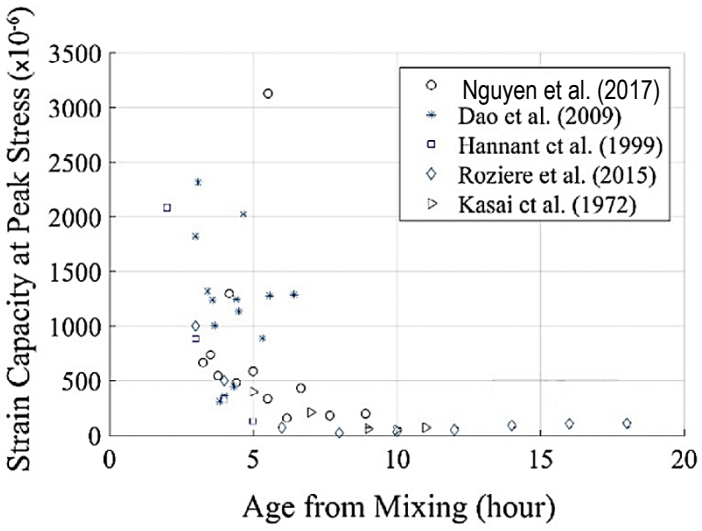

Figure 2.5 Decreasing tensile capacity during early ages (adapted from Nguyen et al., 2017)

2.2.5 Workability

Workability is defined in ASTM C125 (2019) as the property determining the effort required to manipulate a freshly mixed quantity of concrete with minimum loss of homogeneity. The main factor that affects the workability is the water content of the mix. If all mix proportions are fixed

then the workability is governed by the maximum size of the aggregate, the grading, the shape and the texture of the aggregate as well as the cement fineness. If a more workable mix is required with a constant strength concrete, then the water and cement content may be increased while the water to cement ratio remains the same (Mehta and Monteiro, 2006, Domone and Illston, 2010).

2.2.6 Heat of hydration

Cement paste becomes noticeably warm during the early set and hardening period, this is because the hydration process is exothermic. In some cases, the energy released is enough to raise the temperature to 100°C or more in a day if the cement paste is kept in adiabatic conditions i.e. zero heat loss. A more useful indication of the rate of reaction is the measurement of the rate of heat output at a constant temperature (isothermal conditions).

The heat evolution of concrete is strongly influenced by the physical and chemical properties of PC, water-to-cement ratio, mineral and chemical admixtures, concrete mix proportions, curing conditions of the concrete and construction procedures (Schindler and Folliard, 2003, Pan et al., 2008, Mostafa and Brown, 2005, Bentz et al., 2008, Bentz et al., 2009).

A typical rate of heat output curve with time after mixing is shown in Figure 2.6. Immediately after mixing there is a spike in heat output lasting only a few minutes or less (A). A low constant period follows, which is known as the dormant period, when the cement is relatively inactive. The dormant period can last up to a few hours. The hydration rate then starts to increase rapidly and reaches a broad peak (B). The reactions then start to slow down gradually and may have a short spurt in heat output at one or two days giving a further narrow peak (C) (Domone and Illston, 2010).

The shape of the heat evolution plot will be discussed in detail in Section 2.4 as the rate of heat output depends on the mix constituents and proportions of the paste or mortar in the concrete.

2.2.7 Setting time

Setting is usually defined as the onset of rigidity in fresh PC concrete and is usually viewed as the period where the concrete transitions from true fluidity to true rigidity. The setting time of concrete is important because it controls the timing of certain processes like transporting, placing, compacting and finishing. The initial setting time usually corresponds to the time when the concrete can no longer be properly handled and placed. Final set approximates the time when the concrete hardens, and the concrete begins to gain strength. There are two methods used to

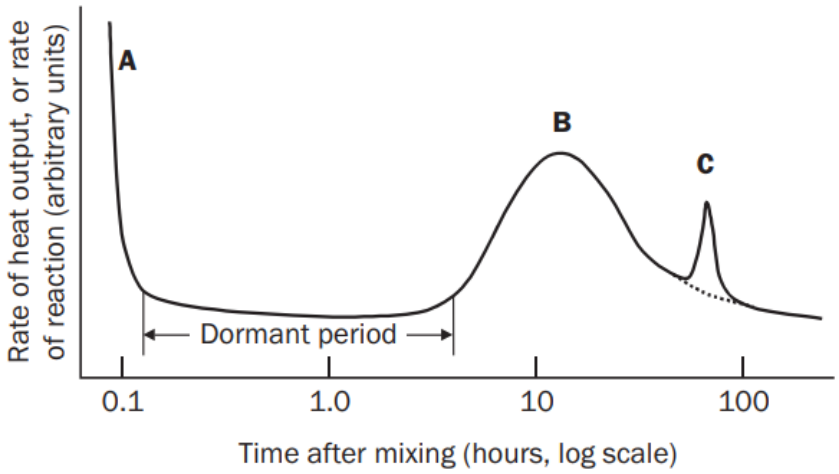

Figure 2.6 Typical rate of heat output of hydrating cement paste at a constant temperature (Domone and Illston, 2010)

determine the setting time. For cement paste the Vicat needle method is used (ASTM C191 (2018), SANS 50196-3 (2006) or EN 196-3 (2016)) and for mortar the penetration resistance test is used (ASTM C403 (1999)). Both cement and mortar test methods give initial and final setting times which are based on arbitrary measurements that do not correspond exactly to any specific change in the concrete properties. The standard tests to determine setting time can also be very time consuming, especially when high volumes of supplemental cementitious materials or admixtures are used. These tests are also user sensitive. Other methods to approximate the setting time has been developed such as calorimetry setting time models (Bobrowicz, 2015, Schindler, 2004, Hu et al., 2014). This new automated setting time measurement approach could provide for a more accurate evaluation of the hydration process and can highlight any compatibility issues (Xu et al., 2010).

The setting time is influenced by the surrounding environment and additions to the concrete. Water-to-cement ratio is one of the most dominant factors affecting cement hydration since the water-to-cement ratio determines the interparticle spacing and how much water is available for each unit volume of cement particle to hydrate. Standard test setting times increases with water-to-cement ratio (Hu et al., 2014). Fly ash (FA), silica fume (SF) and ground granulated blast-furnace slag (GGBS) also increases the setting time of concrete (Dave et al., 2017). High-range-water-reducers (HRWR) or SPs and set retarding admixtures slow down the rate of hydration at early age and extends the setting time (Nocuń-Wczelik and Czapik, 2013, Cheung et al., 2011, Holt and Leivo, 2000). Valtion Teknillinen Tutkimuskeskus (VTT) Technical Research Centre of Finland research data by Holt and Leivo (2000) that explores the setting time with a change in SP

dosage is shown in Table 2.1. The setting time of concrete is highly dependent on the surrounding environment and especially the temperature, as indicated by the VTT research completed by Holt and Leivo (2000) as summarised in Table 2.2.

Table 2.1 Concrete setting times with the addition of melamine-based superplasticiser at a water-to-cement ratio of 0.45 (Holt and Leivo, 2000)

SP Dosage (%)	*Setting time (hr: min)*	
	White cement	*Gray cement*
0	4:10	3:40
0.5	4:20	3:50
1	6:00	4:30
1.5	7:30	5:00

Table 2.2 Influence of curing temperature on concrete final set (Holt and Leivo, 2000)

Temperature (°C)	*Setting time (hr: min)*
5	11 +
20	5:30
30	4:20

2.3 EFFECT OF WATER CONTENT ON HEAT OF HYDRATION

2.3.1 Water-to-binder ratio

Semi-adiabatic calorimetry was carried out by Bentz et al. (2009) to investigate the influence of water-to-cement ratio on the early-age thermal properties of cement pastes and the data is presented in Figure 2.7. The heat capacity of water is much higher than that of cement at 4.18 J/(g·K) and 0.75 J/(g·K) respectively. Consequently, it is expected that a smaller temperature rise will be present when the water-to-cement ratio is increased. Also, the lower amount of cement per unit volume for the higher water-to-cement ratio mixes implies less heat generation within the fixed volume of the semi-adiabatic calorimeter samples.

Figure 2.8 shows the influence of water-to-cement ratio on heat flow and cumulative heat. Early hydration kinetics increased with a decrease in water-to-cement ratio and this is likely due to the higher concentration of alkali ions in the pore solution, promoting the dissolution of the anhydrous phases (Danielson, 1962). The long-term degree of hydration decreased with a lower water-to-cement ratio because less water and space were available for hydrates to grow (Lothenbach et al., 2011). The isothermal calorimetry samples self-desiccated due to chemical shrinkage that occurred during hydration because the samples were sealed, and no external curing water was

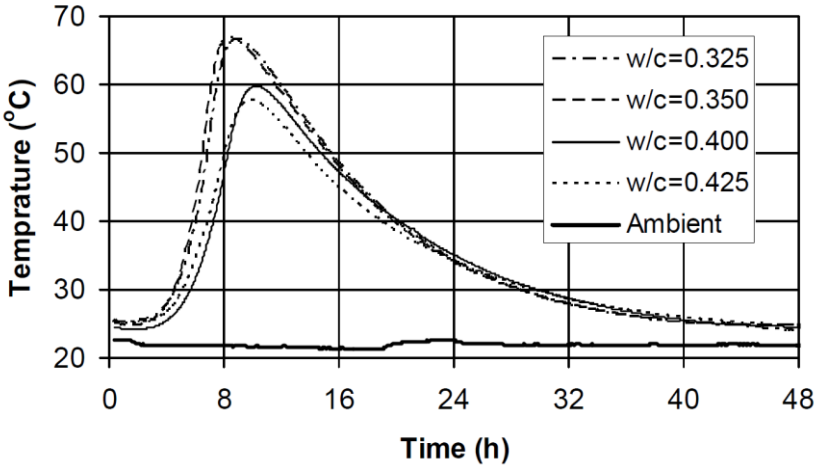

Figure 2.7 Semi-adiabatic temperature rise for four different water-to-cement ratio pastes during the first 48 hours of hydration (Bentz et al., 2009)

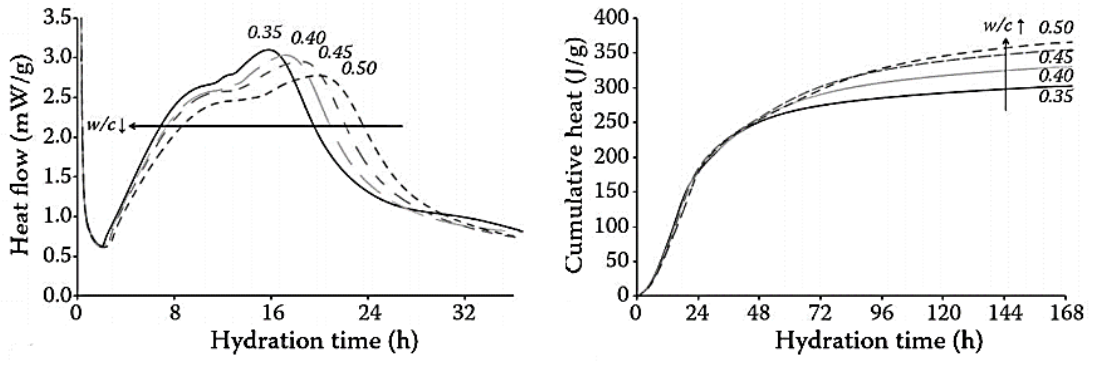

a) *b)*

Figure 2.8 Influence of water-to-cement ratio on the a) heat flow and b) cumulative heat of CEM I 52.5 N (Lura et al., 2017)

available. The on-going hydration rates decreased with time, and the effect was more pronounced in lower water-to-cement samples (Bentz et al., 2009). Results from previous studies are in agreement with the results obtained by Lura et al. (2017) in Figure 2.8 (Pane and Hansen, 2005, Tydlitát et al., 2012, Berodier et al., 2014, Hu et al., 2014, Schöler et al., 2017, De la Varga et al., 2018, Kirby and Biernacki, 2012). Bentz et al. (2009), Lootens and Bentz (2016) and Han et al. (2017) found however, that the heat flow is nearly independent of the water-to-cement ratio, but the cumulative heat followed the same trend as in the previous studies mentioned above. A study done by Quennoz and Scrivener (2013) however reported that the first maximum peak heat flow

increased with an increase in water-to-binder ratio and the time at which this peak occurred was slightly delayed with an increase in water-to-binder ratio.

2.3.2 Chemical admixtures

SPs (also referred to as HRWRs) are used to either permit a high reduction in the water content of a given concrete mix without affecting the consistence or increase the workability without affecting the water content. They are added by percentage of cementitious material weight. They cause a combination of mutual repulsion and steric hinderance between the cement particles (Domone and Illston, 2010).

SPs are efficient at interacting with fine-grained materials such as cement, FA, GGBS and SF resulting in a concrete strength that is higher than expected from the reduction in water-to-cement ratio alone (Neville, 2011).

For any particular binder and SP ratio there is a saturation point. At dosages higher than the saturation point, no further increase in fluidity will occur and segregation, excessive retardation or entrapment of air can take place (Domone and Illston, 2010).

SPs and set retarding admixtures slow down the early hydration process (Łaźniewska-Piekarczyk, 2013, Schindler, 2004, Chaei et al., 2018, Xu et al., 2010, Winnefeld et al., 2007, Kumar et al., 2012, Pan et al., 2008). Figure 2.9 shows the influence of set retarders and SPs on the heat flow of CEM I 42.5R. *R1* and *R2* are phosphate-based set retarders with differing modifiers and *SP1* and *SP2* are polycarboxylate SPs having a chain-like structure and *SP1* has a much lower molecular weight resulting from a lower amount of side chains. SPs or set retarders prolonged the induction period and the main peak was reduced. This effect was stronger at a lower water-to-cement ratio in the presence of set retarders. The delay was more prominent with set retarders. The total heat evolved was not influenced significantly by SPs compared to the plain cement sample but set retarders did however hamper the hydration process and resulted in a lower heat evolved (Nocuń-Wczelik and Czapik, 2013).

2.4 EFFECT OF CEMENT COMPOSITION ON HEAT OF HYDRATION

When discussing high strength concrete, it becomes important to define what is meant by high strength. The compressive strength required for a concrete to be defined as high strength has been revised upwards over the past 20 years and will likely continue to rise in the future (Price, 2003). In 2001 concrete was classified as high strength if the compressive cube strength was 40 MPa or

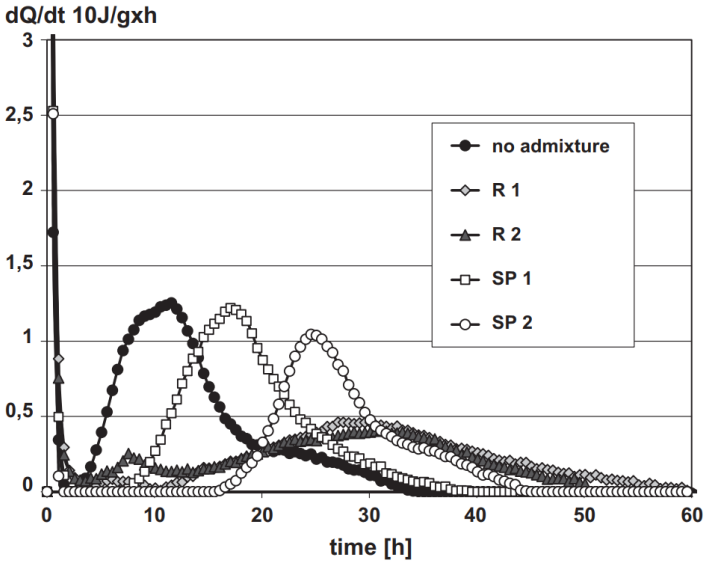

Figure 2.9 Heat flow curves of Portland cement CEM I 42.5R, hydrated in the presence of admixtures added as 2% by mass of cement at water-to-cement ratio 0.3 (Nocuń-Wczelik and Czapik, 2013)

more (Holt, 2001). More recently high strength concrete has been defined as concrete with compressive cube strength greater than 80 MPa (Domone and Illston, 2010). Another proposed definition is that high strength concrete is a concrete with a higher compressive cube strength than that covered by current codes and standards. High strength concrete makes it possible to build smaller sections which in turn will result in more usable space and possible savings in material costs. High strength concrete also has the benefit of being less permeable due to the reduced water-to-cement ratio, this in turn results in lower maintenance cost and a more durable concrete.

The very low water-to-cement ratio values for high strength concrete causes impractically low workability and it is impossible to place concrete using conventional methods, thus SPs must be included in the concrete mix design. Low water-to-cement ratios are not enough to produce high strength concrete and therefore mineralogical additions such as FA, SF and/or GGBS are used (Domone and Illston, 2010).

2.4.1 Cement

Cement clinker consists of two silicate phases, alite (impure C_3S) and belite (C_2S) and two aluminate phases, C_3A and C_4AF. Clinker is ground and mixed with gypsum (calcium sulphate) to produce PC.

Calcium sulphate, clinker and water react and form hydrates resulting in hardening and setting. Calcium silicate hydrate (C-S-H) and Portlandite or calcium hydroxide (CH) form due to the hydration of the silicates and ettringite or trisulfoaluminoferite hydrate (AFt) and monosulfoaluminoferite hydrate (AFm) form due to the hydration of the aluminates. The typical ranges of oxide present in PC is shown in Table 2.3.

Table 2.3 Typical chemical composition for Portland cement (Domone & Illston, 2010)

Oxide	*Range*
CaO	60-67
SiO_2	17-25
Al_2O_3	3-8
Fe_2O_3	0.5-6
$Na_2O + K_2O$	0.2-1.3
MgO	0.1-4
Free CaO	0-2
SO_3	1-3

Figure 2.10 illustrates a typical isothermal calorimetry heat flow curve for the hydration of PC. The fast dissolution of anhydrous phases occurs in stage (0). Calcium sulphate controls the dissolution of C_3A and prevents flash setting. At stage (I) there is a decline in reaction rate and a period of low chemical activity thereafter (II), this is also known as the induction period. A main hydration peak occurs at the end of stage (III) in the acceleratory period resulting from the precipitation of C-S-H and CH due to the hydration of C_3S and C_2S. In stage (IV) there is another deceleration period where a second peak is observed which corresponds to the formation of ettringite when all the sulphate ions are consumed or due to renewed C_3A dissolution. The last stage (V) is a low reactivity period where a third peak is observed corresponding to the formation of AFm, a result of the reaction of ettringite with C_3A when the calcium sulphate is fully consumed (Bazzoni, 2014).

The reaction of alite to portlandite and C-S-H contributes the most to the heat of hydration observed during the early reaction of PC. The other clinker phases do not contribute significantly to the heat release within the first 12 hours (Schöler et al., 2017).

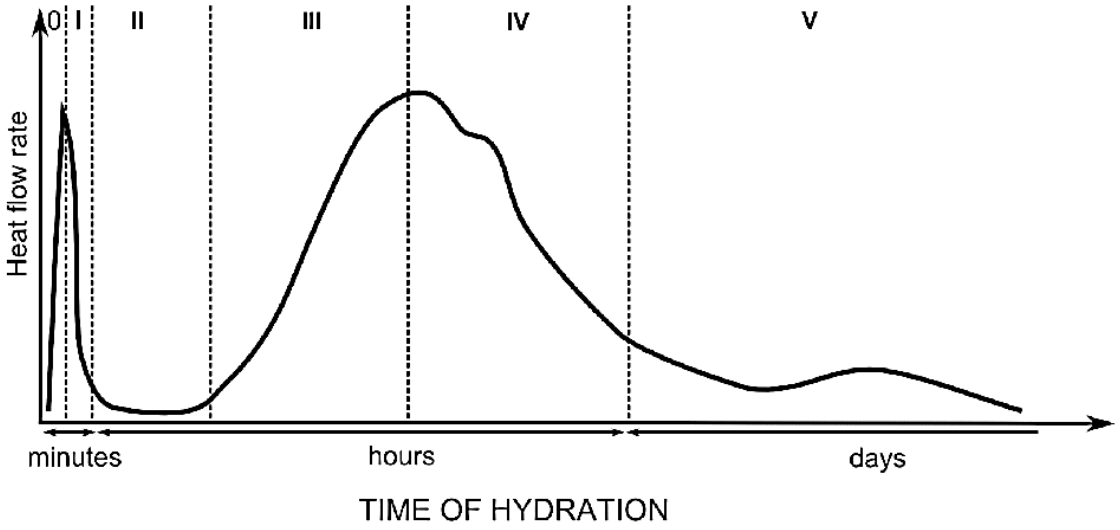

Figure 2.10 Typical calorimetry heat flow curve for the hydration of Portland cement (Bazzoni, 2014)

Amongst others, Gutteridge and Dalziel (1990b) realised that blending even inert materials with cement have a significant influence on the hydration of clinker phases. This is called the filler effect. The reactivity of the SCMs has frequently been confused with this filler effect. The reactions of the SCMs are usually negligible during the first day or so due to the dependence of SCM reactions on the alkalinity of the pore solution, which builds up over the first few days as the cement hydrates. Thus, the filler effect dominates the changes in hydration kinetics. This is particularly the case with SF even though ^{29}Si NMR indicates that almost no reaction of SF occurred at this stage (Hjorth et al., 1988, Justnes, 1988, Lothenbach et al., 2011).

Two main principle mechanisms can be used to explain the filler effect:

1. The filler does not produce hydrates at early ages, the effective water to clinker ratio is higher and there is more space for the hydration products of the clinker phases.
2. The larger surface area provided by the SCMs acts as nucleation sites for the hydration products of the clinker phases to form.

Fernandez Lopez (2009) studied the filler effect. Figure 2.11 show the heat evolution curves for a blend with quartz filler compared to a reference cement at a water-to-cement ratio of 0.4. The quartz gives more space for the hydration products of clinker to form leading to an increase in the induction period. Quartz does not react significantly, there is almost no change in the slope of the heat evolution curve during the acceleration period, but the acceleration period is extended, and the maximum occurs later than the 100% PC curve.

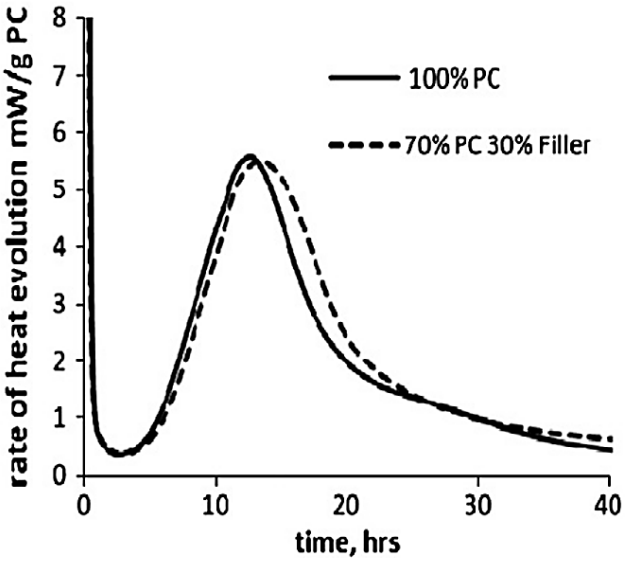

Figure 2.11 Heat flow evolution curves of 100% PC compared to 70% PC with 30% fine quartz filler (Fernandez Lopez, 2009)

2.4.2 Silica fume

SF, also known as microsilica is very fine noncrystalline silica particles condensed from the waste gasses given off in the production of elemental silicon or alloys containing silicon. The particle size range of SF is between 0.03-0.3 μm with a spherical shape. The specific surface area is typically 20 000 m^2/kg with a relative particle density of 2.2 (Domone and Illston, 2010). The typical composition of SF is given in Table 2.4.

Table 2.4 Typical chemical composition ranges of additions (Domone & Illston, 2010)

	FA			
Addition	*Low lime*	*High lime*	*GGBS*	*SF*
Oxides				
SiO_2	44-58	27-52	30-37	94-98
CaO	1.5-6	8-40	34-45	<1
Al_2O_3	20-38	9-25	9-17	<1
Fe_2O_3	4-18	4-9	0.2-2	<1
MgO	0.5-2	2-8	4-13	<1

SF increases the water demand of concrete therefore it is often necessary to include SP into the mix design or reduce the sand content. Due to the high surface area of SF bleeding is reduced if SF is added to the concrete mix. As the SF content is increased the concrete becomes sticky and

more cohesive. The increased cohesiveness leads to reduced segregation and bleed water pockets forming underneath reinforcing bars and coarse aggregate which in turn benefits the hardened structure. Some bleed water however is required to inhibit plastic shrinkage cracking (Mazloom et al., 2004, Sellevold, 1987).

A pozzolanic reaction takes place between the amorphous silica in CSF and calcium hydroxide produced by the hydration of PC. Thus, the CSF can only be activated after the cement has started reacting. CSF also contributes to the hydration of PC due to the extreme fineness of the CSF particles which provide nucleation sites for calcium hydroxide. Early age strength development takes place due to this. CSF dissolves in a saturated solution of calcium hydroxide within a few minutes. Calcium silicate hydrate is formed on the surface of the CSF particles as soon as enough PC has hydrated to result in saturation of the pore water with calcium hydroxide. This reaction initially proceeds at a high rate, but subsequent reaction is very slow (Neville, 2011).

As the calcium silicate hydrates are formed during the reaction of CSF, the voids and pores within the concrete are filled with crystals to bridge the gap between the cement grains and aggregate particles. This physical filling effect of the matrix provides homogenous and dense concrete with improved strength and low permeability. The relatively porous transition zone that usually surrounds the aggregate grains in conventional concrete is virtually absent in high-quality CSF concrete (Newman and Choo, 2003).

Dry curing conditions influence CSF concrete more than normal PC concrete with a higher reduction in strength as the water to cementitious material ratio increases (Atiş et al., 2005). As a consequence of the high reactivity of CSF the mix water is used up rapidly. Water, if available, cannot easily penetrate the dense microstructure of the hydrated cement paste to reach the remnants of unhydrated PC or CSF particles. Self-desiccation takes place and strength development ceases much earlier than compared with PC alone (Neville, 2011).

Kocaba (2009) studied the filler effect and results from this is shown in Figure 2.12a. When comparing the heat flow evolution of 100% PC to 90% PC with 10% CSF it is clear that there is another effect at play than in Figure 2.11. The maximum heat is increased and the slope of the heat evolution curve of the blended mix is steeper than the 100% PC curve. This effect on the heat evolution curve is consistent with an increase in the number of nucleation sites that is shown in Figure 2.12b. The water-to-cement ratio used in this study was however not disclosed.

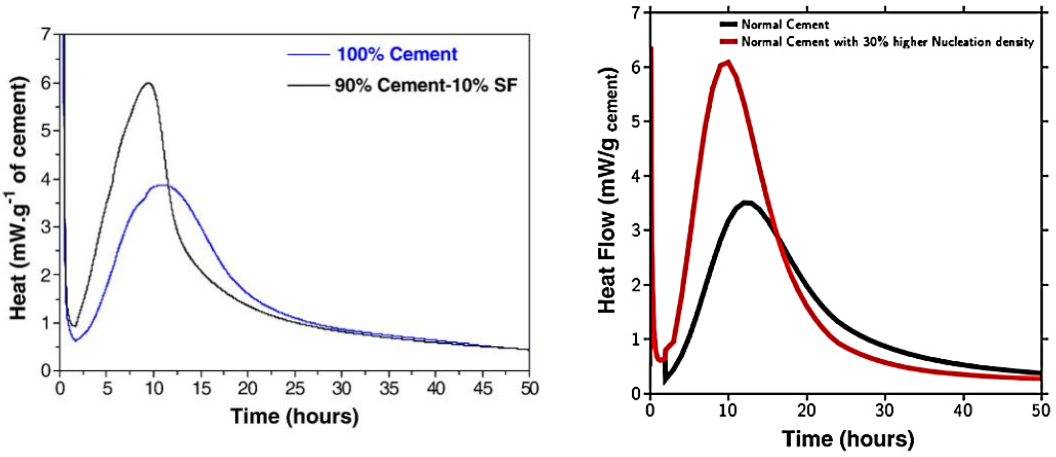

a) *b)*

Figure 2.12 a) Heat flow evolution curve of 100% PC compared to 90% PC with 10% SF and b) simulation results of increasing the number of nucleation sites by 30% (Lothenbach et al., 2011)

It appears that nucleation effects are more significant in the case of the hydration products of the aluminate phase which is normally an indication of the peak in stage (IV) in Figure 2.10. Figure 2.13 demonstrates the effect of fillers on the hydration of cement alone. The fillers are not expected to react. The two finer fillers have a slight effect on the silicate reaction and a significant effect on the aluminate reaction as described above. The aluminate peak is increased and narrowed (Lothenbach et al., 2011).

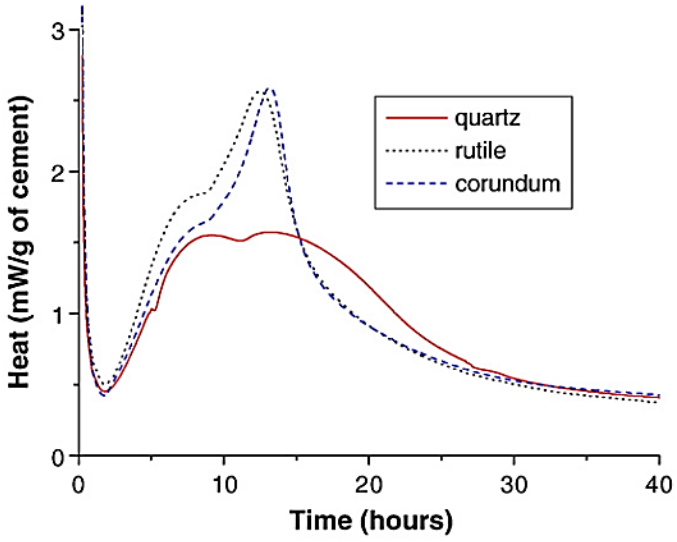

Figure 2.13 Heat evolution curves for PC blended with quartz, rutile and corundum. Fineness: quartz 0.76 m^2/g; rutile 9.1 m^2/g; corundum 5.4 m^2/g (Lothenbach et al., 2011)

In a study by Rossen et al. (2015) PC was replaced by different percentages of SF at a water-to-binder ratio of 0.4 to obtain the heat evolution curves in Figure 2.14. The reaction of C_3S (peak at the end of stage (III) in Figure 2.10) was accelerated by the presence of CSF. The reaction of C_3A (stage (IV) peak in Figure 2.10) occurs earlier and is improved due to the adsorption of sulfate on C-S-H. An earlier study by Rahhal et al. (2007) is in agreement with these trends.

Results from a study by Pane and Hansen (2005) is shown in Figure 2.15. Replacing 25% of PC with CSF produced a higher cumulative heat than the PC paste at a water-to-binder ratio of 0.35 but that was not the case with a water-to-binder ratio of 0.45. Kadri et al. (2010) found that CSF did however produce a higher cumulative heat than the reference PC system at water-to-binder ratio of 0.45 and 10% replacement with CSF.

Kadri et al. (2009) found that the maximum heat released in a semi-adiabatic calorimeter, however, decreased with an increase in CSF replacement. The peak also occurred earlier when CSF was added.

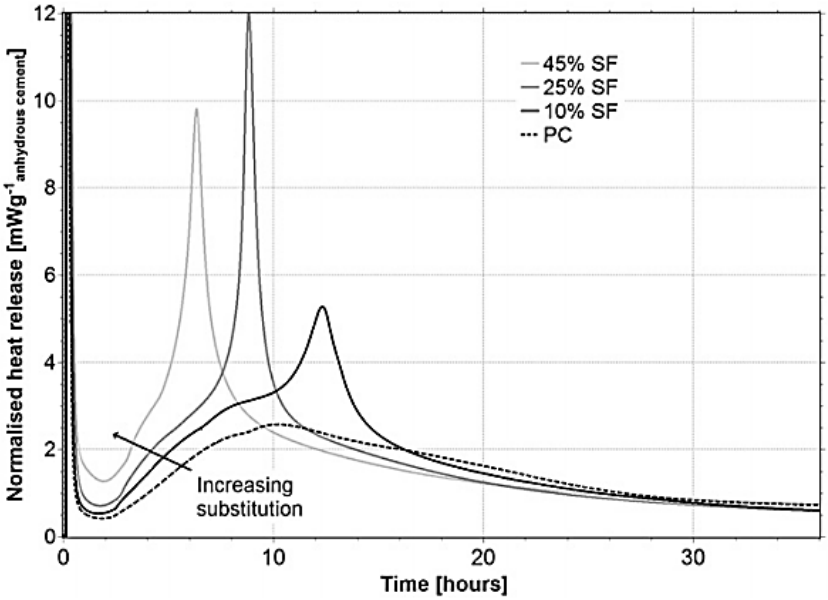

Figure 2.14 Heat evolution curves for different replacement percentages of PC with SF normalised by the anhydrous cement content (Rossen et al., 2015)

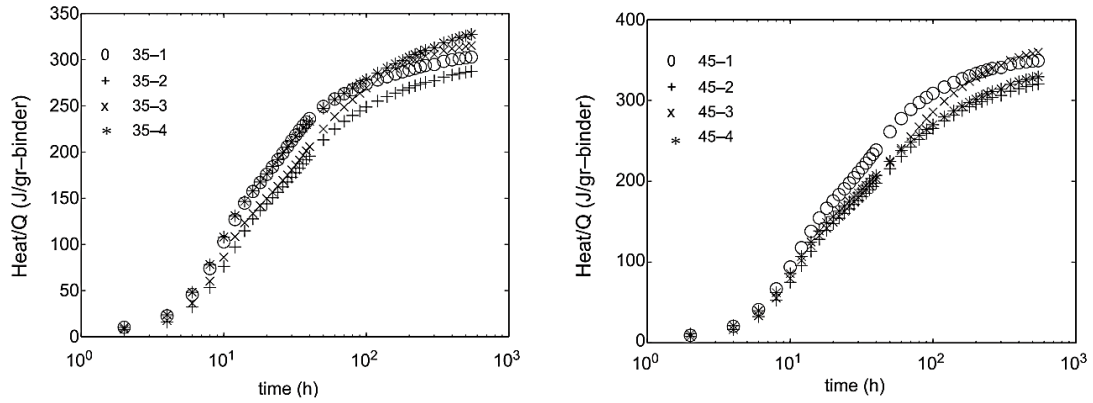

a) *b)*

Figure 2.15 Cumulative heat curves for mixes with the replacement of PC (line #1) with 25% FA (line #2), 25% GGBF (line #3) and 10% SF (line #4) at a water-to-binder ratio of a) 0.35 and b) 0.45 (Pane and Hansen, 2005)

2.4.3 Fly Ash

FA or pulverised fuel ash (PFA) is a by-product from the combustion of pulverised coal. FA varies with the change of the coal supply and the power station demands; this can be a significant problem. Not all FA is suitable for use in concrete due to this variability. The particle size range of FA is between 1-80 μm with a spherical shape. The specific surface area is typically 350 m^2/kg with a relative particle density of 2.3 (Domone and Illston, 2010). The typical composition of FA is given in Table 2.4 with a low lime FA containing between 1.5-6% CaO and a high lime FA containing between 8-40% CaO.

FA limits the amount of early heat of hydration, increases fluidity and suppresses alkali-aggregate reactions but concretes containing FA tends to be vulnerable to carbonation (Sakai et al., 2005). FA is less reactive than cement, which can cause lower strengths at early ages and extended setting time issues. This can be counteracted by reducing the water-to-cement ratio (De la Varga et al., 2018).

The hydration of FA particles can take up to a week to initiate and FA acts as an inert filler before this time. A concrete where cement is replaced with FA is initially more permeable than one without replacement and becomes denser with time (Fraay et al., 1989). FA reacts with calcium hydroxide and alkali in concrete to produce calcium silicate hydrate (C-S-H). Cement-FA blends containing a high volume of FA and a lower water-to-cement ratio displays the dilution or filler effect much more significantly and the hydration degree of cement is notably improved (Wang, 2014).

Chaei et al. (2018) reported a 22% decrease in peak heat flow value with the replacement with 20% FA, a 39% decrease with the replacement of 40% and a 51% decrease with the replacement of 50% FA. The heat evolution curves can be seen in Figure 2.16. FA replacement significantly affects the early age hydration kinetics but does not have an effect after more than about 3 days. Similar results were found in previous studies (Bentz, 2014, Han et al., 2017, Diaz-Loya et al., 2017).

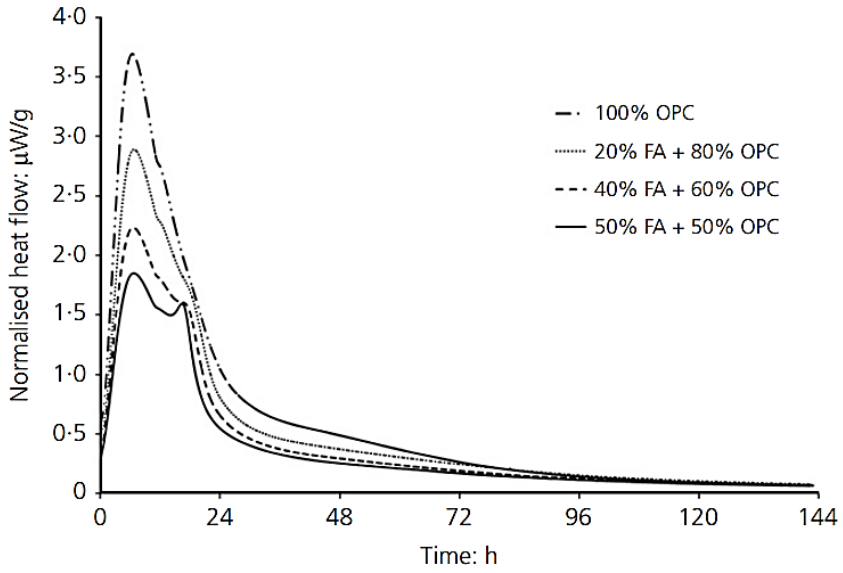

Figure 2.16 Heat evolution curves for pastes with different levels of low lime FA (Chaei et al., 2018)

Xu et al. (2010) reported a "shift" to the right accompanied by a decrease in peak heat flow evolution when the amount of FA was increased by 50% compared to the reference PC and FA blend mix and a "shift" to the left accompanied by an increase in peak heat flow compared to the reference. A high lime FA was used in this study, but similar results were stated by Deschner et al. (2012) and Han et al. (2016) using a low lime FA. De Weerdt et al. (2011), however, found that the heat flow peak increased with 35% replacement of low lime FA and the peak "shifted" right.

The cumulative heat in Figure 2.15 with 25% low lime FA replacement was less than that of the PC system for a water-to-binder ratio of both 0.35 and 0.45 (Pane and Hansen, 2005). Contrary results have been published by De la Varga et al. (2018) where a higher cumulative heat was reported with 60% and 80% high lime FA replacement compared to the reference system at a water-to-cement ratio of 0.3 and the heat flow peak "shifted" right with regards to the PC system, but no significant increase or decrease in heat flow maximum was found. A study by Chen and Poon (2017) found that replacement with 5-20% FA (low lime) had a negligible effect on the peak

heat flow compared to the reference PC system. Berodier et al. (2014) found an increase in heat flow when using a low lime FA at 40% replacement. The difference in chemical composition and particle size distribution of FA used by different researchers could explain the difference in the trends observed.

2.4.4 Ground granulated blast-furnace slag

GGBS is obtained from the production of iron where two products are formed, molten iron that collects in the bottom of the furnace and liquid iron blast-furnace slag floating on the pool of molten iron. Blast-furnace slag consists of silicates and aluminosilicates of calcium and of other bases that is then rapidly chilled and subsequently ground to a similar fineness than PC to form the glassy granular material GGBS. The chemical composition does not vary significantly, there can be some differences in the chemical content of MgO and Al_2O_3, but this does not dramatically change the hydraulic properties of the GGBS when used as a supplementary cementitious material (Aïtcin, 1998). The particle size range of GGBS is between 3-100 μm with an irregular shape. The specific surface area is typically 400 m^2/kg with a relative particle density of 2.9 (Domone and Illston, 2010, ACI, 2014). The typical composition of GGBS is given in Table 2.4.

When GGBS is mixed with water, initial hydration is slower than that of PC. PC, lime or alkali salts are therefore used to increase the reaction rate. Hydration of GGBS in the presence of PC depends largely upon breakdown and dissolution of the glassy slag structure by hydroxyl ions released during the hydration of the PC (ACI, 2014).

Results from a study by Chaei et al. (2018) are shown in Figure 2.17. This illustrates how an increase in GGBS replacement proportionally decreased the peak heat evolution. Replacement with 20% GGBS decreased the peak heat flow by about 19%, replacement with 40% and 50% GGBS reduced the peak heat flow by 34% and 43% respectively. Up until about hour 4, all the hydration curves follow the same linear path indicating that the rate of hydration is consistent for each replacement level. Similar results have been found by Darquennes et al. (2011), Boháč et al. (2014) and Han et al. (2017).

The cumulative heat of the paste containing 25% GGBS replacement was lower than the PC paste at an earlier age but later on surpassed the cumulative heat of the PC paste as indicated in Figure 2.15, and this may be attributed to the slag reaction (Pane and Hansen, 2005). Han et al. (2017) found that the cumulative heat of paste containing 30% GGBS replacement was almost the same as the cumulative heat from the PC paste but slightly less.

Similar effects on the aluminate peak have been reported for PC slag blends than for PC-CSF blends and several researchers have attributed the more significant peak to the early reaction of slag (Lothenbach et al., 2011).

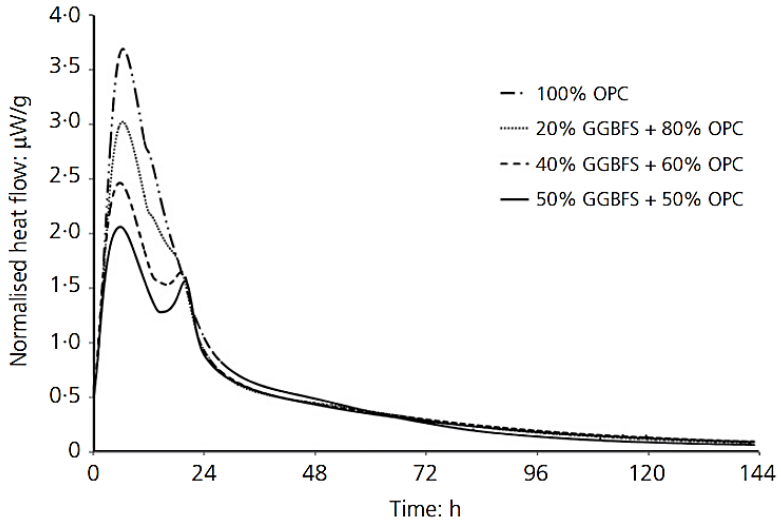

Figure 2.17 Heat flow curves for PC pastes with different replacement levels of GGBS (Chaei et al., 2018)

2.4.5 Blended cements

Blended cements consist of ordinary PC with one or more mineral admixtures such as FA, CSF and/or GGBS. Blended cements have the benefit of reducing carbon dioxide emissions and improving the performance of concrete as well as reducing the cost (Hemalatha and Ramaswamy, 2017, Han et al., 2017, De la Varga et al., 2018). The combination of SF and FA with ordinary PC results in several preferable synergistic effects. FA increases the long-term strength development of CSF concrete, FA offsets the increased water demand of CSF and the relative low cost of FA compensates for the increased cost of CSF. CSF also compensates for the relatively low early age strength of FA concretes (Thomas et al., 1999).

2.5 THERMAL DEFORMATION

When concrete undergoes temperature changes, thermal dilation takes place, also known as thermal expansion, which occurs when there is a temperature rise. Movements can occur due to heating or cooling at any age of the concrete. With a rise in temperature, the concrete will expand and shrink again when cooling takes place. When the rate of temperature change is severe or when a temperature gradient exists in the concrete cross-section, thermal movement causes internal stresses and strains (Holt, 2001).

The importance of thermal movement depends on the structure and on the degree of exposure. The reaction of PC is exothermic and produces large quantities of heat. In small structures the heat dissipates relatively quickly and does not adversely affect the structure. Conversely when casting large concrete masses this becomes critical as a temperature rise of 45°C or more can take place. Concrete is a relatively good insulating material, most of the heat produced accumulates in the concrete. At the surface the heat dissipates faster due to the cooler ambient temperature. A temperature gradient is then present. The hotter inner portion of the concrete tends to expand more than the outer cooler layer of the concrete as depicted in Figure 2.18. Concrete is brittle and elastic in nature and will as a result develop stresses due to the differential expansion. Tensile stresses can develop when the temperature differential between the inner and outer strata is too great and cracking may then occur.

For normal applications, the three major factors that influence the thermal movement of concrete are, the type of aggregate, the volume concentration of aggregate in the mix and the moisture content of the concrete. The cement type, age and strength of the concrete and the curing have far less of an effect.

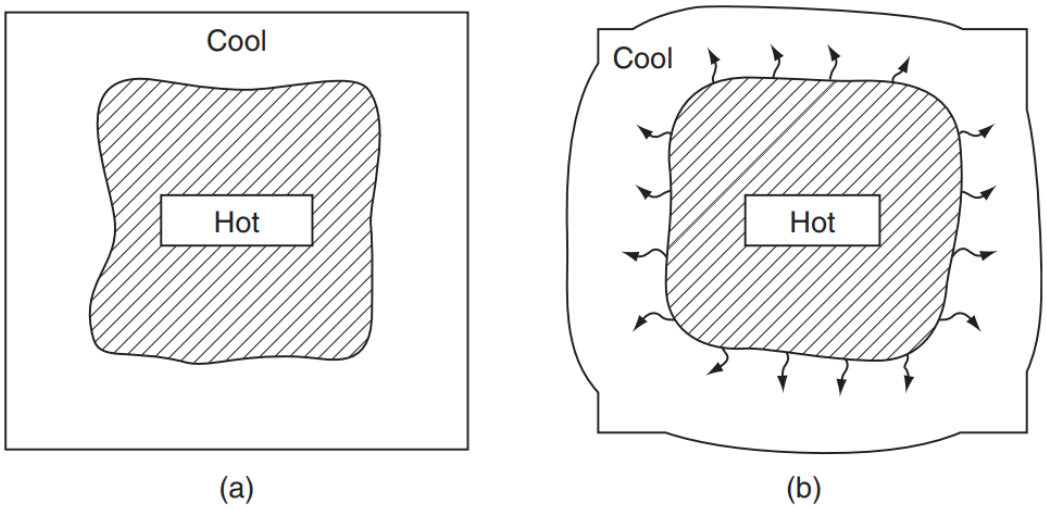

Figure 2.18 Typical temperature development in mass concrete before expansion (a) and after expansion (b) (ICE, 2009)

Concrete that is very dry or saturated has a lower thermal expansion coefficient than a partially dry concrete. The thermal expansion coefficient of stone used in concrete is much lower than that of cement paste, and the thermal expansion coefficient of concrete is thus much lower than that of cement paste. Since concrete usually contains 70-80% stone by volume, there is a considerable

reduction in sensitivity to humidity observed in concrete when compared to cement paste. Normal concrete is then usually assumed to have a constant coefficient of thermal expansion regardless of the humidity. These effects are shown in Figure 2.19. These values are applicable between temperatures of about 0 to 60°C. Internal microcracking can occur at higher temperatures due to the difference in the thermal expansion coefficients of the cement paste and the aggregate and non-linear behaviour will occur (Domone and Illston, 2010).

After casting, the thermal expansion coefficient changes as the concrete inner structure changes and gains strength. Research done by Hedlund (1996) and results obtained by Weigler and Alexanderson (Byfors, 1980) is shown in Figure 2.20. The thermal expansion coefficient has a higher value in the first few hours which then drops significantly and stabilises around 12 με/°C after 24 hours. The thermal expansion coefficient of water at 20°C is 207 με/°C.

Thermal movement at later ages is primarily due to temperature fluctuations in the environment. These changes are dependant to some extent on the amount of free water present in the concrete. Water expands during ice formation when it freezes. If the structure is restrained against movement then there may be no space for the volume change to take place, cracking may then occur (Holt, 2001). The typical values for the coefficient of thermal expansion for mature concrete is between 6 and 12 με/°C according to Mehta and Monteiro (2006) and between 6.8 and 11.9 με/°C according to the ICE (2009). Research done by Cusson and Hoogeveen (2007) shows that the coefficient of thermal expansion of high strength concrete reaches a minimum one day after setting and then slightly increases to stabilise around 10.5 με/°C.

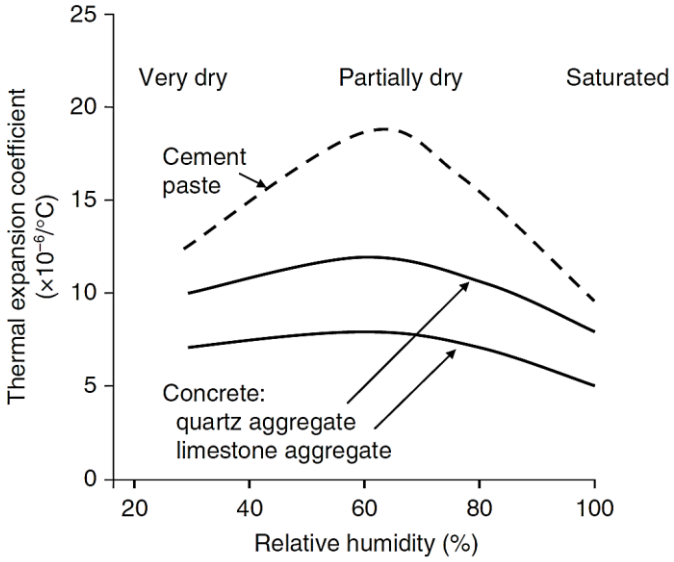

Figure 2.19 The effect of humidity on the thermal expansion coefficient of cement paste and concrete (Domone and Illston, 2010)

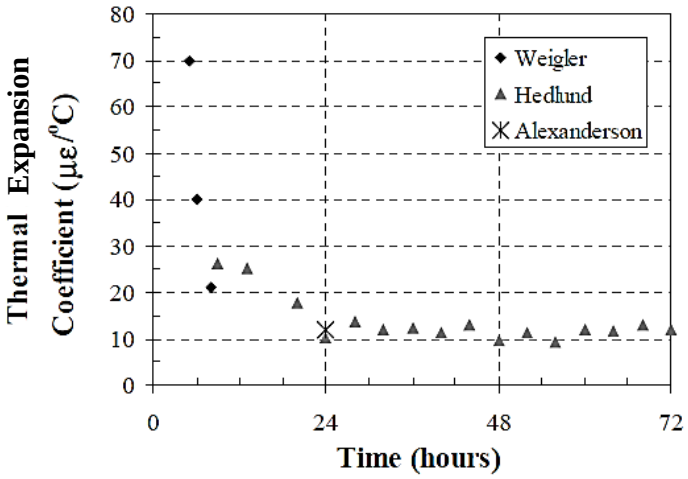

Figure 2.20 Early age thermal expansions coefficients for concrete(Hedlund, 1996, Byfors, 1980)

2.6 PROPERTIES OF HARDENED CONCRETE

Hardened properties of concrete include not only stiffness, compressive strength and tensile strength, but also volume changes over time, such as shrinkage and creep.

Loading causes concrete to deform and, if the load is high enough, failure will occur. All loading on a material can be considered as one or more of three basic types – tension, compression and shear. The mechanical properties of concrete depend on the mix proportions and constituents and the member dimensions.

Typical stress-strain relationship for cement paste, aggregate and concrete is shown in Figure 2.21. Both aggregate and cement paste has a linear elastic relationship, but concrete does not, this implies that the properties of complex composite materials does not necessarily equal the sum of the properties of their components (Mehta and Monteiro, 2006).

Water-to-cement ratio influences the strength and elastic modulus of concrete, the effect can be seen in Figure 2.22. Generally, with an increase in water-to-cement ratio, the compressive strength and modulus of elasticity will decrease.

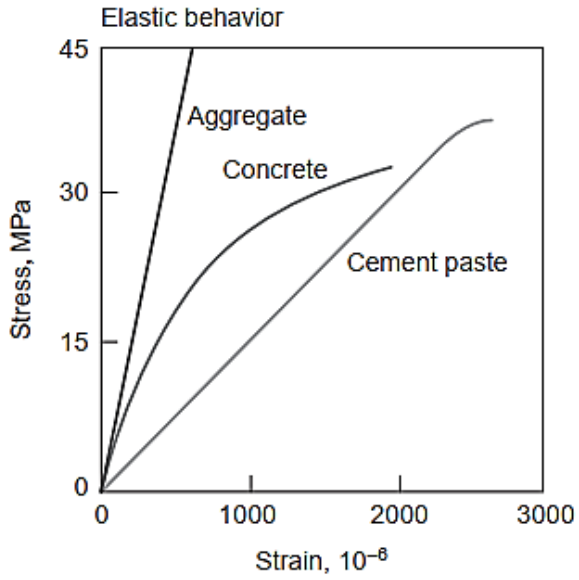

Figure 2.21 Typical stress-strain behaviours of cement paste, aggregate and concrete (Mehta and Monteiro, 2006)

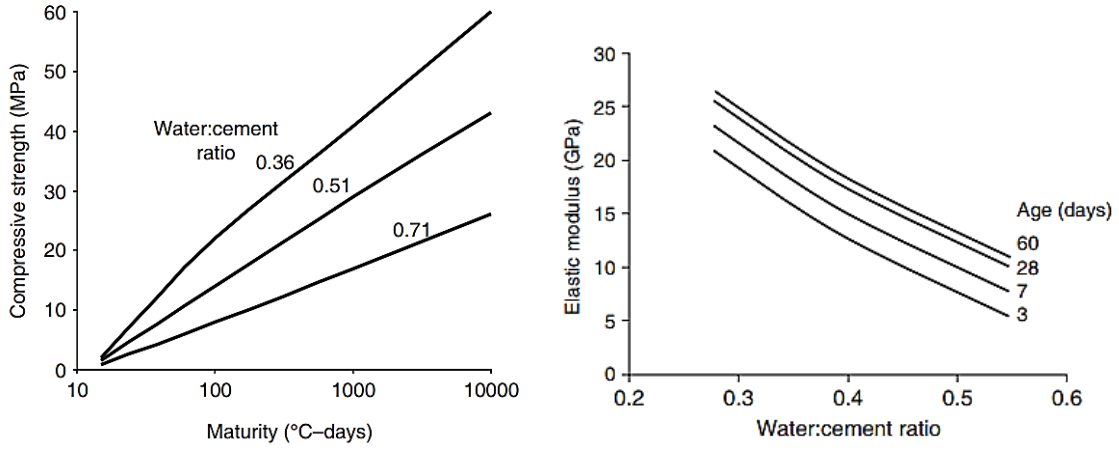

a) *b)*

Figure 2.22 The effect of water-to-cement ratio on a) compressive strength and b) elastic modulus of concrete (Domone and Illston, 2010)

The strength of concrete is governed by porosity and this depends on water-to-cement ratio and degree of hydration. Abrams (1918) demonstrated an inverse relationship of water-to-cement ratio with concrete strength which is now known as Abrams law given in Equation 2.1:

$$f_c = \frac{k_1}{k_2^{w/c}} \qquad \text{(eq. 2.1)}$$

where,

f_c – concrete strength (MPa)

k_1, k_2 – empirical constants (unitless)

w – water content (kg/m^3)

c – cement content (kg/m^3)

The constants k_1 and k_2 are dependent on concrete age, type of materials, porosity, test method and, to a limited extent, aggregate size and type (Domone and Illston, 2010).

Nichols (1982) confirmed that for any given water-to-cement ratio there is an optimum maximum size of aggregate, the effect of aggregate size on concrete strength with a fixed cement content is shown in Figure 2.23. The optimum maximum size of aggregate appears to increase with a decrease in cement content.

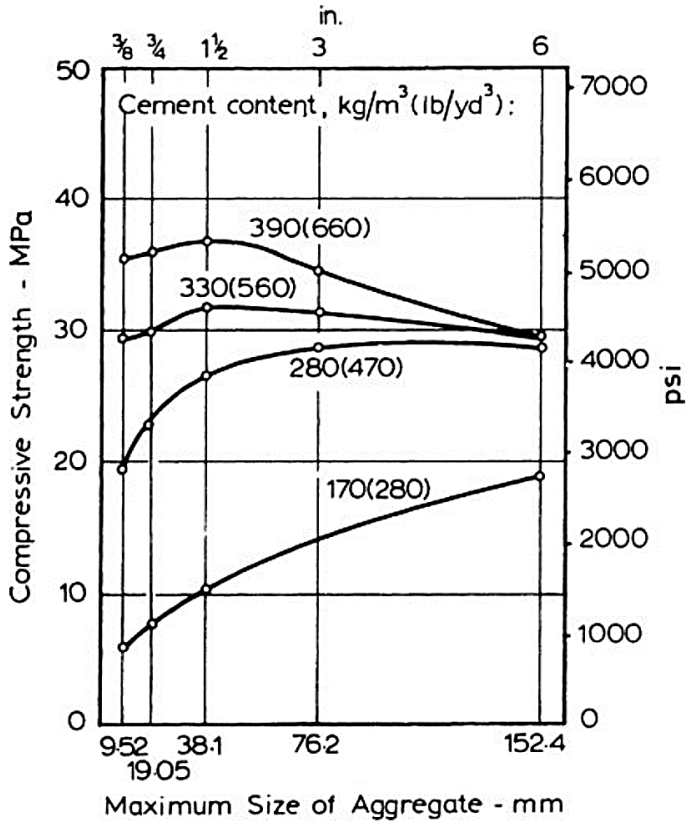

Figure 2.23 Influence of maximum size of aggregate on the 28-day compressive strength of concretes of differing richness (Higginson et al., 1963)

SCMs are used to enhance concrete properties and cement can be replaced in varying amounts depending on the type of SCM. Domone and Illston (2010) suggests maximum effective PC replacement levels of 90% for high-lime FA and GGBS, 40% for low-lime FA and metakaolin and 20% for CSF. They went on to explain that at higher replacement levels there is insufficient PC to produce the required quantities of calcium hydroxide needed to complete the secondary reactions of the SCMs which may lead to low early age concrete strengths.

When SCMs are used, an efficiency factor may be calculated to establish the relative performance of the particular SCM in relation to PC. The cementing efficiency (k) is defined as the number of parts of cement in a concrete mixture that can be replaced to one part of SCM without changing the concrete property under investigation, which is typically strength (Smith, 1967, Wong and Razak, 2003, Khan et al., 2018). Smith (1967) was one of the first to propose this concept, to rationalise the approach for the mixture proportioning of FA concretes, in the form of model given in Equation 2.2:

$$\left(\frac{w}{c}\right)_s = \frac{w}{c}\left(\frac{1}{\left(1+\frac{kF}{c}\right)}\right) \qquad \text{(eq. 2.2)}$$

where,

$\left(\frac{w}{c}\right)_s$ – effective water-to-cement ratio for PC concrete with equivalent strength

c – cement content (kg/m^3)

k – cementing efficiency factor (unitless)

F – FA content in concrete with equal strength (kg/m^3)

w – water content (kg/m^3)

The k-value varies over a wide range depending on type and content of SCM, incorporation of chemical admixture and strength chosen. Researchers have reported k-values between 0.25 and 1.1 for FA replacement levels up to 50% (Babu and Rao, 1993, Kearsley, 1999, Khan et al., 2018), k-values between 2 and 5 for CSF replacement of between 5 and 20% (Telford, 1988, Sellevold and Nilsen, 1987) and k-values between 0.70 and 1.29 for 10 to 80% GGBS replacement (Babu and Rama Kumar, 2000).

Testing of long-term shrinkage usually starts at 24 hours after casting when the specimens are demoulded. The length change over time of standard prismatic specimens are measured according to standards such as SANS 6085 (2006), ASTM C157 (2017), RILEM CPC 9 (1975) and AS 1012.13 (2015). In South Africa, some research facilities conduct natural drying tests, usually

performed in conjunction with creep tests and this is done at 22° ± 2°C as opposed to between 50°C and 55°C for the SANS 6085 (2006) test method.

Holt (2001) illustrated that there is no correlation between the magnitude of early age and long-term shrinkage for concrete, this can be seen in Figure 2.24. The poor curing conditions of the concrete that was subjected to wind illustrates how the early age shrinkage can far exceed the long-term shrinkage. The long-term shrinkage due to drying was equal for all three cases.

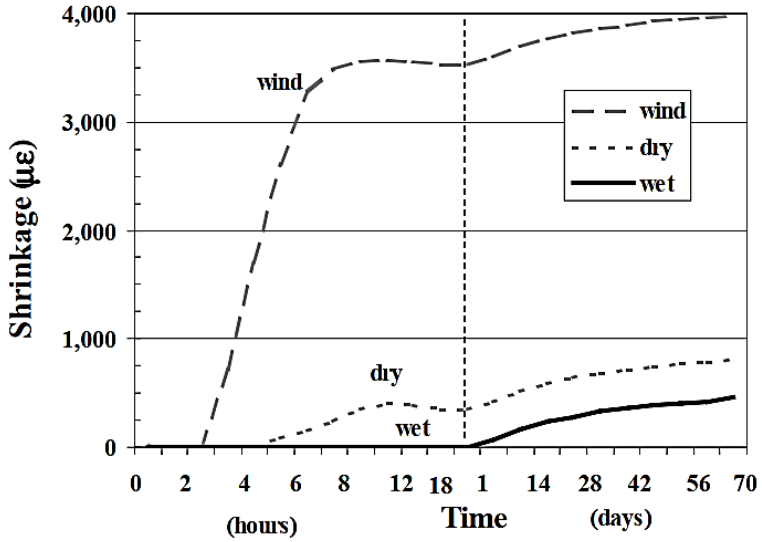

Figure 2.24 Early age and long term shrinkage with different curing environments during the first 24 hours (wind = 2m/s, dry = 40% RH, wet = 100% RH) (Holt, 2001)

Deformation of concrete results from moisture loss or gain, heat, applied stress and/or internal reactions. Often this leads to cracking as the member is almost always under restraint in some way, due to subgrade friction and end constraint of members but usually from reinforcing steel and from differential strains that develop between the exterior and the interior of the concrete (Mehta and Monteiro, 2006). The mechanisms and factors influencing the magnitude of concrete deformation as well as the different types of deformation are discussed in Section 2.7.

2.7 TYPES OF CONCRETE DEFORMATION

Concrete deformation is inevitable, due to not only elastic deformation but also shrinkage, creep and thermal strains. Shrinkage is most often measured over long periods of time and the earlier volume changes during the plastic stage is often deemed to be insignificant. In the following sub-

sections chemical shrinkage, thermal deformation and drying shrinkage are briefly discussed while going into more detail on autogenous shrinkage.

Shrinkage and deformation of concrete is dependent on many intrinsic factors of the concrete mix, concrete member and extrinsic environmental factors. Figure 2.25 lists factors affecting the volume change of concrete.

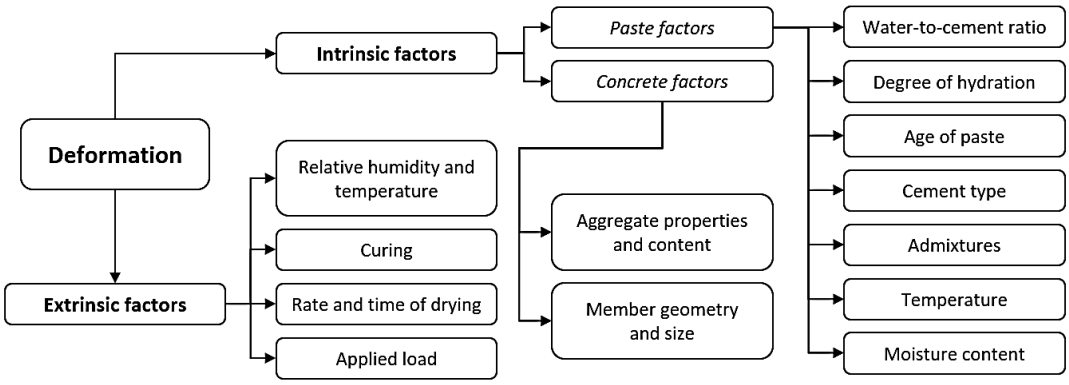

Figure 2.25 Factors affecting deformation of concrete (adapted from Addis, 1994)

Drying shrinkage is caused when water is removed from concrete. When concrete is moved from a dry condition to wet or humid condition, some of the shrinkage can be recovered and swelling can occur. Loss of free water takes place first and causes little to no shrinkage. The volume change is not equal to the volume of water loss. Drying shrinkage is a volumetric effect but is frequently measured as a linear strain. Figure 2.26 illustrates two scenarios where a) the concrete was subjected to drying and subsequent re-saturation and shows that a part of the shrinkage is irreversible and b) the concrete was dried and subjected to drying and wetting cycles also showing the reversable shrinkage. Thus, concrete shrinkage has two components, reversable and irreversible shrinkage. The extension curves in Figure 2.26 indicates swelling of concrete when placed in water. The swelling of the HCP is resisted by the skeletal structure, so the swelling is small when compared to the drying shrinkage strains (Addis, 1994, Neville, 2011).

Member size has a significant effect on the drying shrinkage. Water will only be lost at the surface, hence the inner core acts as a restraint against movement. The rate of shrinkage will also be affected by the rate of moisture transfer from the core to the surface.

Domone and Illston (2010) summarised the four principle mechanisms of shrinkage and swelling namely capillary tension, surface tension or surface energy, disjoining pressure and movement of

interlayer water. Drying shrinkage falls outside the scope of this study and is thus not discussed in further depth.

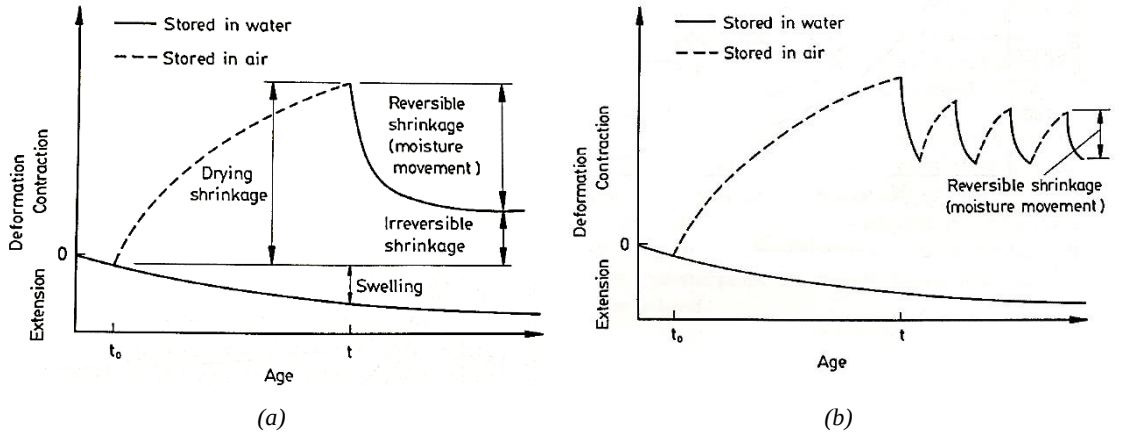

Figure 2.26 Swelling and shrinkage of concrete due to moisture movement: a) concrete dried and was then re-saturated, and b) concrete that dried and was then subjected to wetting and drying cycles (Addis, 1994)

Plastic shrinkage occurs when bleed water rises to an unprotected concrete surface and evaporates at a greater rate than what the bleed water rises. Tensile strains will occur in the topmost region of the concrete and as the concrete tensile strength is almost zero, plastic shrinkage cracking may occur. The cracking pattern resulting from this is fairly regular 'crazing". Plastic shrinkage will be exacerbated by higher environmental or concrete temperatures or if the concrete surface is exposed to wind which will increase the evaporation of surface water (Domone and Illston, 2010).

2.8 AUTOGENOUS SHRINKAGE

2.8.1 Definitions and history

Autogenous shrinkage is the shrinkage that does not include volume change resulting from moisture movement in and out of the environment (sealed conditions), temperature changes or the application of an external force or restraint. It is also referred to as self-desiccation shrinkage. Autogenous shrinkage was defined by a technical committee at the Japan Concrete Institute as the macroscopic volume reduction of cementitious materials when cement hydrates after initial setting (Tazawa, 1996). Mehta defined it as the measured deformation of cement paste in a closed system (Mehta, 1986).

A graphic depicting the relationships between chemical and autogenous shrinkage is given in Figure 2.27. Autogenous shrinkage is a portion of chemical shrinkage. Autogenous shrinkage is

an external volume change while chemical shrinkage is an internal volume change. It can therefore be measured as a linear change on a concrete member. In the plastic stage autogenous shrinkage and chemical shrinkage are equal and the terms may be used interchangeably. However, Holt (2005) has shown that in concrete specimens with a water-to-cement ratio as low as 0.3 these two shrinkage values were not equal. It is also known that addition of SPs in the presence of a low water-to-binder ratio increases chemical shrinkage and autogenous shrinkage but at different rates (Wu et al., 2017).

Chemical shrinkage is the volume change at early ages due to the volume of hydrates being slightly less than the combined volume of the reacting cement and water (Bullard et al., 2011). Chemical shrinkage is the absolute internal volume reduction and is considered the driving force for autogenous shrinkage which represents the external, bulk volume change (Mounanga et al., 2004). The relationship between chemical shrinkage and autogenous shrinkage can be seen in Figure 2.27. As mentioned in the previous section, autogenous shrinkage and chemical shrinkage is the same in the plastic stage.

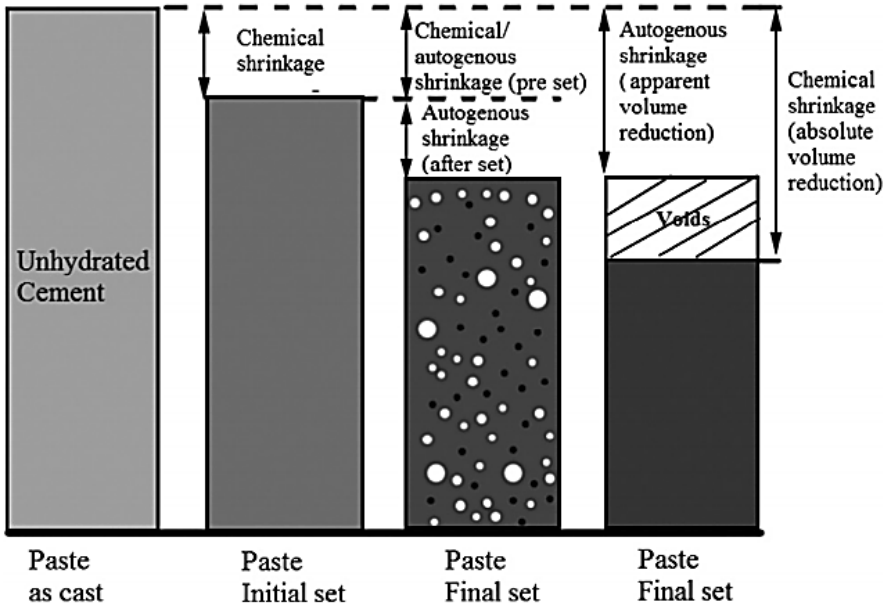

Figure 2.27 The relationship between chemical shrinkage and autogenous shrinkage (Wu et al., 2017)

Factors affecting the magnitude of autogenous shrinkage are often disputed but it is agreed that it cannot be eliminated during casting, placing or curing but must be addressed with the mix design. The material components of concrete and the proportions thereof have the biggest influence as will be discussed in upcoming paragraphs.

Autogenous shrinkage was first described by Lynam (1934) as a factor that forms part of the total shrinkage but was difficult to access. It was noted that autogenous shrinkage only became a problem with low water-to-cement ratios but fell outside the range of practical concretes. Only recently, with the development and frequent use of admixtures, has it been possible to produce concrete susceptible to autogenous shrinkage.

Autogenous shrinkage occurs during the three stages within the first day of mixing described in Section 2.2: liquid, skeleton formation and hardening. The concrete shrinkage after hardening can easily be measured using standard measuring practices.

2.8.2 Liquid Stage

Immediately after mixing when the cement paste is still in liquid phase, chemical shrinkage takes place due to the reduction in volume of the reaction products, resulting fully in external volume change. While the concrete is still liquid, the autogenous shrinkage will be equal to the chemical shrinkage. No cracking potential is caused by this volume change (Huang and Ye, 2017, Holt, 2001, Jensen and Hansen, 2001).

2.8.3 Skeleton Formation Stage

As the cement hydrates, a “stable” solid skeleton is formed in the hardening paste. The chemical shrinkage in this solid skeleton of the hardening cement paste cannot be completely transformed into external volume change. As a result, empty pores are formed inside the paste and water-air menisci occur (Bentz and Jensen, 2004). The bigger pores in the solid skeleton empty first as the water is consumed by cement hydration (Jensen and Hansen, 2001). This is called self-desiccation and produces a drop in the relative humidity (Huang and Ye, 2017).

Water is lost from subsequently smaller pores that causes the water meniscus to be pulled further into the capillary pores and will generate more stress on the capillary pore walls. As the free water in the matrix gradually decrease due to the hydration of cement, the internal relative humidity decreases. The concave surface must remain in equilibrium by increasing the capillary tension by which autogenous shrinkage takes place (Fisher and Israelachvili, 1981). This mechanism of autogenous shrinkage is shown in Figure 2.28.

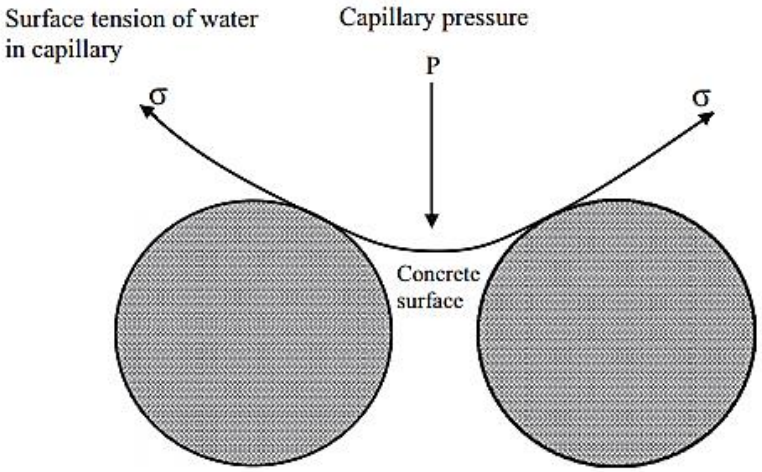

Figure 2.28 Schematic diagram of capillary water tension (Wu et al., 2017)

The point when autogenous shrinkage changes from being a function of chemical shrinkage versus self-desiccation is a function of the degree of cement hydration. The relationship between autogenous shrinkage and degree of hydration can be found in Figure 2.29. When the concrete is still a liquid then the autogenous shrinkage is still a function of the degree of hydration and only due to chemical changes (section AB). Once the skeleton has formed the chemical shrinkage becomes more constrained (section BC). The material is rigid beyond point C and the autogenous shrinkage is less and less due to chemical shrinkage (Acker, 1988, Justnes et al., 1996). Self-desiccation is the driving force for further volume reductions (Boivin et al., 1999).

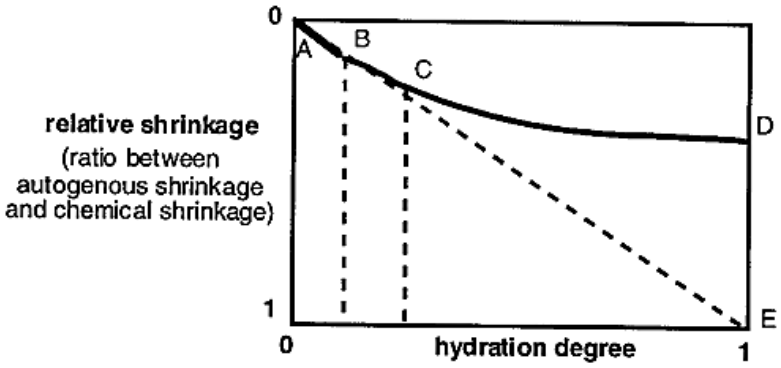

Figure 2.29 Schematic evolution of autogenous shrinkage as a function of degree of hydration (Acker, 1988)

The capillary pressure can be calculated by the Laplace equation and the Kelvin equation as indicated in Equation 2.3 and Equation 2.4 respectively:

$$P_c - P_v = \Delta P = \frac{2\sigma \cos\theta}{r} \quad \text{(eq. 2.3)}$$

$$\frac{M}{\rho} \cdot \frac{2\sigma}{r} \cdot \cos\theta = RT \ln \frac{P_0}{P_r} \quad \text{(eq. 2.4)}$$

where,

σ – surface tension of gas-liquid interface (N/m)

θ – liquid-solid contact angle (°)

P_c – water pressure (kPa)

P_v – water vapor pressure (kPa)

P_0 – actual vapor pressure (kPa)

P_r – saturated vapor pressure (kPa)

r – hydraulic radius of capillary (m)

M – molecular weight of water (g/mol)

ρ – density of water (kg/m^3)

R – ideal gas constant (J/mol)

T – absolute temperature (K)

2.8.4 Hardened Stage

As soon as the concrete has hardened, autogenous shrinkage is no longer the result of chemical shrinkage only. Li and Li (2014) developed a prediction model for early age autogenous shrinkage of self-consolidating concrete based on the capillary tension theory and the pore microstructure of concrete. The negative pressure of capillary and autogenous shrinkage was determined using the capillary tension theory. Autogenous shrinkage was calculated using Equation 2.5:

$$\varepsilon = \frac{1 - 2\mu}{E_s} \cdot \frac{2\sigma}{r} \quad \text{(eq. 2.5)}$$

where,

μ – Poisson's ratio

E_s – elastic modulus of micro-matrix around the capillary (GPa)

r – critical diameter of capillary pore diameter (m)

As time increased, the median pore diameter decreased and micropore porosity content increased which led to an increase in autogenous shrinkage.

The capillary tension theory can be used to explain the influence of a low water-to-cement ratio and the use of admixtures on autogenous shrinkage as these affect the pore structure, relative humidity, self-stress, degree of hydration and interface structure. Previous studies mostly investigated the roles of self-stress, degree of hydration and interface structure through the influence of cement, SCMs, aggregates, chemical admixtures, etc., and only a limited number of studies have addressed the effects of pore structure and relative humidity.

Snoeck et al. (2015) showed that the rate of shrinkage is an important consideration. They studied different mixes with and without SCMs and found that the results at 7 days were not necessarily indicative of which mix would be the better option, when looking to minimise autogenous shrinkage, as the data from 28 days sometimes favoured a different mix.

2.8.5 "Time-zero"

"Time-zero" is defined as the point in time when autogenous shrinkage starts and this is when the system develops a stable skeleton able to transfer tensile stress (Weiss, 2002). It is therefore critical to determine "time-zero" to be able to examine autogenous shrinkage as this can be a major source of scatter in results (Wyrzykowski et al., 2017). ASTM C1698 (2014) suggests the use of the final setting time determined by the Vicat apparatus as "time-zero". Some researchers have questioned the reliability of the final setting time of the Vicat needle test due to the relative arbitrariness of the test method (Bentur, 2002, Sant et al., 2006, Chang-wen et al., 2007, Darquennes et al., 2011, Hu et al., 2014). The above researchers do not believe that the Vicat final setting time precisely corresponds to the "time-zero".

Bentur (2002) found that the final setting time is roughly equal to the final setting time but not exactly. Chang-wen et al. (2007) demonstrated the difficulty in measuring the moisture movement in very early age concrete by the conventional hygrometer method as the material is still in the range of 98% to 100% internal relative humidity. They developed a testing method to determine the meniscus depression within the paste or concrete and determined the "time-zero" from the capillary depression. Darquennes et al. (2011) stated that the development of autogenous shrinkage strongly depends on the definition of "time-zero". Three definitions of "time-zero" were considered based on the free deformation curve tested in their research: (1) initial and final setting time, (2) the time of peak expansions at early ages and (3) the time characterized by the second maximum absolute value of the deformation rate as seen in Figure 2.30. The third

definition, which corresponds to significant stress development inside the specimen, was chosen as the "time-zero" and was confirmed by Temperature Stress Testing Machine (TSTM) testing. A TSTM is an experimental setup that allows for the study of various fundamental properties of concrete from very early ages, to predict and asses the cracking risk.

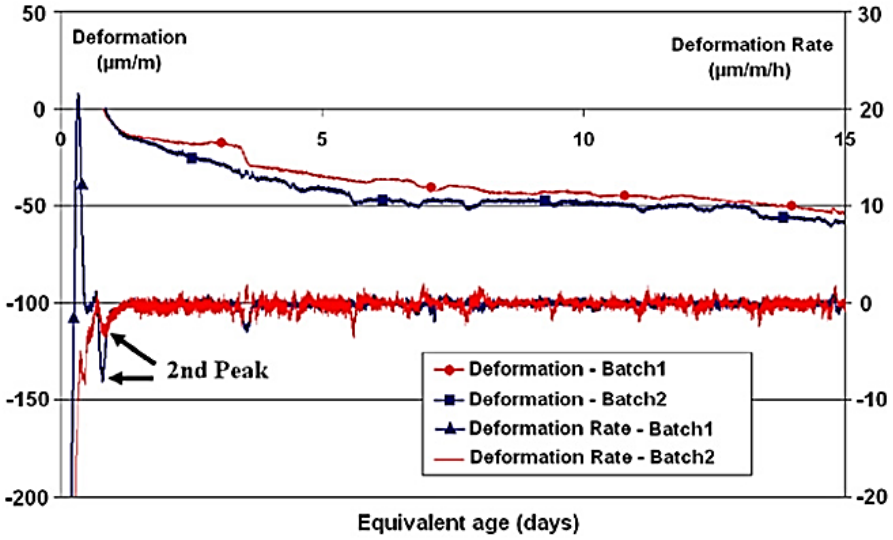

Figure 2.30 Deformation rate and autogenous deformation expressed form the second maximum value of the deformation rate of the CEM I mix (Darquennes et al., 2011)

Chang-wen et al. (2007) used the approach of determining the initiation of self-desiccation to define the "time-zero" while Darquennes et al. (2011) determined the initiation of internal tensile stresses to define the "time-zero". The "time-zero" defined by the last mentioned two methods is expected to be correlative due to the fact that self-desiccation is the main reason for autogenous shrinkage (Jensen and Hansen, 2001). Huang and Ye (2017) found that the Vicat final setting time was an improper way of determining the "time-zero" as the solid skeleton is not yet formed at this stage. They also found that the internal humidity does not drop directly after the Vicat final setting time. They developed an improved hygrometer method to monitor the internal relative humidity in cement pastes and defined a new "time-zero" which corresponds to the onset of internal relative humidity drop. Hu et al. (2014) measured the rate of heat evolution with isothermal calorimetry to determine the time at which a solid skeleton begins to form in the system and found that the setting times correlated positively with the Vicat needle setting times but was later with the isothermal calorimeter. This was attributed to the very different mechanisms and test arrangements.

Another proposed method for determining the "time-zero" is the knee-point method where the transition point between the solid and fluid state determined by the moment when the rate of autogenous strain becomes zero is taken as the reference point (Filho et al., 2019).

2.9 INFLUENCE OF CEMENT COMPOSITION ON AUTOGENOUS SHRINKAGE

The mineral composition of cement influences the autogenous shrinkage. The impact of the C_3A content is the most dominant followed by C_3S, C_4AF and C_2S (van Breugel and van Tuan, 2014). The effect of different types of cement on autogenous shrinkage is basically due to the difference in composition. High-early-strength cements contain higher contents of C_3A and C_3S that cause more autogenous shrinkage than low to moderate heat generating cements in which higher contents of C_2S are used (Wu et al., 2017).

Bullard et al. (2011) showed that increased fineness and larger specific surface area of cement decreased the relative humidity at a higher rate and increased the measured autogenous shrinkage. This may be due to the accelerated cement hydration and water consumption in the matrix. The effect of cement fineness on relative humidity is shown in Figure 2.31.

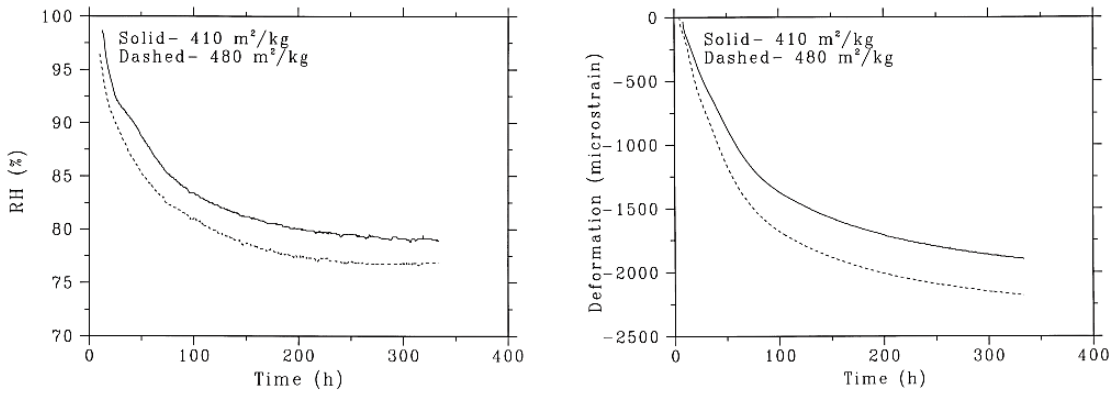

a) *b)*

Figure 2.31 Effect of fineness of cement on a) relative humidity and b) autogenous shrinkage (Bentz et al., 1999)

2.9.1 Influence of silica fume

Jensen and Hansen (1996) showed that SF increased the rate of autogenous shrinkage of HPC. They found that the autogenous shrinkage of cement paste with a water-to-binder ratio of 0.23 increased with the cumulative content of SF within the range of 0-20%. With the presence of 10% SF, the autogenous shrinkage measured was around three times that observed of plain cement paste at 28 days. Zhang et al. (2003) also found that using SF at 5% and 10% increased autogenous

shrinkage and some of the results is shown in Figure 2.32. The autogenous shrinkage increased with an increase in SF content while this effect became more prominent with a decrease in water-to-cementitious material ratio. Some other researchers that also reported the negative effect of SF on autogenous shrinkage include Tazawa and Miyazawa (1995) Maruyama and Teramoto (2013),Lura et al. (2003), Zhang et al. (2003) Holt (2005), Li et al. (2010) Ghafari et al. (2016) and Yang et al. (2005).

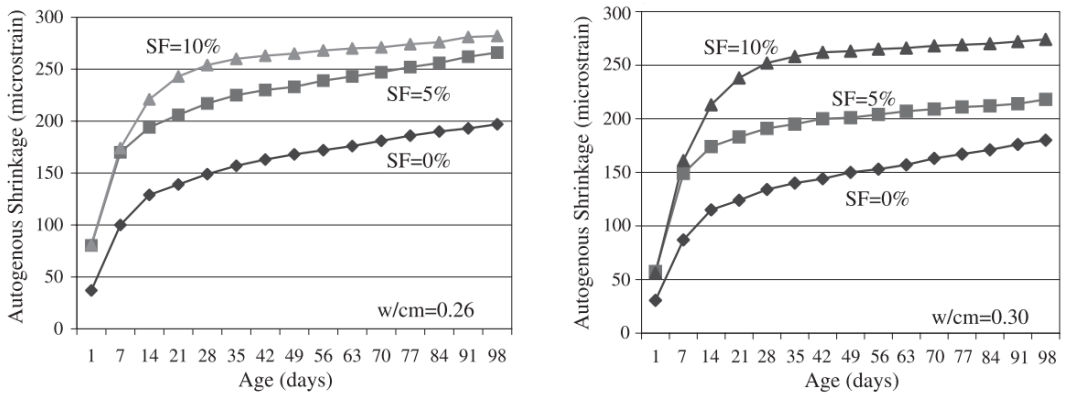

Figure 2.32 Effect of SF on the autogenous shrinkage of concrete (Zhang et al., 2003)

Three mechanisms have been used to explain the results: (1) SF refined the pore structure and the number of small pores increased which led to significant autogenous shrinkage in specimens. (2) During the hydration of clinker, the formed CH was partly distributed into interlayer pores of C-S-H gel and restrained the chain. The CH was consumed by the addition of SF and the porous structure of C-S-H was formed. The consumption of CH caused empty pores and weakened their restraining effect on the C-S-H structure and increased the shrinkage of the cement paste (Mazloom et al., 2004, Wu et al., 2017). (3) SF accelerated the reaction process due to the superfine structure. The large surface area of SF caused the fast combination of SF and mixing water, increased the water shortage in the pore space of the cement paste, reduced the relative humidity inside the cement skeleton and intensified self-desiccation (Paillere et al., 1989, Rao, 2001).

2.9.2 Influence of fly ash

Malhotra (2002) showed that FA decreased autogenous shrinkage because FA reduces the rate at which the internal humidity decreases. The internal relative humidity of concrete specimens was less when FA was used, this decline slowed down as the amount of FA increased from 15% to

60% in a sealed condition with water-to-binder ratio of 0.3. When the mixing amount of FA exceeded 40%, the reduction of internal relative humidity after 120 days was less than 13% compared to 20% in plain cement samples. When more than 60% FA was used, the internal relative humidity was maintained for up to 7 days. Termkhajornkit et al. (2005) found that the replacement with more than 50% FA significantly reduced the autogenous shrinkage of concrete specimens with a water-to-binder ratio of 0.3. They associated the autogenous shrinkage in part with the hydration reactions of PC and reactions of Al_2O_3 to form ettringite and partly with hydration of FA, the hydration of FA causing a slowdown of the shrinkage. Guoxing Huang (1990) studied the autogenous shrinkage of mass concrete with FA. He reported that the incorporation of up to 20% FA halved the autogenous shrinkage and incorporation of 40% FA lowered the autogenous shrinkage to about a tenth of that of the plain specimens. The increased fineness and the content of FA decreased the autogenous shrinkage and increased the initial cracking time (Mehta, 1986). This effect is due to the slow reaction time of FA in comparison to cement which caused a dilution effect and added to the effective water-to-binder ratio, thereby reducing the autogenous shrinkage (Snoeck et al., 2015). But, Jiang et al. (2004) found that this was not necessarily true for a low FA amount of 10% where a portion of the FA contributed to the reduction of autogenous shrinkage and the rest had an adverse effect. Early crack formation could also not be avoided by adding FA alone (Gdoutos et al., 2003, Subramaniam, 2005). FA is more effective at reducing autogenous shrinkage compared to SF and slag (Ghafari et al., 2016).

2.9.3 Influence of slag

Tazawa and Miyahara (1997) showed that the autogenous shrinkage of concrete was dependant on the amount of slag with specific surface area over 400 m^2/kg. When 75% or more slag was used, the autogenous shrinkage of concrete began to decrease. When the fineness increased to 836 m^2/kg the inflection point decreased to 60%. Fineness has a significant effect on reactivity, and this could explain the effect of slag on autogenous shrinkage. With a slag fineness of 338 m^2/kg the autogenous shrinkage had a negative correlation. Lee et al. (2006) found that slag, used in higher contents, increased the autogenous shrinkage. Figure 2.33 shows the effect of slag replacement and water-to-cement ratio on the autogenous shrinkage of concrete. The autogenous shrinkage increased with an increase in slag replacement. A lower water-to-cement ratio increased the autogenous shrinkage even further. This was attributed to the increase in chemical shrinkage and finer pore structure of the concrete with slag compared to the pure PC concrete and also the particle shape of the slag. The slag used in this study has a Blaine of 430 m^2/kg. Almeida and Klemm (2018) also found an increase in autogenous shrinkage with an increase in replacement level with GGBS and attributed this to the so-called filler effect.

The increasing effect of slag on autogenous shrinkage is reportedly less than that of SF since slag concrete contains a smaller volume of fine pores compared to SF concrete. Finer pores contribute to increase capillary pressure in the paste and increases the autogenous shrinkage (Ghafari et al., 2016).

Li et al. (2010) disputed the increasing effect of slag on the autogenous shrinkage of concrete. Volume expansion was observed in a previous study where GGBS cement was used, and the analysis of literature shows that there is still not a consensus on the effect of slag on autogenous shrinkage. Limited materials were used in previous studies and thus the role of slag in autogenous shrinkage is still not clear (Wu et al., 2017). Snoeck et al. (2015) found that GGBS reduced autogenous shrinkage at replacement levels of 15-85% and attributed this to the slag reaction that occurred mostly at later ages which delayed the formation of a denser structure.

The effect of SCMs on the autogenous shrinkage of high-performance concrete with a low water-to-cement ratio is still controversial. Early age shrinkage is tested on site quite often, using prisms and measuring points without corrugated tubes but lack of efficient and practical testing apparatus and methods often prevents the proper systematic research on the influence of these factors on autogenous shrinkage with low water-to-binder ratio and this research is indispensable (Wu et al., 2017).

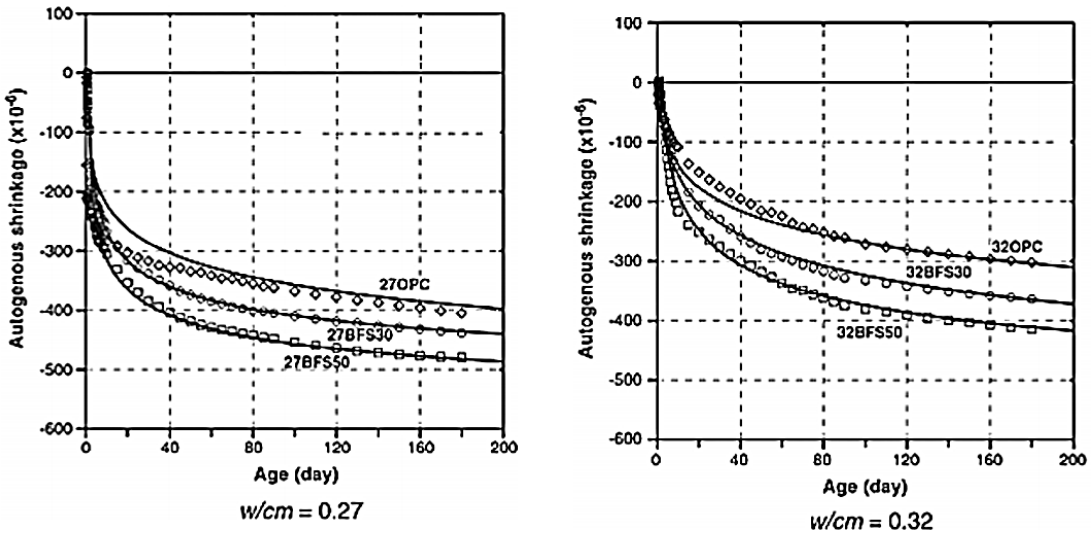

Figure 2.33 Effect of slag content on concrete with a) a water-to-cement ratio of 0.27 and b) a water-to-cement ratio of 0.32 (adapted from Lee et al., 2006)

2.10 INFLUENCE OF WATER-TO-BINDER RATIO ON AUTOGENOUS SHRINKAGE

Water-to-binder ratio has a significant influence on autogenous shrinkage and in particular HPC with a water-to-binder ratio of less than 0.4 (Zhang et al., 2003). Figure 2.34 shows that an increase from water-to-binder ratio 0.26 to 0.30 decreased the autogenous shrinkage and a more significant decrease could be seen with an increase of water-to-binder ratio of 0.30 to 0.35. Although the measured autogenous shrinkage was significantly increased by the inclusion of SF the use of SF in concrete reduced the effect of water-to-binder ratio on autogenous shrinkage.

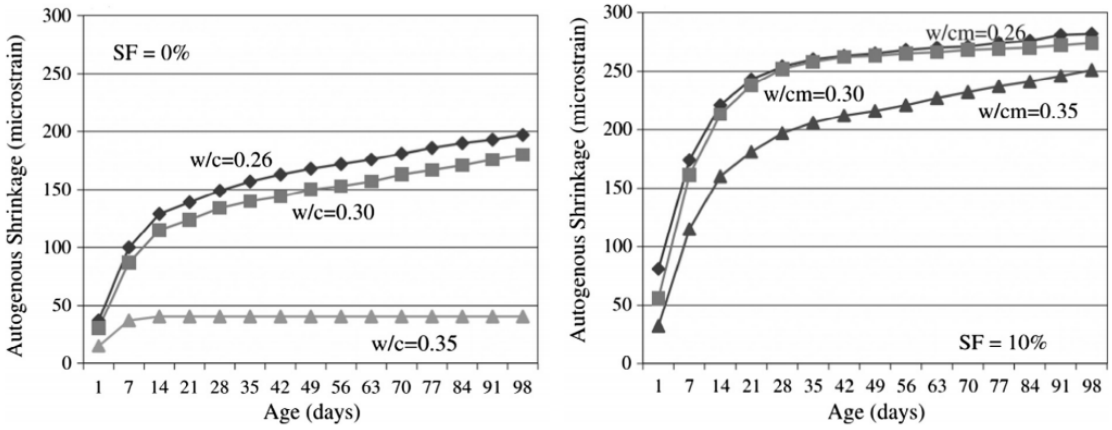

a) *b)*

Figure 2.34 Effect of water-to-binder ratio on autogenous shrinkage of HPC (Zhang et al., 2003)

Jiang et al. (2005) also studied the effect of water-to-cement ratio on autogenous shrinkage in the presence of SF and slag which was in agreement with Zhang et al. (2003). Jiang et al. (2005) found that addition of slag to a cement and SF binary mix decreased the autogenous shrinkage, especially at early ages. Wang et al. (2008) used a segmental screw micrometer to measure the autogenous shrinkage of cement-based materials with ultra-low water-to-binder ratios. The study found that the water-to-binder ratio of 0.25 was critical and when the water-to-binder ratio increased, the autogenous shrinkage decreased. The opposite was found for water-to-binder ratios less than 0.25 where the autogenous shrinkage decreased with a decrease in water-to-binder ratio. This behaviour was attributed to the pore structure and the low degree of hydration of cement-based materials with ultra-low water-to-binder ratios, but further research is required.

A study by Tian (2006) found that a reduction in water-to-binder ratio decreased internal relative humidity of cement slurry especially at an early age and a significant increase in self-desiccation was detected. As the water-to-binder ratio decreased, the total pore volume of HPC decreased and

the pore structure was refined. This resulted in water redistribution toward the inside of smaller micro pores, accelerating the reduction of critical pore radius, increasing the negative capillary pressure and increasing autogenous shrinkage. Wu et al. (2017) defined critical pore radius as the minimum size that must be formed by atoms or molecules clustering together in a gas, liquid or solid matrix, before a new-phase inclusion (a bubble, a droplet or a solid particle) is stable and begins to grow.

2.11 INFLUENCE OF WATER REDUCING AGENTS ON AUTOGENOUS SHRINKAGE

For the sake of maintaining workability while reducing water content, the addition of water reducing agents (WRA) makes it possible to decrease the water-to-binder ratio, therefore causing increased autogenous shrinkage (Tam et al., 2012). Holt (2005) found that the addition of 1% SP to mortar with water-to-cement ratio 0.3 increased the autogenous shrinkage by around 30%. This was attributed to the improved cement dispersion and faster rate of hydration reactions. Conversely, the lower shrinkage of specimens with no added water reducing agents was explained by the increased heterogeneity, such as cluster formation between aggregates and their restraining effect. Beltzung and Wittmann (2002) reported the acceleration of hydration rate and the subsequent increase in autogenous shrinkage for specimen containing WRA.

2.12 SUMMARY

From the information in the literature reviewed it can be seen that the binder composition and content has a significant effect on early age concrete deformation and thermal processes. Concrete deformation is influenced by the binder composition such as addition and replacement of PC with SCMs. The binder content or water-to-binder ratio also significantly affects concrete deformation. The thermal processes evaluated by calorimetry are also influenced by the binder content and binder composition. A strong relationship between the mixture properties and the isothermal heat evolution has not been established. The same could be said with regards to the relationship between SCMs and autogenous shrinkage. As stated in literature, the strength (or reactivity) and thermal processes of concrete are both a function of binder composition and content. There may then exist a relationship between the strength (or reactivity), the thermal processes and autogenous shrinkage. Research is necessary to attempt to establish a link between autogenous shrinkage and the thermal processes and/or strength of concrete.

CHAPTER 3: EXPERIMENTAL PROGRAM

3.1 INTRODUCTION

To investigate the relationship between the thermal processes, strength and autogenous shrinkage of concrete different binder compositions and contents were tested using materials with a wide range of properties to attempt to obtain general relationships between the properties of the tested mixes. Table 3.1 serves as a summary of all tests conducted. Material properties were determined before casting. Workability tests were done to evaluate the effect of the mix constituents and determine SP dosing. Isothermal calorimetry and semi-adiabatic calorimetry tests were initiated immediately after casting. The setting time was determined by two methods and were compared. Autogenous shrinkage tests were conducted to determine the effect of binder content and composition including the effect of SCMs. Mechanical properties were tested along with material properties to assist with analysing results and determining the reactivity. One sample was used for each property tested except in the case of the mechanical properties where two samples were tested at each stage. Two samples were tested where specified to test variation.

Table 3.1 Summary of all tests conducted in this study

Property	*Test method*	*Time frame*
Raw materials	XRF Particle size distribution Relative density Blaine fineness	Before casting
Workability	Flow table	Immediately after mixing
Setting time	Modified Vicat needle Isothermal calorimeter	Immediately after mixing
Hydration	Isothermal calorimetry Semi-adiabatic calorimetry	Minimum 5 days Minimum 3 days
Deformation	Beam - autogenous shrinkage Tubes - autogenous shrinkage	8 days minimum 8 days minimum
Mechanical	Compressive strength Splitting tensile strength Modulus of elasticity	3, 7, 28 days 3, 7, 28 days 3, 7, 28 days

The procedures used to determine all the above are discussed in this chapter as well as the materials and material properties used in this study. The mixture compositions for all the mortar mixes and the mixing and casting procedures are also presented in this chapter.

3.2 MATERIALS AND PROPERTIES

This section describes the materials used throughout the experimental program and the material properties are also discussed.

3.2.1 Cement

Portland cement (PC) conforming to CEM I 52,5 N according to SANS 50197-1 for common cements was used. The measured relative density and specific surface area was 3.15 and 945 m^2/kg respectively. The measured Blaine was 442 m^2/kg. The setting time of the cement was not measured but the setting time of the mortar was. The particle size distribution of all the materials used were determined with a laser diffraction particle size analyser and the results are shown in Figure 3.1.

X-ray fluorescence (XRF) is a non-destructive test technique used to determine the elemental composition of materials. The results of the XRF test done on the cement used in this study is shown in Table 3.2. The chemical composition corresponds to typical ranges from literature (see Table 2.3).

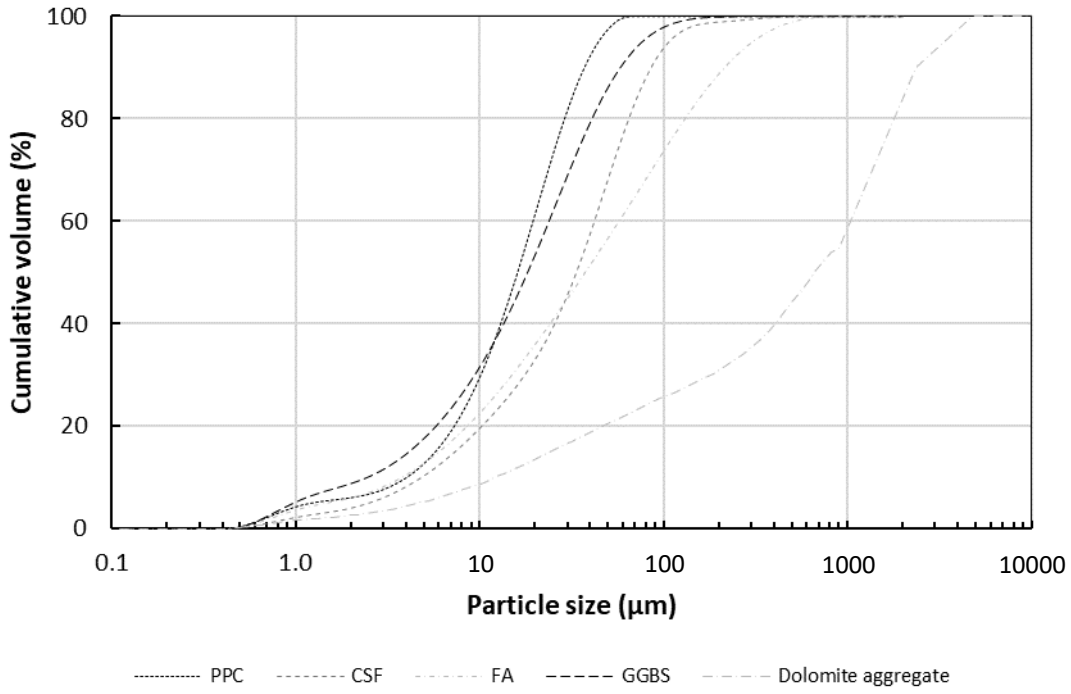

Figure 3.1 Particle size distribution of CEM I PC, CSF, FA, GGBS and dolomite aggregate used in this study

Table 3.2 Chemical composition and physical properties of PC, dolomite, FA, GGBS and CSF

Chemical composition/physical properties	*PC*	*Dolomite*	*FA*	*GGBS*	*CSF*
SiO_2 (wt %)	21.4	22.8	54.1	37.5	86.0
Al_2O_3 (wt %)	4.35	0.84	32.6	15.7	0.34
MgO (wt %)	1.28	18.0	1.23	9.02	1.30
Na_2O (wt %)	*<0.01*	*<0.01*	0.25	0.27	0.62
Fe_2O_3 (wt %)	3.07	0.59	3.15	0.51	1.66
K_2O (wt %)	0.10	0.09	0.72	1.02	2.39
CaO (wt %)	62.39	21.11	4.14	32.05	1.19
TiO_2 (wt %)	0.50	0.05	1.52	0.65	*<0.01*
SO_3 (wt %)	1.31	0.07	0.01	0.89	0.02
LOI (wt %)	4.97	35.86	0.66	0.10	6.01
Relative density	3.16	2.86	2.20	2.90	2.30
Specific surface area (m^2/kg)	945	528	768	1070	503*
D_{10} (µm)	3.96	5.78	3.73	2.41	6.24*
D_{50} (µm)	15.99	139.11	37.23	18.13	43.84*
D_{90} (µm)	36.95	703.36	213.69	57.88	137.56*
Blaine (m^2/kg)	442	-	216	342	-

*Although these values were repeatedly measured, it was not typical and as in literature.

3.2.2 Fly ash

This FA meets the requirements of SANS 50450-1:2014 for a Class N FA, where the mass proportion in percent of FA retained on a 45 µm sieve was less than 40%. The measured relative density and specific surface area was 2.2 and 768 m^2/kg respectively. The measured Blaine was 216 m^2/kg. The particle size distribution is shown in Figure 3.1. The results of the XRF test done on the FA used in this study can be seen in Table 3.2 and indicated a low lime FA which contains less than 6% lime (CaO). The chemical composition corresponds to typical ranges from literature (see Table 2.4).

3.2.3 Condensed silica fume

Condensed silica fume (CSF) with a relative density of 2.30 was used. CSF typically has a surface area of 20 000 m^2/kg and a maximum particle size of 0.3µm. The measured specific surface area however was 503 m^2/kg and the Blaine could not be measured. The particle size distribution was difficult to obtain with the laser diffraction particle size analyser as is shown in Figure 3.2. SP was added in the maximum dosage used in this study during particle size distribution testing in an attempt to mimic the actual particle size distribution obtained when mixing full scale. When only a laser was used to determine the size distribution the two measurements where almost identical. However, when also making use of ultrasound to disperse particles more effectively, a constant result was difficult to obtain. This may be because this specific CSF clumps together and acts as a material possessing a larger particle size. For reference, the cumulative particle size distribution shown in Figure 3.1 is the CSF Laser & Ultrasound 2 series shown in Figure 3.2.

The results of the XRF test done on the CSF used in this study is shown in Table 3.2. The typical content of SiO_2 in CSF from literature is 94-98%, the SiO_2 content of the CSF used was however much less at 86.0%. MgO, Fe_2O_3, K_2O and CaO is typically present at less than 1% but was found to be present at a slightly higher content of 1.30%, 1.66%, 2.39% and 1.19% respectively.

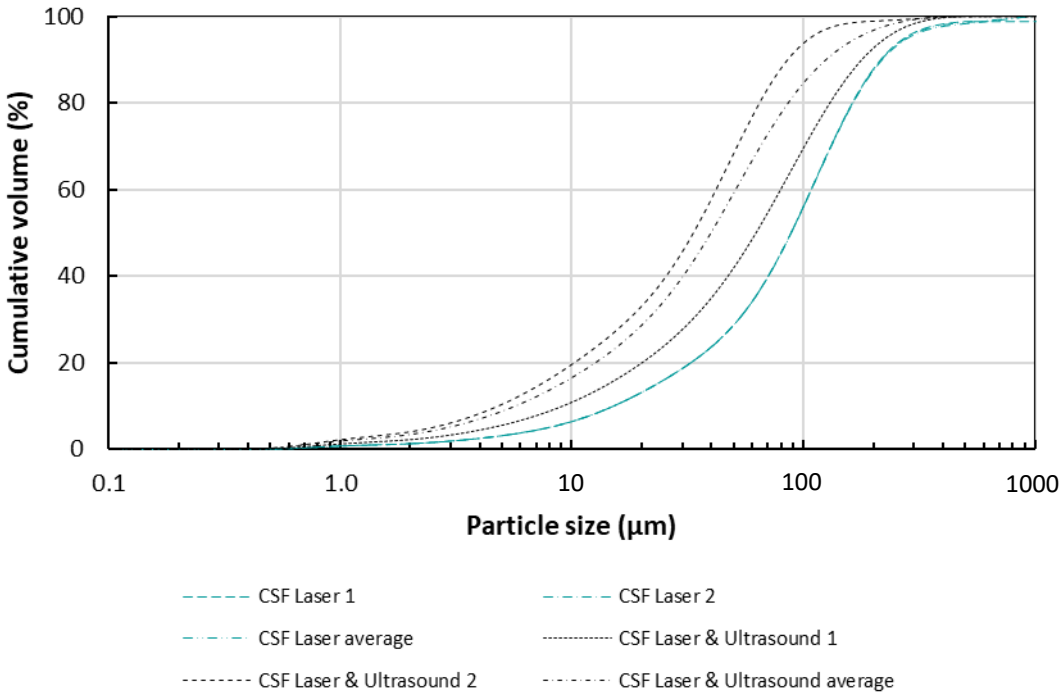

Figure 3.2 Particle size distribution of CSF tested with laser and with and without ultrasound using a laser diffraction particle size analyser

3.2.4 Ground granulated blast furnace slag

GGBS with a measured relative density and specific surface area of 2.89 and 1070 m^2/kg respectively was used. The measured Blaine was 342 m^2/kg. The particle size distribution is shown in Figure 3.1. The results of the XRF test done on the GGBS used in this study is shown in Table 3.2. The chemical composition corresponds to typical ranges from literature (see Table 2.4), except with typical values of CaO where the measured amount was 32% and the typical range is between 34-45%.

3.2.5 Aggregate

Dolomite sand with a relative density of 2.86 was used. The particle size distribution of the aggregate that was used can be seen in Figure 3.1. The results of the XRF test done on the dolomite aggregate used is shown in Table 3.2.

The laser diffraction particle size analyser that was used was limited to a maximum particle diameter size of 1000 µm thus manual sieve analysis was also done to determine the complete particle size distribution of the dolomite aggregate. The results from the laser diffraction particle

size analyser was combined with the sieve analysis to obtain the complete particle size distribution. Figure 3.3 shows the results from both methods. The difference in particle size can be explained by the assumption that the laser diffraction particle size analyser makes which is that the particles are perfect spheres, while the sand used was angular in shape due to the crusher used to manufacture the sand.

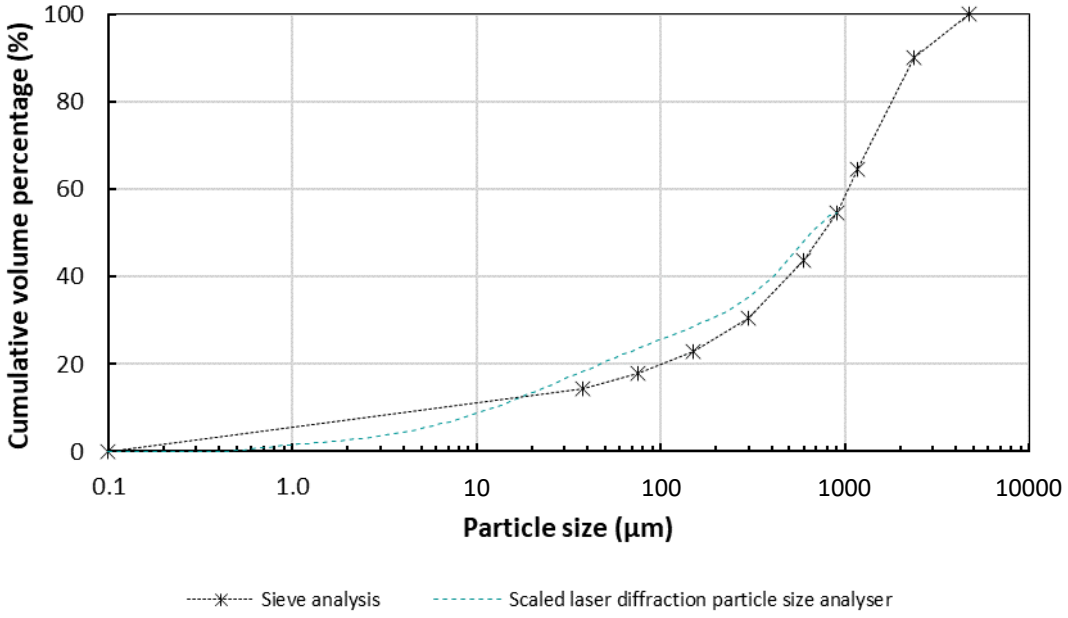

Figure 3.3 Dolomite particle size distribution obtained by sieve analysis and laser diffraction particle size analyser

3.2.6 Superplasticiser

A superplasticiser based on a modified polycarboxylate polymer, with a specific gravity of 1.065, was used. A dosing rate of 0.25 to 2 kg per 100 kg cementitious material by weight was suggested by the manufacturer (Chryso – Premia 100). As SP is known to influence hydration, a minimum dosage for each PC mix was determined based on constant workability. These ratios were retained for all further testing.

3.3 CONCRETE MIX DESIGNS

Based on literature, CSF increased early age heat of hydration and strength, FA decreased early age heat of hydration and early age strength and GGBS varied with source and composition. The above mentioned SCMs were chosen due to the relatively wide range of properties and expected behaviours.

To ascertain the effect of binder composition and content on the strength, heat of hydration and autogenous shrinkage, the water-to-cement ratio was first varied, SCMs were added and PC was replaced with SCMs. The cementitious material used in the different mixture combinations was either PC or a combination of PC and CSF, FA and/or GGBS. The mix designs used in this study are shown in Table 3.3. The percentages of SCMs were selected based on common values used in practise. The first six mixes contained no SCMs and the water content was kept constant at 220 l/m^3 while the water-to-cement ratio was varied from 0.25 up to 0.75. 15% CSF and/or 35% FA was *added* to the 0.45 mixture design for the three mixtures after the first six. With water-to-cement ratios 0.25, 0.45 and 0.75, the PC was first replaced with 15% CSF, secondly with 35% FA and lastly with 15% CSF and 35% FA. Addition and replacement were done by mass. Two additional mixture compositions with water-to-cement ratio 0.45 was done with a 15% CSF replacement and/or 35% GGBS replacement.

Mortar mixtures were chosen for use in small samples. The content of aggregate used was however comparable to that of conventional concrete (Dewar, 2003, Mehta and Monteiro, 2006) and the term concrete will be used in place of mortar from this point forward.

All the water-to-cement ratios and water-to-binder ratios indicated are mass relationships. Where replacement took place with SCMs, the volume of cementitious materials increased because of the relative density of PC being more than the SCMs used. The sand content of all mixes was adjusted to maintain a constant volume of material per mixture. The trends observed would be affected by the increase in volume of reactive material where SCMs were used.

Table 3.3 Mix designs for all the concrete mixes used in the study

	wc 0.25	*wc 0.35*	*wc 0.45*	*wc 0.55*	*wc 0.65*	*wc 0.75*	*wc 0.45 C*	*wc 0.45 F*	*wc 0.45 CF*
w/c	0.25	0.35	0.45	0.55	0.65	0.75	0.45	0.45	0.45
w/b	0.25	0.35	0.45	0.55	0.65	0.75	0.39	0.33	0.30
FA (%)	0%	0%	0%	0%	0%	0%	0%	35%	35%
CSF (%)	0%	0%	0%	0%	0%	0%	15%	0%	15%
GGBS (%)	0%	0%	0%	0%	0%	0%	0%	0%	0%
Water (kg/m^3)	220	220	220	220	220	220	220	220	220
Cement (kg/m^3)	880	629	489	400	338	293	489	489	489
Dolomite aggregate (kg/m^3)	1407	1643	1775	1858	1915	1958	1684	1552	1461
FA (kg/m^3)	0	0	0	0	0	0	0	171	171
CSF (kg/m^3)	0	0	0	0	0	0	73	0	73
GGBS (kg/m^3)	0	0	0	0	0	0	0	0	0
SP (kg/m^3)	8.80	5.47	3.69	2.62	1.93	1.48	3.69	3.69	3.69
Theoretical density (kg/m^3)	2516	2498	2487	2481	2476	2472	2470	2436	2418
Paste (vol %) & (mass %)	51 (44)	42 (34)	38 (29)	35 (25)	33 (23)	31 (21)	41 (32)	46 (36)	49 (40)

	wb 0.25 C	*wb 0.25 F*	*wb 0.25 CF*	*wb 0.45 C*	*wb 0.45 F*	*wb 0.45 CF*	*wb 0.45 G*	*wb 0.45 CG*	*wb 0.75 C*	*wb 0.75 F*
w/c	0.29	0.38	0.50	0.53	0.69	0.90	0.69	0.90	0.88	1.15
w/b	0.25	0.25	0.25	0.45	0.45	0.45	0.45	0.45	0.75	0.75
FA (%)	0%	35%	35%	0%	35%	35%	0%	0%	0%	35%
CSF (%)	15%	0%	15%	15%	0%	15%	0%	15%	15%	0%
GGBS (%)	0%	0%	0%	0%	0%	0%	35%	35%	0%	0%
Water (kg/m^3)	220	220	220	220	220	220	220	220	220	220
Cement (kg/m^3)	748	572	440	416	318	244	318	244	249	191
Dolomite aggregate (kg/m^3)	1363	1289	1247	1750	1709	1685	1764	1738	1943	1918
FA (kg/m^3)	0	308	308	0	171	171	0	0	0	103
CSF (kg/m^3)	132	0	132	73	0	73	0	73	44	0
GGBS (kg/m^3)	0	0	0	0	0	0	171	171	0	0
SP (kg/m^3)	8.60	7.72	6.60	3.61	3.22	2.75	2.40	2.77	1.43	1.29
Theoretical density (kg/m^3)	2472	2396	2354	2463	2421	2397	2475	2450	2458	2432
Paste (vol %) & (mass %)	52 (45)	55 (46)	56 (47)	39 (29)	40 (29)	41 (30)	38 (29)	39 (29)	32 (21)	33 (21)

The dosage of superplasticiser was selected based on obtaining a similar workability for the different mixes and the percentages used as a fraction of cementitious material content are shown in Table 3.4.

Table 3.4 Superplasticiser dosing

Water-to-binder ratio	*Superplasticiser dosing*
0.25	1.00%
0.35	0.87%
0.45	0.75%
0.55	0.65%
0.65	0.57%
0.75	0.50%

3.4 MIXING, CASTING AND CURING

All materials used during this study were pre-conditioned in a climate-controlled room set to 20 ± 2°C and 60 ± 5% RH. A rotatable pan mixer was used to mix the concrete. All the dry components were added to the pan from course to fine and was mixed. The superplasticiser was added to the water and added to the dry components. The concrete was then mixed for five minutes.

The cubes and cylinders used for strength and stiffness testing were cast first followed by the semi-adiabatic temperature flasks, the beams and the tubes for autogenous shrinkage testing. All samples were vibrated until sufficient compaction was achieved (when air bubbles stopped coming to the surface). Setting time test samples were mixed by hand until mixture components were fully incorporated. Isothermal calorimetry samples were mixed in situ. Cubes and cylinders were covered and cured at 20 ± 2°C, demoulded after 24 hours and placed in a water bath at 25 ± 2°C until testing.

Only the mixes without SCMs were tested for workability to determine the SP dosing. Setting time, calorimetry, autogenous shrinkage, strength and stiffness was tested for all the mixes.

3.5 WORKABILITY

Workability was determined according to ASTM C1437 (2015) using a flow table. The diameter of flow was measured to the nearest millimetre and the resulting increase in average base diameter was expressed as a percentage of the original base diameter.

3.6 CALORIMETRY

Calorimetry is the study and measurement of heat and the heat production rate. It is a generic way to study processes as all processes are associated with enthalpy changes. Various types of calorimeters exist but the most common type used in the cement field is isothermal (heat conduction) calorimetry where the heat production from a small sample is directly measured. Semi-adiabatic calorimeters use larger samples and are insulated so that their hydration can be followed by measuring the temperature change of the sample. Perfectly adiabatic calorimeters can be used for mass concrete where the heat losses are negligible. Fully adiabatic calorimeters are surrounded by an adiabatic "shield" that prevents any heat loss from the sample instead of being insulated like semi-adiabatic calorimeters (Scrivener et al., 2016).

3.6.1 Isothermal calorimetry

Isothermal calorimetry measures the heat production rate in a small sample by a heat flow sensor as heat is conducted to a heat sink that is placed in a thermostated environment. It is necessary to use a reference sample with the same properties (especially heat capacity) than the sample but without any heat production. The output of the calorimeter is obtained as the difference between the signals from the sample and the reference.

AfriSam's TAM Air Isothermal Calorimeter was used in this study as is shown in Figure 3.4. The isothermal calorimeter was kept in a temperature-controlled room at 25 °C.

Figure 3.4 TAM Air Isothermal Calorimeter machine used in this study

The available arrangement allowed for 2 ml of liquid to be used which implied the use of 7.1 cm^3 of solids for the mixes in Table 3.3. Glass ampoules with a 20 ml volume was filled with approximately 20 g of material and was placed into the calorimeter to equilibrate. The fluid mixture of water and superplasticiser was then introduced by means of syringes and mixing took place for 5 minutes. The ampoule holder with two 1 ml syringes and mixing system is shown in Figure 3.5. One sample for every mix composition in Table 3.3 was tested for a minimum of about five days.

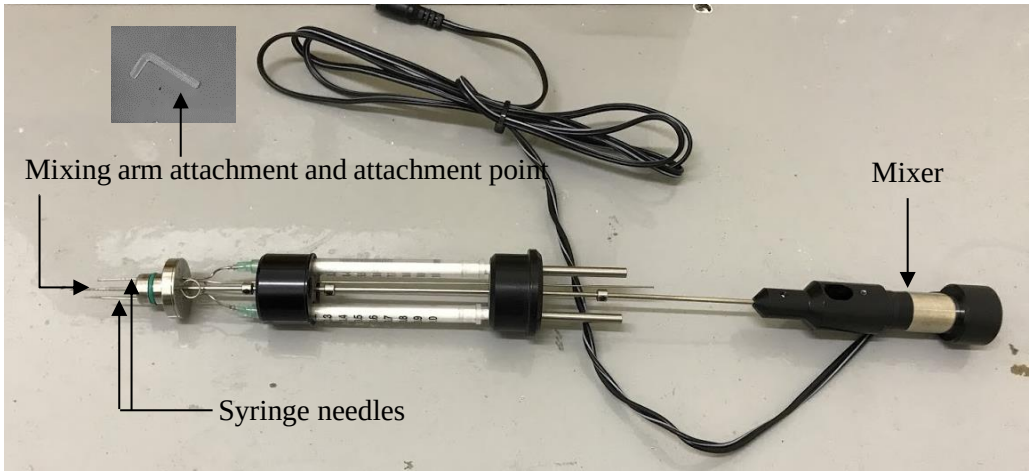

Figure 3.5 Ampoule holder arrangement

A comparative study was done on the heat evolution curves, focusing on the time when peak heat flow occurred and the corresponding magnitude of the peak heat flow.

3.6.2 Semi-adiabatic calorimetry

The semi-adiabatic temperature rise was measured to get an indication of the heat evolution. Samples were cast in metal containers with a thermocouple embedded in the centre. The container was then placed inside a Dewar flask with polystyrene particles surrounding the metal container for insulation and was subsequently sealed. The heat evolution was measured for a minimum of about three days. One sample was tested for every unique mixture and identical 769 ml (27 fl oz) containers were used which were filled completely to keep the volume tested consistent.

The thermocouples were calibrated using a Digitron System Calibration Checker shown in Figure 3.6. The temperature was corrected when data analysis took place.

Figure 3.6 Digitron System Calibration Checker used to calibrate thermocouples

A comparative study was done on the temperature rise curves looking at the time when the peak temperature occurred and the magnitude of the peak curve.

3.7 SETTING TIME

The setting times of all mixes were determined firstly with a method based on SANS 50196-3: 2006 Part 3: Determination of setting times and soundness and secondly with the data from the isothermal calorimeter.

3.7.1 Modified Vicat needle

For the method based on SANS 50196-3 (2006), the samples were not kept in a water bath but rather covered with a slightly damp cloth to prevent drying out. The samples were tested in the mix combinations as stated in Table 3.3 and not using standard consistence. The initial setting time was taken as the time elapsed between mixing and the time when the Vicat apparatus measured 6 mm between the base plate and the end of the needle. The final setting time was taken as the time elapsed between mixing and the time when the Vicat needle ring attachment failed to mark the specimen. Not only were all the mixture combinations tested, but for a and water-to-cement ratio of 0.55 an additional test was conducted without SP.

3.7.2 Isothermal calorimeter

The setting time was also determined using the isothermal calorimeter data. The derivative of the heat flow data was calculated for each mixture composition. The initial setting time was taken as the maximum rate of heat flow and the final setting time was taken as the intercept of the rate of heat flow with the x-axis. These two points are shown in Figure 3.7.

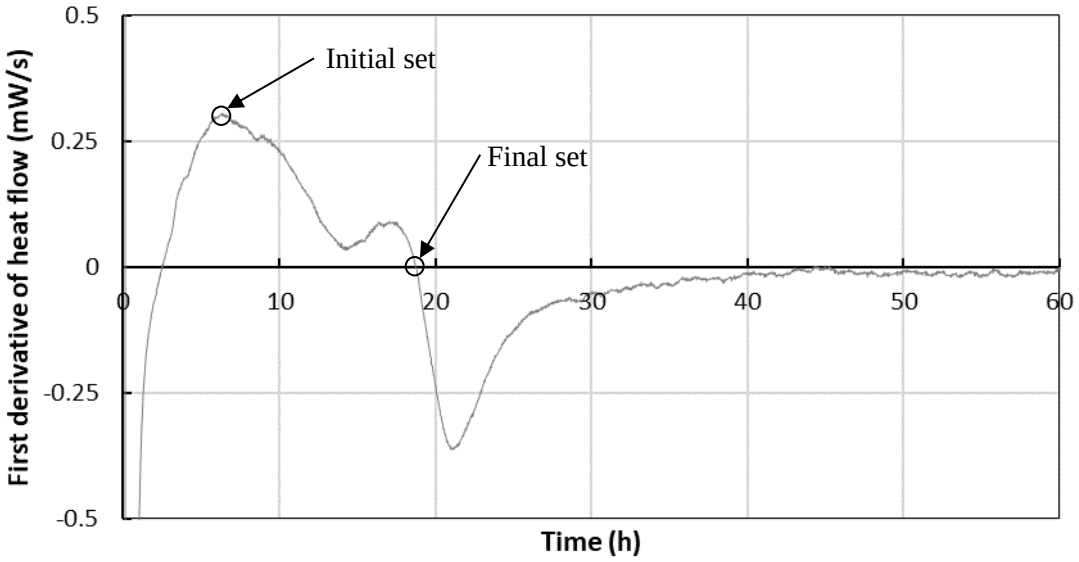

Figure 3.7 First derivative of heat flow and determination of setting times

3.8 AUTOGENOUS DEFORMATION TESTING

3.8.1 Measurements of autogenous deformation

Hammer (2002) stated that there is an enormous difference in autogenous deformation magnitude and even sign between different publications and results are difficult to interpret when different techniques are used (Barcelo et al., 1999). Different measurement techniques are discussed in this section and the methods and procedures used in this study are described.

Cement paste measuring methods

Autogenous deformation can be measured in two ways, volumetric and linear. Jensen and Hansen (2001) explained that volumetric autogenous shrinkage is frequently measured by placing the fresh cement paste in a tight rubber balloon immersed in water. The water displaced by the

immersed sample is measured to obtain the change in volume of the cement paste, as shown in Figure 3.8.

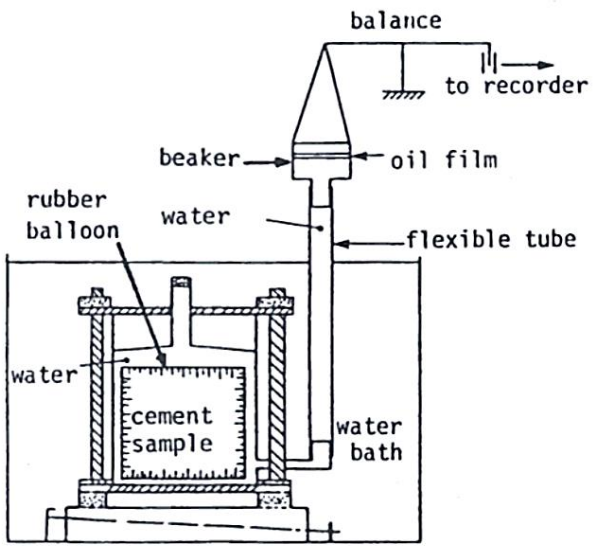

Figure 3.8 Apparatus for the measurement of volumetric autogenous deformation of cement paste (Setter and Roy, 1978)

Linear measurement of autogenous deformation is frequently performed by placing the cement paste in a rigid mould with low friction, see Figure 3.9. The length change is measured by a displacement transducer at the top of the specimen. However, in a vertical setup like this, segregation, bleeding and plastic settlement is expected.

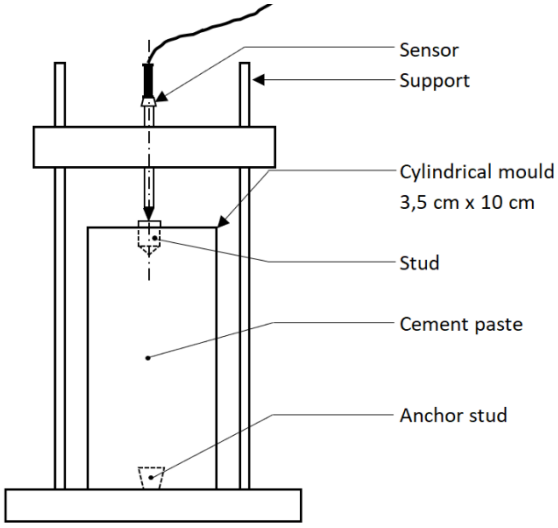

Figure 3.9 Apparatus for the measurement of linear autogenous deformation of cement paste (adapted from Buil, 1979)

These two methods should give the same results, but this is not true as the volumetric method, after being converted to linear strain, yields up to 5 times higher shrinkage than the linear method (Barcelo et al., 1999).

An advantage of the volumetric technique is that the measurement can commence immediately after casting but there is a lack of constant contact between the balloon and the cement paste which is a considerable disadvantage of the volumetric method. Bleed water may interfere with this contact. As the cement paste reacts the water may be reabsorbed as a consequence of chemical shrinkage and the internal volume reduction may also be erroneously measured as outer volume reduction. Buil (1979) also remarks that the pressure caused by the tight rubber balloon could damage the weak structure during the setting period. Osmosis through the latex membrane used in volumetric measurements may be another source of error (Marciniak, 2002). Lastly, volumetric measurements of autogenous deformation produce a large scatter in results (Lura, 2003).

An advantage of the linear autogenous deformation method is the firm anchorage of the measuring points to the set sample which greatly reduces the above-mentioned problems. This comes at a cost since the measurements cannot be carried out before the sample has set. The mould may also restrain the cement paste in the early hours after setting when the cement paste is too weak to overcome the friction against the rigid mould (Barcelo et al., 1999, Hammer et al., 2002). The friction can however be greatly reduced by lubricating the mould. Bleeding may also influence the measurements. Bleed water may be reabsorbed after setting and reduce the autogenous deformation or even cause expansion (Hammer et al., 2002). This may be eliminated by rotating the samples for both the volumetric and linear measuring technique.

The vertical deformation is expected to be different from the deformation in the horizontal directions before setting due to settlement.

Jensen and Hansen (1995) developed a corrugated mould system (see Figure 3.10), which combines the advantages of linear and volumetric measurement of autogenous deformation. The corrugated mould transforms the volumetric deformation into linear deformation before set and linear deformation is measured after set. This technique provides the opportunity to start measuring directly after casting. This method is what the ASTM C1698 (2014) standard test procedure for the measurement of autogenous strain of cement paste and mortar is based on. The moulds suggested by the standard test method has a length of 420 mm and an outer diameter of 29 mm which is too small to test mortar and limits testing to cement paste. Rotation of samples reduces bleeding and researchers have found that rotation leads to a higher shrinkage value in

samples where visible bleeding occurred but also increases the initial shrinkage in cement pastes with a water-to-cement ratio as low as 0.3 (Wyrzykowski et al., 2017).

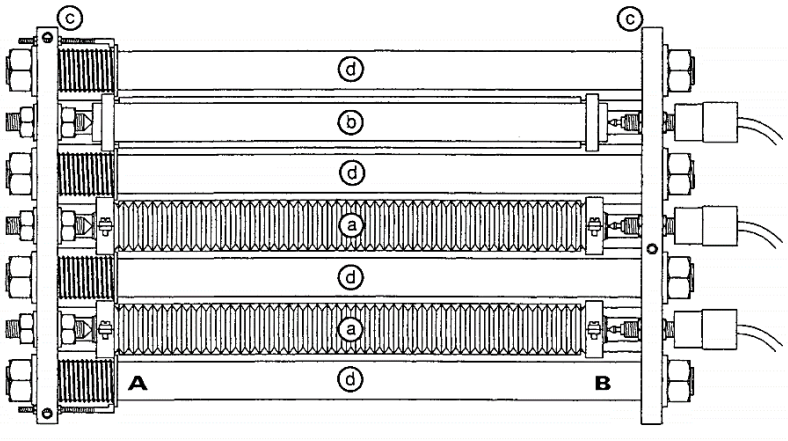

Figure 3.10 Apparatus for the measurement of linear autogenous deformation of cement paste (Jensen and Hansen, 1995)

Concrete

Volumetric autogenous deformation measurement is not possible due to the possibility of aggregates damaging the rubber balloon. Different linear methods have been used to measure the autogenous deformation of concrete. Figure 3.11 shows a system where the autogenous deformation is measured using cast-in rods at the ends of the beam.

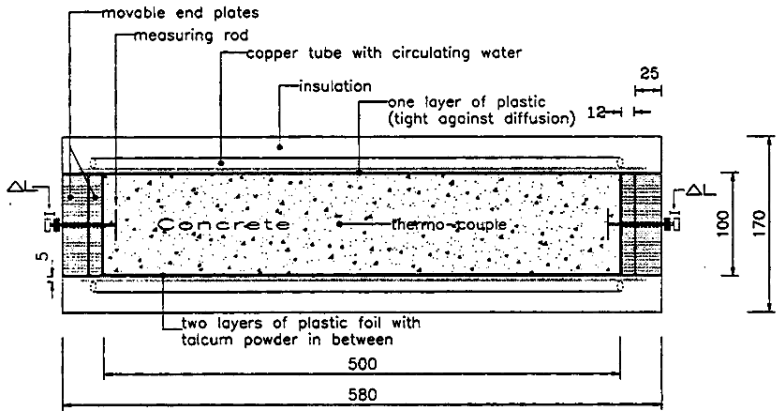

Figure 3.11 Measuring system utilising cast-in pins to measure autogenous deformation (Bjontegaard, 1999)

Figure 3.12 shows a beam with movable endplates with rods cast in to measure autogenous deformation.

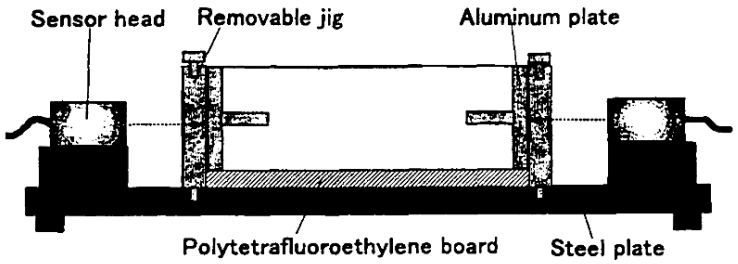

Figure 3.12 Measuring system utilising movable end plates in a 40x40x160 mm beam (Morioka et al., 1999)

Figure 3.13 shows a measuring system using horizontal transverse cast-in bars through a beam.

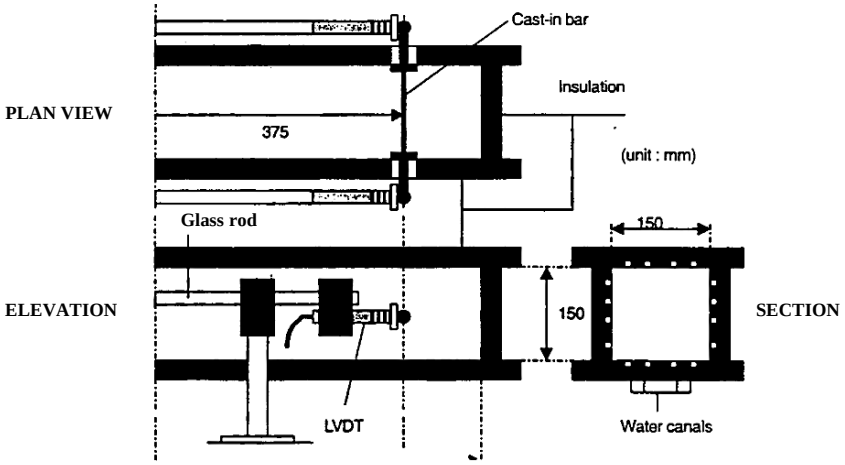

Figure 3.13 Measuring system with horizontal cast-inn bars in a 150x150x1000 mm beam (Lokhorst, 1998)

Figure 3.14 shows a measuring system where vertical rods were cast in to measure autogenous shrinkage.

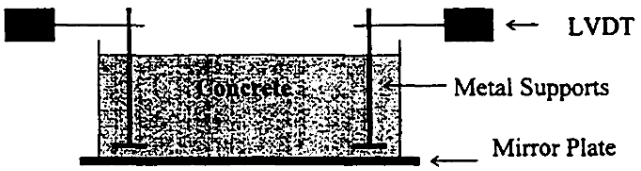

Figure 3.14 Measuring system with vertical cast-in bars in a 270x270x100 mm slab (Holt and Leivo, 1999)

Figure 3.15 details the measuring system using flexible corrugated tubes with metal plates placed on top of specimen to measure autogenous deformation. Again, as with the testing setup in Figure 3.9, segregation, bleeding and plastic settlement is expected.

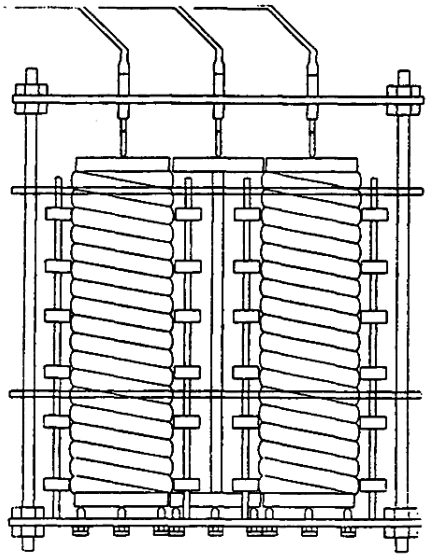

Figure 3.15 Measuring system with flexible corrugated tubes with a diameter of 100 mm and length of 375 mm (Hansen and Jensen, 1997)

The movement was measured either by linear variable differential transformers (LVDT) or non-contact transducers like reflection of electronic pulses or lasers.

For all measuring methods the main problems to overcome included ensuring good contact between the measuring points and the sample, minimising moisture loss and restraint and keeping the temperature constant. Solutions to these problems were to embed rods in the fresh concrete, reduce friction with low-friction foils, reduce moisture loss by sealing upper face with plastic or aluminium foil. A constant temperature was obtained by using temperature-controlled baths or by the circulation of cooling liquid in the mould.

3.8.2 Experimental setup for autogenous deformation

Concrete was to be tested so the size of the specimen was of importance. Two measurement techniques were selected, firstly, a vertical corrugated tube system based on Figure 3.15. and secondly, a beam with cast-in rods based on Figure 3.11.

Corrugated tube

Wirquin Magicflex corrugated tubes were used as moulds. The tubes have a length of 230 mm and an inner diameter of 50 mm. These tubes were relatively easy to obtain from the local hardware store.

A corrugated tube was prepared before casting by inserting a rubber stopper/cap at the bottom and inserting the tube in a steel pipe as shown in Figure 3.16. Two steel plates were slided into the grooves of the tube at the top and the bottom to keep it stretched out and upright during casting. This also provided a constant measuring length across all samples when filled with concrete. Concrete was first poured halfway before vibrating and then filled to the required final level. The tube in the pipe was vibrated again until sufficient compaction was obtained. The top cap was then inserted to seal the corrugated tube thus preventing moisture movement in or out of the system. The tube with the caps fitted securely was then removed from the steel mould, ready to be instrumented in a temperature-controlled room.

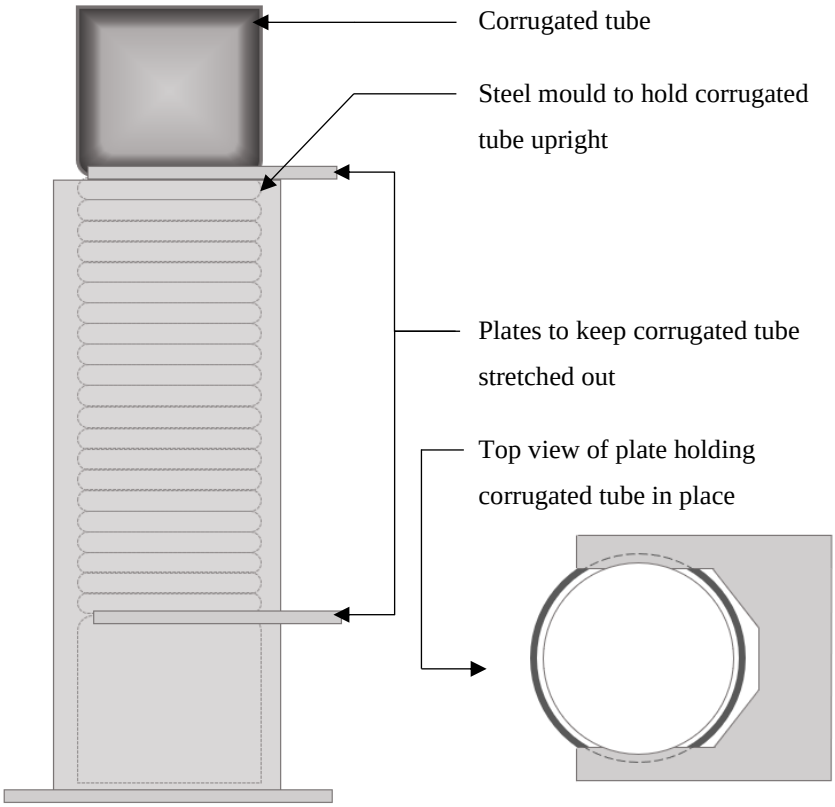

Figure 3.16 Corrugated tube casting setup

The corrugated tube filled with concrete was placed in a frame with four rods holding the tube upright, a schematic of this can be seen in Figure 3.17. The top cap had four screws attached that were embedded into the sample during casting, this ensured contact between the sample and the end cap. A measuring point for the LVDT was located on the outside of the top cap, a small indent was placed on the measuring point for the LVDT to rest on, thus preventing possible horizontal movement after initial setup. The LVDT was fixed in place by a screw located on the side of the LVDT mount and proper range was checked to prevent the need for adjustment during testing.

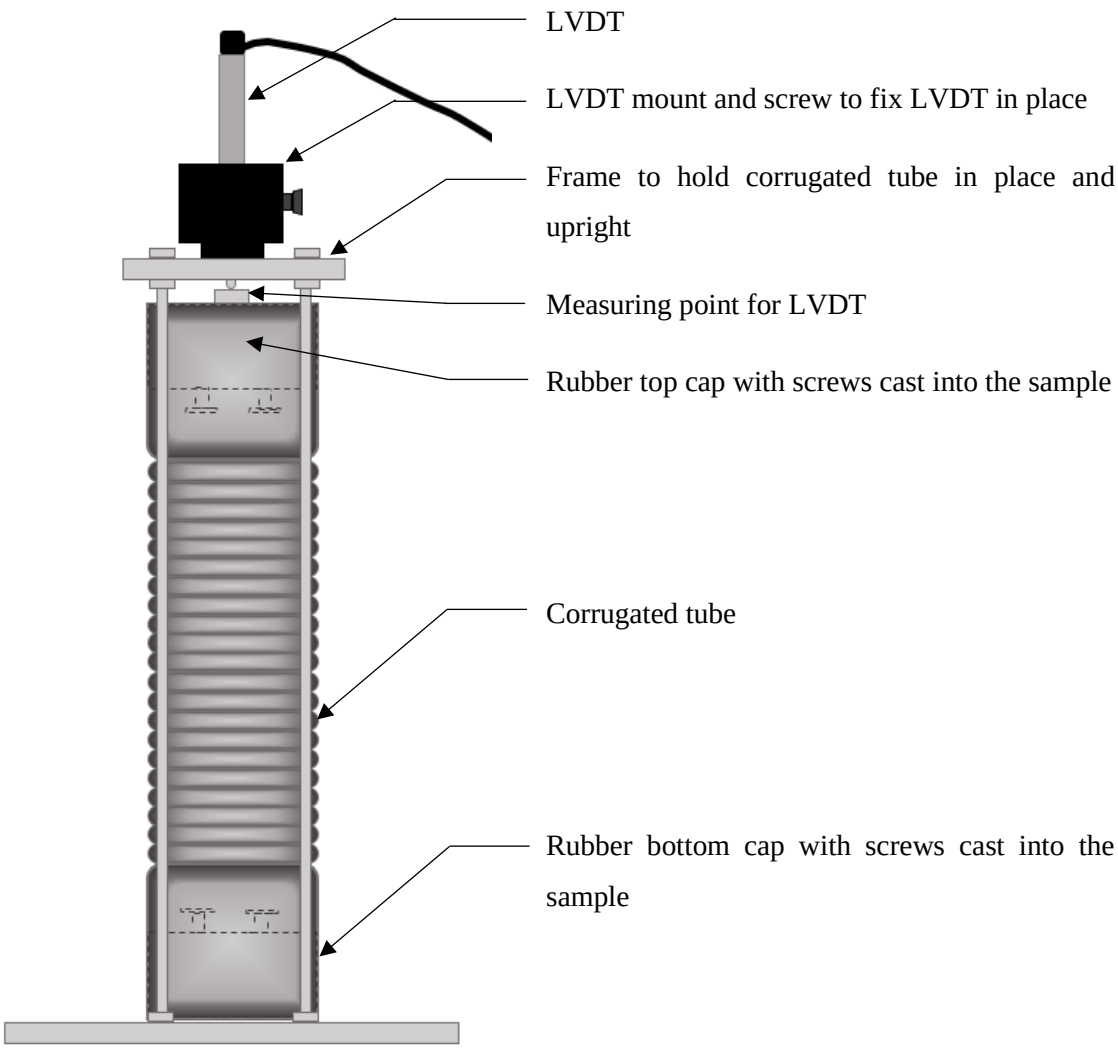

Figure 3.17 Schematic of the corrugated tube autogenous deformation experimental setup

The time when the water was added to the dry mixture components as well as the time at which the LVDT was fixed on the frame was taken down for future use during analysis.

Beam

Steel moulds with a length of 520 mm (20.5 inches) and a height and width of 101.6 mm (4 inches) were used to test beam samples. The moulds were completely taken apart and wrapped in plastic sample bags that were filled with baby powder to reduce friction. The wrapped moulds were also oiled before casting. Mould in the process of being wrapped are shown in Figure 3.18.

Figure 3.18 Moulds in the process of being wrapped in plastic sample bags filled with baby powder

A beam mould was prepared before casting by fixing rods at a spacing of 420 mm in the place where the LVDTs were to be placed. This provided a constant effective length for all the samples. The layout can be seen in Figure 3.19. The rubber end plates were glued with foam around the perimeter to enable the plate to slide over the plastic with the movement of the sample. The mould was filled halfway before vibrating and was then filled to the top and vibrated until sufficient compaction was obtained. The mould was taken to a temperature-controlled room to be instrumented.

A thermocouple was fixed into place in the middle of the sample. The two LVDTs were fixed onto the beam and checked for range. Rather than mainly providing for elongation of the LVDT (shrinkage of the beam), as in the case of the corrugated tube measuring experimental setup, the LVDTs fixed onto the beam was placed so that possible expansion of the beam could also be measured.

Three mixture compositions were tested simultaneously and an example of one set of tests are shown in Figure 3.20. The table was covered by a layer of foamed rubber to dampen any vibrations from the surrounding environment.

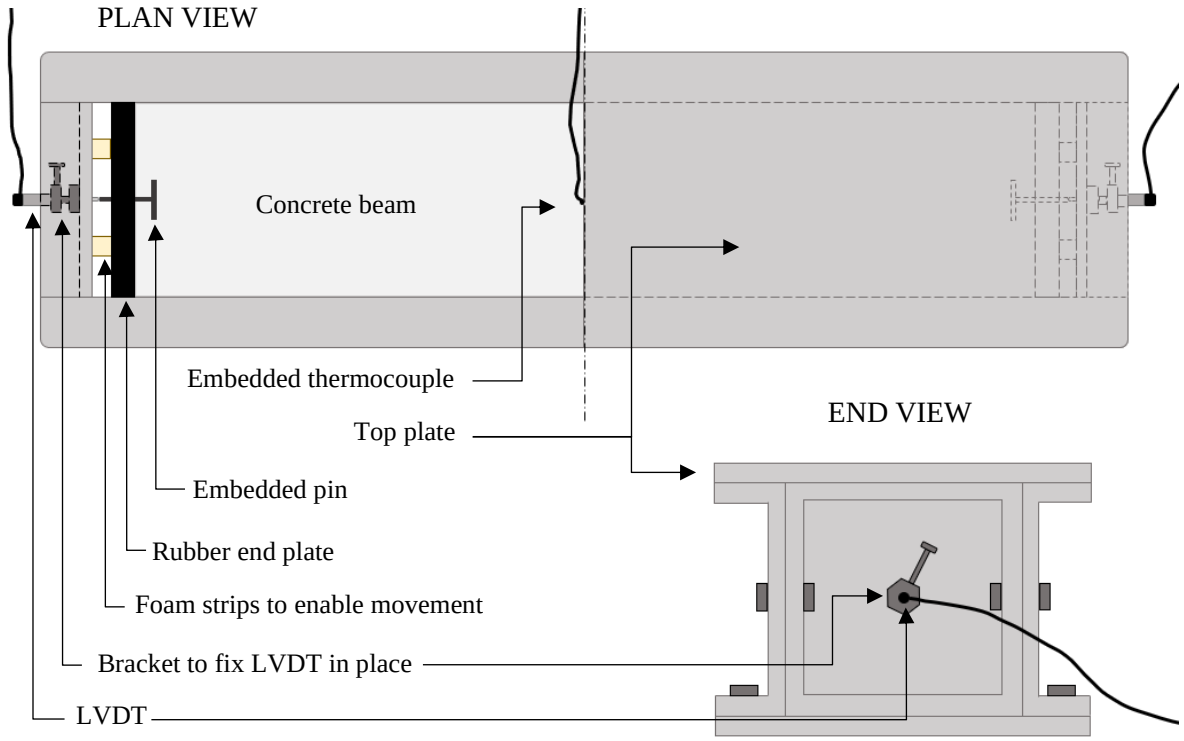

Figure 3.19 Schematic of beam autogenous deformation experimental setup

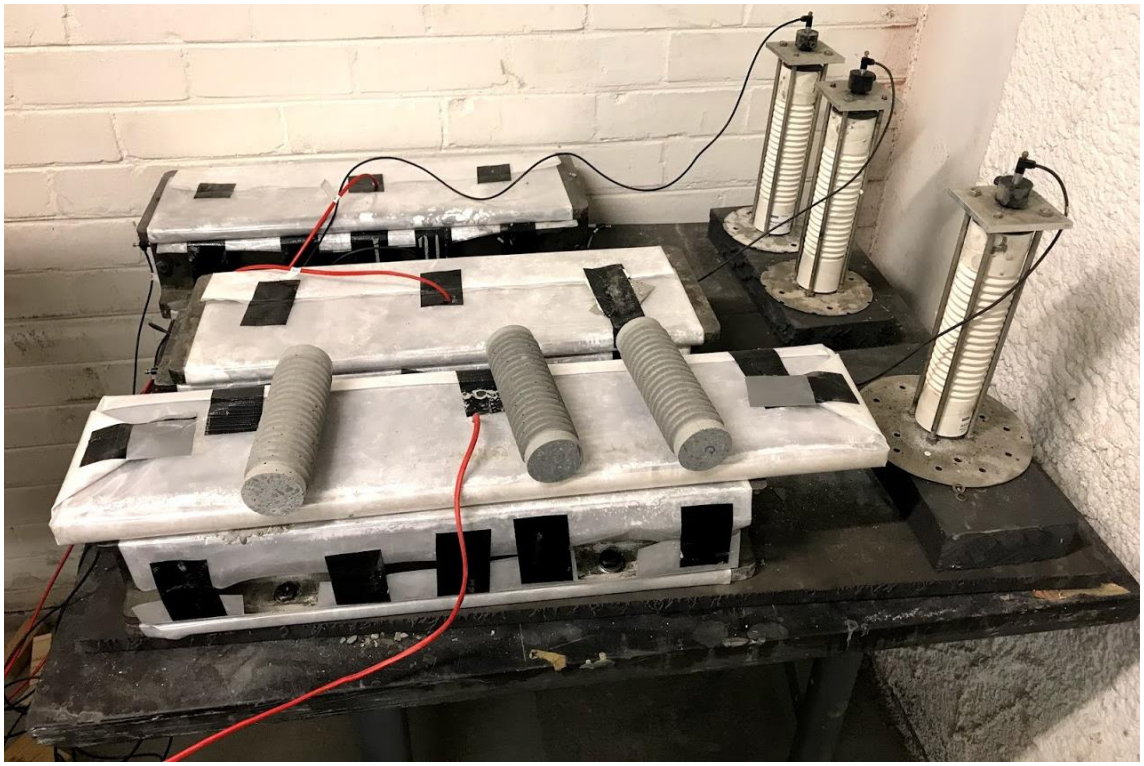

Figure 3.20 Table with complete autogenous deformation experimental setup

All LVDTs were calibrated before being used and the calibration curves can be found in Appendix A.

3.9 MECHANICAL PROPERTIES

3.9.1 Compressive strength

The compressive strength of the concrete was determined using SANS 501-1:2006 Part 1: Determination of strength. Load was applied to a 100 mm cube until failure. Two cubes were tested for each mixture combination at each age and the values recorded in this dissertation is the average of these two results.

3.9.2 Static modulus of elasticity

The modulus of elasticity was determined according to ASTM C469 (2014) on concrete specimens with a diameter of 105 mm and 210 mm length. Strain measuring equipment was fixed to the specimen and placed in a loading press. Load was applied at 270 kPa/s and the strain was

measured up until 40% of the failure load of the concrete (it was assumed that the cylinder strength was 80% that of the cube strength). The samples were then cut into two 105 mm long specimen that were used to determine the tensile splitting strength.

3.9.3 Tensile splitting strength

The tensile splitting strength was determined according to SANS 6253:2006 Concrete tests – Tensile splitting strength of concrete. The cylinder that was first used to determine the modulus of elasticity (Section 3.9.2) was then cut in half to obtain two cylinders with a diameter of 105 mm to test the tensile splitting strength. One cylinder that was cut in half to yield two samples were tested at each age for all the concrete mixture compositions. The experimental setup is shown in Figure 3.21. The average of these two test results was used in this dissertation.

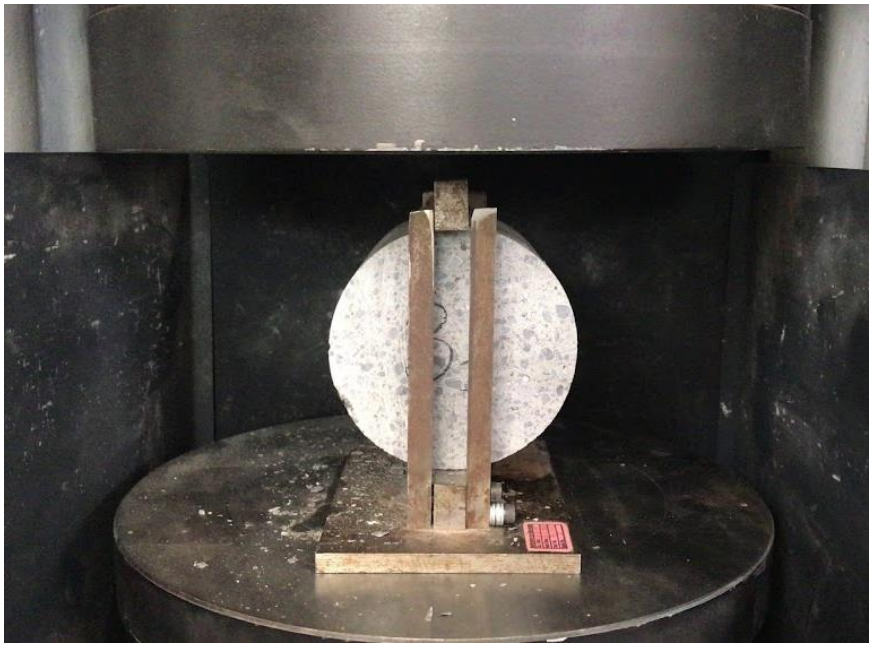

Figure 3.21 Cylinder splitting strength testing setup before being loaded

CHAPTER 4: RESULTS AND DISCUSSION

4.1 WORKABILITY

The flow percentages measured with change in water-to-cement ratio is shown in Figure 4.1. Although the data points were not enough for statistical analysis, dashed lines were placed through the data to indicate a general trend and assist in interpretation, this was done throughout Chapter 4. Overall it can be seen that the water-to-cement ratio affected the workability. The workability followed a parabolic curve. The workability of the mixes increased with an increase in water-to-cement ratio up to a water-to-cement ratio of 0.55. The flow then decreased with an increase in water-to-cement ratio. The mix with a water to cement ratio of 0.55 flowed off the flow table during the test and is indicated with the arrow in Figure 4.1. This could be due to the amount of superplasticiser exceeding the optimal dosage. All of the mixtures were deemed to have a high workability indicating that the chosen SP dosages of 0.5-1% of cementitious content were suitable for the relatively large range of water-to-cement ratios.

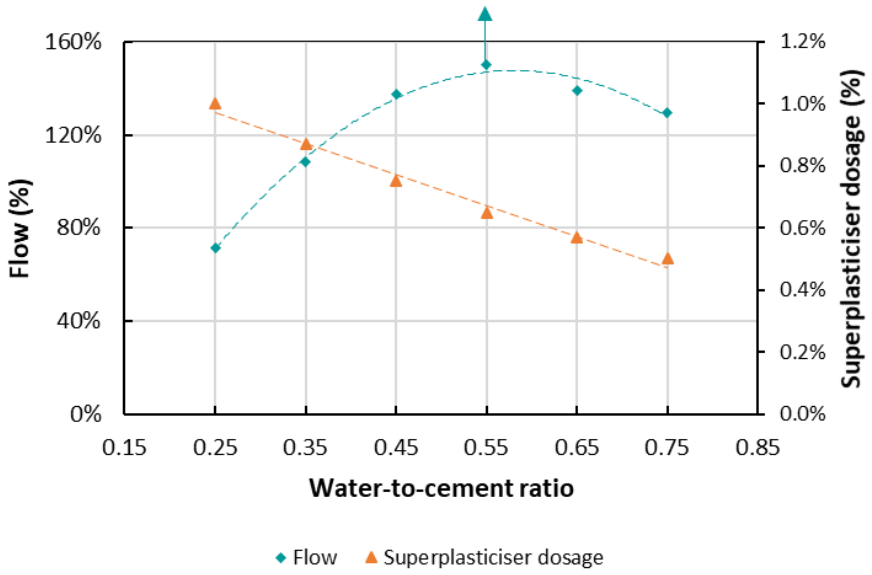

Figure 4.1 Flow percentage measured and superplasticiser dosage with change in water-to-cement ratio

4.2 SETTING TIME

The setting times obtained from the modified Vicat needle method and calculated from isothermal calorimetry data were compared, the effect of SCMs on the setting time versus the setting time of the PC samples discussed and the influence of the different testing methods highlighted.

4.2.1 Modified Vicat needle

Figure 4.2 and Figure 4.3 show the results for initial setting time with water-to-cement-ratio and cementitious material content respectively. The initial setting time for the mixes with no SCMs, indicated as *PC* in Figure 4.2 and Figure 4.3, increased on average with an increase in water-to-cement ratio, which is expected. The initial setting time of the sample tested at water-to-cement ratio 0.55 without SP, indicated as *PC w/o SP* in Figure 4.2 and Figure 4.3, was delayed when compared to the sample with SP. This may be due to the SP acting as a dispersant which leads to particles that are arranged with more sites for nucleation because of less flocculation that may in turn accelerate the reactions.

Although it is widely accepted that CSF does not significantly affect the setting time of concrete, an increase in initial setting time was observed with an addition of CSF (ACI, 2000). A larger increase in initial setting time was observed when cement was partially replaced by CSF. It is expected that the setting time of the mixes with CSF replacement will increase with an increase in water-to-cement ratio, however, a parabolic relationship was observed. The test method specified in SANS 50196-3 (2006) is user sensitive, the results will be discussed with this in mind. CSF is frequently used to gain early age strength in high strength concrete, but the results indicated that the setting time was increased especially in the case of mixes containing more than 600 kg/m^3 cementitious material. There may not have been enough PC to provide a high enough pH to start the reaction for the amount of CSF present.

As expected, an increase in initial setting time was observed with FA addition or replacement, as FA only participates in the reaction process at later ages and can have a retarding effect (ACI, 2002). The initial setting time for FA replacement increased with an increase in water-to-binder ratio. The initial setting time followed a parabolic curve with the peak at water-to-binder ratio 0.45. In Figure 4.3 FA has the same tendency to increase initial setting time when comparing PC-FA mixes at different cementitious material contents (and constant replacement levels).

An increase in initial setting time was observed when cement was partially replaced by GGBS and a larger increase in initial setting time was observed with both CSF and GGBS replacement. Previous research has shown that GGBS can increase setting time (ACI, 2003).

When cement was replaced by CSF and FA or when CSF and FA were added, the initial setting time increased. Addition results in a smaller increase in initial setting time than replacement.

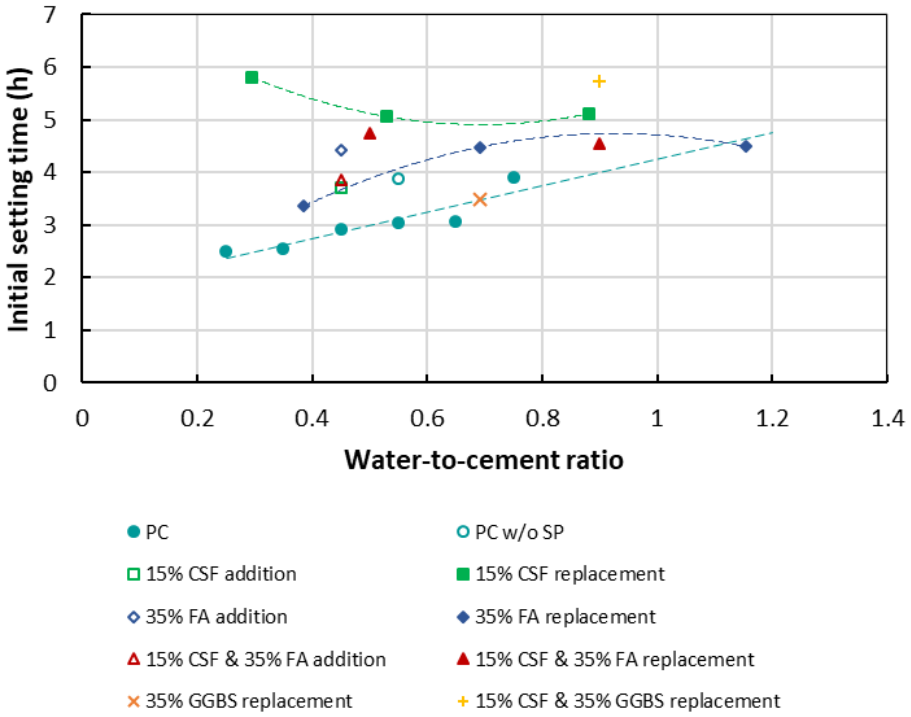

Figure 4.2 Effect of water-to-cement ratio on modified Vicat needle initial setting time

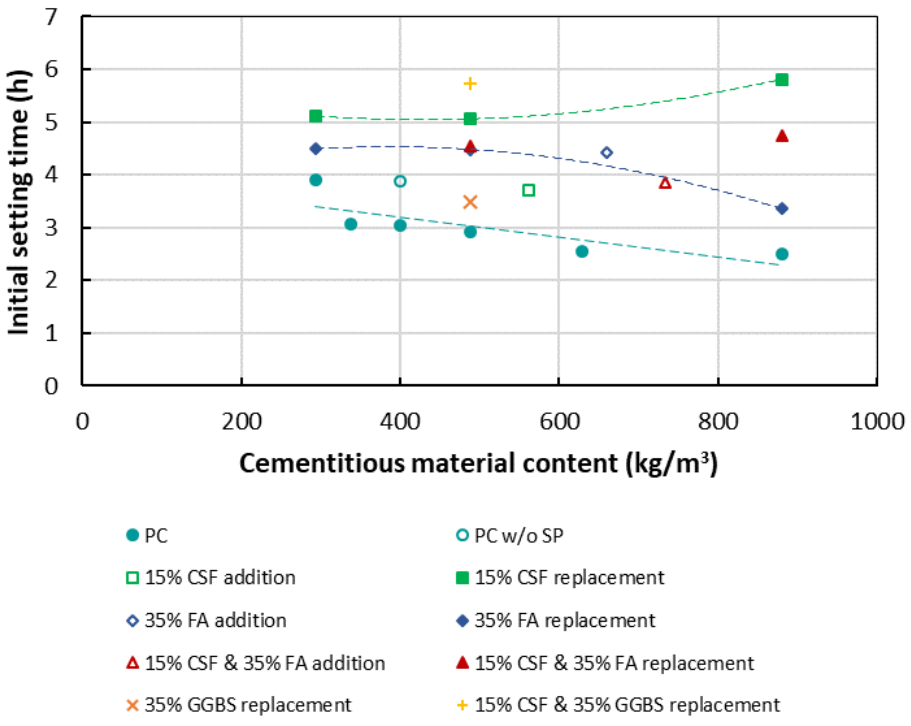

Figure 4.3 Effect of cementitious material content on modified Vicat needle initial setting time

The final setting times in Figure 4.4 and Figure 4.5 followed the same type of trends as the initial setting times with the exception that CSF and FA addition did not affect the final setting time. The average elapsed time between initial and final setting time for all mixes was approximately 3 hours, with a minimum and maximum time of approximately 2 and 5 hours.

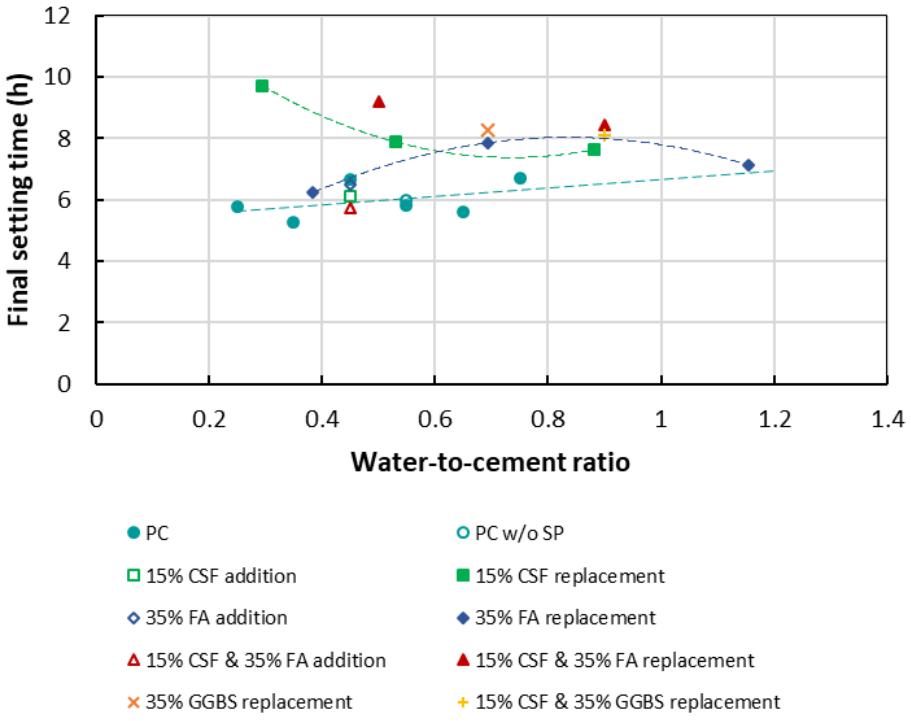

Figure 4.4 Effect of water-to-cement ratio on modified Vicat needle final setting time

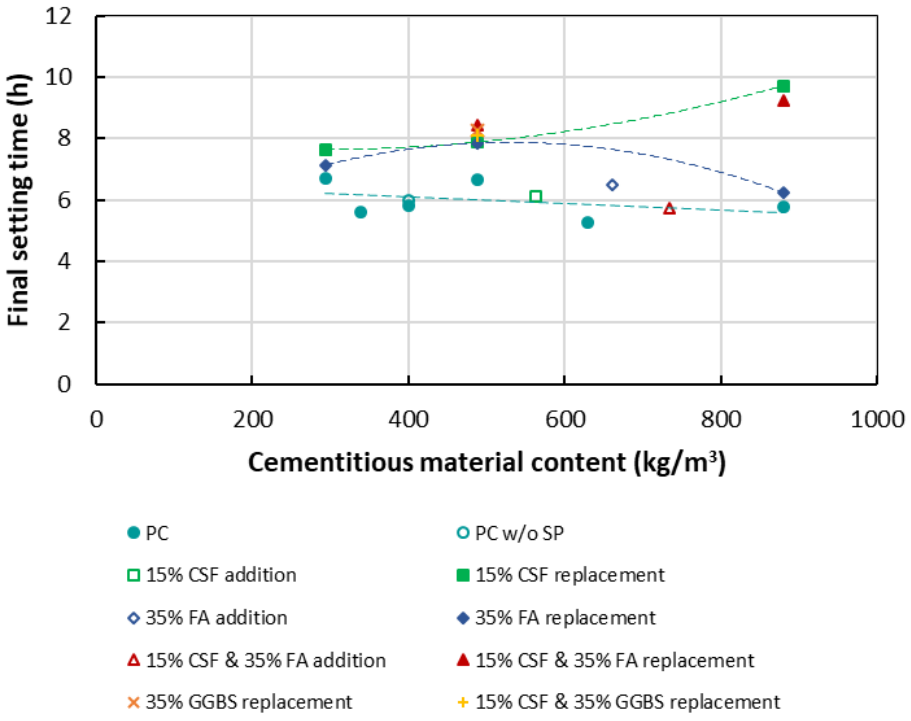

Figure 4.5 Effect of cementitious material content on modified Vicat needle final setting time

4.2.2 Isothermal calorimeter

The initial setting time calculated using the isothermal calorimeter data is shown in Figure 4.6 for water-to-cement ratio and Figure 4.7 for cementitious material content. The initial setting time decreased on average with an increase in water-to-binder ratio for the *PC* samples, and this could possibly be explained by the addition of SP delaying the reactions and thus the heat development. The lower the water-to-cement ratio the higher the dose of SP.

CSF addition and replacement brought on a delay in initial setting time. The increase in initial setting time with CSF replacement followed a parabolic curve and the increase in setting time was more pronounced at water-to-binder ratio 0.45 with respect to both water-to-cement ratio and cementitious material content (Figure 4.6 and Figure 4.7 respectively). CSF and FA addition also resulted in a delay in initial setting time. CSF and FA replacement increased the initial setting time at water-to-cement ratio 0.5 but reduced the initial setting time at water-to-cement ratio 0.9. This again may be due to the fact that the CSF content may be in excess of what could react with the available hydrates that formed during PC hydration. The same trends were observed when initial setting time was compared with respect to water-to-cement ratio and cementitious material content.

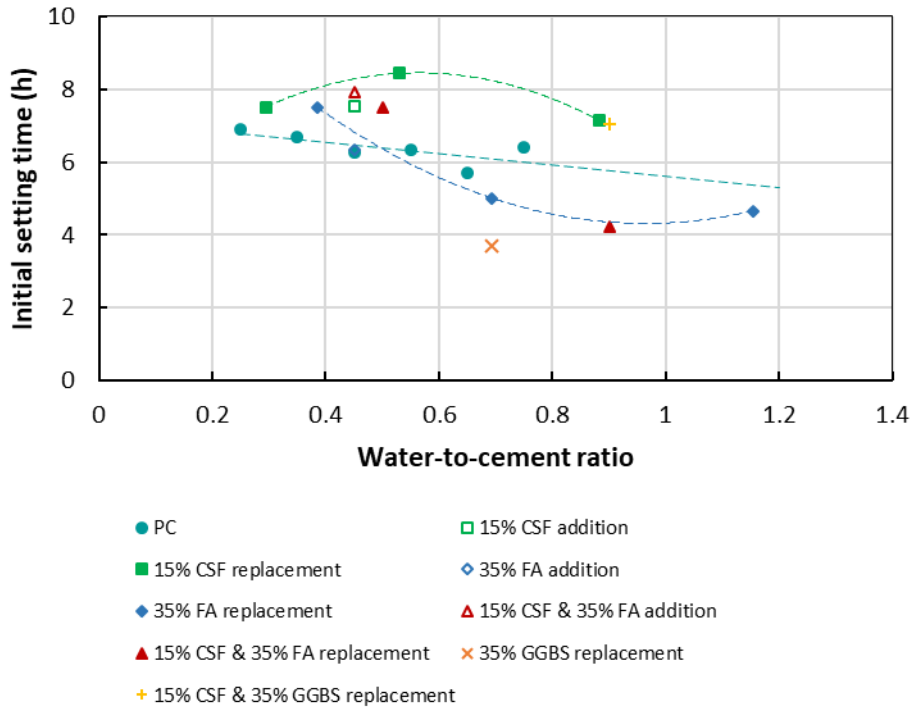

Figure 4.6 Effect of water-to-cement ratio on isothermal calorimeter initial setting time

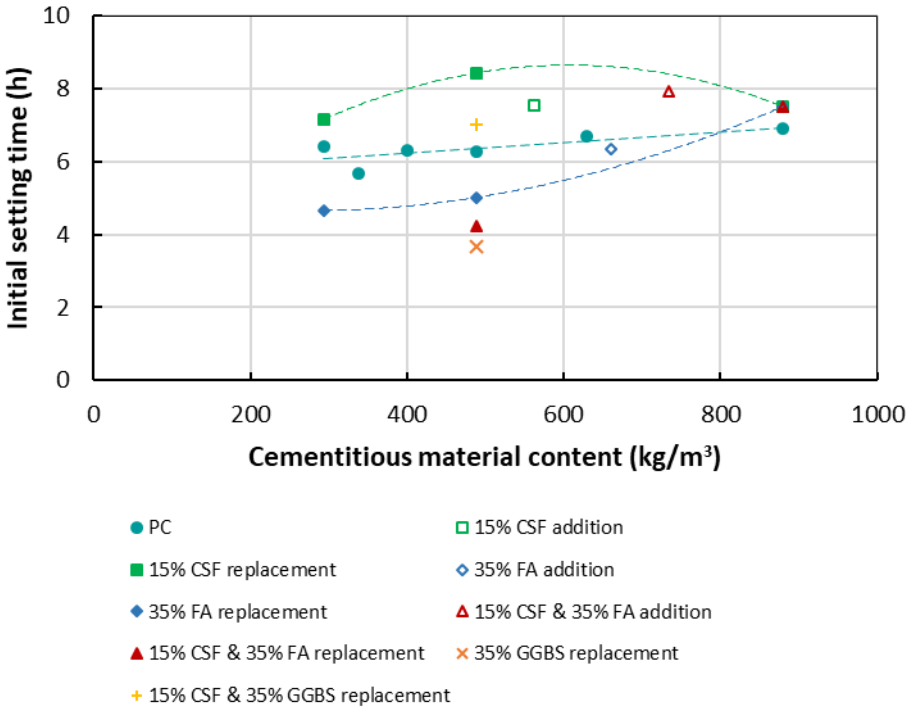

Figure 4.7 Effect of cementitious material content on isothermal calorimeter initial setting time

FA replacement increased the initial setting time at water-to-cement ratio 0.38 or at a cementitious material content of 880 kg/m^3 but decreased the initial setting time at higher water-to-cement ratios and cementitious material contents, this may have been due to the fact that more SP was used at the lower water-to-binder ratios.

GGBS replacement decreased the setting time and CSF and GGBS replacement increased the initial setting time.

The final setting time calculated using the isothermal calorimeter data is shown in Figure 4.8 for water-to-cement ratio and Figure 4.9 for cementitious material content. The final setting time for the PC samples decreased with an increase of water-to-cement ratio similar to the results from initial set. CSF addition decreased the final setting time while CSF replacement increased final setting time with respect to water-to-cement ratio. The same was observed with respect to cementitious material content except for a low cementitious material content which resulted in a decrease is final setting time.

FA addition decreased final setting time and FA replacement delayed final setting time at water-to-cement ratio 0.38 and water-to-cement ratio 1.15 but slightly decreased final setting time for water-to-cement ratio 0.69 in Figure 4.8. The final setting time with respect to cementitious

material content was delayed only at a cementitious material content of above 700 kg/m^3. CSF and FA addition decreased final setting and CSF and FA replacement decreased the final setting time when comparing equivalent cementitious material contents but increased final setting time with respect to equivalent water-to-cement ratios. GGBS replacement decreased final setting time. CSF and GGBS replacement increased final setting time with respect to cementitious material content and increased final setting time with respect to water-to-cement ratio.

The average time elapsed from initial set to final set was approximately 13 hours with the minimum and maximum time being 5.5 hours and 23.5 hours respectively.

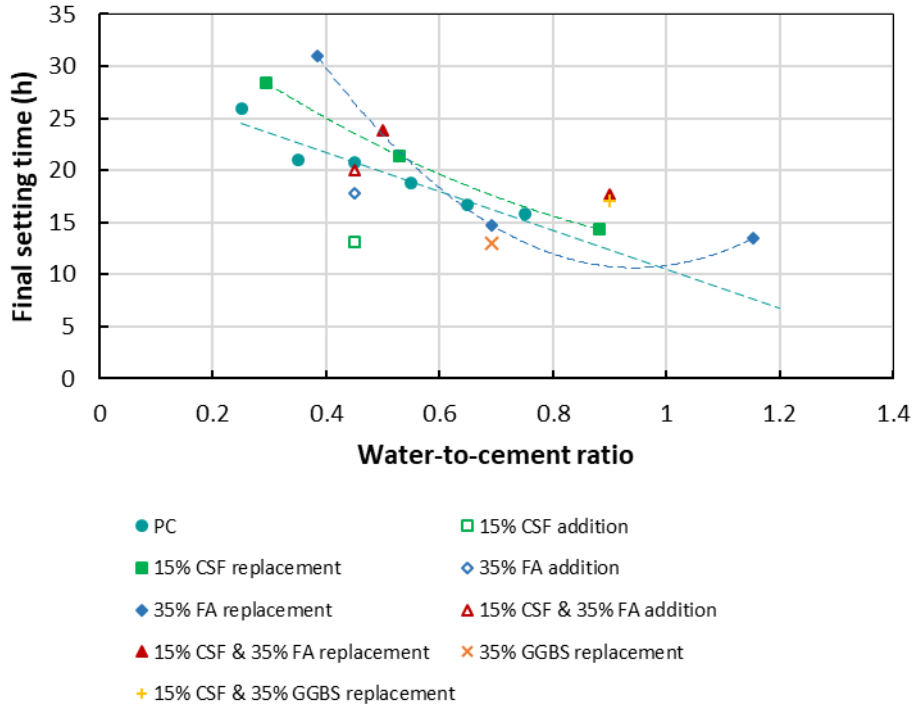

Figure 4.8 Effect of water-to-cement ratio on isothermal calorimeter final setting time

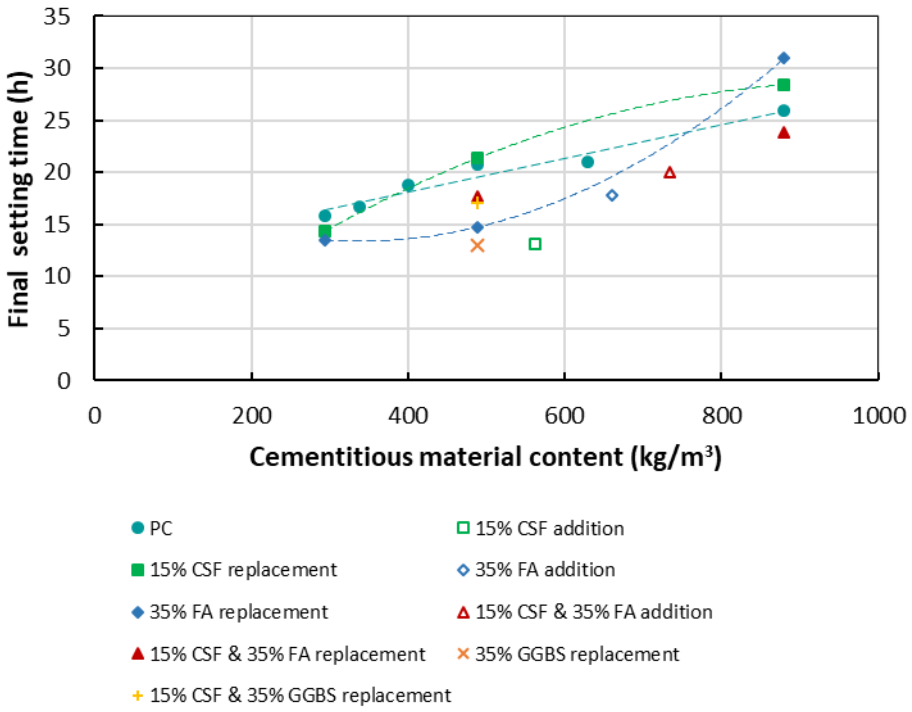

Figure 4.9 Effect of cementitious material content on isothermal calorimeter final setting time

4.2.3 Comparison of setting times

The relationship between water-to-binder ratio and initial or final setting time for both the modified Vicat needle test and isothermal calorimeter data is shown in Figure 4.10 and Figure 4.11 respectively. The setting times determined from the isothermal calorimeter were longer that that determined from the modified Vicat needle method. This difference in time is due to the fact that the two methods have very different mechanisms for determining the setting time. The calorimetry method is based on the heat of hydration which is a measure of the chemical reactions while the modified Vicat needle method is based on the penetration force against microstructure development which is a physical process. Another reason for the shorter setting time from the modified Vicat needle method is the accumulation from the exothermic reaction from cement hydration which can result in acceleration of hydration from the increased temperature of the larger specimen compared to the isothermal calorimeter specimen (Wyrzykowski et al., 2017).

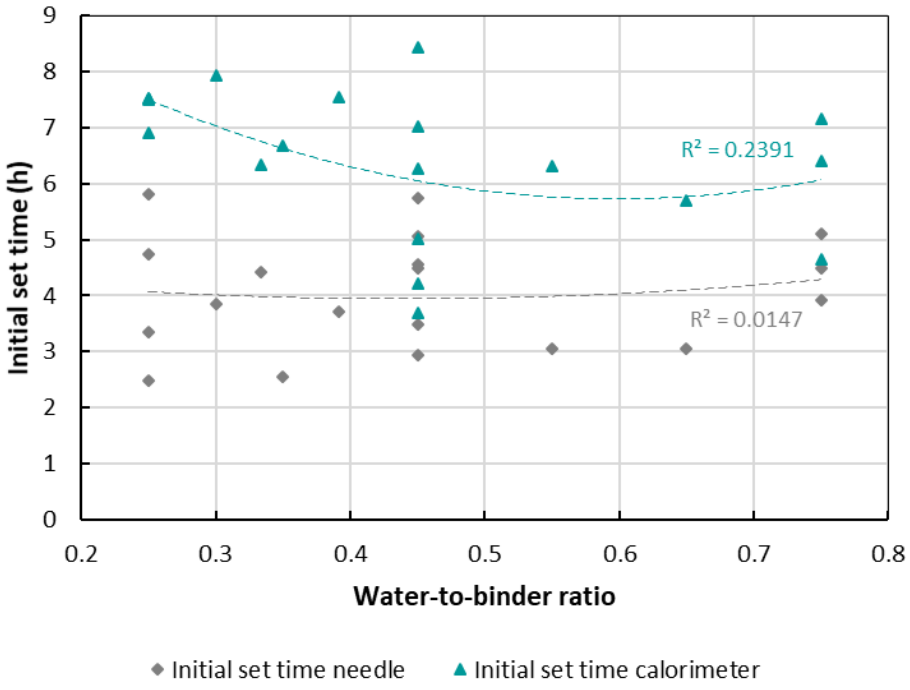

Figure 4.10 Initial setting time for modified Vicat needle versus isothermal calorimeter

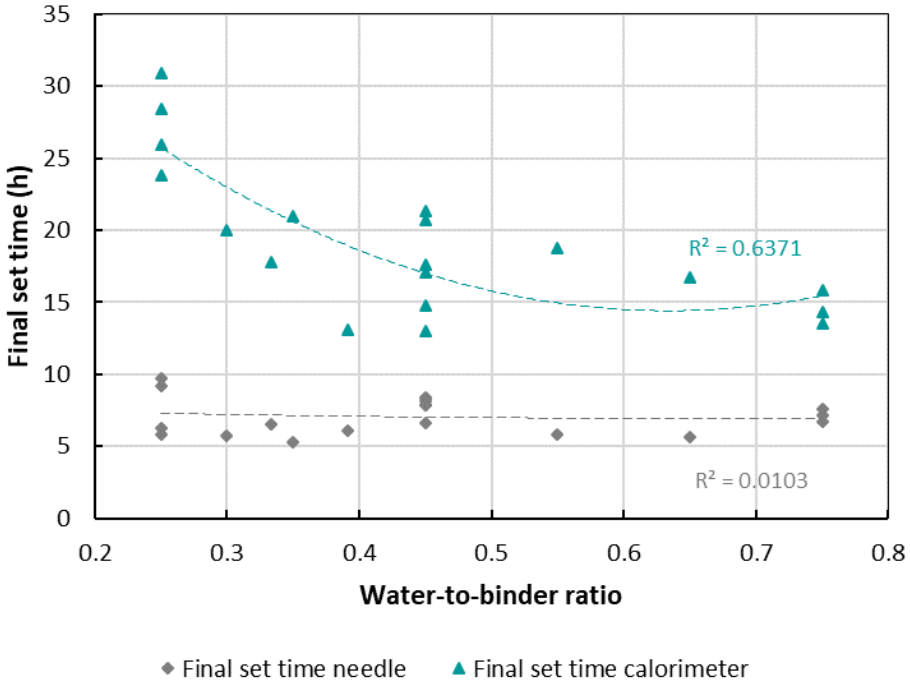

Figure 4.11 Final setting time for modified Vicat needle versus isothermal calorimeter

Figure 4.12 illustrates a moderate correlation between the isothermal calorimeter setting time and modified Vicat needle setting time. Calibration of setting times obtained from isothermal calorimeter data may be necessary to account for the use of SP, SCMs, and even the type of cement used, to relate the time with the modified Vicat needle time. It should be noted that an alternative method as well as a more accurate method than the modified Vicat needle test to determine the setting time used for autogenous shrinkage initiation is desired.

The modified Vicat needle testing method indicated an increase in setting time when any SCM was used where the setting time calculated with isothermal calorimeter results varied with the specific SCM. The setting time will have an effect on autogenous shrinkage, and "time zero" values based on different methods may significantly change the trends that are observed.

It is assumed that the initial setting time from the isothermal calorimeter corresponds to the time when an initial skeleton structure is formed in the system and this was used as the "time zero" for autogenous shrinkage. The shrinkage results will be interpreted using the isothermal calorimeter setting times as calculated and emphasis will not be put into calibrating the curve to fit the equality line.

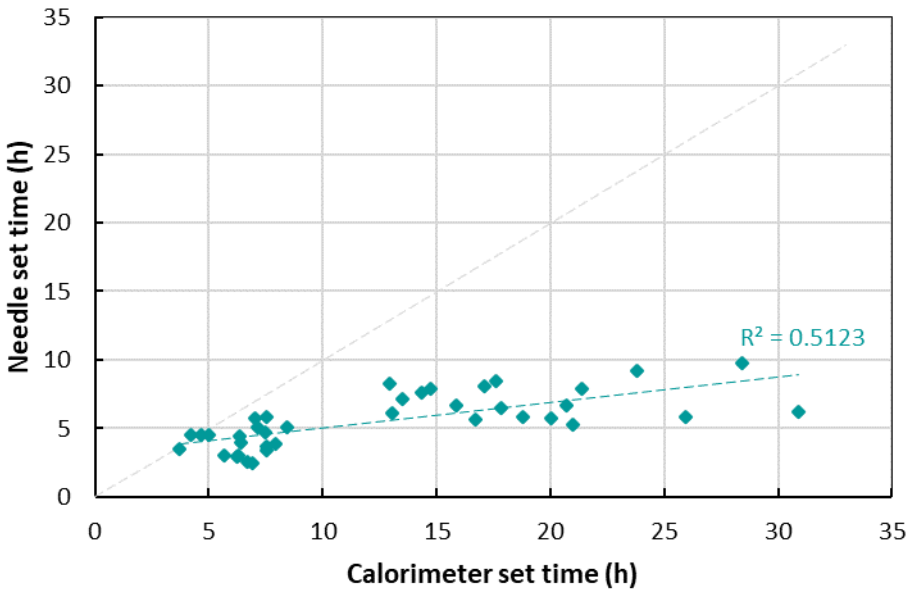

Figure 4.12 Relationship between the modified Vicat needle and isothermal calorimeter setting times

4.3 THERMAL EFFECT

Thermal effects are discussed in this section. The semi-adiabatic temperature rise is discussed first followed by the isothermal calorimetry data. The temperature data measured in the beams can be seen in Appendix B.

4.3.1 Semi-adiabatic Temperature Rise

As all the mixes were not tested on the same day but weeks apart, some environmental temperature effects were observed. The temperature in the temperature-controlled room where the tests were conducted was not constant. Figure 4.13 clearly shows the effect of ambient temperature on the semi-adiabatic temperature rise results. *Ambient 1* was the ambient temperature for *wc 0.25*, *wc 0.35*, *wc 0.45* and *wc 0.55* and *Ambient 2* was the ambient temperature for *wc 0.65* and *wc 0.75*. The temperature of the mixes converges to the ambient temperature after some time. The first four mixes were tested for approximately 75 hours while the other two mixes were tested for approximately 290 hours. A similar trend was seen for all mixes and another example is shown in Figure 4.14 where the effect of ambient temperature between seasons can be observed for *wc 0.75* which converges to ambient temperature *Ambient 2* and for *wb 0.75 C* and *wb 0.75 F* which converges to ambient temperature *Ambient 6*.

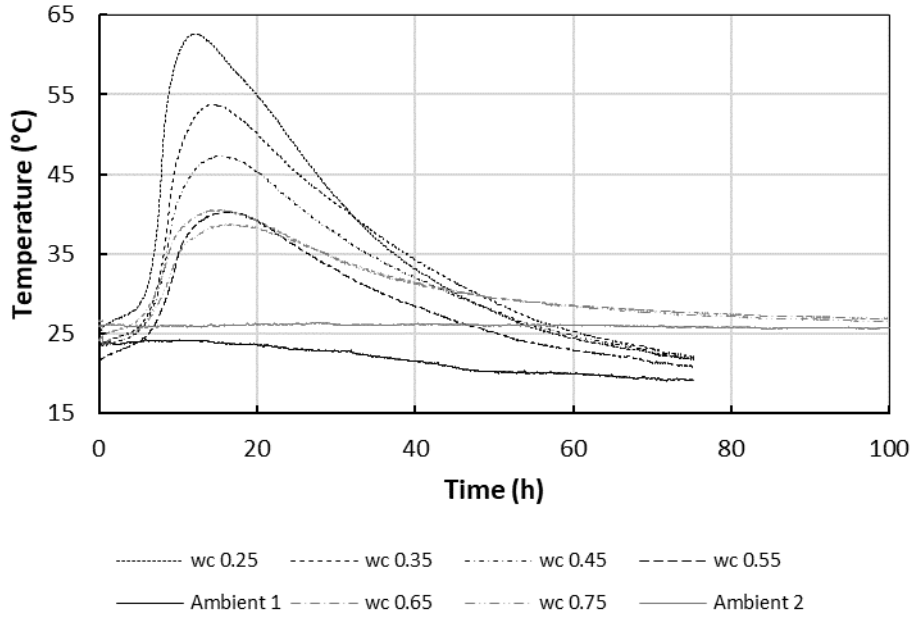

Figure 4.13 Semi-adiabatic temperature rise with time for wc 0.25, wc 0.35, wc 0.45, wc 0.55, wc 0.65 and wc 0.75

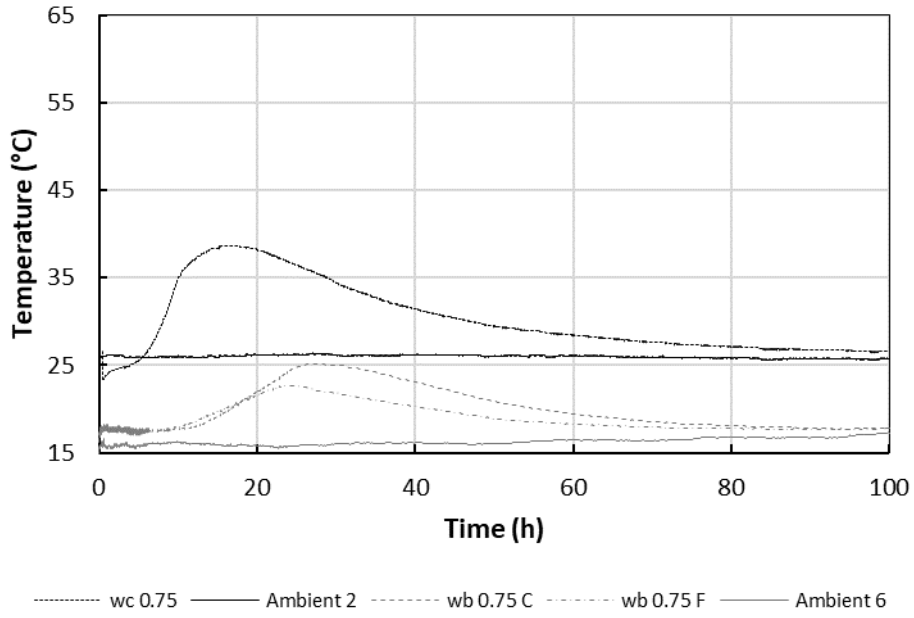

Figure 4.14 Semi-adiabatic temperature rise with time for wc 0.75, wb 0.75 C and wb 0.75 F

In an effort to be able to better compare the semi-adiabatic temperature rise, the temperature change was calculated and is used in the rest of the document.

Influence of water-to-binder ratio

The semi-adiabatic temperature changes for the PC only mixtures are shown in Figure 4.15. Generally, the time of maximum temperature rise increased with an increase in water-to-cement ratio but there was a shift for the *wc 0.65* and *wc 0.75* mixes. However, this can be explained by the average ambient temperature being 5°C higher than the other four mixes. The higher ambient temperature had an accelerating effect on the hydration reactions and gave rise to the maximum peaks occurs earlier than expected.

Water has a much larger heat capacity than cement, 4.18 J/(g·K) vs. 0.75 J/(g·K) thus a smaller temperature rise is expected when the water-to-binder ratio increased (Bentz and Peltz, 2008). The amount of cement in the sample decreased with an increase in water-to-cement ratio which implies less heat generation with an increase in water-to-cement ratio.

The temperature for the *wc 0.25* sample decreased more rapidly after the maximum peak than the other high water-to-cement ratio samples. Free water, if available, may not have been able to

penetrate the dense microstructure of the hydrated cement paste to reach the remnants of the unhydrated PC particles and self-desiccation took place as suggested in literature (Neville, 2011).

The maximum temperature change of 37.6 °C occurred in the *wc 0.25* sample and the minimum temperature change of 15.1 °C occurred in the *wc 0.75* sample.

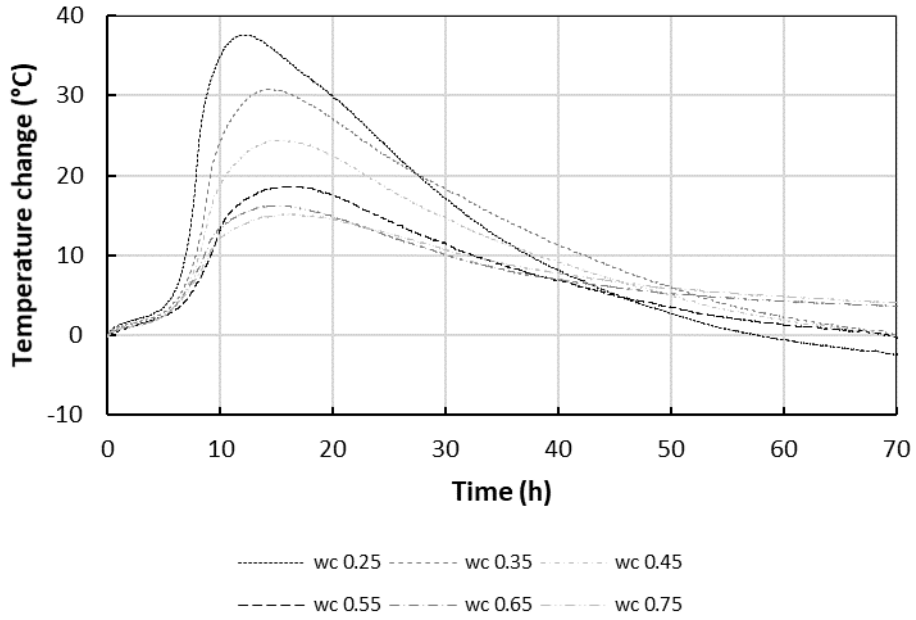

Figure 4.15 Semi-adiabatic temperature change with time for PC mixtures

The maximum semi-adiabatic temperature change with cement content and cementitious material content for all mixes are shown in Figure 4.16 and Figure 4.17 respectively. The maximum temperature decreased with a decrease in cement content (and by default cementitious material content) for the PC mixtures. When the cement content was increased from 293 kg/m^3 to 880 kg/m^3, the maximum temperature change increased about 2.5 times.

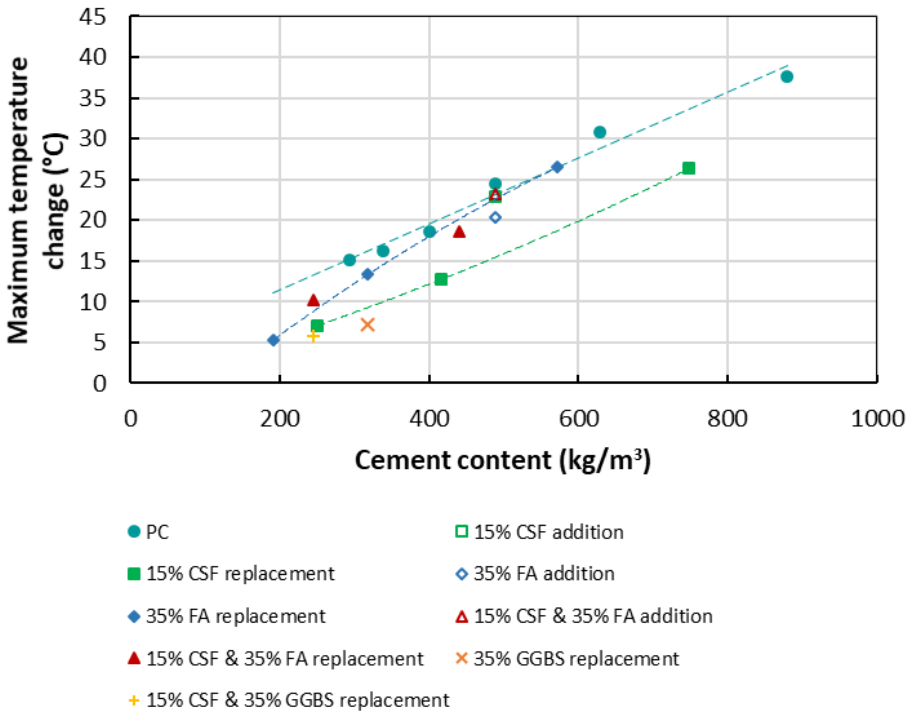

Figure 4.16 Maximum semi-adiabatic temperature change with cement content

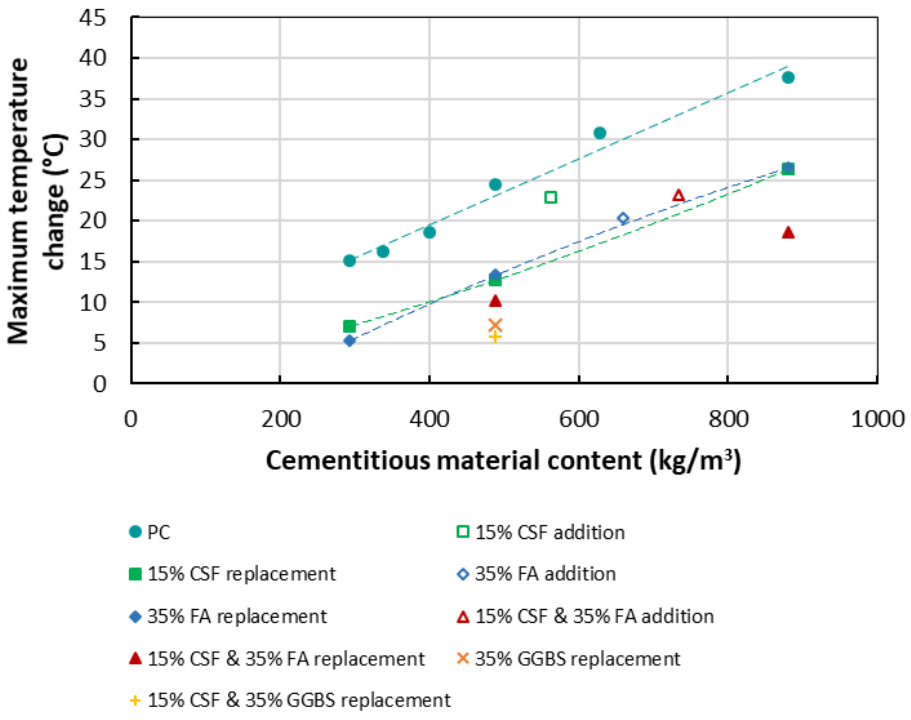

Figure 4.17 Maximum semi-adiabatic temperature change with cementitious material content

Influence of CSF

The semi-adiabatic temperature change with time graphs for mixes containing SCMs can be found in Appendix C. For all cement contents, the maximum temperature change was reduced by CSF replacement as shown in Figure 4.16. The time at which the maximum temperature occurred was also delayed. This is expected and corresponds to literature on semi-adiabatic calorimetry.

The percentage reduction of maximum temperature change due to CSF replacement decreased with an increase in cementitious material content as shown in Figure 4.17. Conversely, the percentage delay in maximum temperature change time increased with an increase in cementitious material content. The percentage reduction in maximum temperature change at 293 kg/m^3, 489 kg/m^3 and 880 kg/m^3 with CSF replacement (green markers and line) was 53%, 47% and 30% respectively and the percentage delay time at which this occurred was 58%, 81% and 93% respectively. The maximum temperature change for CSF addition was slightly reduced (6%) and the maximum change time delayed by 25%. The maximum temperature change with cementitious material content for CSF replacement and PC samples followed almost the same trend and in this case was offset by approximately 8°C in Figure 4.17. The reduction in temperature and delay in maximum temperature may be explained by the CSF particles conglomerating as explained in Section 3.2.3 or by the high replacement rate resulting in a dense microstructure where water cannot penetrate, and hydration ceased. Literature suggests that SF only reacts later and only the filler effect is present at this earlier stage which can also explain this behaviour (Hjorth et al., 1988, Justnes, 1988, Lothenbach et al., 2011).

Influence of FA

FA replacement did not have an effect on the maximum temperature change at higher cement contents when comparing the same cement contents as can be seen in Figure 4.16 at a cement content of 572 kg/m^3. The maximum temperature change with FA replacement converges with the PC line when the cement content is increased. FA addition did however lower the maximum temperature change.

The percentage reduction of maximum temperature due to FA replacement decreased with cementitious material content (blue markers and line in Figure 4.17) (65%, 45% and 30% for 293 kg/m^3, 489 kg/m^3 and 880 kg/m^3 cementitious material contents respectively), conversely, the percentage delay in time at which this occurred increased with cementitious material content (36%, 49% and 71% for 293 kg/m^3, 489 kg/m^3 and 880 kg/m^3 cementitious material contents respectively). The FA addition produced a reduction in maximum temperature change of 16%

and a 20% delay in the time at which this occurs. The maximum temperature change with FA addition followed the same trend as with FA replacement for each unit cementitious material in Figure 4.17. The reduction and delay in maximum temperature change time can be explained by the tendency of FA to retard the hydration of a PC-FA system explained in Section 2.4.3.

Influence of GGBS

The maximum temperature change was significantly reduced by 71% compared to the effect of CSF and FA at a cementitious material content of 489 kg/m^3. The time at which this occurred was also delayed by 43%. This is expected because of the slow reaction speed of GGBS which is explained in Section 2.4.4.

Influence of multiple SCMs

The effects of the SCMs on their own were compounded when used in a ternary blend. When PC was replaced by both CSF and FA the maximum temperature change was reduced by 58% and 50% at 489 kg/m^3 and 880 kg/m^3 cementitious material contents respectively (in Figure 4.17) and the time at which these maximum temperature changes occurred were delayed by 78% and 153% respectively. The maximum temperature change was decreased by only 5% when both CSF and FA were added at a cementitious material content of 489 kg/m^3 and the time at which this maximum took place was delayed by 43%. When PC was replaced by both CSF and GGBS the maximum temperature change was reduced by 76% and the time at which this occurred was delayed by 133%. CSF and FA addition had the same effect on maximum temperature change than FA addition and FA replacement with respect to cementitious material content in Figure 4.17.

In summary for Figure 4.16, the addition of SCM had less of an effect on maximum temperature change with respect to cement content than SCM replacement. FA addition lowered the maximum temperature change while both CSF and FA addition while CSF addition had a negligible effect. GGBS had the biggest temperature lowering effect when used alone or with CSF. FA replacement was more effective in lowering the temperature at a lower cement content but had no effect at higher cement contents. CSF replacement lowered the maximum temperature consistently with all cement contents. This may be caused by agglomeration of CSF particles and the material behaving like a coarser material.

With respect to cementitious material content in Figure 4.17, CSF replacement, FA replacement and FA addition had the same temperature lowering effect with cementitious material content.

CSF addition had the least of an effect of all the SCM additions or replacements. GGBS replacement and CSF and GGBS replacement lowered the temperature the most of all the SCM additions and replacements. Interestingly, when CSF was used with another SCM, the other SCM effects governed because of the higher replacement or addition level at 35% compared to the replacement or addition level of 15% for CSF.

4.3.2 Isothermal Calorimetry

Influence of water-to-binder ratio

The heat flow and cumulative heat with time for the PC samples is shown in Figure 4.18. The heat flow curves are labelled "HF" and the cumulative heat curves are labelled "CH". The results are in agreement with studies conducted by Lura et al. (2017) and Pane and Hansen (2005) which found that a lower water-to-binder ratio mix produces a lower cumulative heat compared to a higher water-to-binder sample. This is due to the fact that more space is available for hydration products to form in a higher water-to-binder environment than a lower water-to-binder environment and full hydration may not be possible for a water-to-binder ratio of about 0.4 or less and self-desiccation may occur (Lothenbach et al., 2011). Research done by Nocuń-Wczelik and Czapik (2013), Kumar et al. (2012) and Łaźniewska-Piekarczyk (2013) concluded that superplasticisers may significantly increase the induction period on the heat evolution curve and retard the hydration overall. The retarding effect of the SP can be seen in Figure 4.18 where the peak heat flow of the mixes "shifted" right with an increase in SP content (which corresponded to a decrease in water-to-binder ratio). A decrease in maximum heat flow and cumulative heat with a decrease in water-to-binder ratio is also observed.

The cumulative heat per gram cement with cement content and cementitious material content for all of the mixes are shown in Figure 4.19 and Figure 4.20 respectively. The total and normalised graphs for maximum heat flow with cement content and cementitious material content can be found in Appendix D. The total cumulative heat with cement content and cementitious material content can be found in Appendix D as well.

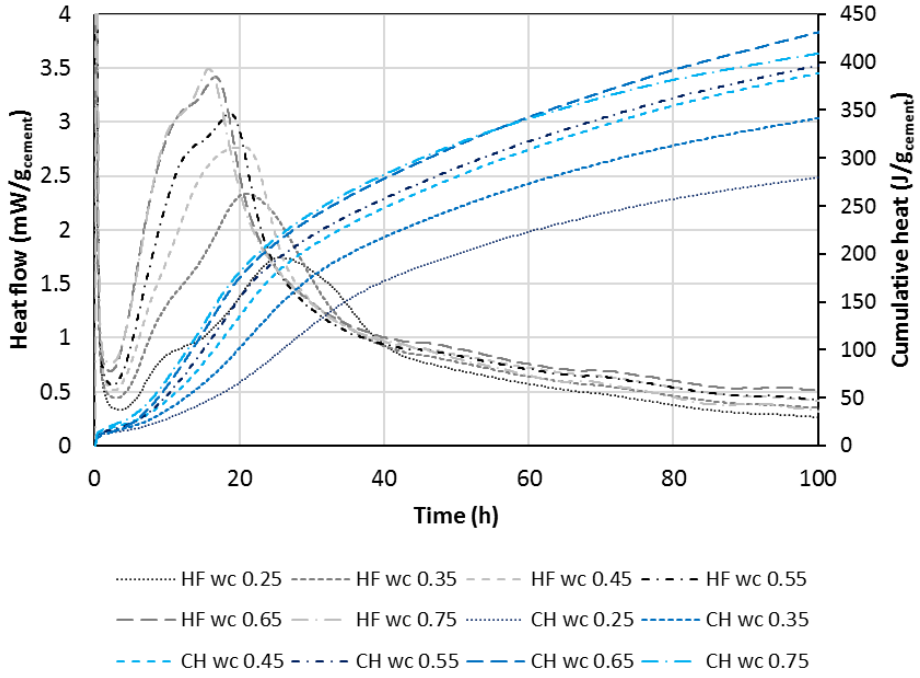

Figure 4.18 Isothermal calorimetry heat flow and cumulative heat with time for PC samples (HF=heat flow; CH=cumulative heat)

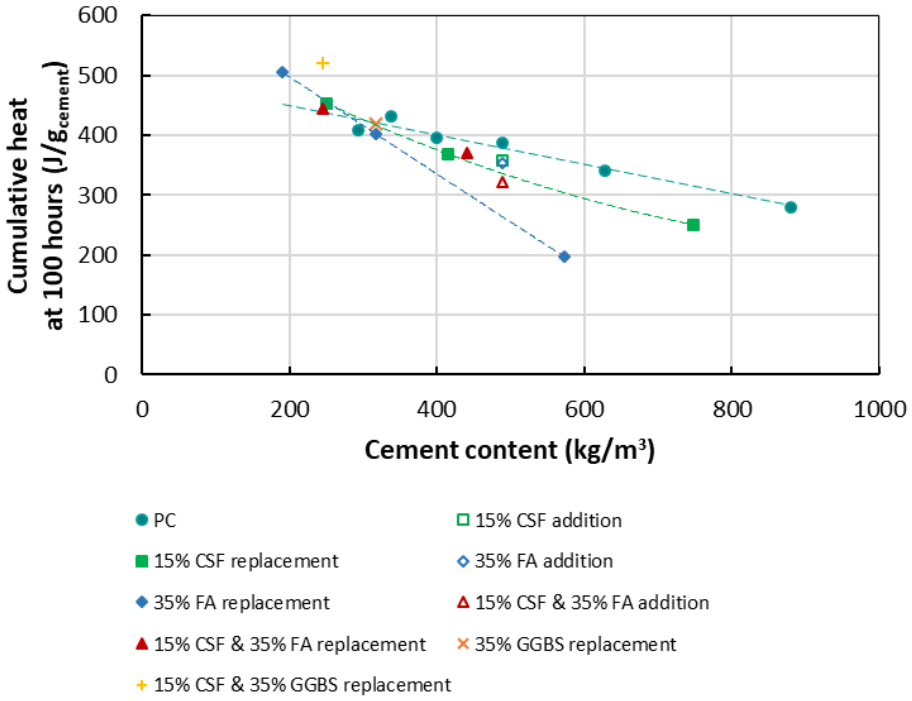

Figure 4.19 Normalised cumulative heat released at 100 hours with cement content

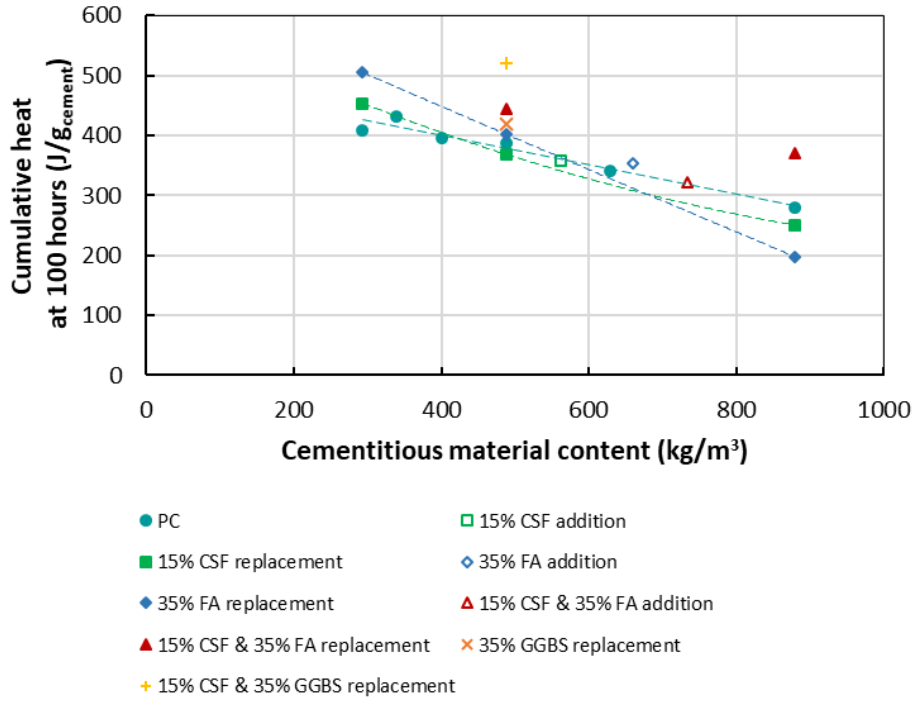

Figure 4.20 Normalised cumulative heat released at 100 hours with cementitious material content

Influence of CSF

The heat flow and cumulative heat curves for the mixes containing SCMs are in Appendix D. The peak heat flow was reduced when PC was replaced by CSF which is not in agreement with literature but can be explained by the CSF particles possibly behaving as larger particles due to flocculation as explained in Chapter 3.2.3. Hu et al. (2014) found that the heat flow peak was reduced when the fineness of the cement was reduced which corresponds to the belief that the particles may have clumped together to act as bigger particles.

The cumulative heat was reduced with respect to cement content in Figure 4.19 when PC was partially replaced with CSF for cement contents above approximately 300 kg/m^3. CSF addition also reduced the cumulative heat but only by 8%.

It appears that CSF addition and CSF replacement did not affect the cumulative heat significantly with respect to cementitious material content in Figure 4.20 showing only about a 10% variation in cumulative heat at 100 hours.

Influence of FA

The peak heat flow was reduced when PC was replaced by FA for *wc 0.25* and *wc 0.45* and increased for *wc 0.75*. Adding FA also resulted in an increase in peak heat flow.

FA replacement increased the cumulative heat at cement contents below about 300 kg/m^3 but reduced the cumulative heat above 300 kg/m^3 as can be seen in Figure 4.19. This effect was less noticeable with cementitious material content in Figure 4.20. FA addition produced a relatively small difference in cumulative heat with respect to both cement content and cementitious material content.

Influence of GGBS

The peak heat flow was reduced as expected when PC was partially replaced by GGBS while Figure 4.19 and Figure 4.20 indicated no increase in cumulative heat per unit cement, an increase in cumulative heat was observed per unit cementitious material.

Influence of multiple SCMs

The peak heat flow was increased by partially replacing PC with CSF and FA for *wc 0.25* and *wc 0.45* or replacing with CSF and GGBS in *wc 0.45*. The peak heat flow was reduced when CSF and FA were added to *wc 0.45*.

Similarly, the cumulative heat was not significantly influenced when PC was partially replaced by CSF and FA when compared to PC samples with similar cement contents, but the cumulative heat was higher when the cementitious material content was compared. CSF and GGBS replacement resulted in the highest cumulative heat.

Figure 4.19 and Figure 4.20 both indicate that for a higher cement content or cementitious material content enough time may not have elapsed for the SCMs to begin hydrating properly thus contributing to the reactions and thus the thermal processes. The replacement levels were possibly too high, and enough hydration products might not have been present at 100 hours to allow for contribution to the reactions.

4.4 AUTOGENOUS SHRINKAGE TESTING

Autogenous shrinkage measurement was done as described in Section 3.8.2. The shrinkages in the beams were measured in the horizontal direction and the corrugated tubes were measured in the vertical direction.

Figure 4.21 shows the autogenous shrinkage results of a beam and a corrugated tube for the concrete with a water-to-cement ratio of 0.25. Shrinkage was measured at both ends of the beam and the total shrinkage is given. The test results presented in Figure 4.21 is from the start of measurement and is not zeroed to any reference point in time (see Section 2.8.5). Four distinct shrinkage stages were observed (Holt, 2011):

- **I**: For the first 5 hours approximately, the shrinkage increased at a relatively slow rate in the beam samples. Rapid settlement took place in the corrugated tube samples followed by the same relatively slow rate than for the beam shrinkage.
- **II**: An inflection point was present at about 4 hours where after shrinkage occurred more rapidly and slowed down after approximately 8 hours. Some mixes reabsorbed bleed water through small capillary suction and expansion took place. This was present in mixes with a higher water-to-cement ratio.
- **III**: Another inflection point was present at 8 hours, and shrinkage resumed and slowed down after approximately 10 hours. The maximum temperature in the beam was measured around the end of this stage.
- **IV**: A third inflection point was present at about 10 hours where after steady but slow shrinkage took place.

These trends were visible for the majority of the mixtures cast. The rest of the data captured from the time of instrumentation up until 200 hours can be found in Appendix E.

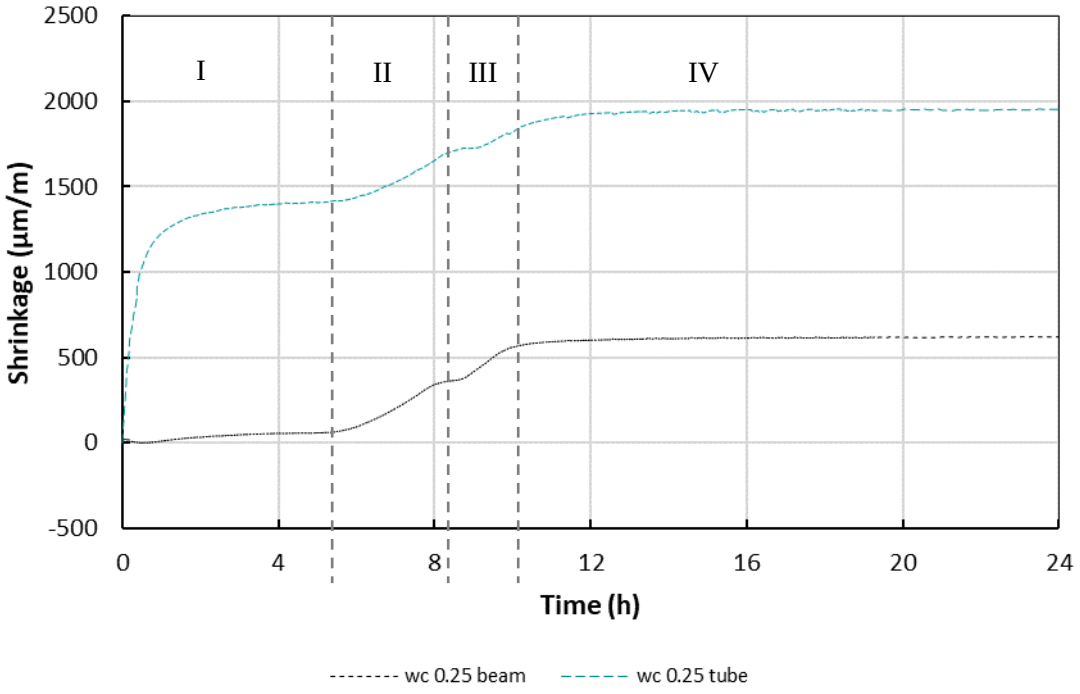

Figure 4.21 Autogenous shrinkage results from testing in a beam and a corrugated tube for the concrete with a water-to-cement ratio of 0.25

The same mixture compositions were casted twice and results for the water-to-binder ratio 0.25 can be seen in Figure 4.22. The values obtained from the beam test method were within 35 µm/m of each other while the data from the tubes differed by 894 µm/m. This difference changed to 45 µm/m and 132 µm for the beam and corrugated tube respectively when the data was zeroed with the modified Vicat needle setting time and to 35 µm/m and 98 µm/m for the beam and corrugated tube respectively when the data was zeroed with the isothermal calorimeter initial setting time. A typical within-operator standard deviation for the same mix has been reported at 130 µm/m and the highest precision obtained by a single operator in both automatic and standard measurements corresponded to a standard deviation of about 50 µm/m (Wyrzykowski et al., 2017). The results of the beam method were far better than the results of the corrugated tube testing method, but the latter is still valuable to be able to determine the propensity for settlement of the various mixture compositions. To prove repeatability, more samples would need to be tested to be able to carry out statistical analysis. A possible reason for the larger variation in the results from the corrugated tube setup include variations in the corrugated tube moulds providing possible restraint against movement and early age settlement of the specimen before a solid structure was developed.

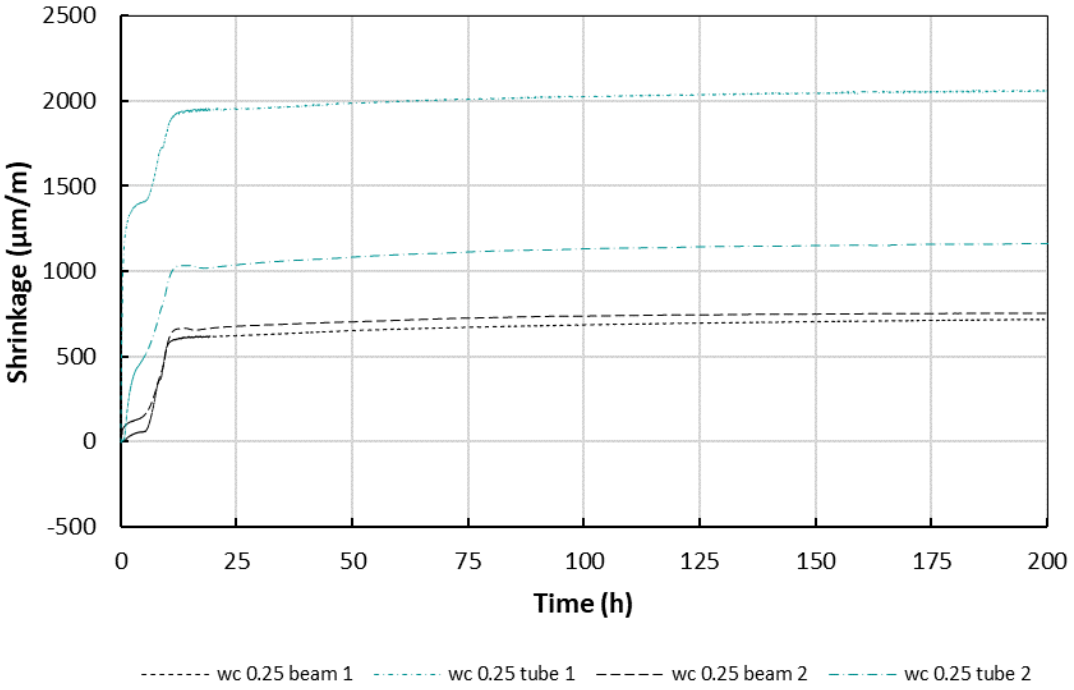

Figure 4.22 Two sets of autogenous shrinkage testing for water-to-cement ratio 0.25

Thermal expansion or contraction is present in all the shrinkage measurements. As the qualitative effect of altering material properties is of interest, the thermal component was not removed, making it possible to interpret the effect of binder composition and content on actual autogenous shrinkage in a field situation. When autogenous shrinkage is referred to from this point forward it is implied that the thermal movements are included and will be referred to as shrinkage to simplify explanations.

The data was zeroed using the modified Vicat needle final setting time and the isothermal calorimeter initial setting time. The results were compared to determine the influence of the binder content and composition on shrinkage at 75 hours which is roughly equal to 3 days. The effect of mixture design on early age shrinkage is discussed in this section.

4.4.1 Influence of Water-to-cement Ratio

Figure 4.23 shows the effect of water-to-cement ratio on shrinkage. The effect of water-to-cement ratio was clear in the results obtained for the beam testing method but the results from the corrugated tube were difficult to interpret. By using the isothermal calorimeter initial setting time to zero the results, all the samples experienced shrinkage although expansion occurred at early

ages for all the water-to-cement ratios above 0.25 for the beam testing method, but the isothermal calorimeter initial setting time zero method excluded the expansion period for the water-to-cement ratio mixtures below 0.55 and less shrinkage was observed overall.

The expected higher amount of settlement from the mixtures with a higher workability influenced the corrugated tube shrinkage reading significantly, to the point that the *wc 0.35* and *wc 0.45* shrinkage exceeded the shrinkage of *wc 0.25* when the modified Vicat needle final setting time was used, which is unlikely. Only the results from the beam testing method will be discussed as the results from the corrugated tube method was deemed inconclusive.

Early age shrinkage increased with a decrease in water-to-cement ratio for both reference points used in the beam samples as was expected from literature due to the increase in cement content and increased tendency for self-desiccation to be present. The shrinkage for *wc 0.25* was 18 times that of *wc 0.55* when zeroed with the modified Vicat needle final setting time and 9 times that of *wc 0.55* when zeroed with the isothermal calorimeter initial setting time.

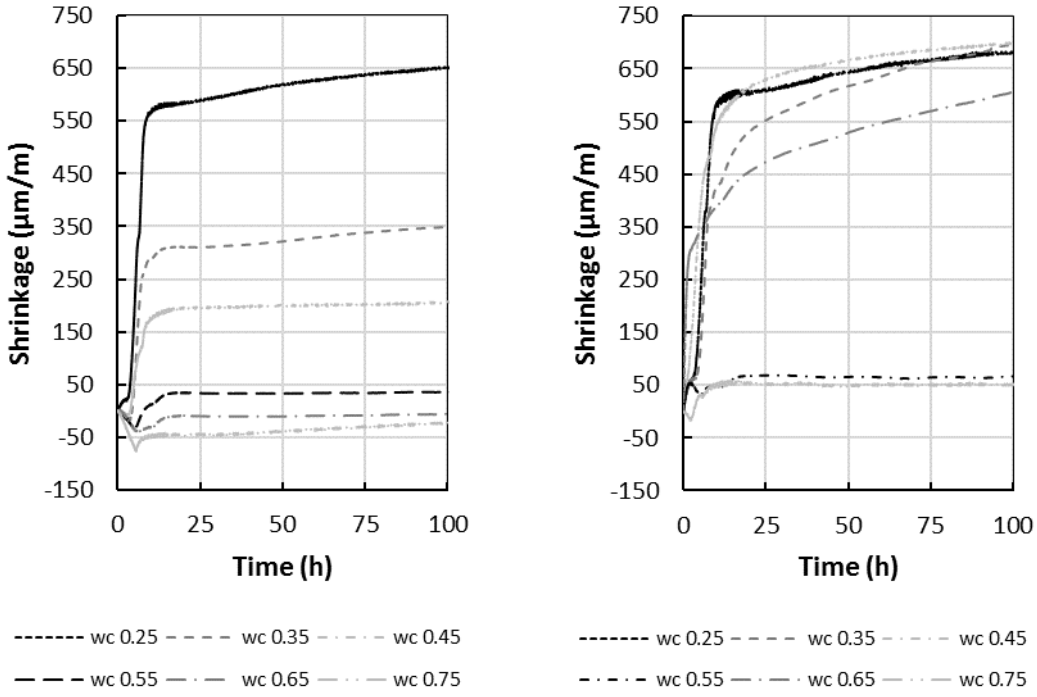

a) *b)*

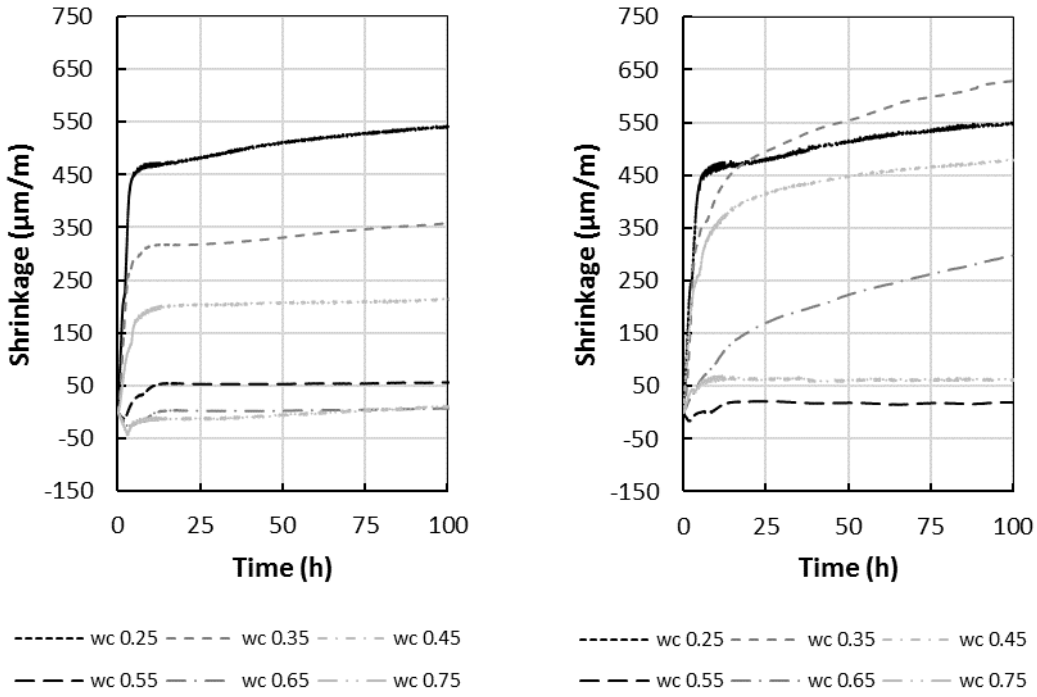

c) *d)*

Figure 4.23 Autogenous shrinkage for mixtures without additions tested in beams (a & c) and corrugated tubes (b & d) and zeroed with the modified Vicat needle setting time (a & b) and zeroed with the calorimeter setting time (c & d)

The beam shrinkage at 100 hours for both reference points are shown in Figure 4.24 and indicates that the initial setting time from isothermal calorimeter data may be used to estimate the starting point for autogenous shrinkage for this study. As suggested by literature, shrinkage was only significant at lower water-to-cement ratios where unhydrated cement was present and further hydration was constrained by lack of space available for hydrates to form, the relative humidity decreased and self-desiccation was intensified (Paillere et al., 1989, Addis, 1994, Rao, 2001, Tian, 2006, Lothenbach et al., 2011).

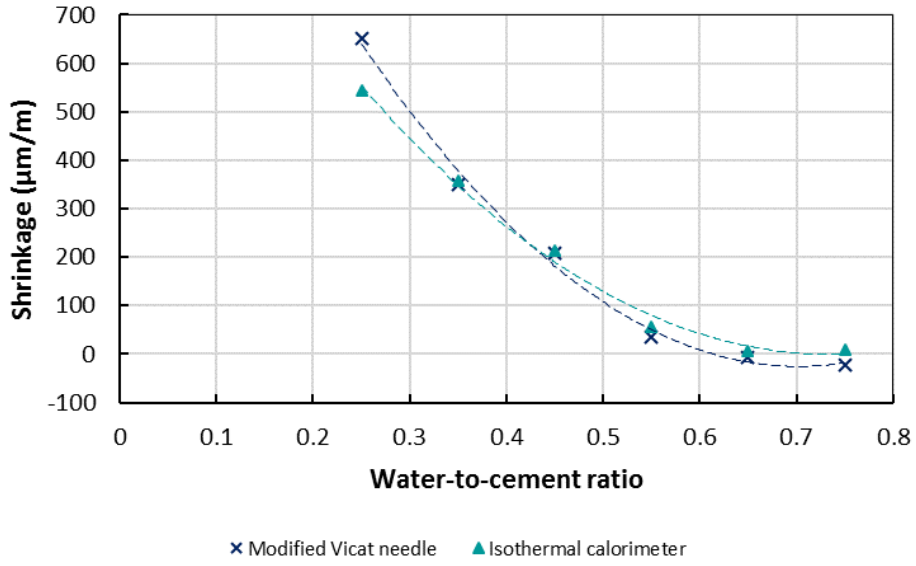

Figure 4.24 Beam shrinkage with reference to modified Vicat needle and isothermal calorimeter setting time

4.4.2 Influence of CSF

Figure 4.25 shows the effect of cement content and Figure 4.26 the effect of cementitious material content on shrinkage with modified Vicat needle reference. The same graphs with respect to the isothermal calorimeter setting time is located in Appendix E. Generally, the shrinkage was reduced by replacing with or even adding CSF. A decrease in water-to-binder ratio in the samples containing CSF brought on a decrease in shrinkage.

When comparing Figure 4.25 and Figure 4.26 it is apparent that by incorporating CSF the shrinkage can be reduced significantly, by replacing 15% of PC with CSF the shrinkage was decreased by 25%. Shrinkage appears to be strongly related to cement content.

Generally, it is expected to observe an increase in shrinkage when CSF is used but this was not the case for all the measurements.

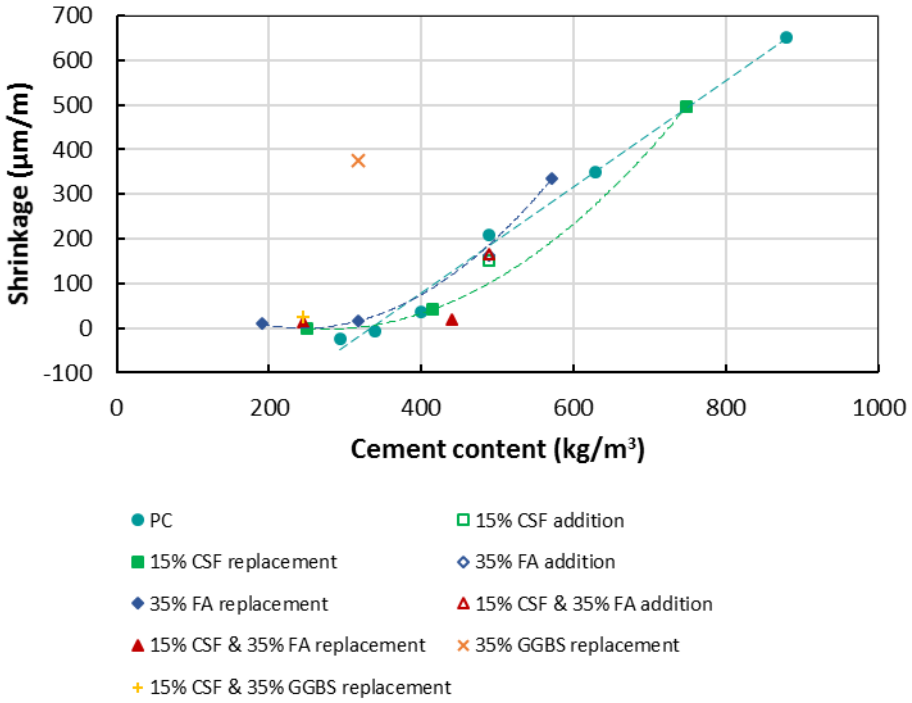

Figure 4.25 Beam shrinkage with cement content for modified Vicat needle setting time reference

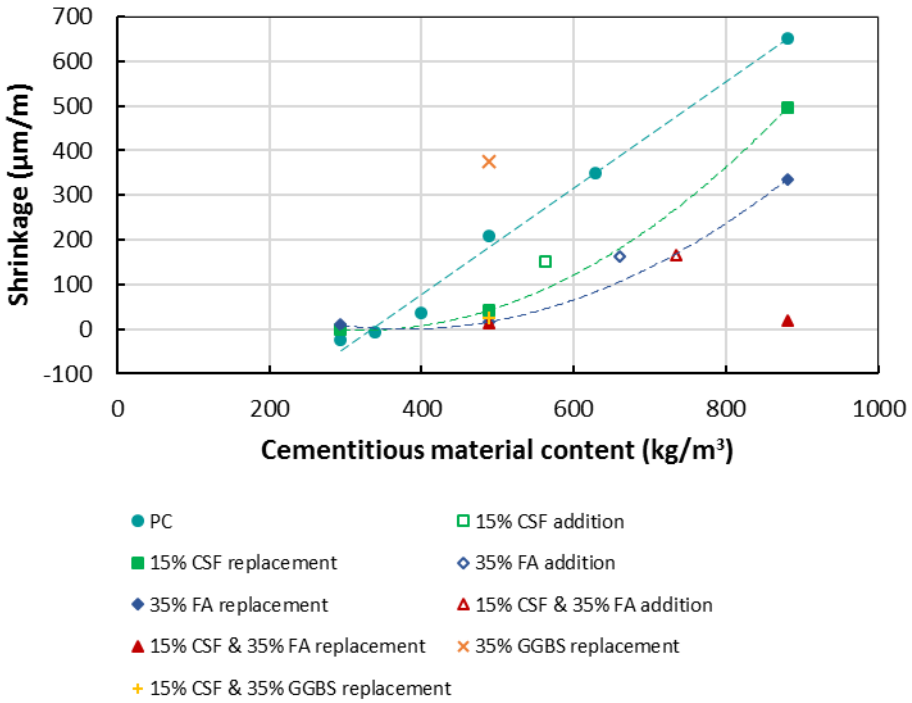

Figure 4.26 Beam shrinkage with cementitious material content for modified Vicat needle setting time reference

The CSF used in this study may have acted as a material possessing a larger particle size and the SP used did not disperse particles effectively in the mixture thus preventing the typical refinement of pore structure found in literature. This may be the reason why the CSF used in this study affected the shrinkage observed in a positive way in most cases.

4.4.3 Influence of FA

Shrinkage was reduced in all samples when FA was incorporated. This is expected as it is widely known that FA inhibits autogenous shrinkage due to the reduction in the rate at which the internal relative humidity decreases (Malhotra, 2002). The slow reaction time of FA may also have reduced the shrinkage by effectively diluting the system and thus increasing the water-to-cement ratio. The shrinkage was also reduced when the cement content was not altered but FA was added. FA replacement reduced shrinkage by almost 50% at a cementitious material content of 880 kg/m^3.

Again, when comparing Figure 4.25 and Figure 4.26 it appears that shrinkage is dependent on cement content rather than cementitious material content.

4.4.4 Influence of GGBS

Shrinkage was increased by approximately 45% with GGBS replacement. Shrinkage did not appear to be dependent on either the cement content or the cementitious material content when looking at Figure 4.25 and Figure 4.26. The increasing effect was also observed in literature when GGBS with a similar Blaine than the GGBS used in this study was used and where the fines content of the GGBS was more than that of the cement and vice versa for the coarser particles as is the case for the GGBS used in this study. The increasing effect of shrinkage can be attributed to the filler effect since the reaction rate of GGBS is lower and there is relatively more space for the formation of the clinker hydrates at early ages. The presence of GGBS may also lead to a refinement of the pore structure which would explain the increase in shrinkage (Almeida & Klemm, 2018). Interestingly, the combination of the increase in autogenous shrinkage combined with a lower heat of hydration has also been reported by Wyrzykowski & Lura (2014).

4.4.5 Influence of Multiple SCMs

CSF and FA replacement significantly reduced shrinkage compared to equivalent cementitious material PC samples by around 95%. CSF and FA addition reduced shrinkage by about half of that at around 40%. CSF and GGBS replacement reduced shrinkage by approximately 90%. The

CSF used in this study was beneficial when used either alone or with another SCM. The increasing effect of GGBS on shrinkage was mitigated by CSF replacement of PC.

When comparing Figure 4.25 and Figure 4.26, shrinkage was more cement content dependent than cementitious material content dependant.

Figure 4.27 illustrates the effect of cumulative heat at 100 hours on shrinkage at 100 hours. Samples containing SCM that produced the same heat as pure PC samples generally underwent less shrinkage. The samples with either CSF addition or FA addition exhibited the same behaviour as pure PC samples. Notably, GGBS replacement did not generate heat but caused high shrinkage.

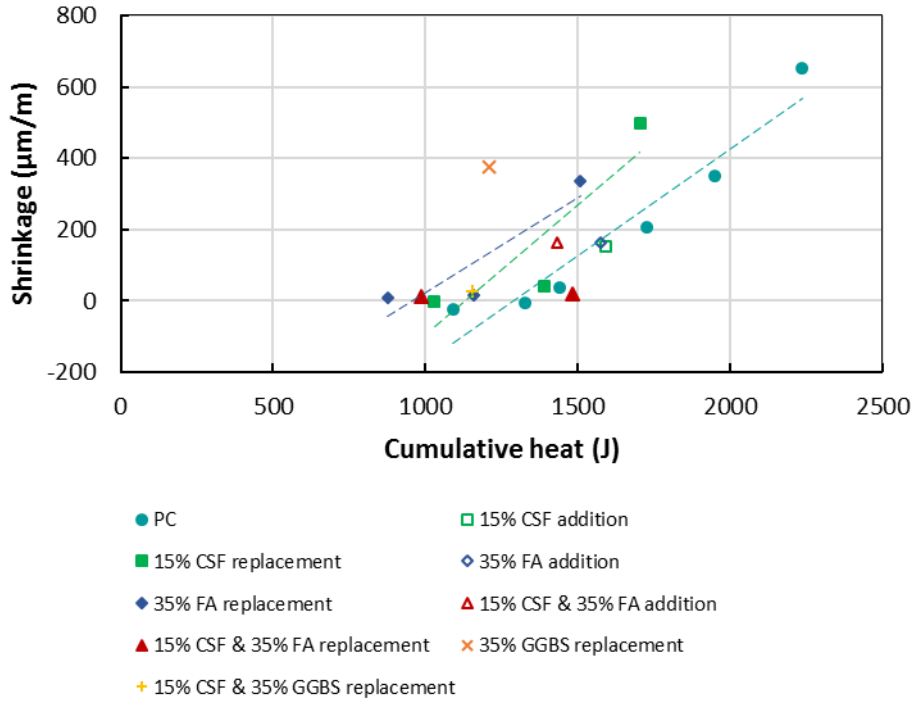

Figure 4.27 Shrinkage with cumulative heat at 100 hours

4.5 MECHANICAL PROPERTIES

4.5.1 Compressive Strength

The 28-day compressive strength for the mixture compositions used in this study is shown in Figure 4.28. Generally, the strength increased with a reduction in water-to-binder ratio. CSF addition and replacement had the biggest effect on the concrete strength with an increase when PC was replaced, or CSF added to the mixture. Adding FA or adding both CSF and FA did not

have a significant effect on the concrete strength. FA replacement slightly reduced the 28-day strength for all water-to-binder ratios. Replacement with both CSF and FA or CSF and GGBS reduced the 28-day strength. The strength development curves for all samples are shown in Appendix F.

The results were as expected as FA generally retards the hydration process and reduces the early age strength and at some point, the strength for a PC-FA sample could be more than that of a PC sample. This can happen at a later stage than 28 days, so the strengths observed were as expected. GGBS can have a varying effect on strength depending on the slag activity index. CSF typically increase strength which was the case for the samples tested. The grey trend line in Figure 4.28 is for all the samples and the cyan line for the PC samples. The samples with SCM seem to have a higher strength than PC samples at higher water-to-binder ratios. The reactivity of the SCMs individually may shed light on the behaviour.

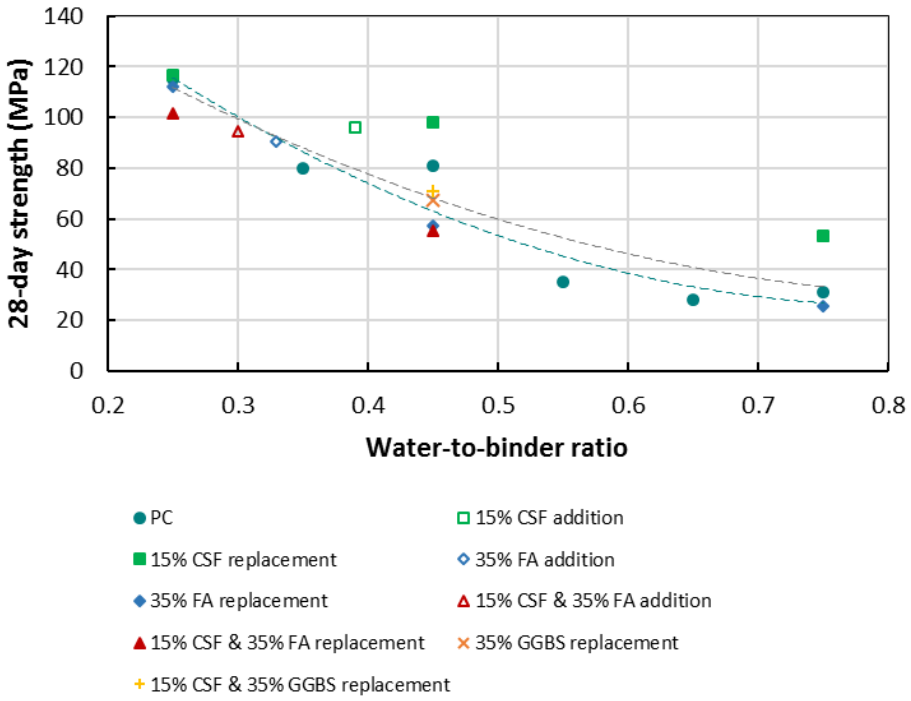

Figure 4.28 28-day cube strength with water-to-binder ratio (grey dashed line = trendline for all data points & cyan dashed line = trendline for PC samples)

Using Equation 2.1, k_1 and k_2 was calculated such that the error from the fitted compressive strength curve using Abrams law was minimised. The resulting fitted curve is shown in Figure 4.29. The strength at water-to-cement ratio 0.45 was taken as an outlier. The fitted function

equation in shown in Figure 4.29 and was used to calculate an effective water-to-cement ratio for each mix composition containing SCM(s).

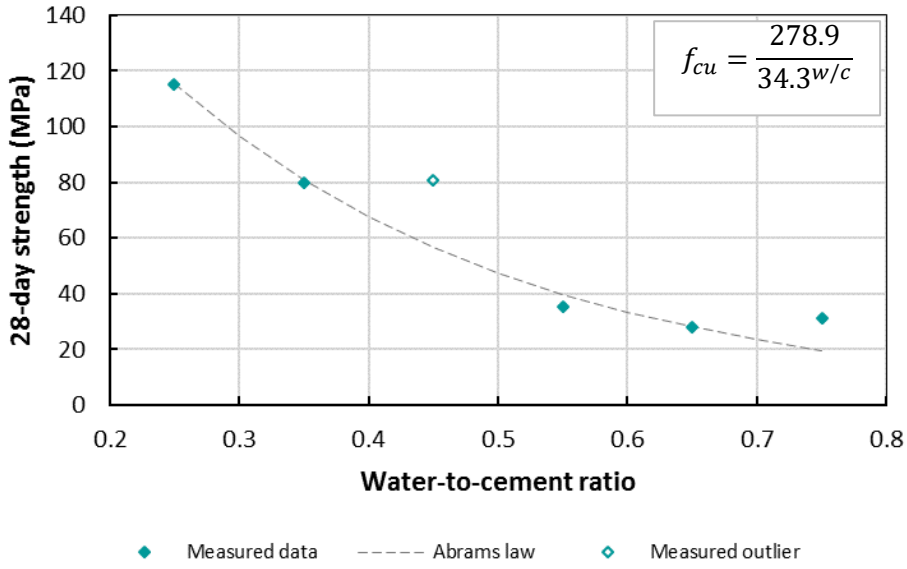

Figure 4.29 Compressive strength results and fitted Abrams law curve

Equation 2.2 was used to calculate the k-value after 28 days for each mix composition and is shown in Figure 4.30. A k-value of 1 would indicate that the contribution of the SCM was identical to that of the cement that was replaced. The k-values calculated was between 0.75 and 1.3 for all mixes except for CSF replacement at higher water-to-cement ratios. CSF replacement yielded a k-value of around 4.3 at water-to-cement ratio 0.45 and water-to-cement ratio 0.75. The k-values calculated was within ranges obtained in literature. For this study the k-value did not vary significantly with SCM or content of SCM except with CSF replacement and CSF addition at water-to-cement ratio 0.45 and higher. Below a water-to-cement ratio of 0.4 the CSF did not contribute to the strength as efficiently as with higher water-to-cement contents and there probably was not enough water for the mixture to fully hydrate. Addition (hollow markers in Figure 4.30) was more efficient than replacement for FA and GGBS but this was not the case with CSF. Although there is not a significant increase in k-values with water-to-cement ratio there is a definite incline indicating that the efficiency of SCMs increased with water-to-cement ratio as indicated by the grey dashed line in Figure 4.30.

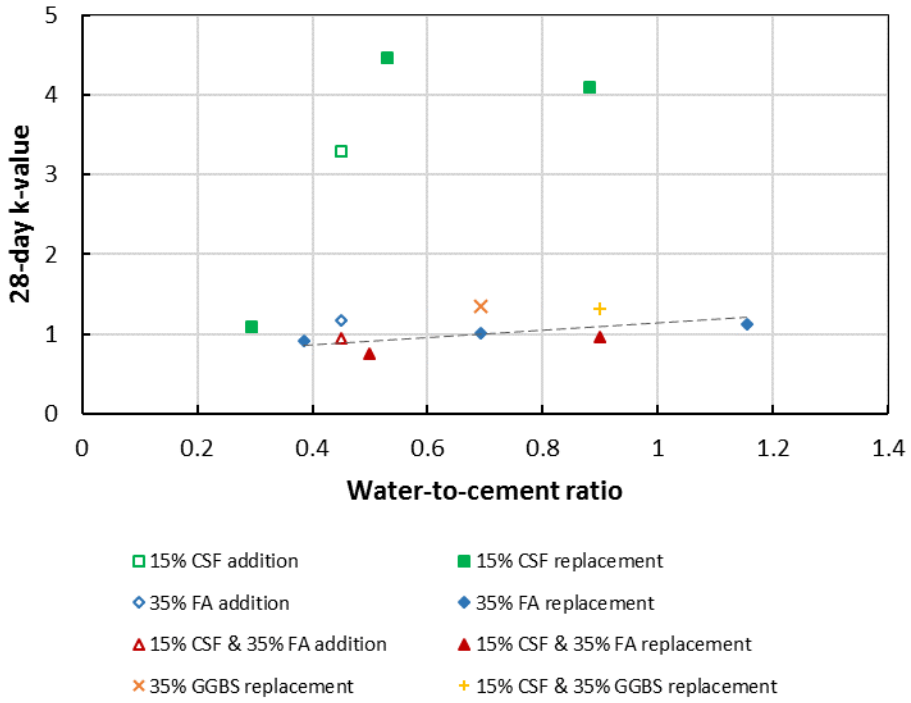

Figure 4.30 Calculated 28-day k-values for SCMs at different water-to-cement ratios (grey dashed line = all data points except CSF addition or replacement)

The 3-day strength with cumulative heat at 72 hours can be seen in Figure 4.31. There appears to be a relatively strong correlation between 3-day strength and cumulative heat at 72 hours for samples with SCM replacement regardless of which SCM was present. With SCM addition the cumulative heat was not increased significantly in relation to strength compared to PC samples.

The shrinkage with compressive strength at 3 days (grey dashed line) and 7 days (cyan dashed line) is shown in Figure 4.32 and indicates that early strength gain is related to more shrinkage. This is to be expected as hydrates formed faster than in the other mixes with a lower early strength and formed a dense microstructure. Water, if available, could not easily reach the remnants of unhydrated PC or SCM and self-desiccation took place and shrinkage was increased (Addis, 1994, Neville, 2011).

The 7-day k-values with corresponding shrinkage is shown in Figure 4.33 and illustrates that there is no correlation between reactivity and shrinkage. The 28-day k-values with shrinkage at 200 hours is shown in Figure 4.34, the mixtures containing highly reactive SCMs (k>2) did not shrink significantly. The mixes with the highest shrinkage to k-value ratio was the low water-to-binder ratio CSF replacement mix, the GGBS replacement mix (at a water-to-binder ratio of 0.45) and the low water-to-binder FA replacement mix in both Figure 4.33 and Figure 4.34.

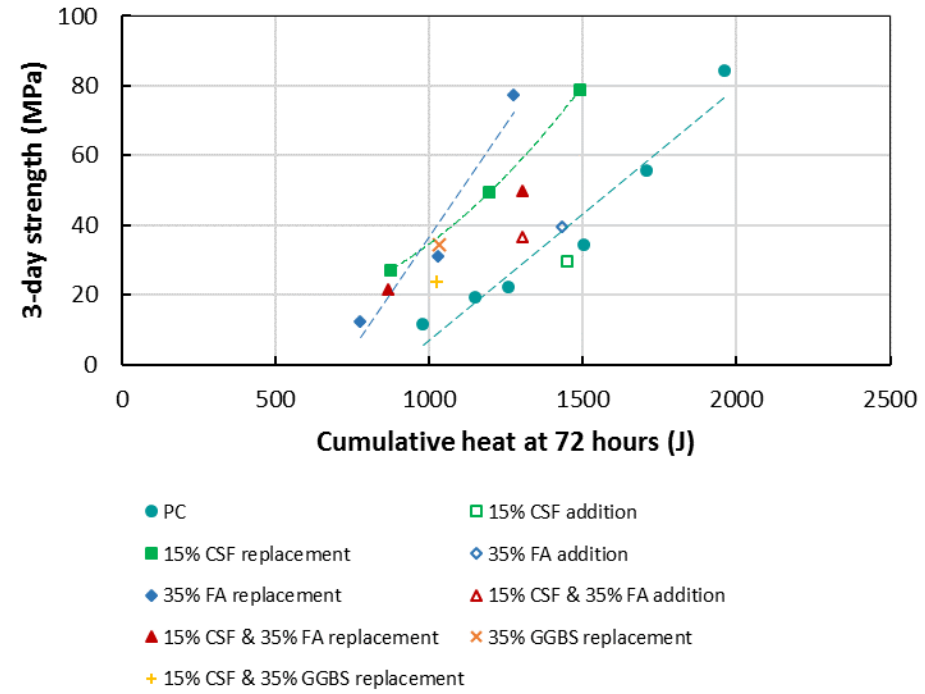

Figure 4.31 3-day compressive strength with cumulative heat at 72 hours

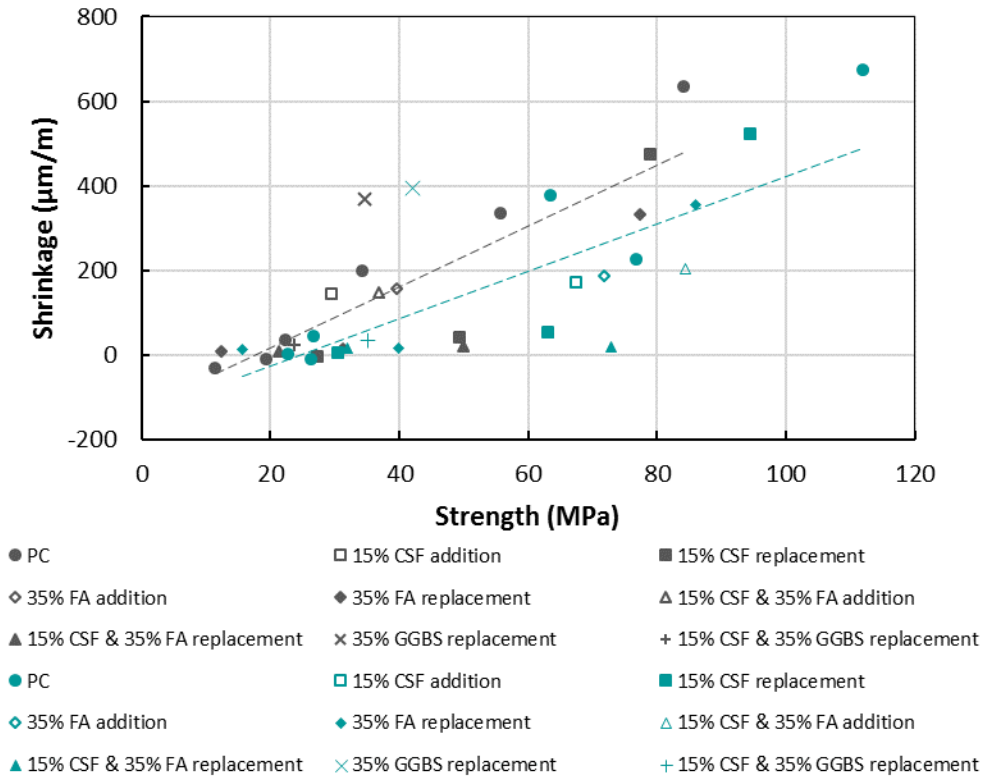

Figure 4.32 Shrinkage with compressive strength at 3 days (grey) and 7 days (cyan)

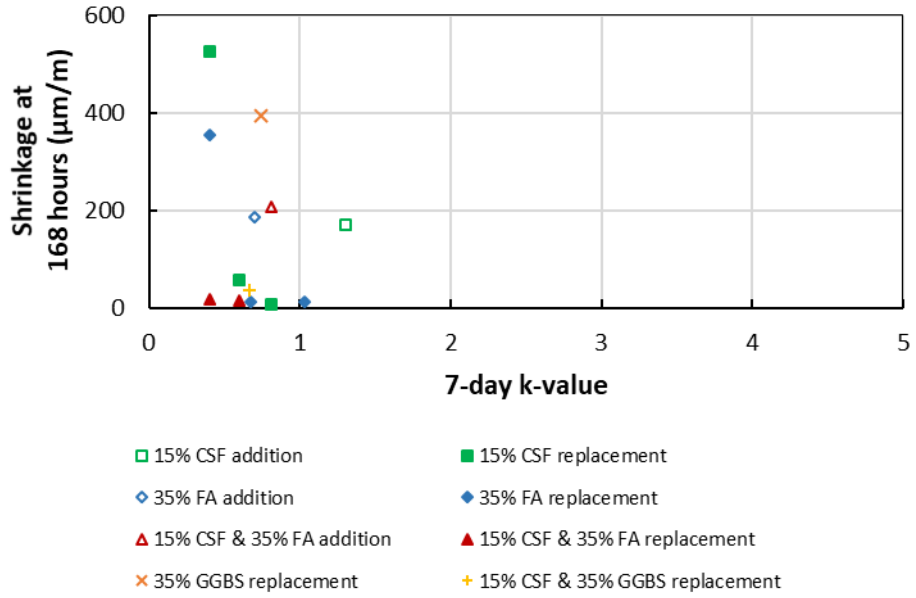

Figure 4.33 Shrinkage at 168 hours with 7-day k-value

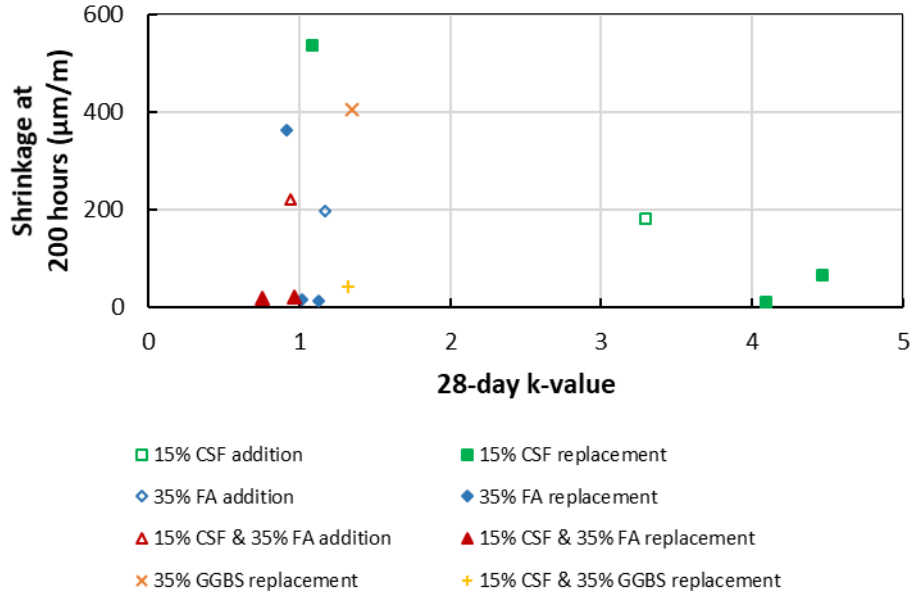

Figure 4.34 Shrinkage at 200 hours with 28-day k-value

4.5.2 Static Modulus of Elasticity

Figure 4.35 shows the static modulus of elasticity with water-to-binder ratio at 28 days. The modulus of elasticity increased on average with a decrease in water-to-binder ratio. The modulus of elasticity was not significantly affected with addition or replacement with CSF, FA and/or

GGBS. This however was not the case for water-to-binder ratio 0.75 where CSF increased the modulus of elasticity and FA decreased the modulus of elasticity.

The modulus of elasticity of CSF concrete is similar to that of PC concrete (Løland, 1983, Luther, 1989). Lane and Best (1982) reported that the modulus of elasticity of low lime FA concrete is slightly less at early ages and slightly more at later ages when compared to similar concretes without FA. Brooks et al. (1992) conducted research and concluded that the modulus of elasticity for concrete containing slag cement was similar at early ages and higher at later ages than that of similar concrete containing pure PC.

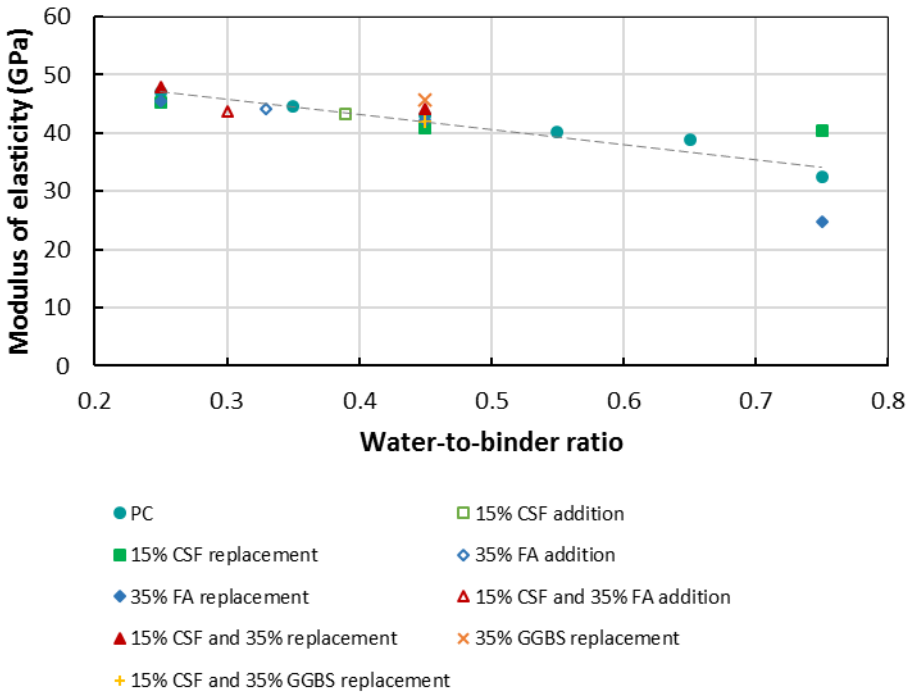

Figure 4.35 28-day modulus of elasticity with water-to-binder ratio at 28 days (dashed line indicates the trendline for all data points)

4.5.3 Splitting cylinder tensile strength

Figure 4.36 shows the 28-day splitting tensile strength with water-to-binder ratio for different additions and replacements. The split cylinder tensile strength generally increased with a decrease in water-to-binder ratio, the grey dashed line indicates the average for all samples and the cyan dashed line indicates the trend for PC samples. The tensile strength generally increased when SCM(s) were incorporated and the increase was constant over all water-to-binder ranges.

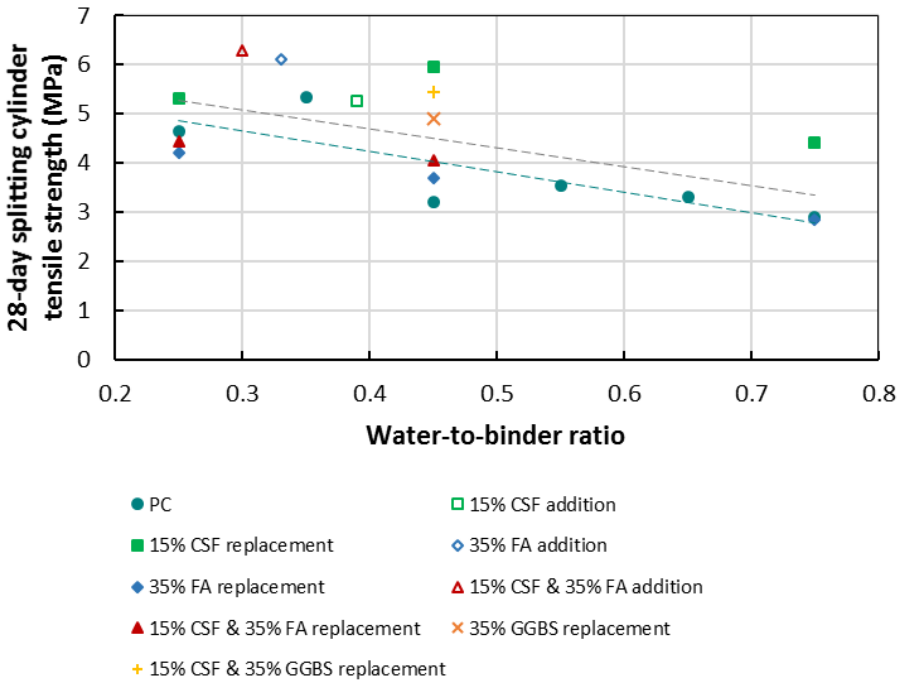

Figure 4.36 28-day split cylinder tensile strength with water-to-binder ratio (grey dashed line = trendline for all data points & cyan dashed line = trendline for PC data points)

4.6 SUMMARY

Mechanical properties, thermal processes and shrinkage were recorded for mixtures with different water-to-binder ratios and SCM additions and replacements to investigate the relationship between autogenous shrinkage, reactivity and thermal processes. The results found that there was no correlation between autogenous shrinkage and reactivity. There seems to be a correlation between autogenous shrinkage and cumulative heat released which is expected as both processes are a function of water and cement content (Danielson, 1962, Zhang et al., 2003, Tian, 2006, Bentz et al., 2009, Lothenbach et al., 2011). GGBS replacement did not behave like the other SCMs and more shrinkage was observed with less heat released. A correlation was observed between the compressive strength and cumulative heat released regardless of which SCM was used.

4.6.1 Setting time

Two methods of determining the setting times were investigated and the observations from results are discussed.

Modified Vicat needle method:

- Both CSF addition and CSF replacement delayed initial setting time the most except when GGBS replacement was also present.
- CSF replacement delayed final setting time, but CSF addition did not influence final setting time. When GGBS replacement was also present, the final setting time was similar to the final setting time of a CSF replacement sample.
- Both the initial and final setting times for samples containing CSF replacement was more delayed at a lower water-to-cement ratio or higher binder content which could have been due to the higher level of SP present.
- Both FA replacement and FA addition delayed the initial setting times, but a similar initial setting time was observed for PC samples and PC-FA samples at a water-to-cement ratio of around 1.15.
- FA replacement delayed final setting time, but less so for water-to-binder ratio 0.45 than for water-to-binder ratios of 0.25 and 0.75. FA addition did not influence the final setting time significantly.
- Comparing equal cementitious material contents, the initial setting time of mixes containing both CSF and FA replacement was similar to FA replacement samples, except at a high cementitious material content (880 kg/m^3) where the initial setting time was delayed more significantly as with CSF replacement alone. The initial setting time of CSF and FA addition samples were similar to the initial setting time of FA replacement samples containing only FA replacement.
- The final setting time with CSF and FA replacement was increased to a similar extent than for CSF replacement samples, while CSF and FA addition did not seem to have an effect on final setting time.
- GGBS replacement had a negligible effect on the initial setting time but delayed final setting.
- Notably, all SCMs delayed setting or had a negligible effect on setting.

Isothermal calorimeter method:

- The initial and final setting time determined by this method showed an increase in setting time with a decrease in water-to-cement ratio which could suggest a strong link to the SP dosing which is increased with a decrease in water-to-cement ratio.
- Both CSF addition and CSF replacement delayed initial setting time the most significantly. When GGBS replacement was also present the initial setting time was comparable to a sample with CSF replacement at an equivalent cement content.

- The final setting time with CSF replacement only differed by a maximum of 10% compared to PC samples with equivalent cementitious material contents but CSF addition decreased the final setting time considerably by about 40%. When GGBS replacement was present as well, the final setting time was delayed or decreased depending on the comparison with either equivalent water-to-cement ratios or equivalent cementitious material contents respectively.
- Both FA replacement and FA addition decreased initial setting time below a cementitious material content of about 800 kg/m^3.
- Similarly, FA replacement decreased final setting time below cementitious material contents of about 750 kg/m^3. FA addition decreased final setting time as well.
- CSF and FA replacement decreased initial setting time at a cementitious material content of less than about 800 kg/m^3 and CSF and FA addition yielded an initial setting time close to CSF replacement which delayed the initial setting time.
- CSF and FA replacement and CSF and FA addition decreased final setting time compared to PC samples containing equivalent cementitious material contents.
- GGBS replacement decreased both the initial setting time and final setting time and the smallest results indicated that this mix was the first to set out of all the mixes.

The setting times obtained by the isothermal calorimeter data was longer than the setting times obtained from the modified Vicat needle method, but this is explained by the different mechanisms used in the different methods. The setting times obtained from the two methods were opposing in terms of the setting time generally increasing with water-to-cement ratio for the modified Vicat needle method and the opposite being true for the isothermal calorimeter setting time in general. This may be explained by the difference in sample size and again by the difference in mechanisms present in both methods, and the probability that the isothermal calorimeter results are strongly linked to SP dosing. There seems to be a correlation between the setting times of the two different measuring methods. Calibration or further investigation however fell outside of the scope of this study.

4.6.2 Thermal effect

Thermal effects were measured by semi-adiabatic calorimetry, isothermal calorimetry and thermocouples in beam shrinkage samples. The first and second method was focussed on and the general observations made from both methods are listed.

Semi-adiabatic calorimetry:

- The maximum temperature change increased with a decrease in water-to-binder content.
- CSF replacement lowered the maximum temperature change with a constant offset at all binder contents in relation to the PC samples. CSF addition resulted in a similar maximum temperature change than a PC sample with the same cement content.
- FA replacement lowered the maximum temperature change at lower cement contents (lower than about 500 kg/m^3) but did not influence the maximum temperature change at higher cement contents.
- Both CSF and FA replacement and CSF and FA addition lowered the maximum temperature change at lower cement contents (below about 480 kg/m^3).
- GGBS replacement lowered the maximum temperature change. CSF and GGBS replacement lowered the maximum temperature change as well.

Isothermal calorimetry:

- The peak heat flow increased with a decrease in water-to-binder content and the time at which this peak occurred increased as well. The time at which the peak occurred seem to be strongly linked to SP content.
- CSF replacement lowered the peak heat flow; the lowering effect was more prominent at a high cementitious material content (880 kg/m^3). CSF addition resulted in a slight increase in peak heat flow.
- FA replacement did not influence the peak heat flow at cement contents of less than about 320 kg/m^3 but lowered peak heat flow at higher cement contents. FA addition, however, slightly increased the peak heat flow.
- The peak heat flow was not influenced by either CSF and FA replacement or CSF and FA addition when compared with PC samples with equivalent cement contents.
- GGBS lowered the peak heat flow. CSF and GGBS replacement did not influence the peak heat flow when compared to PC samples with the same cement content.

The semi-adiabatic temperature and peak heat flow was either reduced or the influence was negligible when SCMs were present depending on the specific SCM.

4.6.3 Autogenous shrinkage

During autogenous shrinkage measurements the following main observations were made:

- The data from the corrugated tube method was inconclusive and this was attributed to the possible variance in the stiffness of the moulds or the measuring method including

settlement in the shrinkage measurements. Interpretable results may possibly be obtained from mixes with limited variations in consistency.

- Starting autogenous shrinkage measurements at the initial setting times from the isothermal calorimeter data resulted in only positive shrinkage for all mixtures, where using the final setting times of the modified Vicat needle method resulted in slight negative shrinkage values for some mixes. The shrinkage from the two reference points did however display the same trends and it was concluded that the setting times may be used interchangeably to make qualitative conclusions for the data in this study.
- Significant shrinkage was only observed below water-to-cement ratios of around 0.4 and this is in agreement with the belief that self-desiccation and thus autogenous shrinkage will take place only below this point as discussed in Chapter 2 (Addis, 1994, Zhang et al., 2003).
- Shrinkage generally increased with an increase in cement content.
- Shrinkage was more dependent on cement content than cementitious material content for all mixes, whether SCM(s) were present or not, with the exception of GGBS replacement, where a lower cement content resulted in more shrinkage.
- In hindsight, consideration of the knee-point method of determining the "time-zero" could have been useful to compare to the modified Vicat needle "time-zero" results.

4.6.4 Mechanical properties

Compressive strength tests were conducted, and the following observations were made:

- The compressive strength decreased on average with an increase in water-to-binder ratio with variations when SCMs were used.
- The variation in reactivity of the mixes was deemed to be negligible for all mixes except where CSF was used above a water-to-cement ratio of 0.4.
- The cumulative heat at 72 hours correlates with the 3-day compressive strength where mixes containing SCMs were stronger per unit cumulative heat than the PC mixes. Replacement with SCM(s) was more effective than addition with SCM(s).
- The shrinkage with strength at 3 days and 7 days were compared and it was observed that a higher shrinkage was expected at 3 days with a certain compressive strength than the shrinkage that was expected at the same strength at 7 days indicating that early age strength attributed more to the shrinkage measured.
- The reactivity or k-value did not show a correlation with shrinkage.

The modulus of elasticity and splitting cylinder tensile strength was tested and the following observations were made:

- A negligible variation in modulus of elasticity was observed for mixes containing SCM(s) compared to PC mixes and the modulus of elasticity decreased generally with an increase in water-to-binder ratio.
- The splitting cylinder tensile strength decreased with an increase in water-to-binder ratio.

CHAPTER 5:

CONCLUSIONS AND RECOMMENDATIONS

5.1 CONCLUSIONS

The primary objective of this study was to investigate the relationship between autogenous shrinkage, the thermal processes and the strength development of concrete. The influence of binder composition and content on the early age volume change of concrete was studied. The results indicated a correlation between autogenous shrinkage and cumulative heat released where the autogenous shrinkage observed increased with cumulative heat released. A weak correlation was found between compressive strength and autogenous shrinkage. Generally, the shrinkage increased with concrete strength and the earlier age strength contributed more to autogenous shrinkage than later age strength. A correlation was observed between the compressive strength and cumulative heat released. SCM replacement led to a lower cumulative heat but SCM addition was detrimental in that more heat was released for an equivalent strength to SCM replacement samples.

Notably, GGBS replacement led to more shrinkage with a lower cumulative heat released and a lower strength as well. This was mitigated by additional CSF replacement which was also not expected as CSF is known to exacerbate autogenous shrinkage. The results seem to indicate that the particles of the CSF used in this study conglomerated to behave as a material with larger particles.

It was also found that:

- Autogenous shrinkage measurements conducted in a corrugated tube mould were inconclusive and the beam mould testing method provided interpretable results and seem to indicate that the results are repeatable.
- The initial and final setting time was obtained by means of the modified Vicat needle testing method as well as from the isothermal calorimeter data. When autogenous shrinkage taken from the reference point of the modified Vicat needle final setting time and compared to the autogenous shrinkage measured from the isothermal calorimeter initial setting time the results were observed to be almost interchangeable. By using isothermal calorimeter

data to determine the setting time of mixes, the impractical Vicat needle testing procedure may be bypassed and the process automated. Isothermal calorimetry is less user sensitive which may assist in obtaining repeatable reliable results.

- The reactivity of SCM was determined in each mix through the calculation of k-values that were comparable to that found in literature. Although this was not successful in explaining the behaviour observed, interesting observations could be made in terms of the reactivity of CSF and GGBS.

5.2 RECOMMENDATIONS

- Testing of more samples would enable future researchers to carry out statistical analysis on the results obtained to be able to plot statistically meaningful graphs.
- The effects of CSF on concrete behaviour observed in this study should be further investigated to determine the cause. The use of Microsilica, when the fine particles are in solution and cannot conglomerate could significantly affect the results and further testing is recommended.
- GGBS should be used with caution as early age cracks could form due to the lower early age strength combined with a higher autogenous shrinkage.
- CSF may be used to increase early age strength without increasing the risk of cracking.
- Heat of hydration and autogenous shrinkage can be reduced with the use of SCMs.
- The knee-point method of determining the “time-zero” could be helpful.

CHAPTER 6: REFERENCES

ACI Committee 201 2014. ACI Manual of Concrete Practice. *ACI 201.2R-08 Guide to Durable concrete.* Farmington Hills, MI.

ACI Committee 232 2002. ACI Manual of Concrete Practice. *ACI 232.2R-96 Use of Fly Ash in Concrete.* Farmington Hills, MI.

ACI Committee 233 2003. ACI Manual of Concrete Practice. *ACI 233R-03 Slag Cement in Concrete and Mortar.* Farmington Hills, MI.

ACI Committee 234 2000. ACI Manual of Concrete Practice. *ACI 234R-96 Guide for the Use of Silica Fume in Concrete*. Farmington Hills, MI.

Acker, P. 1988. *Comportement Mecanique du Beton: Apports de L'Approche Physico-Chimique*, France, Central Laboratory of Bridges & Highways.

Addis, B.J. 1994. *Fulton's Concrete Technology*, Midrand, South Africa, Portland Cement Institute.

Aïtcin, P.C. 1998. *High Performance Concrete*, London, E & FN Spon.

Almeida, F.C.R. & Klemm, A.J. 2018. Efficiency of internal curing by superabsorbent polymers (SAP) in PC-GGBS mortars. *Cement and Concrete Composites*, 88, pp 41-51.

ASTM Committee C01 2015. ASTM standard C1437 – 15: *Standard Test Method for Flow of Hydraulic Cement Mortar.*

ASTM Committee C09 1999. ASTM standard C403 – 99: *Standard Test Method for Time of Setting of Concrete Mixtures by Penetration Resistance.*

ASTM Committee C09 2002. ASTM Standard C469 – 02: *Standard Test Method for Static Modulus of Elasticity and Poisson's Ratio of Concrete in Compression.*

ASTM Committee C09 2014. ASTM standard C1698 – 09: *Standard Test Method for Autogenous Strain of Cement Paste and Mortar*.

ASTM Committee C09 2017. ASTM standard C157 – 17: *Standard Test Method for Length Change of Hardened Hydraulic-Cement Mortar and Concrete*.

ASTM Committee C09 2018. ASTM standard C191 – 18a: *Standard Test Methods for Time of Setting of Hydraulic Cement by Vicat Needle*.

ASTM Committee C09 2019. ASTM standard C125 – 19: *Standard Terminology Relating to Concrete and Concrete Aggregates*.

Atiş, C.D., Özcan, F., Kılıç, A., Karahan, O., Bilim, C. & Severcan, M.H. 2005. Influence of dry and wet curing conditions on compressive strength of silica fume concrete. *Building and Environment*, 40(12), pp 1678-1683.

Babu, K.G. & Rama Kumar, V.S., 2000. Efficiency of GGBS in concrete, *Cement and Concrete Research*, 30, pp 1031–1036.

Babu, K.G. & Rao, G.S.N. 1993. Efficiency of fly ash in concrete, *Cement and Concrete Composites*, 15, pp 223-228.

Barcelo, L., Boivin, S., Rigaud, S., Acker, P., Clavaud, B. & Boulay, C. 1999. Linear vs. volumetric autogenous shrinkage measurement: Material behaviour or experimental artefact? In *Proceedings of the 2nd International Seminar on Self-desiccation and its Importance in Concrete Technology*, Lund, Sweden, pp 109-125.

Bazzoni, A. 2014. *Study of early hydration mechanisms of cement by means of electron microscopy*. Doctorate, Federal Institute of Technology in Lausanne.

Beltzung, F. & Wittmann, F 2002. Influence of cement composition on endogenous shrinkage. In *Self-Desiccation and its importance in concrete technology: proceedings of the third international research seminar in Lund.* Eds. Persson, B. & Fagerlund, G. Lund: Lund Institute of Technology.

Bentur, A. 2001. Terminology and definitions. In *International RILEM Conference on Early Age Cracking in Cementitious Systems—EAC, RILEM TC 181-EAS*. Haifa, Israel.

Bentz, D.P. 2014. Activation energies of high-volume fly ash ternary blends: Hydration and setting. *Cement and Concrete Composites*, 53, pp 214-223.

Bentz, D.P., Garboczi, E.J., Haecker, C.J. & Jensen, O.M. 1999. Effect of particle size distribution on properties of cement-based materials. *Cement and Concrete Research,* 29(10), pp. 1663-1671.

Bentz, D.P. & Jensen, O.M. 2004. Mitigation strategies for autogenous shrinkage cracking. *Cement and Concrete Composites,* 26(6), pp 677-685.

Bentz, D.P. & Peltz, M.A. 2008. Reducing the Thermal and Autogenous Shrinkage Contributions to Early-Age Cracking. *ACI Materials Journal,* 105(4), pp 414 - 420.

Bentz, D.P., Peltz, M.A. & Winpigler, J. 2009. Early-Age Properties of Cement-Based Materials: II. Influence of Water-to-Cement Ratio. *ASCE Journal of Materials in Civil Engineering,* 21(9), pp 512-517.

Bentz, D.P., Sant, G. & Weiss, J. 2008. Early-Age Properties of Cement-Based Materials. I: Influence of Cement Fineness. *ASCE Journal of Materials in Civil Engineering,* 20(7), pp 502-508.

Berodier, E. & Scrivener, K. 2014. Understanding the Filler Effect on the Nucleation and Growth of C-S-H. *Journal of the American Ceramic Society,* 97(12), pp 3764-3773.

Bjontegaard, Ø. 1999. *Thermal dilation and autogenous deformation as driving forces to self-induced stresses in high performance concrete.* Ph.D., Norwegian University of Science and Technology.

Bobrowicz, J. 2015. Study of cements initial setting time determination using curves of hydration rate evolution, measured by isometric calorimetry. *Cement Wapno Beton,* 20, pp 401-410.

Boháč, M., Palou, M., Novotný, R., Másilko, J., Všianský, D. & Staněk, T. 2014. Investigation on early hydration of ternary Portland cement-blast-furnace slag–metakaolin blends. *Construction and Building Materials,* 64, pp 333-341.

Boivin, S., Acker, P., Rigaud, S. & Clavaud, B. 1999. Experimental Assessment of Chemical Shrinkage of Hydrating Cement Pastes. *Autogenous Shrinkage of Concrete.* London: E & FN Spon.

Brooks, J.J., Wainwright, P.J. & Boukendakji, M. 1992. Influence of Slag Type and Replacement Level on Strength Elasticity, Shrinkage and Creep of Concrete. *Special Publication,* 132, pp 1325-1342.

Buil, M. 1979. *Contribution à l'étude du retrait de la pâ Studies of the shrinkage of hardening cement paste (in French).* Ph.D.

Bullard, J.W., Jennings, H.M., Livingston, R.A., Nonat, A., Scherer, G.W., Schweitzer, J.S., Scrivener, K.L. & Thomas, J.J. 2011. Mechanisms of cement hydration. *Cement and Concrete Research,* 41(12), pp 1208-1223.

Byfors, J. 1980. *Plain Concrete at Early Ages.* PhD. Thesis report FO 3:80, Swedish Cement and Concrete Research Institute, Stockholm.

Chaei, M.G., Akbarnezhad, A., Castel, A., Lloyd, R., Keyte, L. & Foster, S. 2018. Precision of cement hydration heat models in capturing the effects of SCMs and retarders. *Magazine of Concrete Research,* 70(23), pp 1217-1231.

Chang-wen, M., Qian, T., Wei, S. & Jia-ping, L. 2007. Water consumption of the early-age paste and the determination of "time-zero" of self-desiccation shrinkage. *Cement and Concrete Research,* 37(11), pp 1496-1501.

Chen, Z. & Poon, C.S. 2017. Comparative studies on the effects of sewage sludge ash and fly ash on cement hydration and properties of cement mortars. *Construction and Building Materials,* 154, pp 791-803.

Cheung, J., Jeknavorian, A., Roberts, L. & Silva, D. 2011. Impact of admixtures on the hydration kinetics of Portland cement. *Cement and Concrete Research,* 41 (12), pp 1289-1309.

Chryso 2018. CHRYSO Fluid Premia 100.

Cusson, D. & Hoogeveen, T. 2007. Test method for determining coefficient of thermal expansion of high-performance concrete at early age. In *12th International Congress on the Chemistry of Cement.* Montréal, QC: National Research Council Canada.

Danielson, U.H. 1962. Heat of hydration of cement as affected by water-cement ratio. In *Proceedings of the 4th International Symposium on the Chemistry of Cement*. Washington DC, U.S., pp 519-526.

Darquennes, A., Staquet, S., Delplancke-Ogletree, M.-P. & Espion, B. 2011. Effect of autogenous deformation on the cracking risk of slag cement concretes. *Cement and Concrete Composites,* 33(3), pp 368-379.

Dave, N., Misra, A.K., Srivastava, A. & Kaushik, S.K. 2017. Setting time and standard consistency of quaternary binders: The influence of cementitious material addition and mixing. *International Journal of Sustainable Built Environment,* 6(1), pp 30-36.

De la Varga, I., Castro, J., Bentz, D.P., Zunino, F. & Weiss, J. 2018. Evaluating the hydration of high volume fly ash mixtures using chemically inert fillers. *Construction and Building Materials,* 161, pp 221-228.

Dewar, J. 2003. Concrete mix design. In *Advanced Concrete Technology.* Eds. Newman, J. & Choo, B. S., Elsevier Ltd.

De Weerdt, K., Haha, M.B., Le Saout, G., Kjellsen, K.O., Justnes, H. & Lothenbach, B. 2011. Hydration mechanisms of ternary Portland cements containing limestone powder and fly ash. *Cement and Concrete Research,* 41(3), pp 279-291.

Deschner, F., Winnefeld, F., Lothenbach, B., Seufert, S., Schwesig, P., Dittrich, S., Goetz-Neunhoeffer, F. & Neubauer, J. 2012. Hydration of Portland cement with high replacement by siliceous fly ash. *Cement and Concrete Research,* 42(10), pp 1389-1400.

Diaz-Loya, I., Juenger, M., Seraj, S. & Minkara, R. 2019. Extending supplementary cementitious material resources: Reclaimed and remediated fly ash and natural pozzolans. *Cement and Concrete Composites,* 101, pp 44-51.

Domone, P. & Illston, J. 2010. *Construction Materials: Their Nature and Behaviour,* 4th ed. London, United Kingdom, Taylor & Francis Ltd.

Fernandez Lopez, R. 2009. *Calcined Clayey Soils as a Potential Replacement for Cement in Developing Countries.* Doctorate, Federal Institute of Technology in Lausanne.

Filho, J.R.T., de Araújo, M.A.P.G., Snoeck, D. & De Belie, N. 2019. Discussing Different Approaches for the Time-Zero as Start for Autogenous Shrinkage in Cement Pastes Containing Superabsorbent Polymers. *Materials,* 12(18), pp 2962.

Fisher, L.R. & Israelachvili, J.N. 1981. Experimental studies on the applicability of the Kelvin equation to highly curved concave menisci. *Journal of Colloid and Interface Science,* 80(2), pp 528-541.

Fraay, A.L.A., Bijen, J.M. & de Haan, Y.M. 1989. The Reaction of Fly Ash in Concrete. *Cement and Concrete Research,* 19(2), pp 235-246.

Gdoutos, K.M.S., Shah, S.P. & Dattatraya, D.J. 2003. Relationships between engineering characteristics and material properties of high strength- high performance concrete. In *Role of Concrete In Sustainable Development: Proceedings of the International Symposium dedicated to Professor Surendra Shah*, University of Dundee, Scotland, UK., pp 37–46.

Ghafari, E., Ghahari, S.A., Costa, H., Júlio, E., Portugal, A. & Durães, L. 2016. Effect of supplementary cementitious materials on autogenous shrinkage of ultra-high performance concrete. *Construction and Building Materials*, 127, pp 43-48.

Guoxing Huang, R.H. 1990. The Shrinkage of Concrete. *Railway Publishing House*, pp 1-30.

Gutteridge, W.A. & Dalziel, J.A. 1990a. Filler cement: The effect of the secondary component on the hydration of Portland cement: Part 2: Fine hydraulic binders. *Cement and Concrete Research*, 20(6), pp 853-861.

Gutteridge, W.A. & Dalziel, J.A. 1990b. Filler cement: The effect of the secondary component on the hydration of Portland cement: Part I. A fine non-hydraulic filler. *Cement and Concrete Research*, 20(5), pp 778-782.

Hammer, T.A. 2002. Is there a relationship between pore water pressure and autogenous shrinkage before and during setting? In *Proceedings of the 3rd International Seminar on Self-desiccation and Its Importance in Concrete Technology*, Lund, Sweden, pp 27-38.

Hammer, T.A., Bjøntegaard, Ø. & Sellevold, E.J. 2002. Measurement methods for testing of early age autogenous strain. In *Early age cracking in cementitious systems.* Eds. Kovler, K. & Bentur, A., Cachan, France: RILEM.

Han, F., He, X., Zhang, Z. & Liu, J. 2017. Hydration heat of slag or fly ash in the composite binder at different temperatures. *Thermochimica Acta*, 655, pp 202-210.

Han, F., Zhang, Z., Liu, J. & Yan, P. 2016. Effect of water-to-binder ratio on the hydration kinetics of composite binder containing slag or fly ash. *Journal of Thermal Analysis and Calorimetry*, 128, pp 855-865.

Hansen, K.K. & Jensen, O.M. 1997. Equipment for Measuring Autogenous RH-Change and Autogenous Deformation in Cement Paste and Concrete. In *Proceedings of International Seminar on Self-desiccation and its Importance in Concrete Technology.* Lund, Sweden.

Harrison, T. 2003. Concrete properties: setting and hardening. In *Advanced Concrete Technology: 4 Volume Set*, Eds. Newman, J. & Choo, B.S. Jordan Hill, Oxford: Elsevier Ltd.

Hedlund, H. 1996. *Stresses in High Performance Concrete Due to Temperature and Moisture Variations at Early ages.* Licentiate, Luleå University of Technology.

Hemalatha, T. & Ramaswamy, A. 2017. A review on fly ash characteristics – Towards promoting high volume utilization in developing sustainable concrete. *Journal of Cleaner Production,* 147, pp 546-559.

Higginson, E.C., Wallace, G.B. & Ore, E.L. 1963. Effect of Maximum Size Agregate on Compressive Strength of Mass Concrete. *Special Publication,* 6, pp 219-256.

Hjorth, J., Skibsted, J. & Jakobsen, H.J. 1988. 29Si MAs NMR studies of Portland cement components and effects of microsilica on the hydration reaction. *Cement and Concrete Research,* 18(5), pp 789-798.

Holt, E. & Leivo, M.T. 1999. Autogenous shrinkage at very early ages. In *Proceedings of International Workshop on Autogenous Shrinkage*. Eds. Tazawa, E. Hiroshima, Japan: E & FN SPON, London.

Holt, E. 2001. *Early age autogenous shrinkage of concrete.* PhD, University of Washington in Seattle.

Holt, E. 2005. Contribution of mixture design to chemical and autogenous shrinkage of concrete at early ages. *Cement and Concrete Research,* 35(3), pp 464-472.

Holt, E. & Leivo, M. 2000. Methods of Reducing Early Age Shrinkage. In *Shrinkage 2000: Proceedings of the International RILEM Workshop.* Eds. Baroghel-Bouny, V. & Aïtcin, P., Paris, France: RILEM Publications.

Hu, J., Ge, Z. & Wang, K. 2014. Influence of cement fineness and water-to-cement ratio on mortar early-age heat of hydration and set times. *Construction and Building Materials,* 50, pp 657-663.

Huang, H. & Ye, G. 2017. Examining the "time-zero" of autogenous shrinkage in high/ultra-high performance cement pastes. *Cement and Concrete Research,* 97, pp 107-114.

ICE 2009. *ICE manual of construction materials Volume 1,* London, UK, Thomas Telford Limited.

Jensen, O.M. & Hansen, P.F. 1995. A dilatometer for measuring autogenous deformation in hardening Portland cement paste. *Materials and Structures*, 28(7), pp 406-409.

Jensen, O.M. & Hansen, P.F. 1996. Autogenous deformation and change of the relative humidity in silica fume-modified cement paste. *ACI Materials Journal*, 93(6), pp 539-543.

Jensen, O.M. & Hansen, P.F. 2001. Autogenous deformation and RH-change in perspective. *Cement and Concrete Research*, 31(12), pp 1859-1865.

Jiang, Z., Sun, Z., Wang, P. & Wang, X. 2004. Study on self-desiccation effect of high performance concrete. *Journal of Building Materials*, 7.

Jiang, Z., Sun, Z. & Wang, P. 2005. Autogenous relative humidity change and autogenous shrinkage of high-performance cement pastes. *Cement and Concrete Research*, 35(8), pp 1539-1545.

Justnes, H. 1988. Kinetics of reaction in cementitious pastes containing silica fume as studied by 29Si MAS NMR. In *Nuclear Magnetic Resonance Spectroscopy of Cement-Based Materials.* Eds. Colombet, P., Zanni, H., Grimmer, A.-R. & Sozzani, P. Springer-Verlag Berlin Heidelberg.

Justnes, H., Van Gemert, A., Verboven, F. & Sellevold, E.J. 1996. Total and external chemical shrinkage of low w/c ratio cement pastes. *Advances in Cement Research*, 8(31), pp 121-126.

Kadri, E.H., Aggoun, S., De Schutter, G. & Ezziane, K. 2010. Combined effect of chemical nature and fineness of mineral powders on Portland cement hydration. *Materials and Structures*, 43(5), pp 665-673.

Kadri, E.H., Duval, R., Aggoun, S. & Kenai, S. 2009. Silca Fume Effect on Hydration Heat and Compressive Strength of High-Performace Concrete. *ACI Materials Journal*, 106(2), pp 107-113.

Kearsley, E.P. 1999. *The effect of high volimes of ungraded fly ash on the properties of foamed conrete.* PhD. The University of Leeds, Leeds.

Khan, A.N., Magar, R.B. & Chore, H.S. 2018. Efficiency Factor of Supplementary Cementitious Materials: *A State of Art. International Journal of Optimization in Civil Engineering*, 8(2), pp 247-253.

Kirby, D.M. & Biernacki, J.J. 2012. The effect of water-to-cement ratio on the hydration kinetics of tricalcium silicate cements: Testing the two-step hydration hypothesis. *Cement and Concrete Research*, 42(8), pp 1147-1156.

Kocaba, V. 2009. *Development and evaluation of methods to follow microstructural development of cementitious systems including slags.* Doctorate, Federal Institute of Technology in Lausanne.

Kronlöf, A., Leivo, M. & Sipari, P. 1995. Experimental study on the basic phenomena of shrinkage and cracking of fresh mortar. *Cement and Concrete Research*, 25(8), pp 1747-1754.

Kumar, M., Singh, S.K. & Singh, N.P. 2012. Heat evolution during the hydration of Portland cement in the presence of fly ash, calcium hydroxide and super plasticizer. *Thermochimica Acta*, 548, pp 27-32.

Lane, R.O. & Best, J.F. 1982. Properties and Use of Fly Ash in Portland Cement Concrete. *Concrete International: Design & Construction*, 4(7), pp 81-92.

Łaźniewska-Piekarczyk, B. 2013. The influence of chemical admixtures on cement hydration and mixture properties of very high performance self-compacting concrete. *Construction and Building Materials*, 49, pp 643-662.

Lee, K.M., Lee, H.K., Lee, S.H. & Kim, G.Y. 2006. Autogenous shrinkage of concrete containing granulated blast-furnace slag. *Cement and Concrete Research*, 36(7), pp 1279-1285.

Li, Y., Bao, J. & Guo, Y. 2010. The relationship between autogenous shrinkage and pore structure of cement paste with mineral admixtures. *Construction and Building Materials*, 24(10), pp 1855-1860.

Li, Y. & Li, J. 2014. Capillary tension theory for prediction of early autogenous shrinkage of self-consolidating concrete. *Construction and Building Materials*, 53, pp 511-516.

Lokhorst, S.J. 1998. Deformational behaviour of concrete influenced by hydration related changes of the microstructure. Delft, The Netherlands: Delft University of Technology.

Løland, K.E. 1983. "Fasthets — og deformasjonsegenskaper i herdnet tilstand — Herdebetingelser," ("Strength and Deformation Properties of Hardened Concrete"). *Bruk av Silika i Betong.* Oslo, Norway.

Lootens, D. & Bentz, D.P. 2016. On the Relation of Setting and Early-Age Strength Development to Porosity and Hydration in Cement-Based Materials. *Cement and Concrete Composites*, 68, pp 9-14.

Lothenbach, B., Scrivener, K. & Hooton, R.D. 2011. Supplementary cementitious materials. *Cement and Concrete Research*, 41(12), pp 1244-1256.

Lura, P. 2003. *Autogenous Deformation and Internal Curing of Concrete.* PhD, Technische Universiteit Delft.

Lura, P., Jensen, O.M. & van Breugela, K. 2003. Autogenous shrinkage in high-performance cement paste: An evaluation of basic mechanisms. *Cement and Concrete Research*, 33(2), pp 223-232.

Lura, P., Winnefeld, F. & Fang, X. 2017. A simple method for determining the total amount of physically and chemically bound water of different cements. *Journal of Thermal Analysis and Calorimetry*, 130, pp 653-660.

Luther, M.D. 1989. Comparison of Creep and Shrinkage of High-Strength Silica Fume Concretes with Fly Ash Concretes of Similar Strengths. In *CANMET/ACI Third International Conference on the Use of Fly Ash, Silica Fume, Slag, and Natural Pozzolans in Concrete*, Eds. Malhotra, V. M., Trondheim. American Concrete Institute, pp 573-592.

Lynam, C.G. 1934. *Growth and Movement in Portland Cement Concrete*, London, Oxford University Press.

Malhotra, V.M. 2002. High-Performance High-Volume Fly Ash Concrete. *Concrete International*, 24(7), pp 30-34.

Marciniak, S. 2002. *Autogenous deformations and relative humidity change: experimental studies.* M.Sc., Aalborg University.

Morioka, M., Hori, A., Hagiwara, H., Sakai, E. & Daimon, M. 1999. Measurement of autogenous length changes by laser sensors equipped with digital computer systems. In *Proceedings of International Workshop on Autogenous Shrinkage.* Eds. Tazawa, E., Hiroshima, Japan. E & FN SPON, London, pp 191-200.

Maruyama, I. & Teramoto, A. 2013. Temperature dependence of autogenous shrinkage of silica fume cement pastes with a very low water–binder ratio. *Cement and Concrete Research*, 50, pp 41-50.

Mazloom, M., Ramezanianpour, A.A. & Brooks, J.J. 2004. Effect of silica fume on mechanical properties of high-strength concrete. *Cement and Concrete Composites*, 26(4), pp 347-357.

Mehta, P.K. 1986. *Concrete. Structure, Properties and Materials*.

Mehta, P.K. & Monteiro, P.J.M. 2006. *Concrete: Microstructure, Properties and Materials, Third Edition*, United States of America, McGraw-Hill.

Mostafa, N.Y. & Brown, P.W. 2005. Heat of hydration of high reactive pozzolans in blended cements: Isothermal conduction calorimetry. *Thermochimica Acta*, 435(2), pp 162-167.

Mounanga, P., Khelidj, A., Loukili, A. & Baroghel-Bouny, V. 2004. Predicting $Ca(OH)_2$ content and chemical shrinkage of hydrating cement pastes using analytical approach. *Cement and Concrete Research*, 34(2), pp 255-265.

Neville, A.M. 2011. *Properties of Concrete*, Harlow, United Kingdom, Pearson Education Limited.

Newman, J. & Choo, B.S. 2003. *Advanced Concrete Technology 3: Processes*, Oxford, United Kingdom, Elsevier Science & Technology.

Nguyen, D.H., Dao, V.T.N. & Lura, P. 2017. Tensile properties of concrete at very early ages. *Construction and Building Materials*, 134, pp 563-573.

Nichols Jr., F.P. 1982. Manufactured Sand and Crushed Stone in Portland Cement Concrete. *Concrete International, 4(8)*, pp 56-63.

Nocuń-Wczelik, W. & Czapik, P. 2013. Use of calorimetry and other methods in the studies of water reducers and set retarders interaction with hydrating cement paste. *Construction and Building Materials*, 38, pp 980-986.

Paillere, A.M., Buil, M. & Serrano, J.J. 1989. Effect of fiber addition on the autogeneous shrinkage of silica fume concrete. *ACI Materials Journal*, 86(2), pp 139-144.

Pan, L.S., Qiu, X.Q., Pang, Y.X. & Yang, D.J. 2008. Effect of water-reducing chemical admixtures on early hydration of cement. *Advances in Cement Research*, 20(3), pp 93-100.

Pane, I. & Hansen, W. 2005. Investigation of blended cement hydration by isothermal calorimetry and thermal analysis. *Cement and Concrete Research*, 35(6), pp 1155-1164.

Powers, T.C. & Brownyard, T.L. 1947. Studies of the physical properties of hardened Portland cement paste, Bulletin 22, Research and Development Laboratories of Portland Cement Association, Skokie, IL, U.S.A., reprinted from *Journal of the American Concrete Institute*, Proceedings,43, pp 101 – 132, 249 – 336, 469 – 505, 549 – 602, 669 – 712, 845 – 880, 933 – 992.

Price, B. 2003. High Strenth Concrete. In *Advanced Concrete Technology: 4 Volume Set*, Eds. Newman, J. & Choo, B.S. Jordan Hill, Oxford: Elsevier Ltd.

Quennoz, A. & Scrivener, K.L. 2013. Interactions between alite and C3A-gypsum hydrations in model cements. *Cement and Concrete Research,* 44, pp 46-54.

Rahhal, V., Cabrera, O., Talero, R. & Delgado, A. 2007. Calorimetry of Portland cement with silca fume and gypsum additions. *Journal of Thermal Analysis and Calorimetry,* 87(2), pp 331–336.

Rao, G.A. 2001. Long-term drying shrinkage of mortar - influence of silica fume and size of fine aggregate. *Cement and Concrete Research*, 31(2), pp 171-175.

Rossen, J.E., Lothenbach, B. & Scrivener, K.L. 2015. Composition of C–S–H in pastes with increasing levels of silica fume addition. *Cement and Concrete Research,* 75, pp 14-22.

Sakai, E., Miyahara, S., Ohsawa, S., Lee, S.-H. & Daimon, M. 2005. Hydration of fly ash cement. *Cement and Concrete Research,* 35(6), pp 1135-1140.

Sant, G., Rajabipour, F., Lura, P. & Weiss, J. 2006. Examining Time-zero and Early Age Expansion in Pastes Containing Shrinkage Reducing Admixtures (SRA's). In *2nd International RILEM Symposium on Advances in Concrete through Science and Engineering.* Quebec City, Canada.

Schindler, A.K. Prediction of Concrete Setting. In *Proceedings of the RILEM international symposium on advances in concrete through science & engineering.* Eds. Weiss, J., Kovler, K., Marchand, J. & Mindess, S. Illinois. RILEM Publications SARL.

Schindler, A.K. & Folliard, K.J. 2003. Influence of supplementary cementing materials on the heat of hydration of concrete. In *Advances in Cement and Concrete IX Converence.* Colorado.

Schöler, A., Lothenbach, B., Winnefeld, F., Haha, M.B., Zajac, M. & Ludwig, H.-M. 2017. Early hydration of SCM-blended Portland cements: A pore solution and isothermal calorimetry study. *Cement and Concrete Research,* 93, pp 71-82.

Scrivener, K., Snellings, R. & Lothenbach, B. 2016. *A Practical Guide to Microstructural Analysis of Cementitious Materials,* Boca Raton, FL, CRC Press.

Seddik Meddah, M. & Tagnit-Hamou, A. 2011. Evaluation of Rate of Deformation for Early-Age Concrete Shrinkage Analysis and Time Zero Determination. *Journal of Materials in Civil Engineering,* 23(7), pp 1076-1086.

Sellevold, E.J. 1987. The Function of Condensed Silica Fume in High Strength Concrete. In *Symposium on Utilization of High Strength Concrete*. Eds. Holand, I., Helland, S., Jakobsen, B. & Lenschow, R., Trondheim. Tapir Publishers, pp 39-49.

Sellevold, E.J. & Nilsen, T., 1987. Condensed silica fume in concrete: A world review In: *Supplementary Cementing Materials for Concrete*. Eds.V.M. Malhotra, Canadian Government Publishing Centre, Ottawa, Canada, pp. 167– 243.

Setter, N. & Roy, D.M. 1978. Mechanical features of chemical shrinkage of cement paste. *Cement and Concrete Research,* 8(5), pp 623-634.

Snoeck, D., Jensen., O.M. & De Belie, N. 2015. The influence of superabsorbent polymers on the autogenous shrinkage properties of cement pastes with supplementary cementitious materials. *Cement and Concrete Research,* 74, pp 59–67.

Standards South Africa, 2005. SANS 50196-3:2005: Methods of testing cement. *Part 3: Determination of setting times and soundness.* SABS.

Standards South Africa, 2006. SANS 50196-1:2006 Methods of testing concrete: *Part 1: Determination of strength.* SABS.

Standards South Africa, 2006. SANS 50196-3:2006 Methods of testing concrete: *Part 3: Determination of setting times and soundness.* SABS.

Standards South Africa, 2006. SANS 6253:2006 Concrete Tests – *Tensile splitting strength of concrete.* SABS.

Standards South Africa, 2014. SANS 50450-1: 2014 Fly ash for concrete: *Part 1: Definition, specifications and conformity criteria*. SABS.

Subramaniam, K.V. 2005. Influence of ultrafine fly ash on the early age response and the shrinkage cracking potential of concrete. *Journal of Materials in Civil Engineering*, 23(17), pp 1076-1086.

Tam, C.M., Tam, W.Y. & Ng, K.M. 2012. Assessing drying shrinkage and water permeability of reactive powder concrete produced in Hong Kong. *Construction and Building Materials*, 26(1), pp 79-89.

Tazawa, E.-i. & Miyazawa, S. 1995. Influence of cement and admixture on autogenous shrinkage of cement paste. *Cement and Concrete Research*, 25(2), pp 281-287.

Tazawa, E. 1996. Technical committee report on Autogenous shrinkage. *The Journal of Clinical Investigation*, 18, pp 29-38.

Tazawa, E. & Miyahara, S. 1997. Influence of constituents and composition on autogenous shrinkage of cementitious materials. *Magazine of Concrete Research*, 48(178), pp 15-22.

Telford, T. FIP, State of the Art Report: Condensed Silica Fume in Concrete, London, 1988.

Termkhajornkit, P., Nawa, T., Nakai, M. & Saito, T. 2005. Effect of fly ash on autogenous shrinkage. *Cement and Concrete Research*, 35(3), pp 473-482.

Thomas, M.D.A., Shehata, M.H., Shashiprakash, S.G., Hopkins, D.S. & Cail, K. 1999. Use of ternary cementitious systems containing silica fume and fly ash in concrete. *Cement and Concrete Research*, 29(8), pp 1207–1214.

Tian, Q. 2006. *Study on shrinkage and mechanism of cement-based material at low water to binder ratio incorporating high volume mineral admixtures.* Southeast University.

Tydlitát, V., Zákoutský, J., Schmieder, M. & Černý, R. 2012. Application of large-volume calorimetry for monitoring the early-stage hydration heat development in cement-based composites as a function of w/c. *Thermochimica Acta*, 546, pp 44-48.

van Breugel, K. & van Tuan, N. 2014. Autogenous Shrinkage of HPC and Ways to Mitigate it. *Key Engineering Materials*, 629-630, pp 3-20.

Wang, C., Pu, X.C., Chen, K., Liu, F., Wu, J.H. & Peng, X.Q. 2008. Measurement of Hydration Progress of Cement Paste Materials with Extreme-Low W/B. *Journal of Materials Science and Engineering*, 26, pp 852-857.

Wang, X.-Y. 2014. Effect of fly ash on properties evolution of cement based materials. *Construction and Building Materials*, 69, pp 32-40.

Weiss, J. 2002. Experimental determination of the 'Time Zero', t0 ('Maturity-Zero', M0). In *International RILEM Conference on Early Age Cracking in Cementitious Systems—EAC, RILEM TC 181-EAS*. Haifa, Israel.

Winnefeld, F., Becker, S., Pakusch, J. & Götz, T. 2007. Effects of the molecular architecture of comb-shaped superplasticizers on their performance in cementitious systems. *Cement and Concrete Composites*, 29(4), pp 251-262.

Wu, L., Farzadnia, N., Shi, C., Zhang, Z. & Wang, H. 2017. Autogenous shrinkage of high performance concrete: A review. *Construction and Building Materials*, 149, pp 62-75.

Wyrzykowski, M. & Lura, P. 2015. Reduction of Autogenous Shrinkage in OPC and BFSC Pastes with Internal Curing. *XIII International Conference on Durability of Building Materials and Components*, pp 999-1005.

Wyrzykowski, M., Hu, Z., Ghourchian, S., Scrivener, K. & Lura, P. 2017. Corrugated tube protocol for autogenous shrinkage measurements: review and statistical assessment. *Materials and Structures*, 50(57).

Xu, Q., Hu, J., Ruiz, J.M., Wang, K. & Ge, Z. 2010. Isothermal calorimetry tests and modeling of cement hydration parameters. *Thermochimica Acta*, 499(1-2), pp 91-99.

Yang, Y., Sato, R. & Kawai, K. 2005. Autogenous shrinkage of high-strength concrete containing silica fume under drying at early ages. *Cement and Concrete Research*, 35(3), pp 449-456.

Zhang, M.H., Tam, C.T. & Leow, M.P. 2003. Effect of water-to-cementitious materials ratio and silica fume on the autogenous shrinkage of concrete. *Cement and Concrete Research*, 33(10), pp 1687-1694.

APPENDIX A: CALIBRATION CURVES

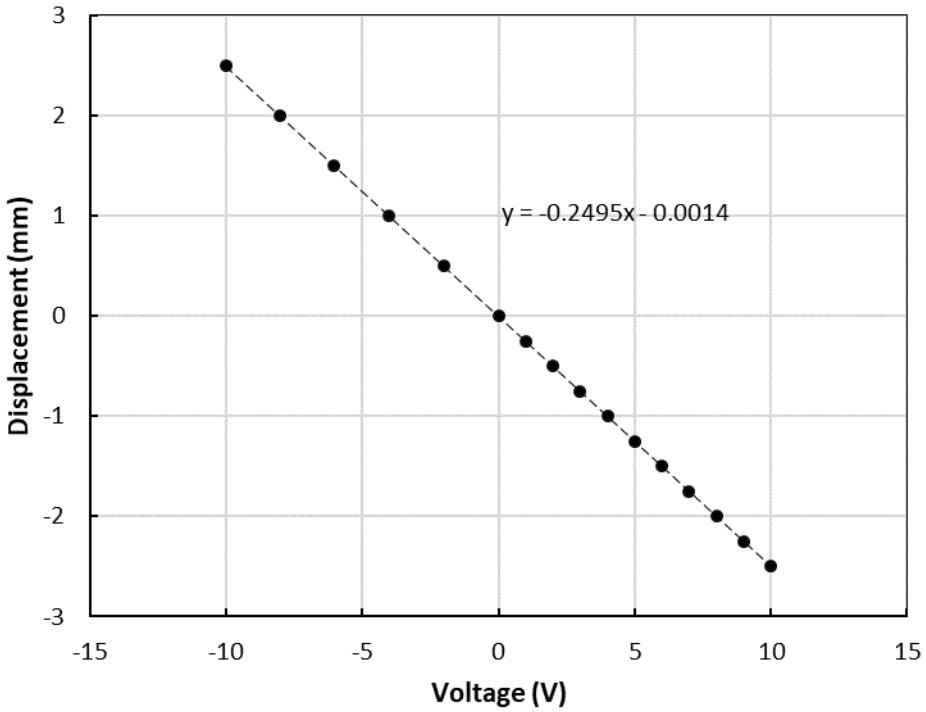

Figure A.1 Calibration curve for LVDT 1

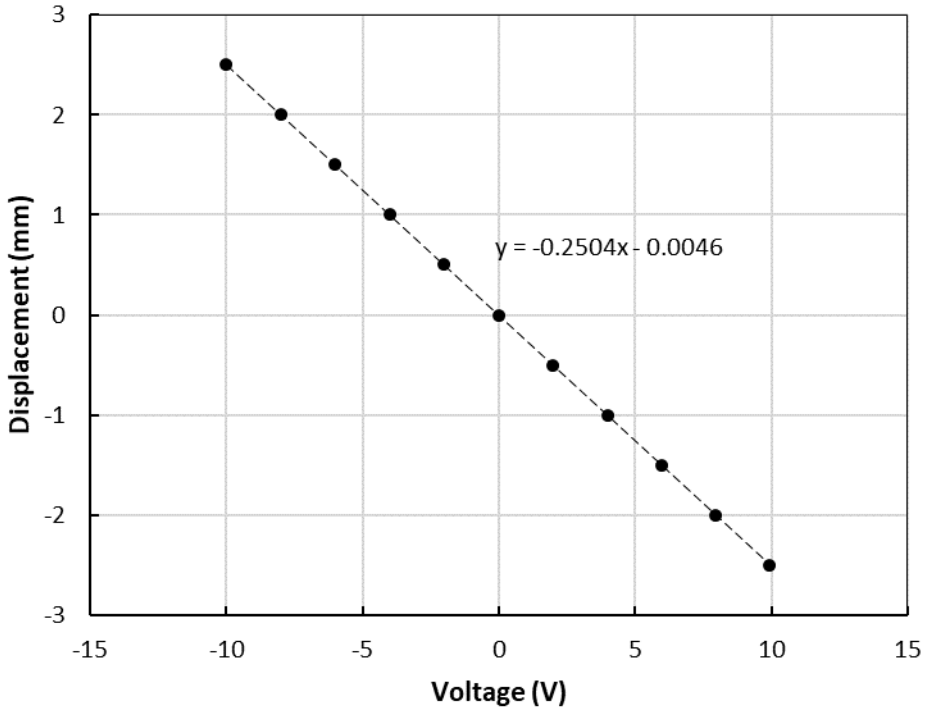

Figure A.2 Calibration curve for LVDT 2

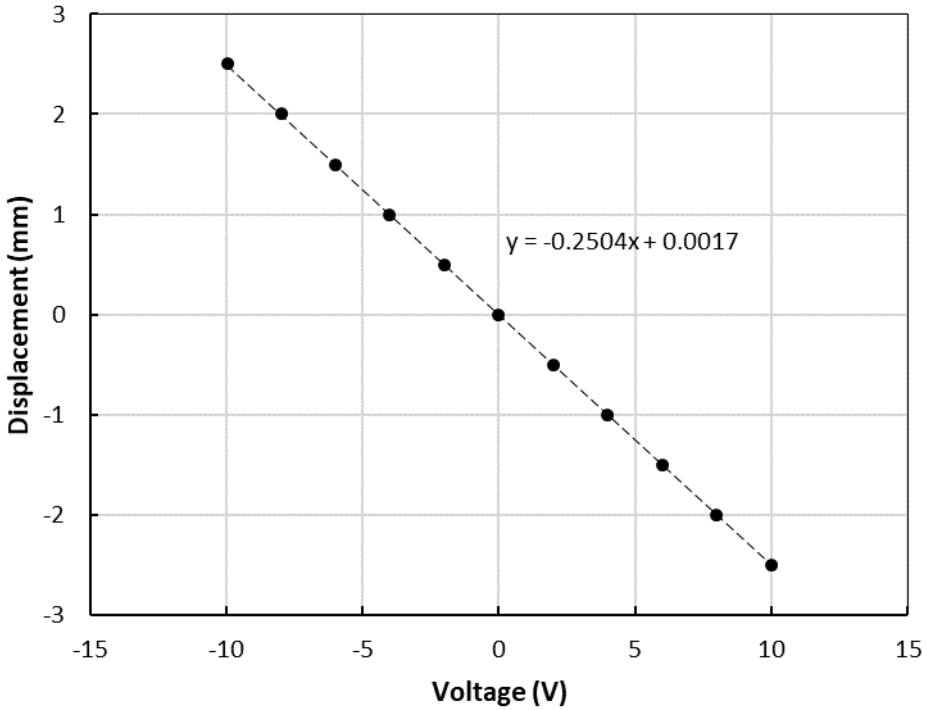

Figure A.3 Calibration curve for LVDT 3

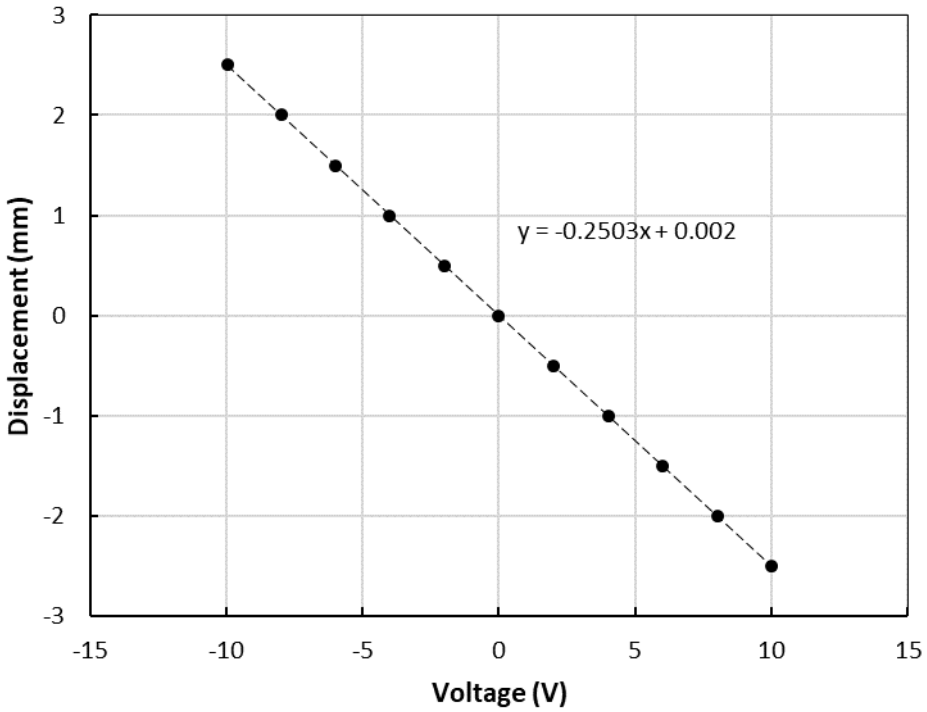

Figure A.4 Calibration curve for LVDT 4

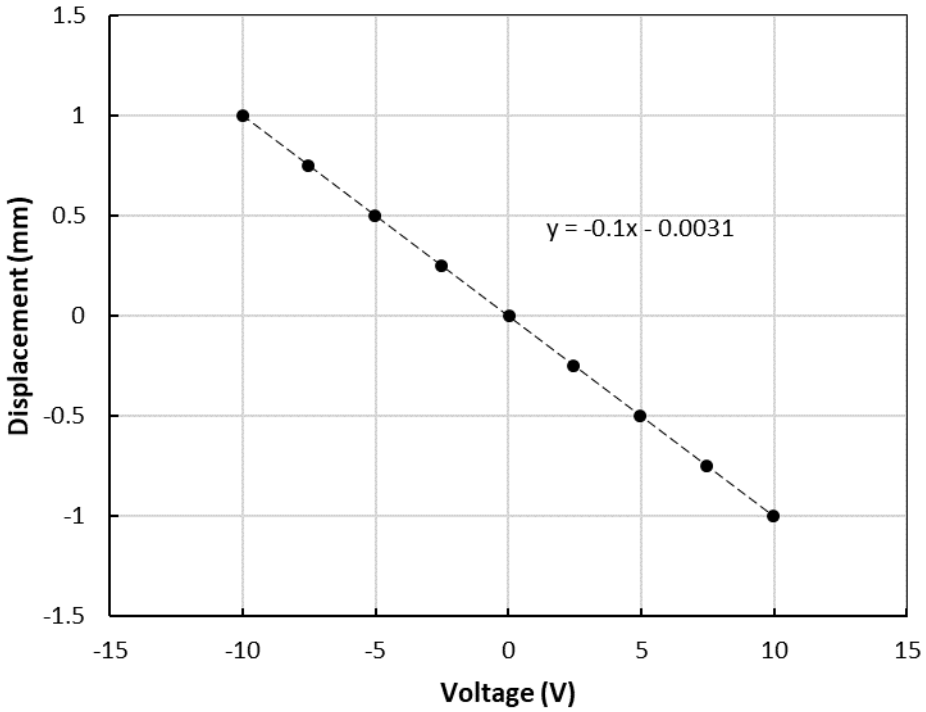

Figure A.5 Calibration curve for LVDT 5

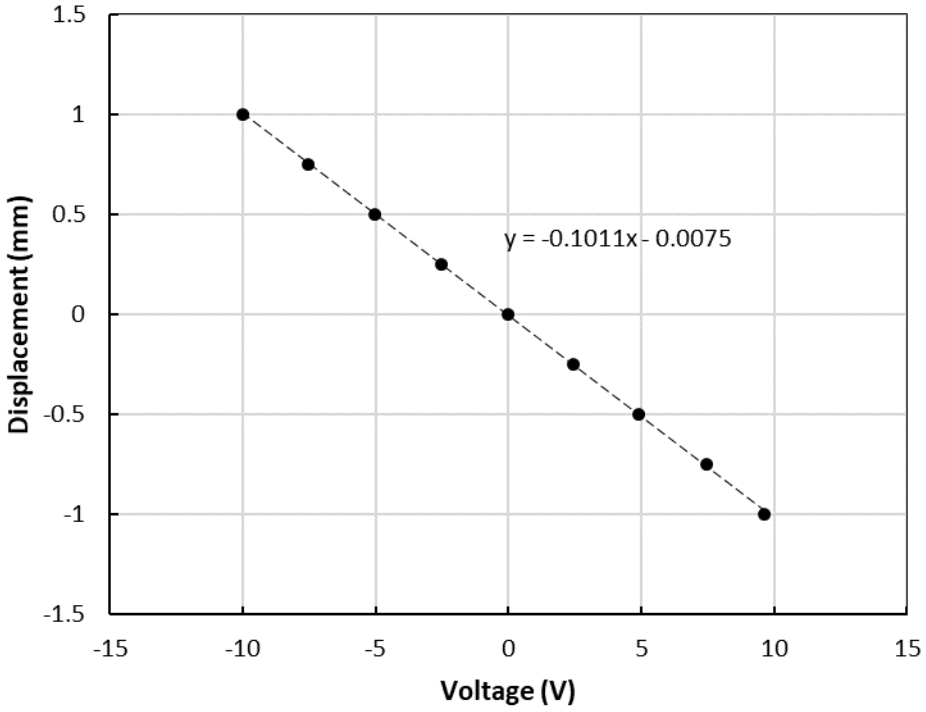

Figure A.6 Calibration curve for LVDT 6

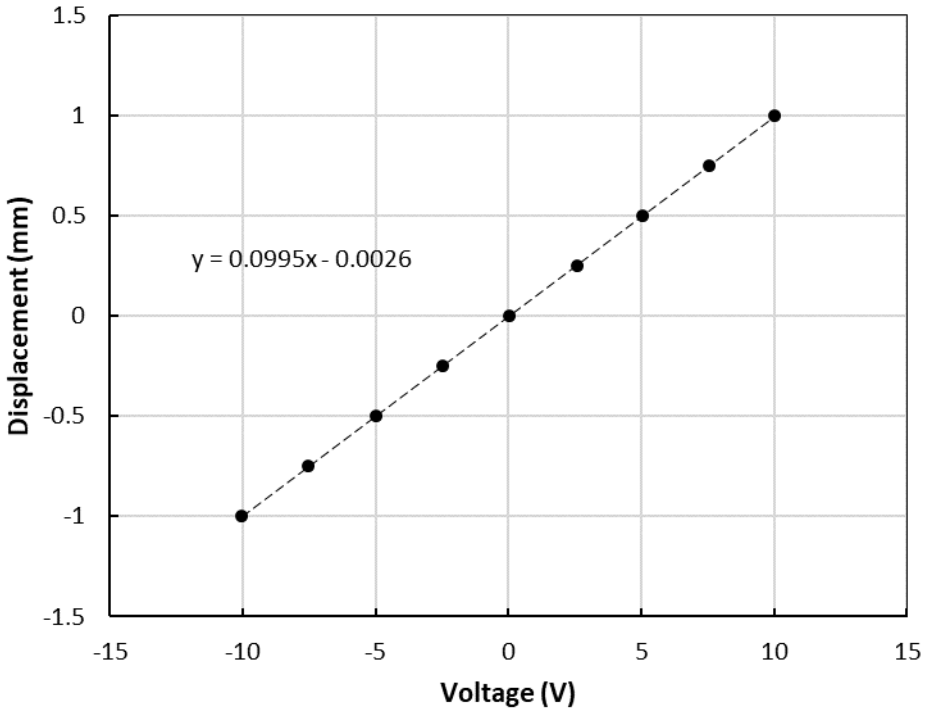

Figure A.7 Calibration curve for LVDT 7

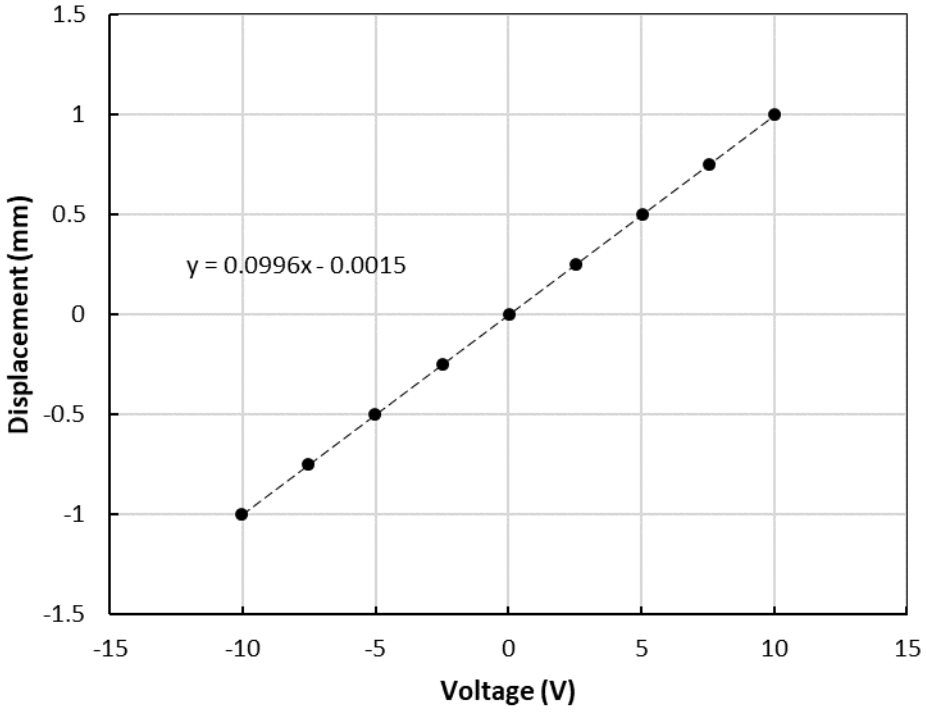

Figure A.8 Calibration curve for LVDT 8

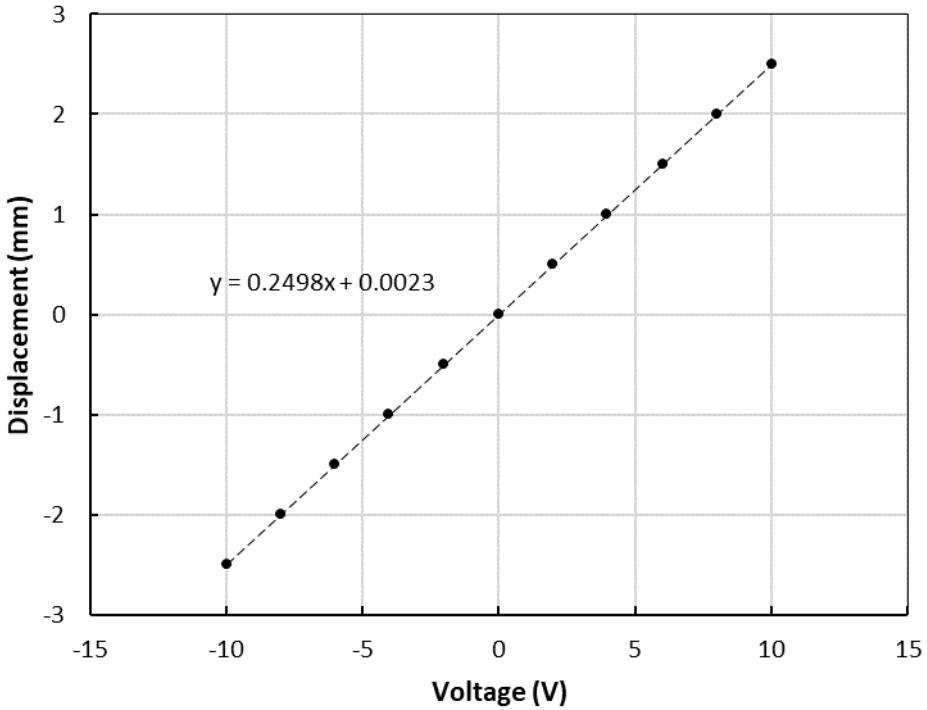

Figure A.9 Calibration curve for LVDT 9

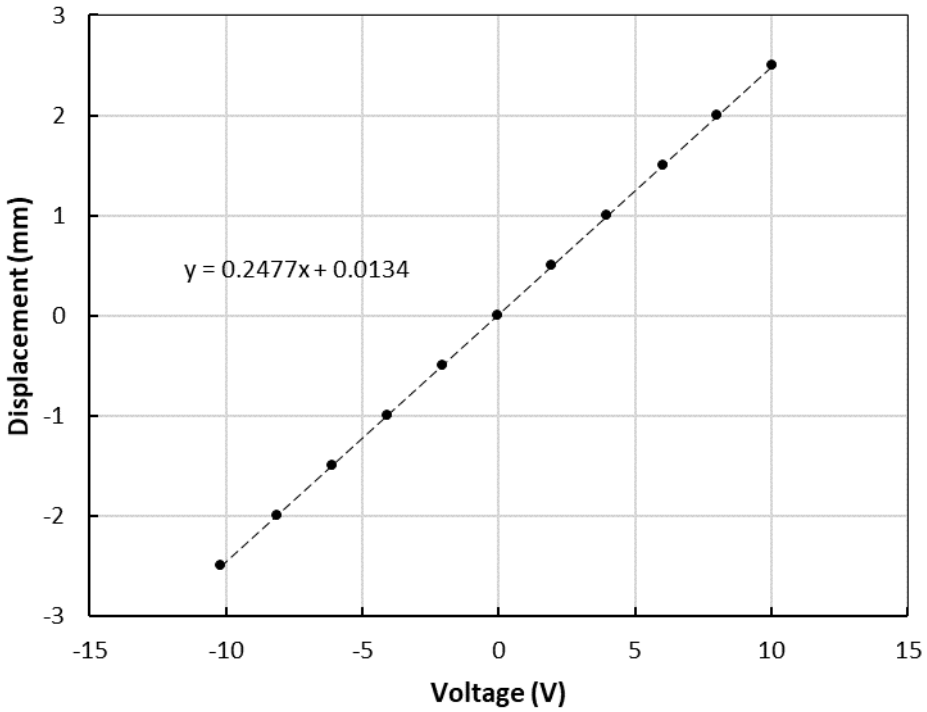

Figure A.10 Calibration curve for LVDT 10

APPENDIX B: BEAM TEMPERATURES

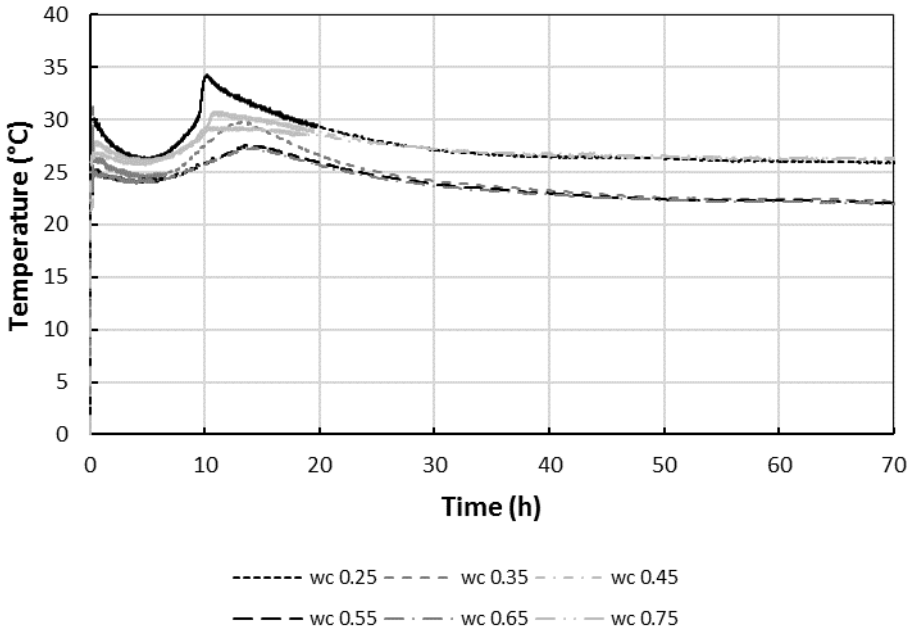

Figure B.1 Beam temperatures for PC mixtures

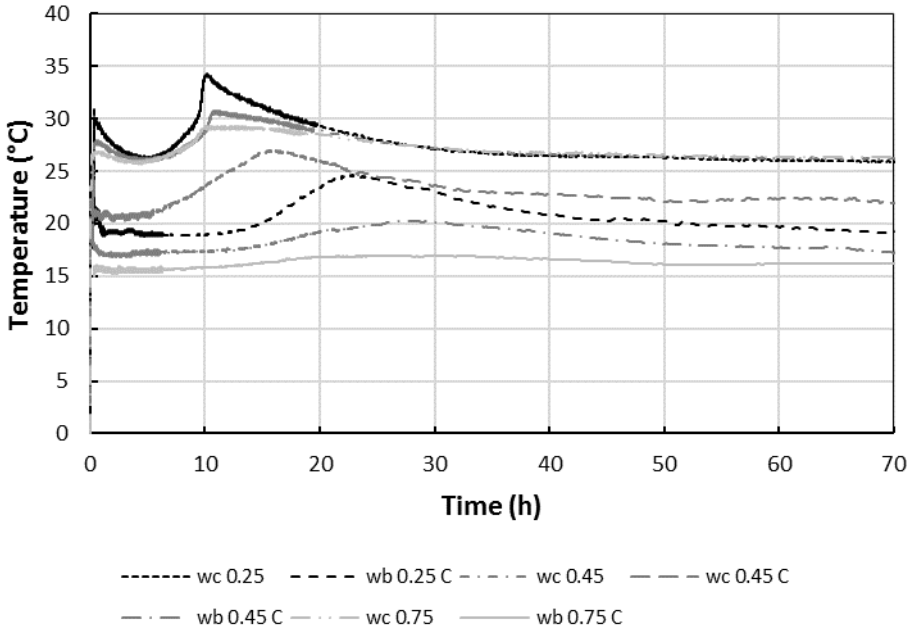

Figure B.2 Beam temperatures for mixtures with CSF

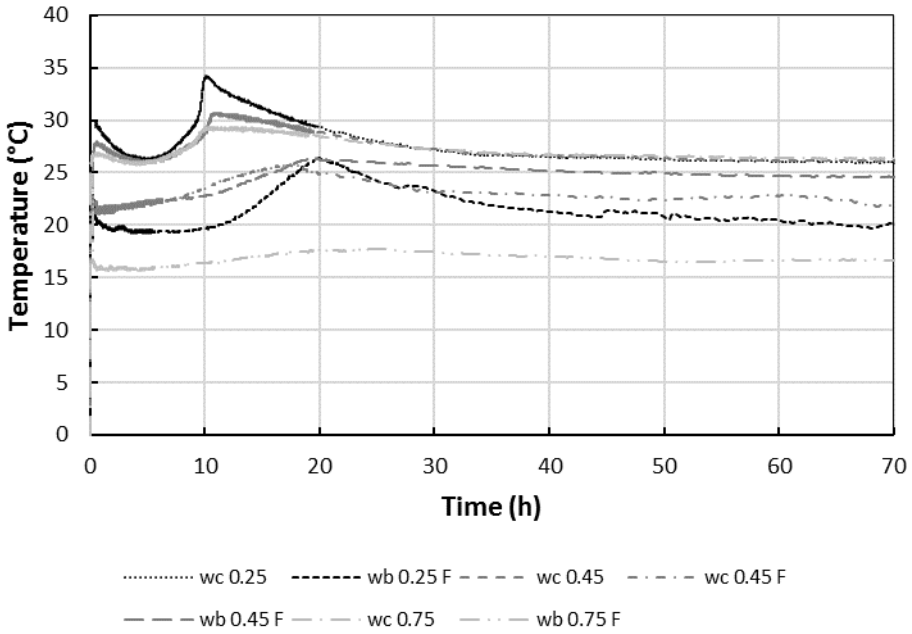

Figure B.3 Beam temperatures for mixtures with FA

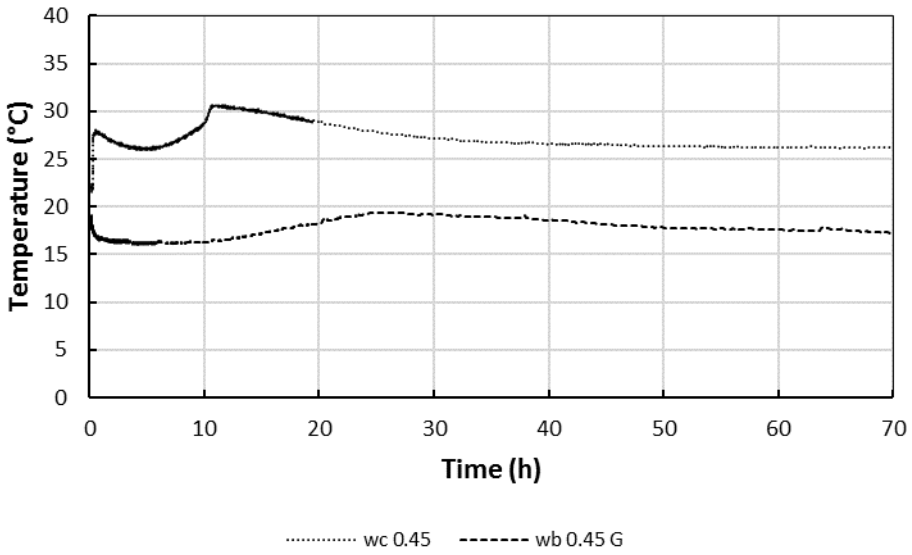

Figure B.4 Beam temperatures for mixtures with GGBS

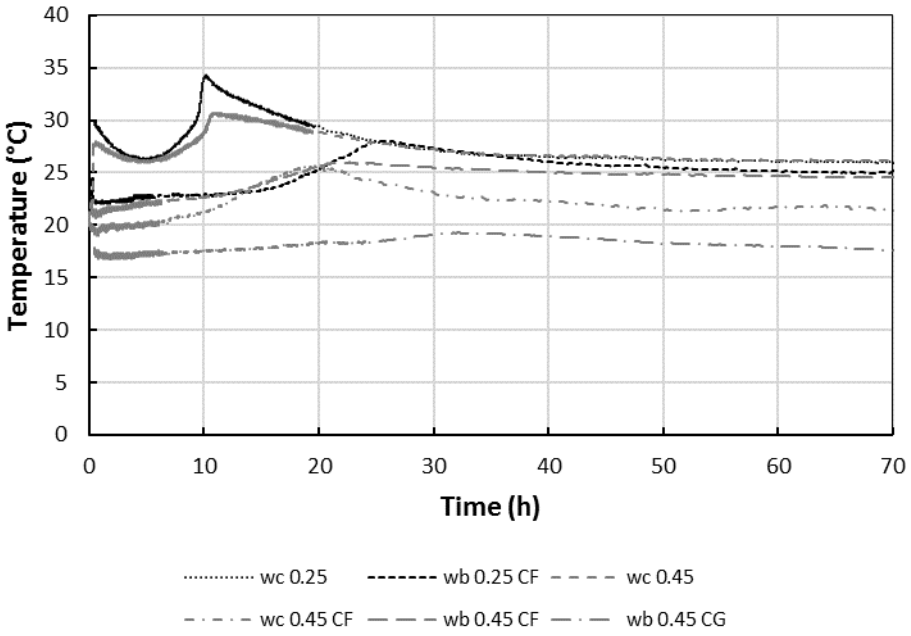

Figure B.5 Beam temperatures for mixtures with multiple SCMs

APPENDIX C:

SEMI-ADIABATIC TEMPERATURE CHANGE

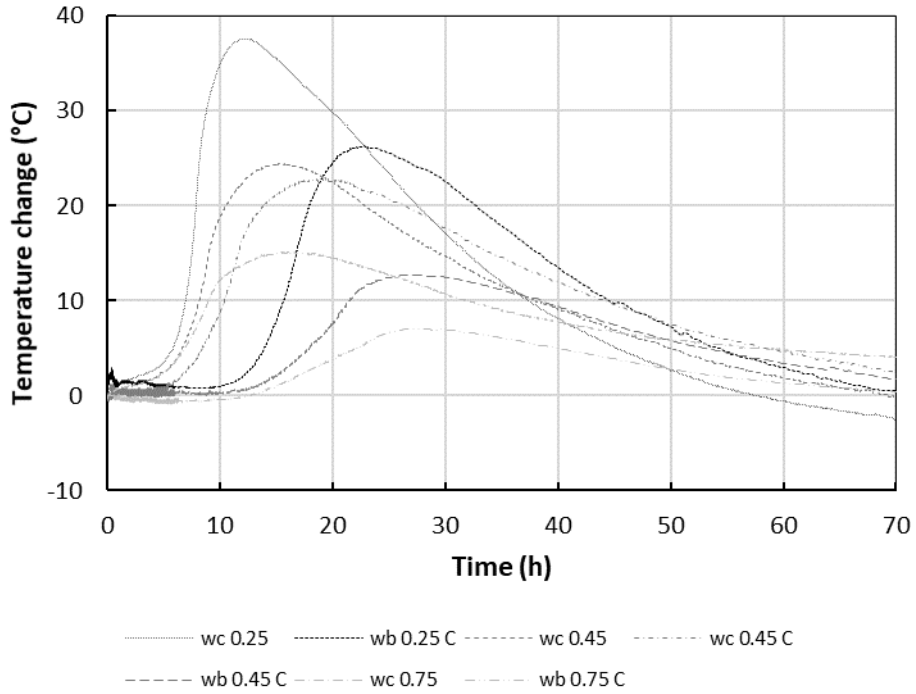

Figure C.1 Semi-adiabatic temperature change with time for mixtures with CSF

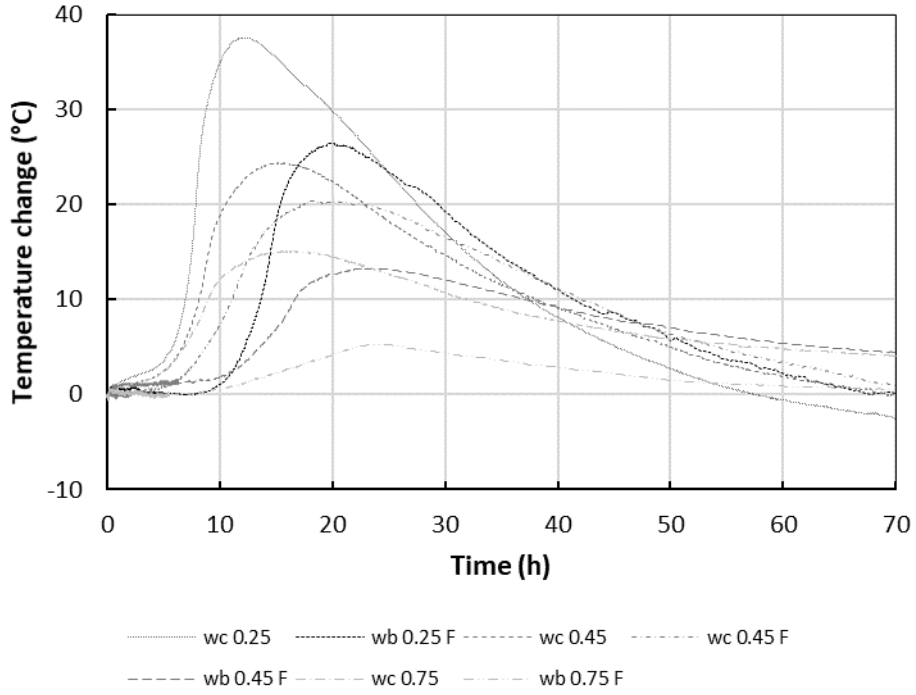

Figure C.2 Semi-adiabatic temperature change with time for mixtures with FA

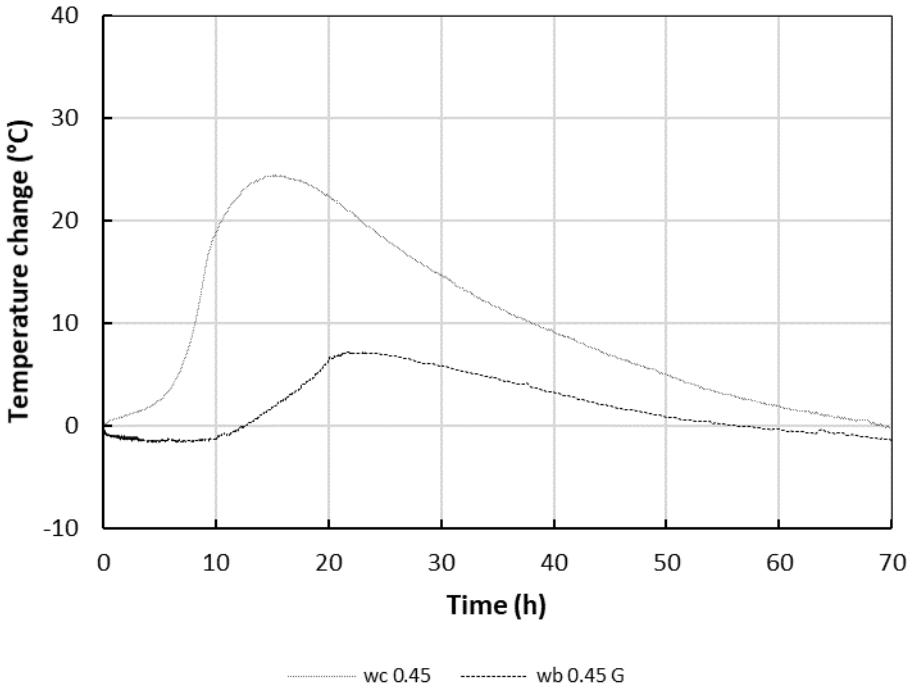

Figure C.3 Semi-adiabatic temperature change with time for mixtures with GGBS

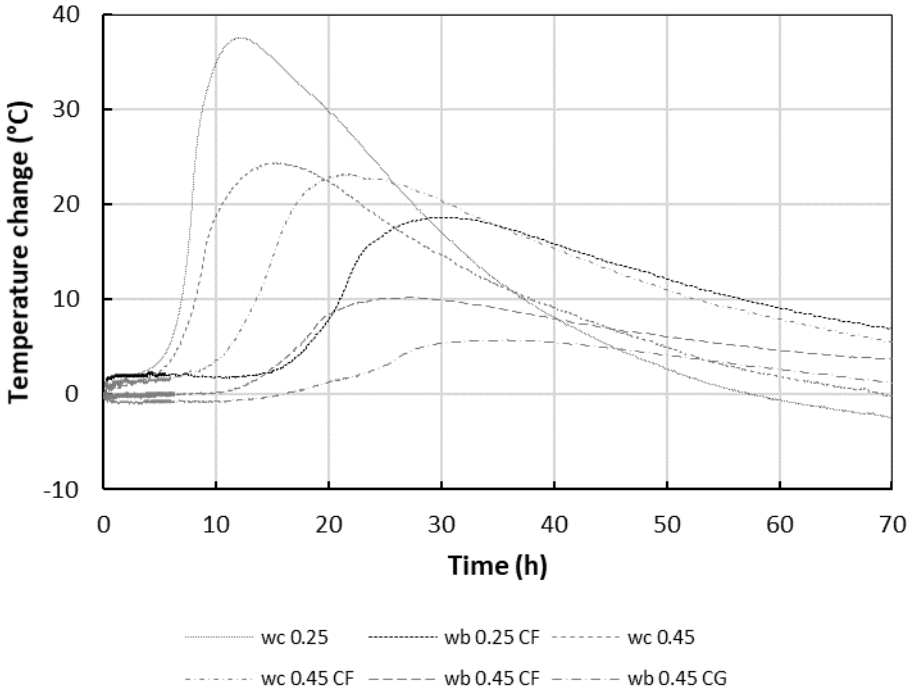

Figure C.4 Semi-adiabatic temperature change with time for mixtures with multiple SCMs

APPENDIX D:

ISOTHERMAL CALORIMETRY DATA

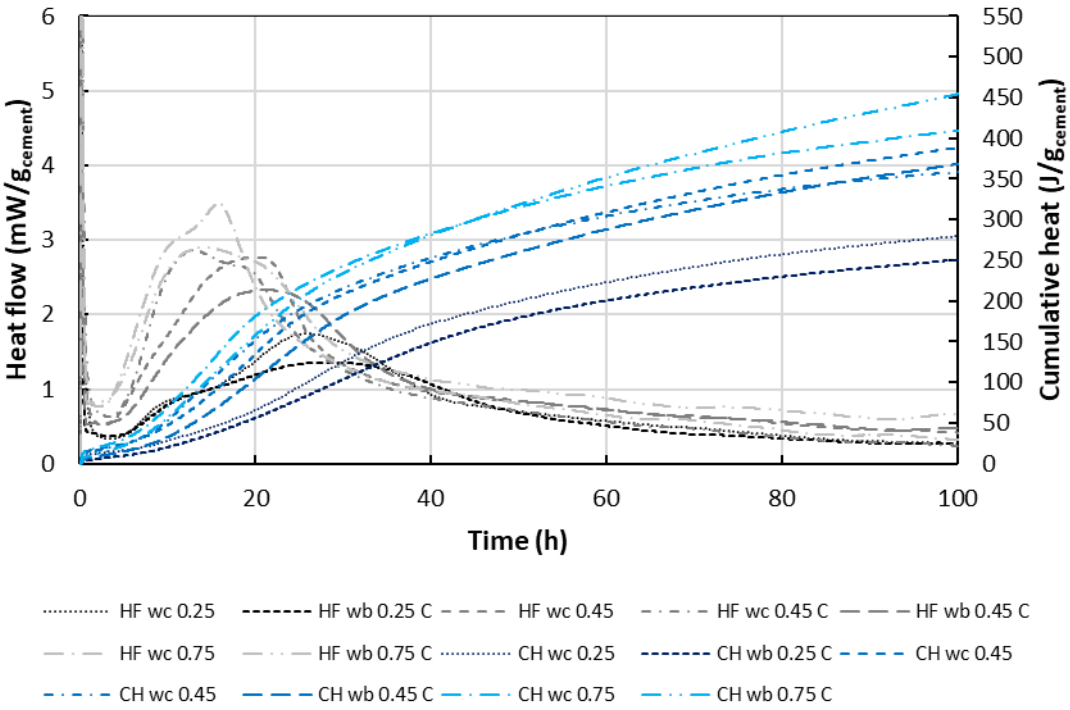

Figure D.1 Isothermal calorimetry heat flow and cumulative heat with time for mixtures with CSF

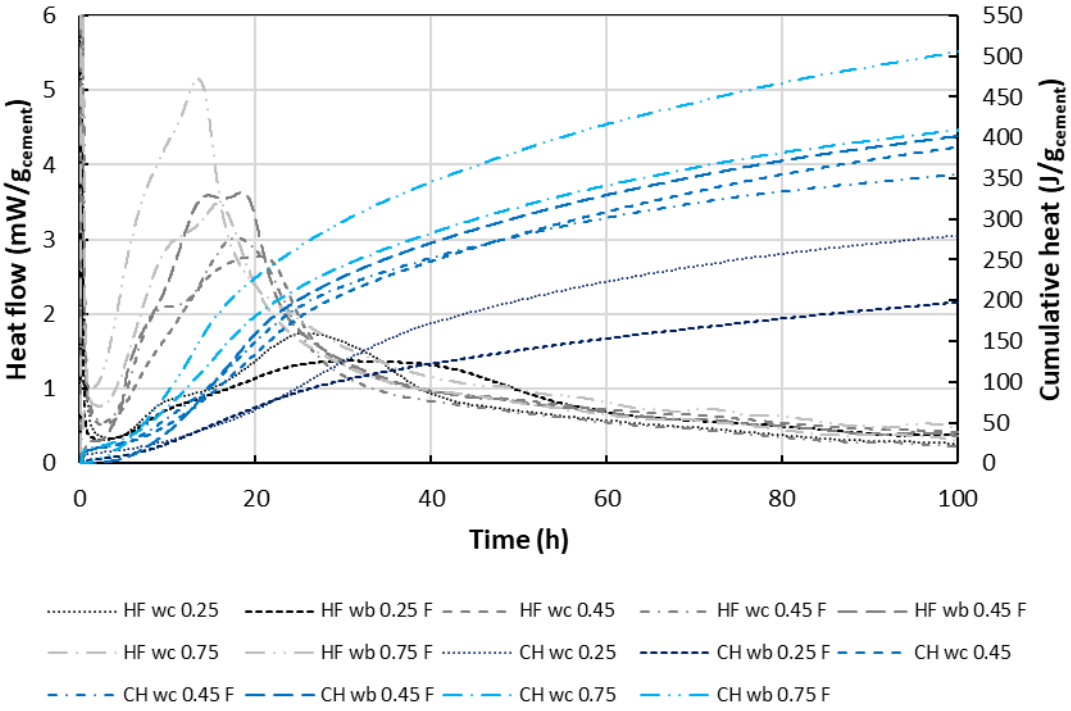

Figure D.2 Isothermal calorimetry heat flow and cumulative heat with time for mixtures with FA

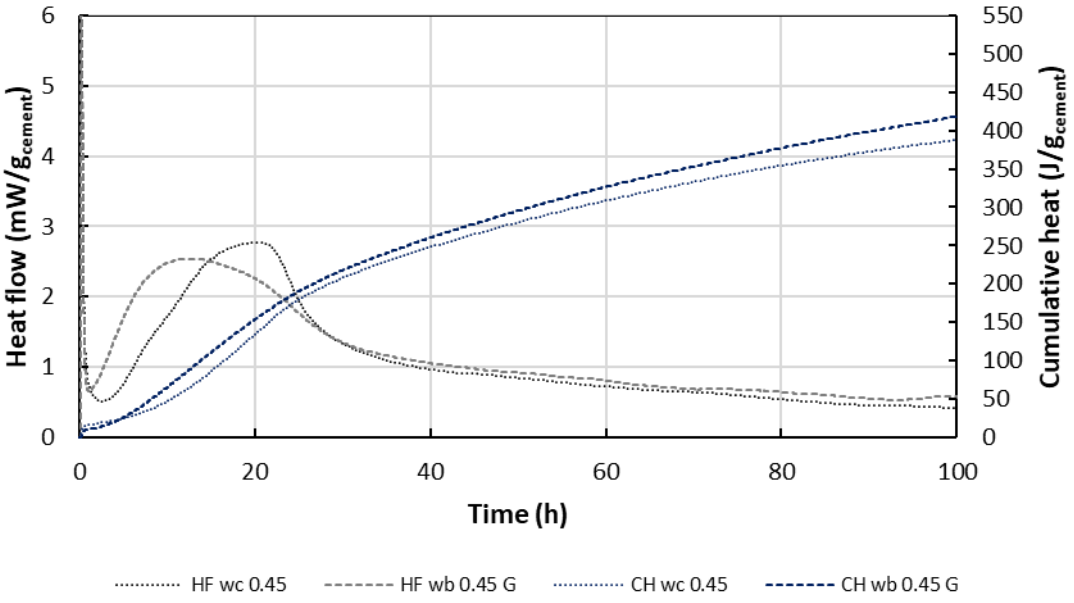

Figure D.3 Isothermal calorimetry heat flow and cumulative heat with time for mixtures with GGBS

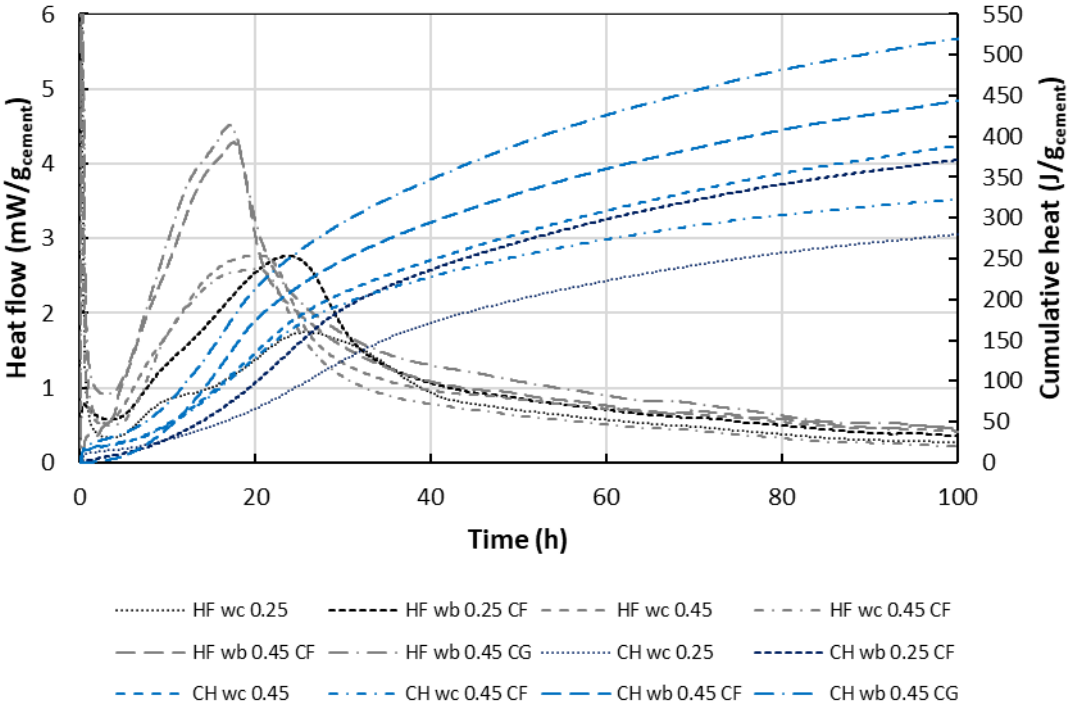

Figure D.4 Isothermal calorimetry heat flow and cumulative heat with time for mixtures containing multiple SCMs

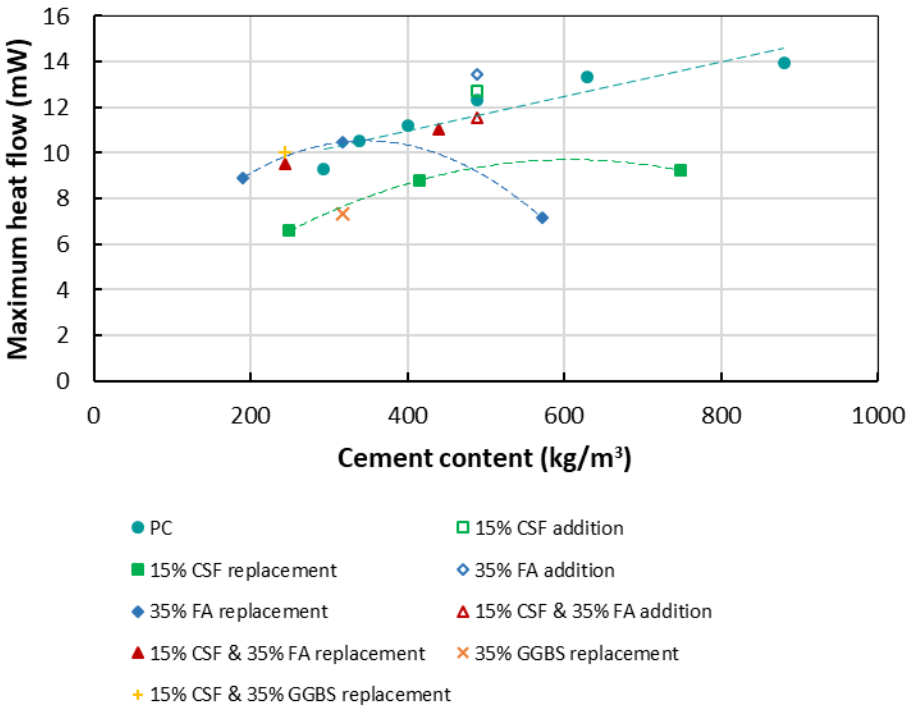

Figure D.5 Total maximum heat flow with cement content

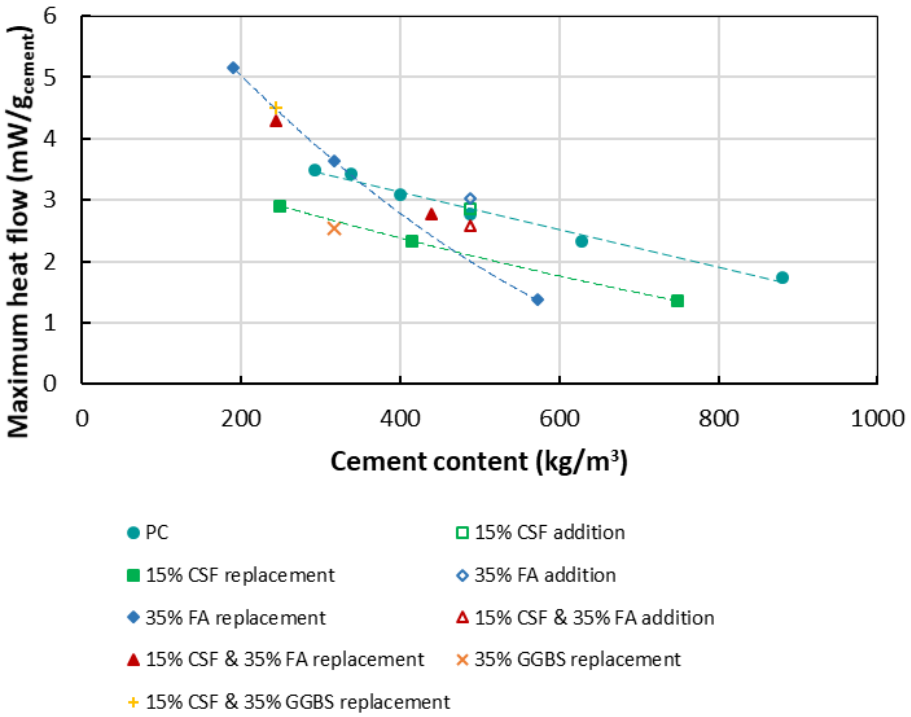

Figure D.6 Normalised maximum heat flow with cement content

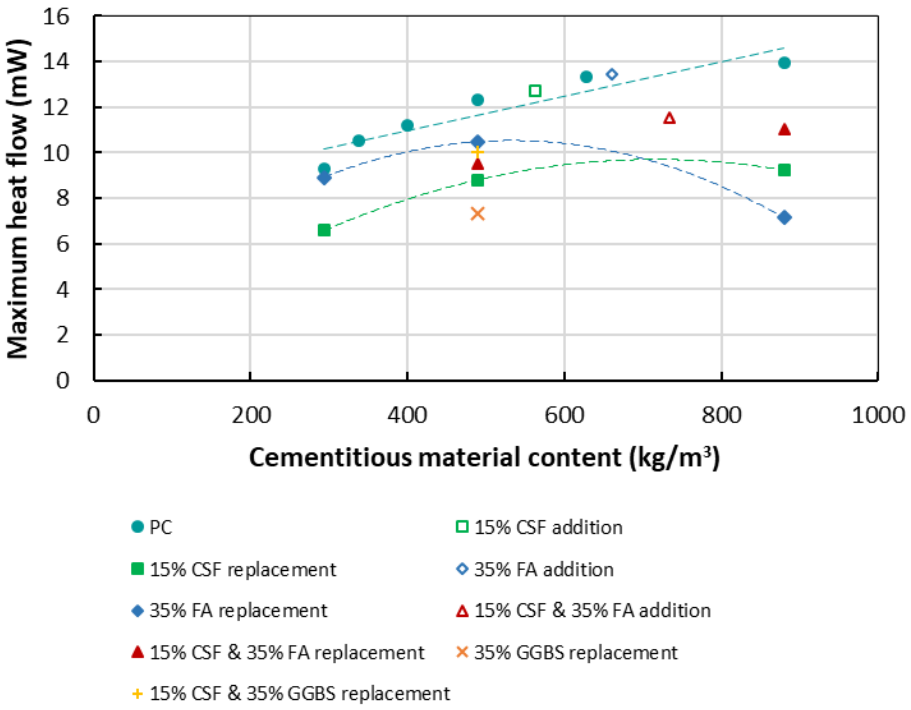

Figure D.7 Total maximum heat flow with cementitious material content

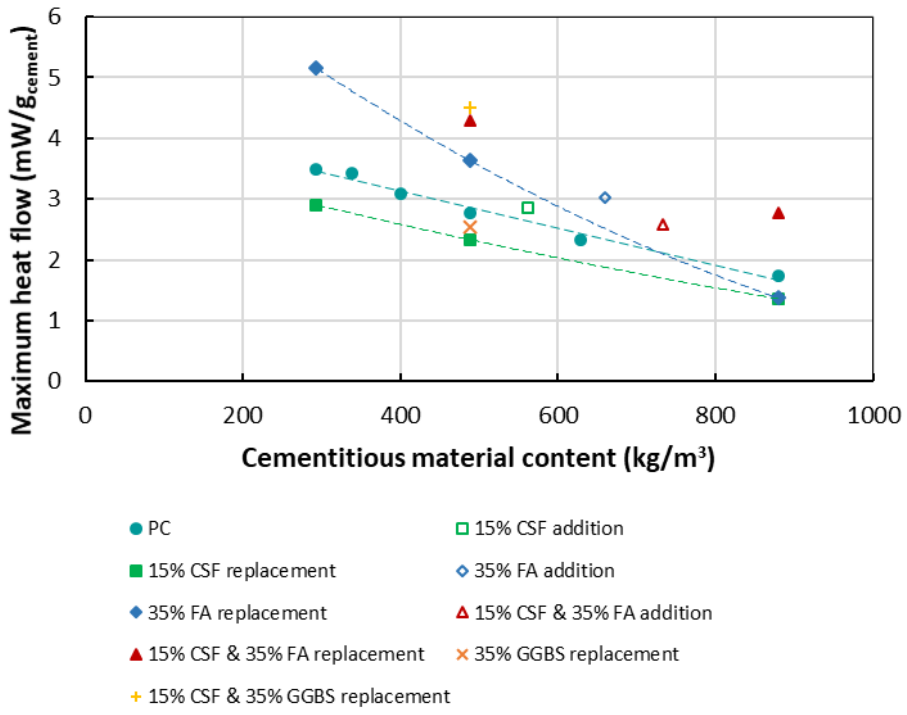

Figure D.8 Normalised maximum heat flow with cementitious material content

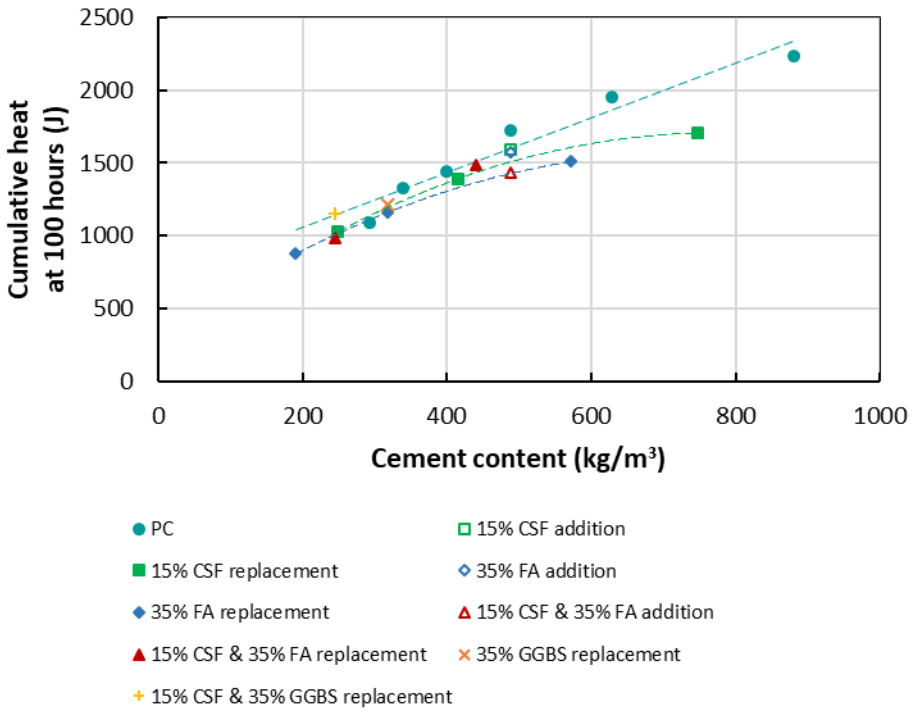

Figure D.9 Total cumulative heat released at 100 hours with cement content

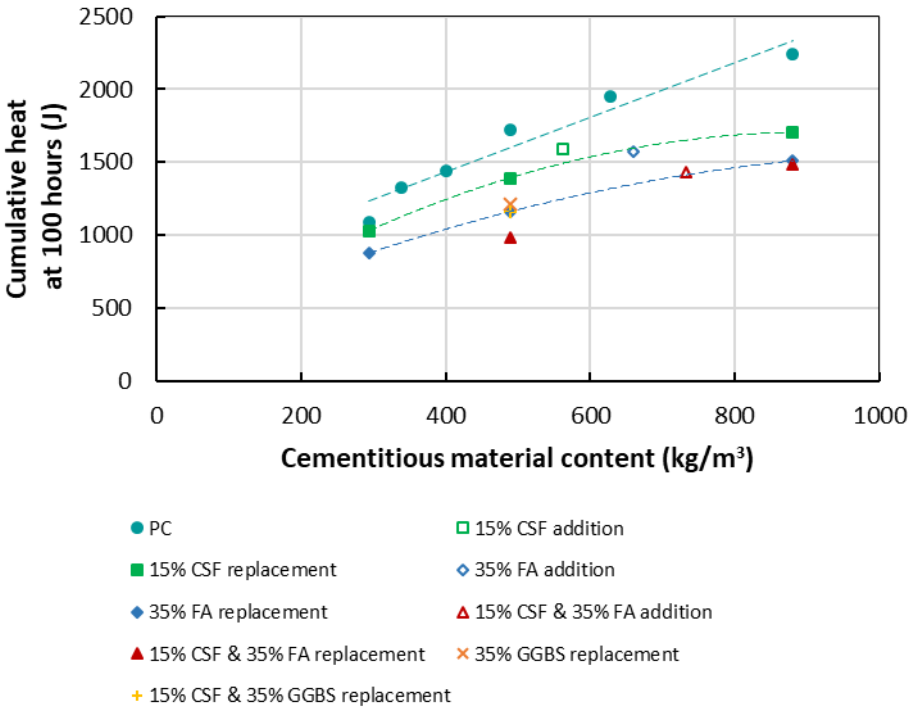

Figure D.10 Total cumulative heat released at 100 hours with cementitious material content

APPENDIX E:

AUTOGENOUS SHRINKAGE DATA

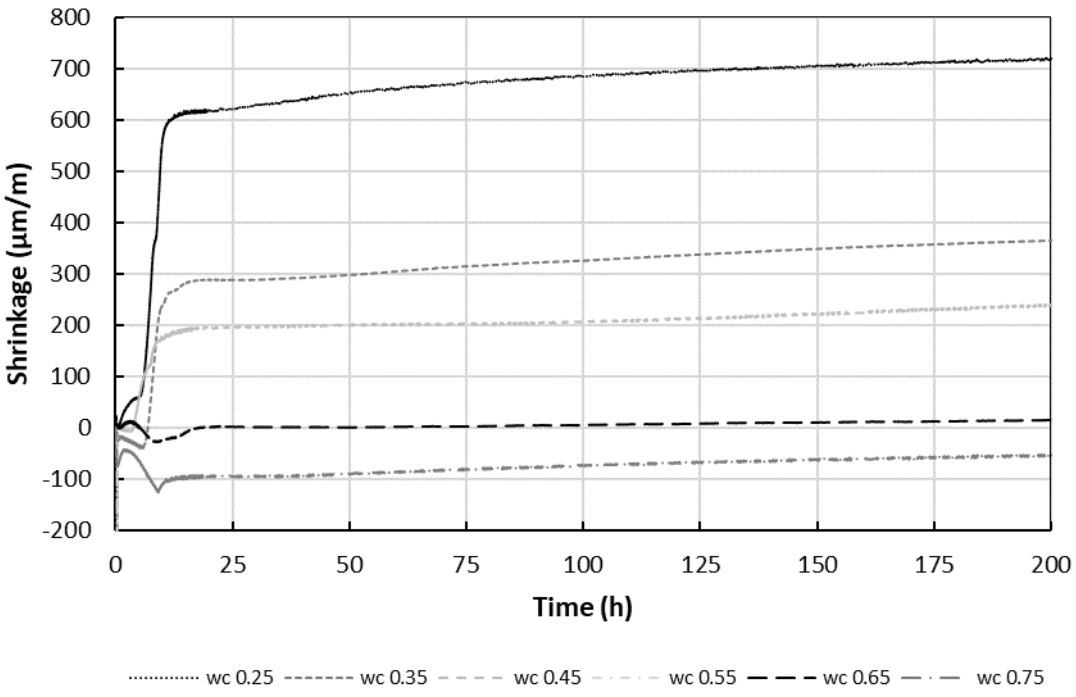

Figure E.1 Beam shrinkage for PC mixtures

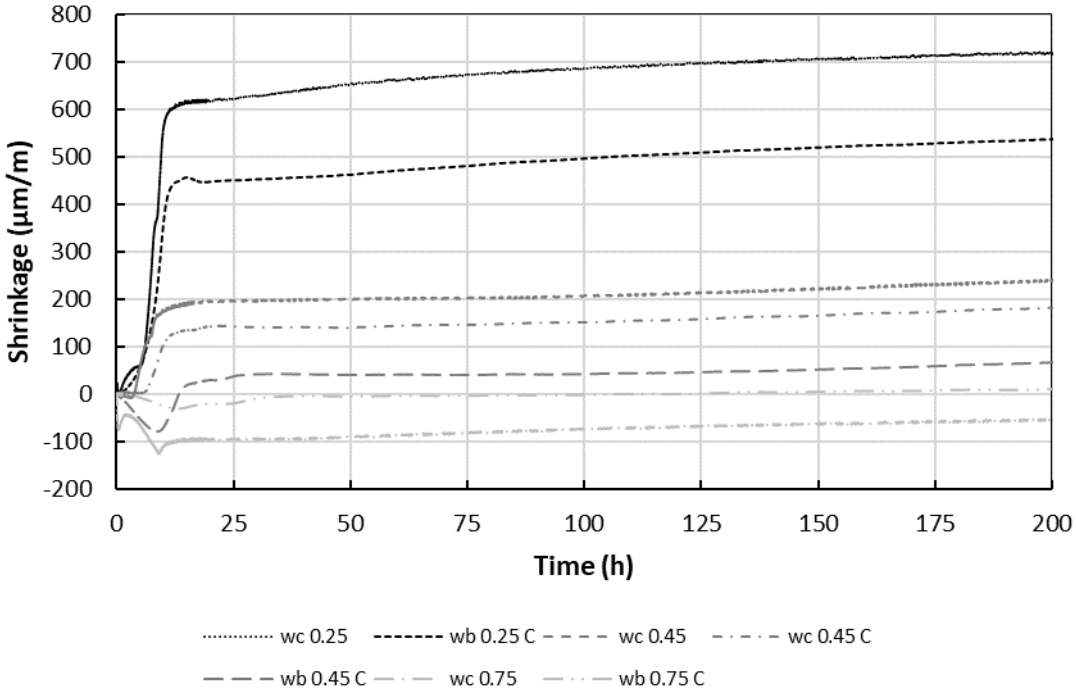

Figure E.2 Beam shrinkage for samples containing CSF

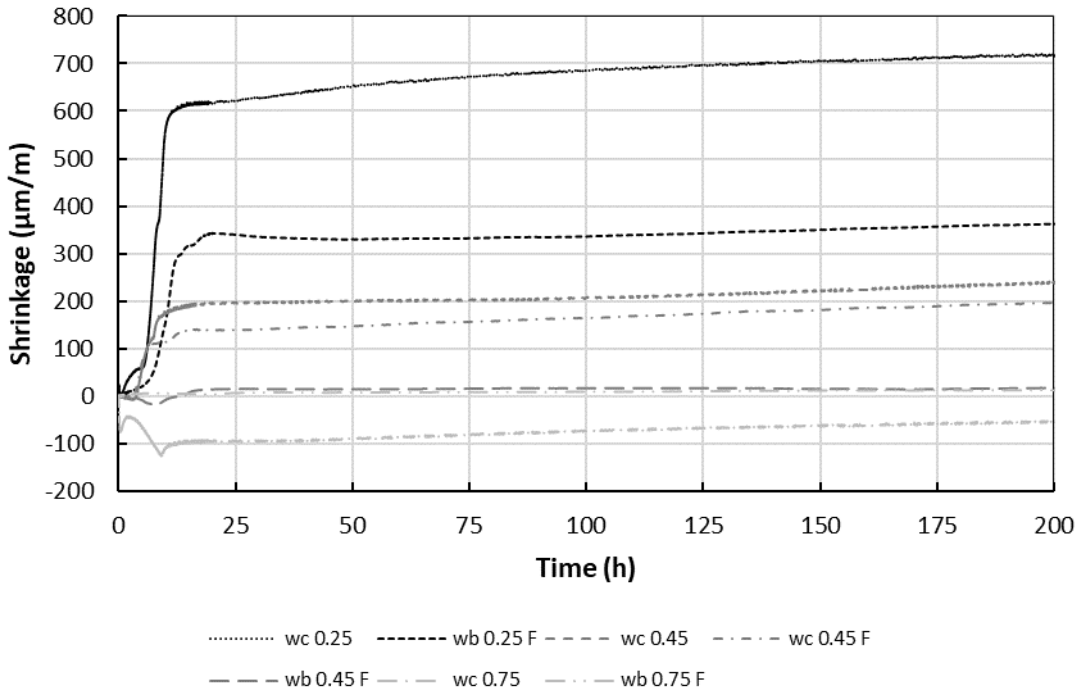

Figure E.3 Beam shrinkage for samples containing FA

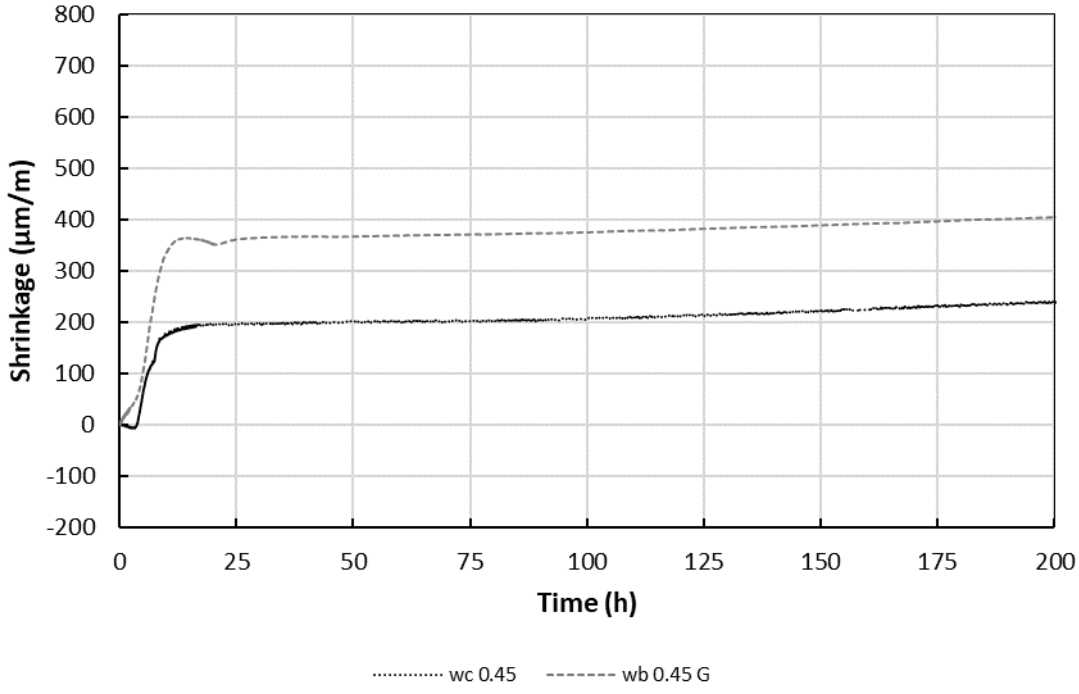

Figure E.4 Beam shrinkage for samples containing GGBS

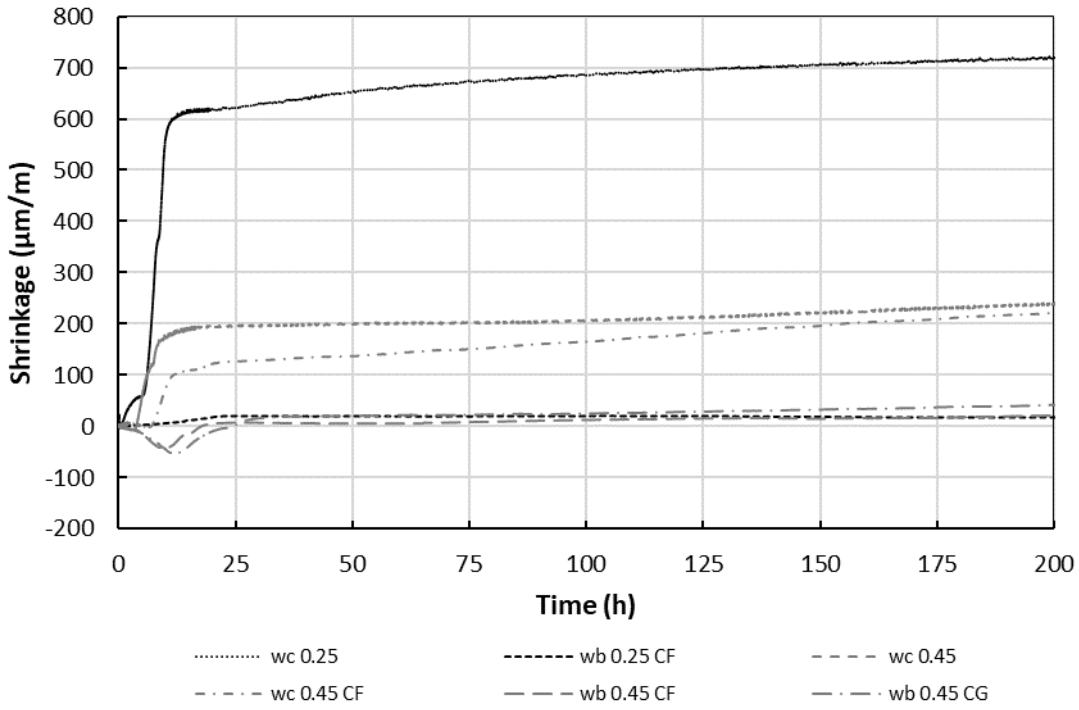

Figure E.5 Beam shrinkage for samples containing multiple SCMs

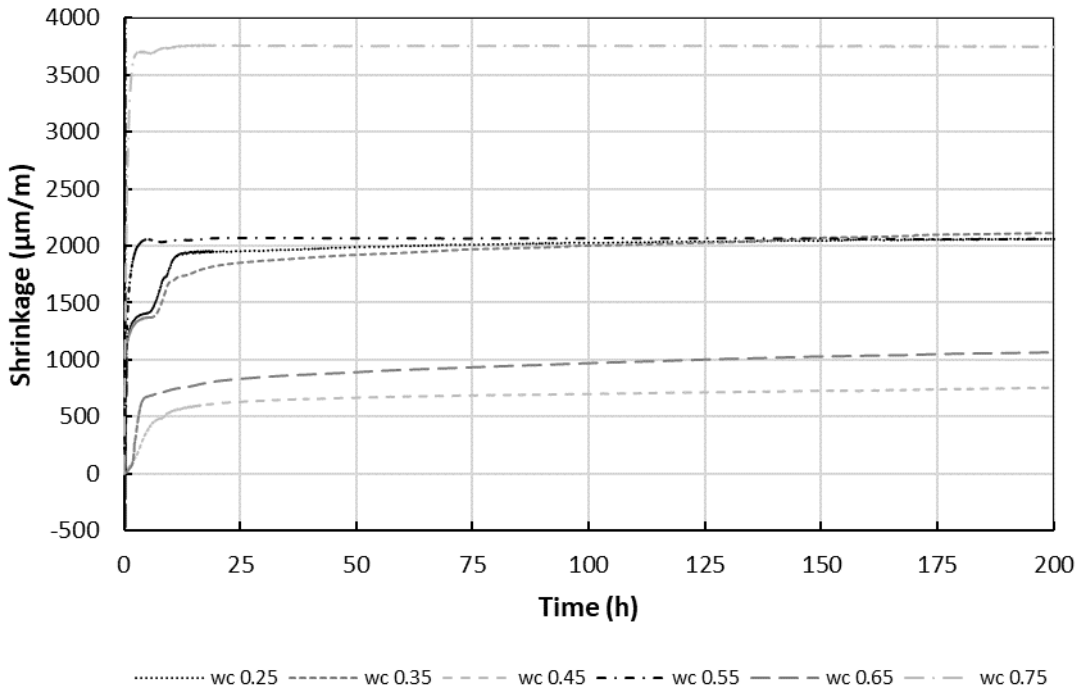

Figure E.6 Corrugated tube shrinkage for PC samples

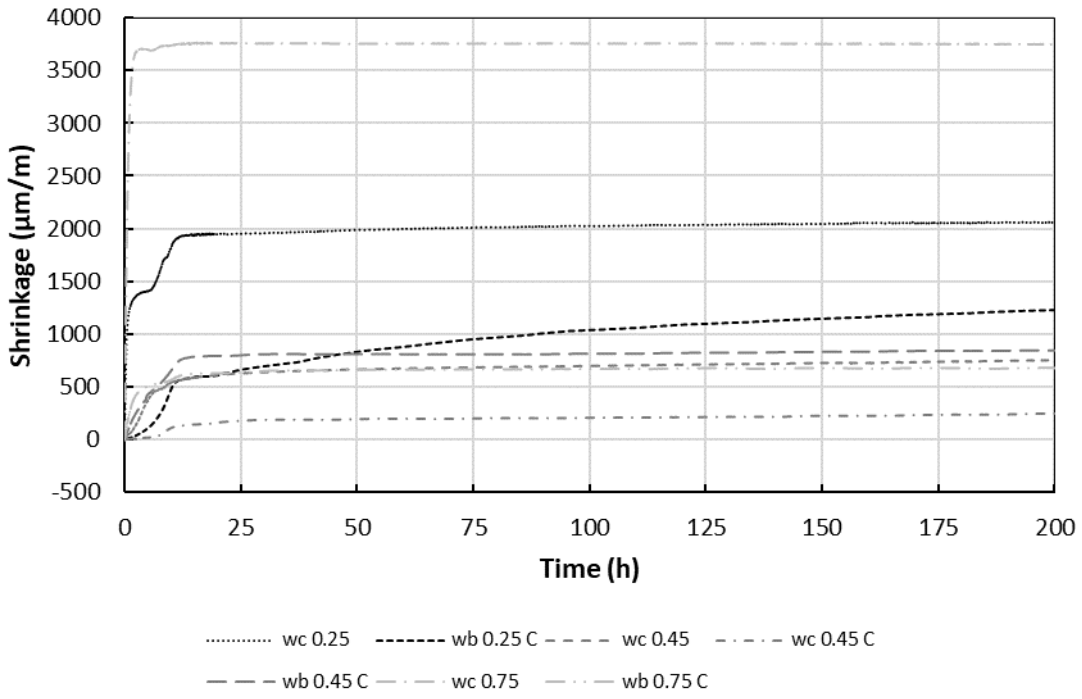

Figure E.7 Corrugated tube shrinkage for samples containing CSF

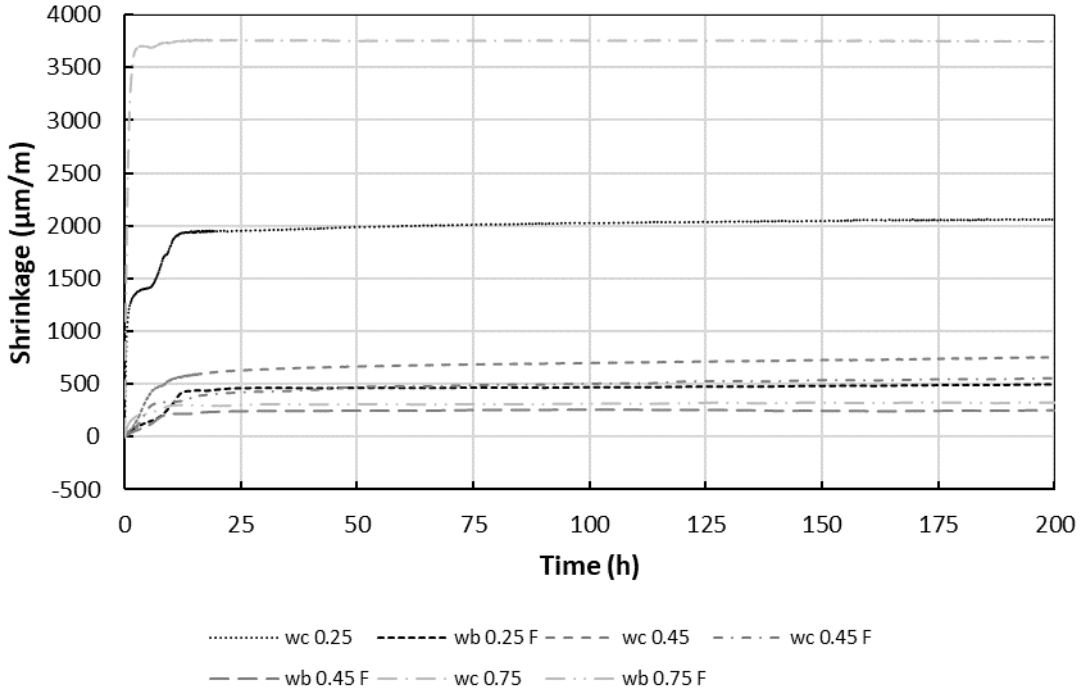

Figure E.8 Corrugated tube shrinkage for samples containing FA

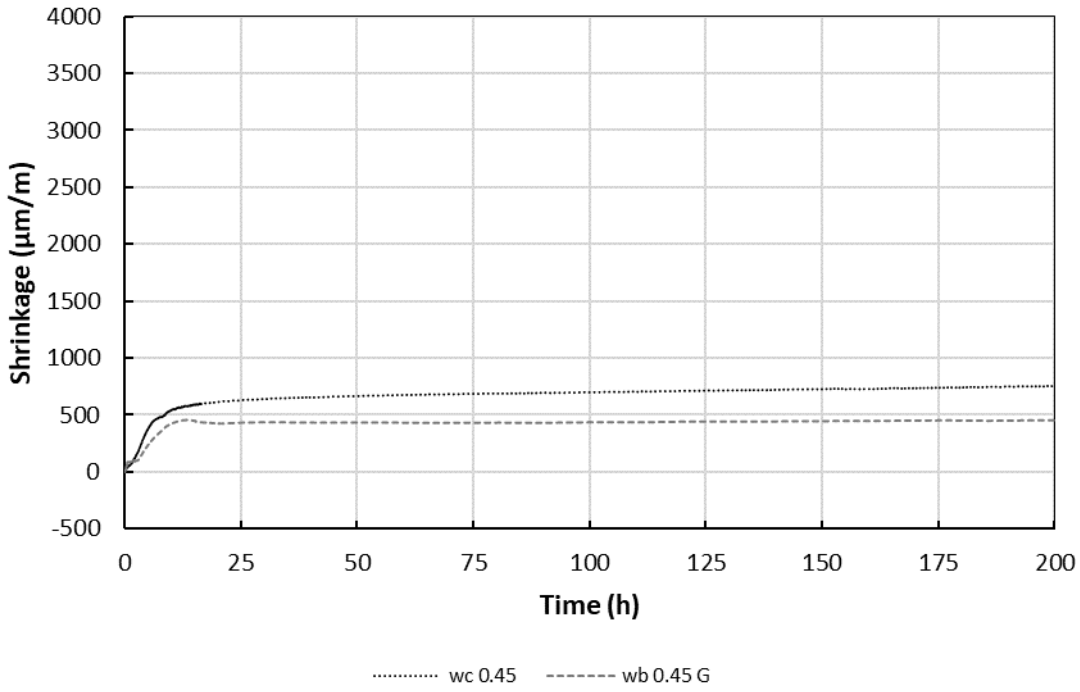

Figure E.9 Corrugated tube shrinkage for samples containing GGBS

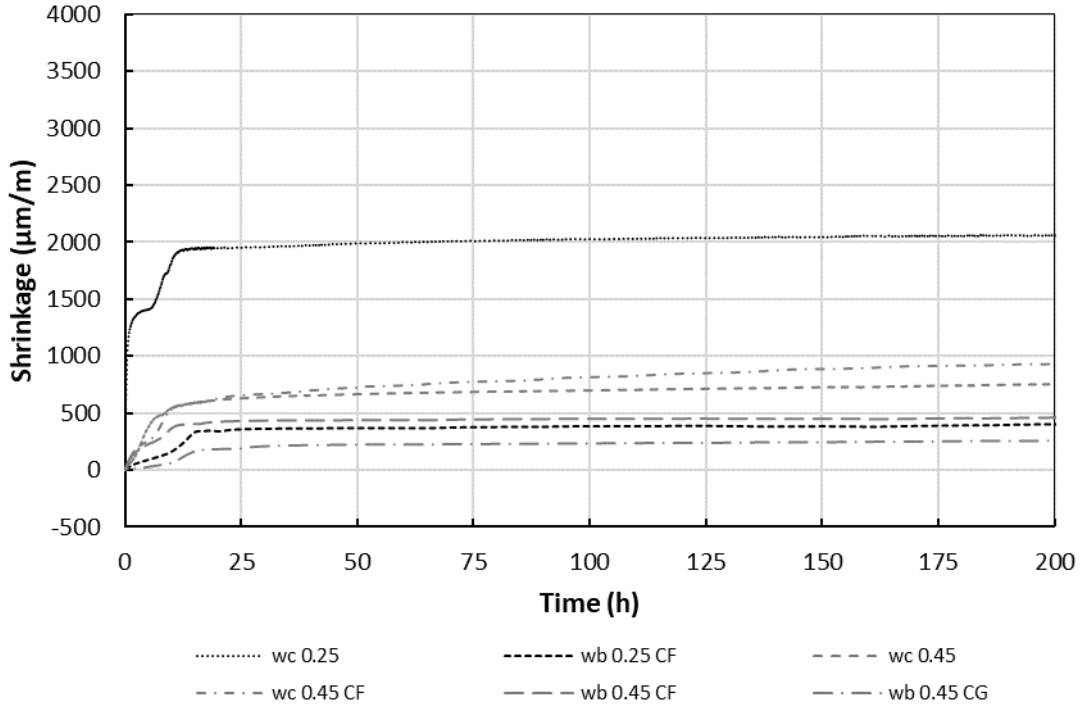

Figure E.10 Corrugated tube shrinkage for samples containing multiple SCMs

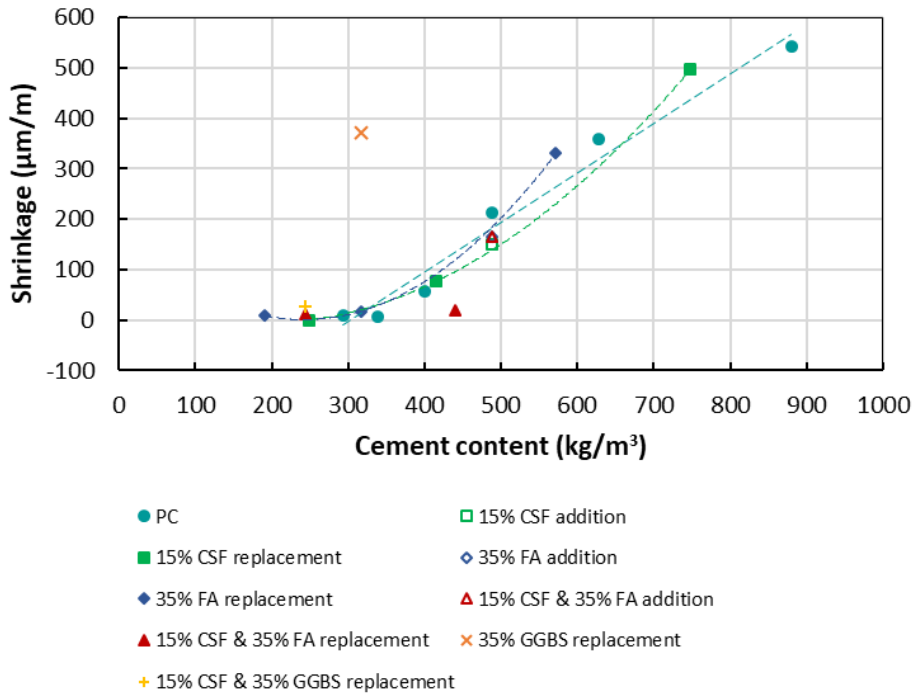

Figure E.11 Beam shrinkage with cement content for isothermal calorimeter setting time reference

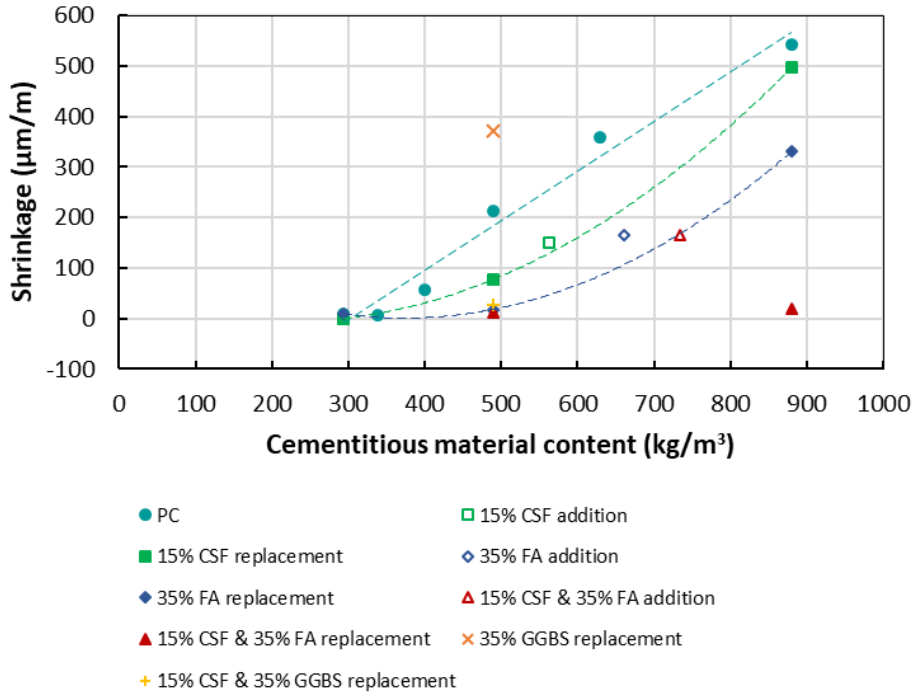

Figure E.12 Beam shrinkage with cementitious material content for isothermal calorimeter setting time reference

APPENDIX F:

STRENGTH DEVELOPMENT CURVES

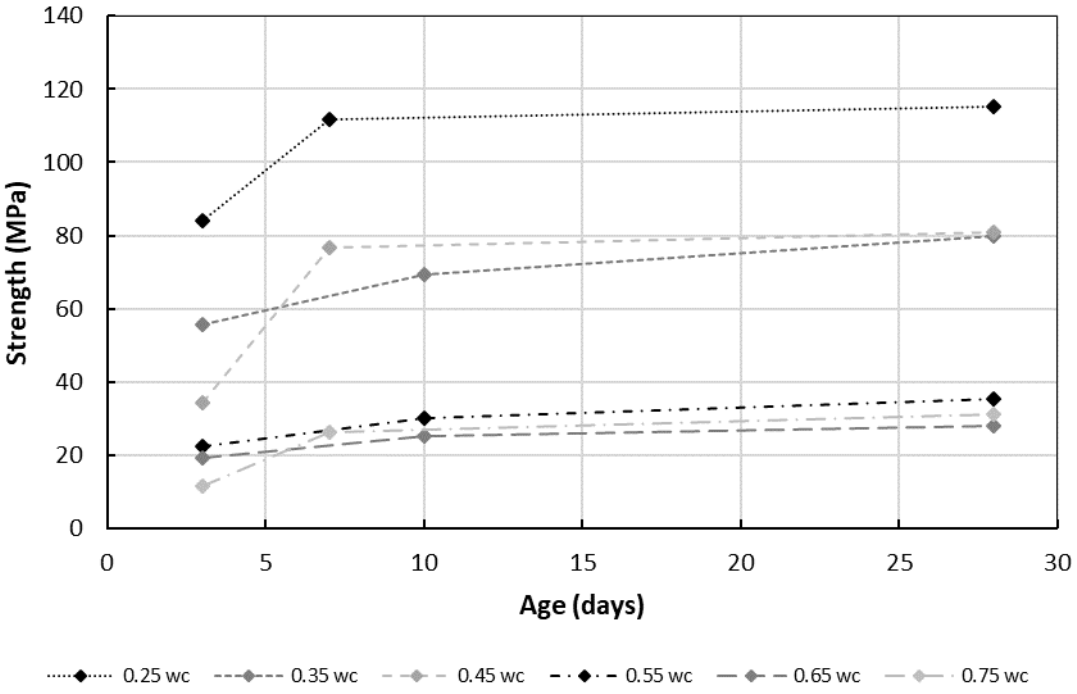

Figure F.1 Strength development for PC samples

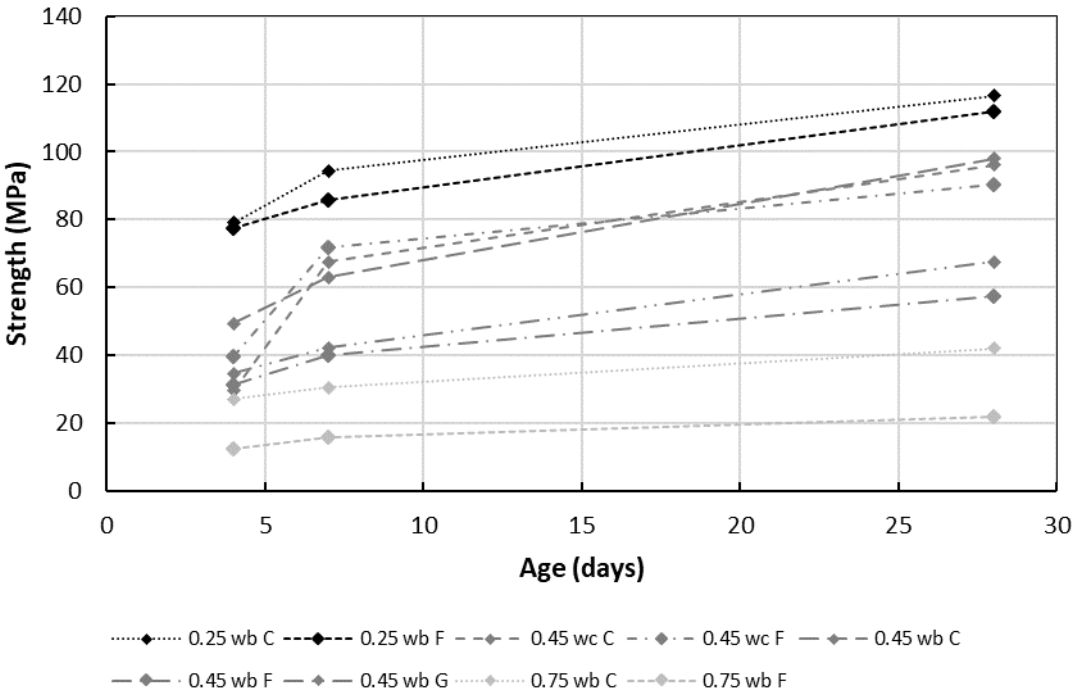

Figure F.2 Strength development for mixes with CSF, FA and GGBS

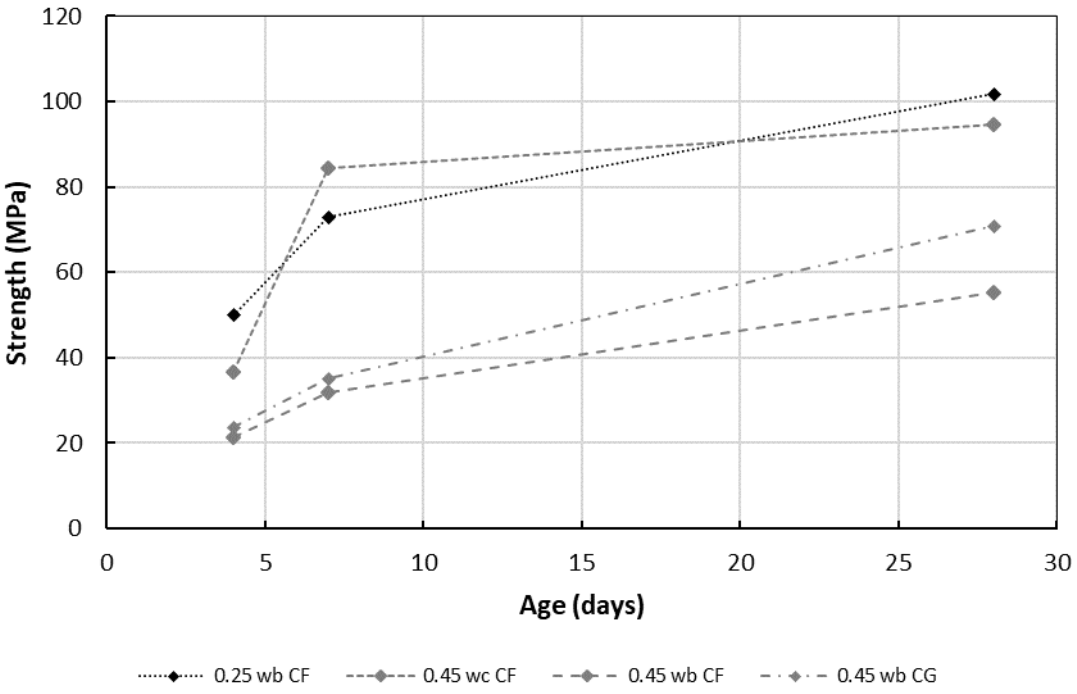

Figure F.3 Strength development curves for samples with multiple SCMs